Influence of Offshore Wind Farms on Atmosphere and Ocean Dynamics

Dissertation zur Erlangung des Doktorgrades
an der Fakultät für Mathemaitk, Informatik und Naturwissenschaften
Fachbereich Geowissenschaften
der Universität Hamburg

vorgelegt von
Elke Ludewig

angefertigt am
Institut für Meereskunde der Universität Hamburg
im Rahmen der
Max Planck Research School for Maritime Affairs, Hamburg

Hamburg 2013

Als Dissertation angenommen vom Fachbereich Geowissenschaften der Universität Hamburg auf Grund der Gutachten von
PD Dr. Thomas Pohlmann und Prof. Dr. Heinke Schlünzen

Die Disputation fand am 17.01.2014 statt.
Die vorliegende Fassung ist eine korrigierte Fassung.

Hamburg, den 30.01.2014
(Datum der vorläufigen Bescheinigung)

Prof. Dr. Dirk Gajewski
Leiter des Fachbereichs Geowissenschaften

EIDESSTATTLICHE VERSICHERUNG

Hiermit erkläre ich an Eides statt, dass ich die vorliegende Dissertationsschrift selbst verfasst und keine anderen als die angegebenen Quellen und Hilfsmittel benutzt habe.

Hamburg,

DECLARATION ON OATH

I hereby declare, on oath, that I have written the present dissertation by my own and have not used other than the acknowledged resources and aids.

Hamburg,

“ Die Welle beugt sich jedem Winde gern.”

Johann Wolfgang von Goethe, Faust II, Vers7853 /Thales

ZUSAMMENFASSUNG

Heutzutage spielen erneuerbare Energien eine Schlüsselrolle in der Diskussion zukünftiger Energieversorgung. Besonders ein verstärktes Interesse an Windenergie bewirkt einen intensiven Ausbau von Windfarmen. Im Zuge der erhöhten Nachfrage an erneuerbaren Energien gewinnen Offshore Windfarmen (OWFs). vermehrt an Popularität, zumal auf See größere und vorallem zuverlässig Erträge erzielt werden können. In diesem Zusammenhang nimmt Deutschland, infolge des nationalen Offshore Windenergieausbauprogramm, welches eine intensive Errichtung von Windkraftanlagen in der Ostsee und besonders in der Nordsee beinhaltet, eine Vorreiterrolle ein. Vor diesem Hintergrund ist es sehr bedeutsam abschätzen zu können, ob und in welchem Ausmaß ein solcher offshore Windfarmausbau unsere Meere und lokale Klima beeinflusst.

OWFs bewirken eine Reduktion der Windgeschwindigkeit in Windrichtung hinter der Windfarm. Diese Reduktion der Windgeschwindigkeit wird als Wake-Effekt bezeichnet. Der Wake-Effekt beeinflusst die atmosphärische Grenzschicht und lokal die Windeigenschaften, was wiederum Auswirkungen auf die Ozeandynamik zur Folge hat. Um den ganzen komplexen Sachverhalt der OWF Auswirkungen zu erfassen, wurden **Modellsimulationen und Messungen** für die Analyse herangezogen**.** Bei den verwendeten Modellen handelt es sich um das atmosphärische Modell **METRAS** (**ME**soskaliges **TRA**nsport und **S**trömungsmodell) und das Ozeanmodell **HAMSOM** (**Ham**burg **Schelf**meer/**O**zean **M**odell). Simulationen mit METRAS wurden in Zusammenarbeit mit dem Meteorologischen Institut der Universität Hamburg erstellt und freundlicherweise dieser Arbeit zur Verfügung gestellt. Diese mit METRAS simulierten Daten dienen als meteorologischen Antrieb der Ozeansimulationen. Messungen wurden rund um den deutschen Testwindpark alpha ventus genommen. Die Messkampagne wurde vom Bundesamt für Schifffahrt und Hydrographie (BSH) unterstützt.

Analysen des OWF-Effekts auf Atmosphäre und Ozean umfassen zwei Hauptstudien, um den möglichen OWF-Einfluss und dessen physikalisches Auftreten theoretisch zu erfassen und mögliche Änderungen des marinen Systems der Nordsee bedingt durch den geplanten Offshore Ausbauplan für 2030. Untersuchungen berücksichtigen verschiedene Mengen und Anordnungen von Windturbinen, Windgeschwindigkeiten und Modellantrieben. Modellergebnisse und Messungen zeigen eine angemessene Übereinstimmung, die den gewählten Modellansatz und prinzipielle Annahmen bestätigen.

Hauptergebnisse dieser Arbeit bezeugen signifikante dynamische Änderungen, zum einen in Bezug auf das Windfeld mit einer Reduzierung der Windgeschwindigkeit über ein Gebiet, welches hundertmal größer ist als die Windfarmfläche, bis 70 % und zum anderen in Bezug auf den Ozean durch das Auftreten von Wasserstandänderung mit Dipolstruktur, Up- und Downwellingzellen mit einer horizontalen Ausdehnung von rund 30x30 Kilometer über die ganze Meerestiefe. Die damit verknüpften vertikalen Geschwindigkeiten erreichen drei bis vier Meter pro Tag und bewirken eine Änderung in der Ozeanschichtung von Temperatur und Salzgehalt mit einer Auslenkung der Thermoklinen um 10 m rund um den OWF. Daher muss man davon ausgehen, dass OWFs intensives vertikales Mischen verursachen, welches eventuell Änderungen im Ökosystem der Nordsee bewirkt.

ABSTRACT

Nowadays renewable energy resources play a key role in the energy supply discussion and especially a heightened interest in wind energy induces intensified installation of wind farms. In the course of a larger demand of renewable energy, offshore wind farms (OWFs) gain increasingly in popularity, since over sea yields are larger and more reliable than over land. In this context Germany adopts the position of a pioneering nation due to its national interurban offshore wind energy program comprising an intensified construction of wind turbines in Baltic Sea and mainly North Sea. Against this background it becomes particularly urgent to enquire whether and to what extent such OWF expansion affects our oceans and local climates.

OWFs excite wind speeds reduction downstream of wind farms, the so-called wake-effect, which impacts atmosphere's boundary layer, locally disturbs the wind characteristics and in turn affects ocean dynamics. To study the whole complex in more detail investigations comprises **model simulations and measurements**. Used models are the atmosphere model **METRAS** (**ME**soscale **TRA**nsport and **S**tream model) and the ocean model **HAMSOM** (**HAM**burg **S**helf **O**cean **M**odel). METRAS simulations were generated in collaboration with and by courtesy of the Institute for Meteorological of the university of Hamburg. These METRAS data represent the meteorological forcing for simulations of the ocean. Measurements were taken around German test wind farm alpha ventus supported by the German Federal Maritime Service (BSH).

Analysis regarding OWF effect on atmosphere and ocean comprises two main studies to determine possible OWF effects and their physical appearance in theory and to estimate possible future integrated changes of North Sea's marine system based on the offshore construction plan for 2030. Investigation consider different amount of wind turbines, wind speeds and directions, ocean depths and forcing assumptions. Model results and measurements show a reasonable agreement supporting the principle validity of the used model approach.

Main results of this study show significant dynamical changes including a **wind speed reduction** downstream of OWF up to 70 % over an area being 100 times larger than OWF itself, an evolving **dipole structure** of the sea **surface elevation** around OWFs and **up- and downwelling cells** with an horizontal extension of approximately 30 x 30 kilometer, spanning the whole ocean depth. The connected vertical velocities reach magnitudes of three to four meter per days. In turn, these vertical motions introduce changes in stratification of temperature and salinity, which results in a maximal **excursion of the thermocline** by possibly 10 m. Hence it can be concluded that offshore wind farms cause an intensified vertical mixing in the ocean, which may result in a fundamental change of North Sea ecosystem.

CONTENT

1 INTRODUCTION

Presently, we are living in an era of a turnaround in energy policy with strong interests in renewable energies, focusing wind energy. Increased incident issues on living conditions based on climate change on the one hand and otherwise the fear of nuclear power hazards, bearing problems of nuclear waste and common protests again nuclear energy result in intense political discussions on applying renewable energies as main energy source. Especially Germany official heralds the energy turnaround in 2010. On September 28th 2010 the German Federal Cabinet enact the, in German so-called, 'Energiekonzept' (translation: energy concept). In this concept the Federal Government postulates the aim to form Germany to one of the most energy efficient and most environmentally friendly national economy in near future by offering competitive energy prices and conserving the high prosperity level of Germany. Main aim of this procedure is the phase-out of nuclear energy and the reduction of greenhouse gases by 40% till 2020 and about 80% till 2050 [*BMWi*, 2013]. At this juncture renewable energies, notably wind energy, play an important role to reach such aims. The percentage of renewable energy electricity generation on gross electricity consumption shall add up to 50% in 2030 and 80% in 2050 [*BMWi*, 2013]. Whereas the German Federal Government highlights the importance of offshore wind energy as major element for an environmentally friendly, reliable and affordable energy supply [*BMWi*, 2013]. Additional offshore is favored due to geographical useable areas, a higher reliability due to consequent high wind speeds over ocean supported by less friction than for onshore structures and even less political opposition of the population by avoiding the so-called 'Nimby-Effect', an effect describing shadow and noise disruption realizing health effects for humans. Taking for granted these facts, so Germany commands a huge area in the North and Baltic Sea. Accordingly the development goal of offshore energy is ambitious – a minimum of 25 GW offshore energy supply till 2030 in North and Baltic Sea, which accords 15% of Germany's total energy demand. Based on year 2012, counting an energy demand of around 617.6 TWh, partitioned in 19.1% stone coal, 25.7% brown coal, 11.3% natural gas, 5.7% mineral oil and others, 22% renewable energy (wind, biomass, water, photovoltaic, biogenic garbage) and 16.1% nuclear energy [*BMWi*, 2013], offshore wind energy can be a replacement for nuclear energy.

But Germany is not alone with using wind energy. There exist attractive locations for the wind industry, used in near future, worldwide. The Global Wind Energy Council and Greenpeace International present in their 4th edition of the *Global Wind Energy (GEWC) Outlook 2012* [GWEC, 2012] in three different scenarios the total installed capacity of world wide installed wind farms by 917,798MW up to 2,541,135MW for the year 2030. Based on GWEC's statistics of mid

2013 has been 4,630 MW of offshore wind power installed globally today, representing about 2% of total installed wind power capacity. More than 90% of it is installed in northern Europe alone and most of the rest is in two demonstration projects off China's east coast. However, there are also great expectations placed for major deployment elsewhere; governments and companies in Japan, Korea, the United States, Canada, Taiwan and even India have shown enthusiasm for developing offshore in their waters. According to the more ambitious projections, a total of 80 GW offshore wind could be installed by 2020 worldwide, with three quarters of this in Europe, so GWEC [2012].

And political energy plans show that Europe prefers offshore wind farming, like other countries having access to the ocean. That underlines that in future wind power will increase worldwide which leads to scientific questions dealing with the effects of wind turbines on our environment, atmospheric and oceanic surrounding. So what significant does wind farming have for us? What will happen if we establish wind farms near our coasts? To clarify the impact one has to take into account that the term 'wind farm' can be defined as a power plant using a congeries of wind turbines to generate a high total power of electricity. In case of Germany this again means the construction of diverse offshore wind farms (OWFs) in Germany's exclusive economic zone (EEZ), a huge area that can be filled with hundreds of wind turbines. Here such a develop will change North Sea's appearance and leads to the question what impact such a shift can have on atmosphere and ocean considering the energy transformation of atmospheric energy over mechanical to electrical energy.

The effect of wind turbines can be treated in different ways. Done scientific studies are separated into industrial and technical aspects, analyzed effects on the atmosphere, analyzes of biosphere, ecosystem and medical impacts.

The **technical sector** concentrate on the potential of energy, the arrangement of wind turbines in a field, the size and form of rotor blades, power of turbines and duration life for example treated of in Jenkins [1993], Mosetti et al. [1994], Sutherland and Mandell [1996], Polinder et al. [2005], Castro et al. [2007] and Lackner and Elkinton [2009], just to list a handful examples cross the last decades. Based on industrial impacts and profit thinking these topics are well analyzed and optimized but still in active research for more optimizing and aiming reduction of costs.

Beside technical analysis some **studies deal with effects on biosphere and ecosystem and human life**, for example Zettler and Pollehne [2006], Lange et al. [2010], Nunneri et al. [2008] and Wolsink [2000]. These studies underline issues regarding beards, bats, sea mammal or lobster and other sea animals as well as noise and shadow effects (Nimby-Effect) bothering humans.

If we refrain from the medical and biosphere causes of wind turbines and having a closer look on other studies regarding wind turbine then these studies concentrating on the effect of wind turbines on their surrounding. Focus of these **studies** is the **change in wind field and energy and their effects on the atmosphere**, like changes in temperature and wind field on **higher scales** [*Baidya Roy and Traiteur*, 2010, *Christiansen and Hasager*, 2005, *Hasager et al.*, 2013, *Zhou et al.*, 2012] and **small scales** [*Jimenez et al.*, 2007; *Porté-Agel et al.*, 2011, *Wu and Porté-Agel*, 2010, *Lu and Porté-Agel*, 2011].
There exist studies how strong a wind farm can influence meteorological situations and **changing weather** [*Fiedler and Bukovsky*, 2011; *Fitch et al.*, 2012, *Baidya Roy*, 2004, *Kirk-Davidoff and Keith*, 2008, *Keith et al.*, 2004]. Experiments were done dealing with the question what happen to **global energy distribution** by demanding big wind farms everywhere [*Wang and Prinn*, 2010]. The overall aspects of these studies are a reduction in wind speed behind wind farm in wind direction, the so-called wind wake, a mostly cooling at offshore and warming at onshore as well as possible dynamical changes in atmosphere due to wind wake.

Studies on effects on ocean dealing with dynamical effects on the ocean, like this dissertation, are quite new and rare documented. First Broström [*Broström*, 2008] indicates a change on sea surface elevation due to wind farms which is even documented in [*Paskyabi and Fer*, 2012].

Nerge and Lehnhart picked up Broström's concept. Their results are summarized in the LOICZ 2010 report, which shows effect of wind farms on ocean in various scientific areas. Here it becomes clear that offshore wind farms have an important influence on ocean. That is why this thesis uptakes Nerge and Lehnhart first results to engross and discuss important physical aspects of offshore wind farm effects roundly.

This dissertation concentrates whether and in what manner will dynamics change if we extract energy from the atmosphere over a big areal domain? Based on listed known studies and considering political situation that core question of this thesis is analyzed adapted to Germany's situation in the North Sea. But all results can be also associated to other coastal regions. The focusing on Germany and the North Sea follows practicable reasons, on the one hand the strong interests of Germans in this subject as well as the work's frame including financial and scientific support by German institutions the IMPRS for Maritime Affairs, the University of Hamburg and the Federal Maritime and Hydrographic Agency (BSH).
In this connection the main aim is to analyze and explain the dynamical effects offshore wind farms have on ocean due to mentioned wind reduction and wake production and to provide this information for further studies with an economical background to answer the question of the possibility of reef building, mussel farming and other ecological changes in future as well as to

support additional projects in that field. To get closer to those oceanic questions it is necessary to include the atmosphere why here also common influences of wind farms on the atmosphere are presented even though it is now easily found in literature.

The analysis of offshore wind farm effects on ocean and atmosphere comprises model simulations as well as measurements and is organized as follows:
To become acquainted with thesis' topic chapter 2 gives an introduction into wind energy and here especially offshore wind energy. Chapter 3 explains used data and models and gives an overview of applied methods. The heart of this work is chapter 4 comprising three analysis. Section 4.1 describes the effect of wind farms on the atmosphere based on theoretical assumptions, which spans explanation of forcing for ocean modeling. Section 4.2 presents the effect of OWF on an idealized ocean box, including different wind forcing, analysis of physically ocean processes triggered by OWFs and model evaluation with measurements. Last analyze in section 4.4 gives an insight into the future of the German Bight regarding the demand of offshore wind farms in the North Sea. Finally chapter 5 summarizes and gives an outlook.

2 RENEWABLE ENERGY WIND

This thesis deals with the current most important and effective renewable energy, the wind energy. Countries all over the world want to place wind turbines into nature for producing 'green energy'. In the last decades renewable energies were fixed in our society aiming on protecting resources and providing a new greener and hence more healthful live. Common press coverage delivers spread information on status and developing in this field. Therefore this chapter gives an insight into the renewable energy wind, it's current state and technique. Assuming the crucial point that this thesis concentrates on offshore wind farms this chapter finishes with a description of Germany's wind farming in the North Sea including description of the first German test wind farm, called alpha ventus and possible future offshore expansion.

2.1 Utilization of Wind Energy: Historical and Technical Background

Transforming wind power into mainly mechanical energy is established in our civilization since centuries. A nice overview of wind turbine's history is given by Hau [2008].
The first historical source of a windmill's existence is dated with 644 AD and describes a windmill with vertical rotation axes placed in Persian-Afghan border district used for grinding grain. Across the centuries, references arise of windmills in China used to drain paddy fields. Windmills with a horizontal axis of rotation were developed in Europe, may independent of Orient's construction. Documentable indications come from the year 1180 proving the existence of 'Bock wind mill' in the Normandy. Over the centuries windmills has been technical improved and spread over Europe and Russia. So various types of windmills arise – the ancestors of nowadays wind turbines. Windmills which are similar to turbines of todays were developed in the 19th century in the mid-western United States. They were mainly used for water pumping. Proposed by the Danish government looking for possibilities to supply rural areas with electricity, the Danish professor Poul La Cour built 1891 an experimental wind turbine gearing a dynamo in Askov, Denmark. While in the past windmills were mainly used for transforming wind energy into mechanical energy, generating electricity is prioritized today.
Enhancing Poul La Cour's construction, nowadays wind turbines comprise a huge development in engineering. A sophisticated technique transforms wind energy into electricity by controlling blades and turbine conditions focused on high efficient. Over the years wind turbines of a high technical standard were developed to transform wind energy to electrical power.

Nowadays Wind Turbine

The main concept of nowadays wind mill is a tower, mostly three rotor blades and a turbine in a nacelle [*Morris*, 2006]. Such a wind turbine is illustrated in figure 2.1.1.

Today various turbines are available arranged for different conditions and power supply. Such first turbines dealt with energies of 2 Mega Watt (MW). Now 5 MW turbines are common but the turbines will be developed by ten, fifteen (promoted by Spanish companies Gamesa, Iberdrola and Acciona in 2010) and may more MW-turbines in further times. The diameter of the rotor started with a couple of meter, eighty to hundred meters are currently used and bigger rotor blades up to 200 m are in testing phase [*Vestas Wind Systems*, 2013]. For energy production exist two difference styles of nacelles – construction with gear mechanism and without it. At construction with gear mechanism the power is lead from rotating motion of the rotor through driveshaft and gear in the dynamo. A dynamo can only work with a high driving speed, which cannot be supported by wind turbines. This issue is solved with help of the gear, which transform power with low driving speed and high turning moment into power with high driving speed and low turning moment. In contrast constructions without gear have an advantage of less machine components. This means less rotating materials, hence less maintenance works. Therefore they are proposed for offshore turbines where maintenance is complicated, time and cost intensive and weather dependent.

Such construction offers a synchronous generator activated by a permanent magnet. They transform the rotor motion directly into electricity. In sum nearly 45% of the wind energy can be transformed to electrical power. The rest is loosed during transformation process, shown in figure 2.1.2. Around 41% of wind energy cannot be extracted; the rest of 59% is reduced by aerodynamic rotor losses, mechanical losses and electrical losses through driveshaft and generator.

Wind turbines need a strong basement structure to fix them. On the one hand a rotating turbine leads to imbalance and vibration during rotation and on the other hand wind and waves exert force on construction. While onshore turbines mostly fixed by a monopole and a cement basement, offshore wind turbines can be fixed by various basement structures, shown in figure 2.1.3. Swimming basements are still in testing phase (FLOATGEN project) while currently mostly tripods are used. In case of offshore wind park alpha ventus (described in 2.2.3) tripods and jackets are tested. Piles will be ignored in this study due to the fact that the model resolution cannot resolve such small turbulences. But that assumption will not influence analysis because turbines itself have a really weak effect on ocean dynamics, they just support weak vertical mixing, which lead to very small changes being smaller than natural variability [*Burchard et al.*, 2008].

Although hub height of towers and rotor diameter show an increase by time, figure 2.1.4 and 2.1.5, having common heights of 135 m and diameters of 126 m in 2008.

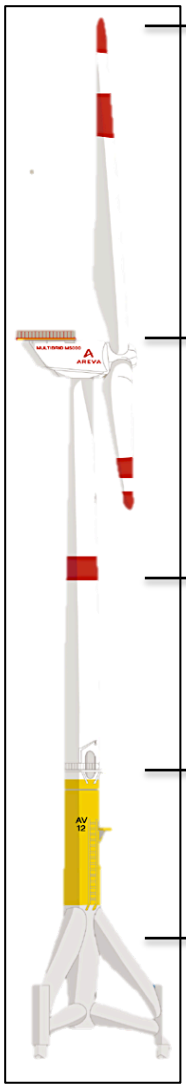

Rotor blade with a diameter of 80m and more, consist of two half-shell connected with internal bars. Half-shells are covered with glass or carbon fiber and are drenched in polyester and epoxy resin and then colored with special surface technology colors to survive them from atmospheric conditions. The blades can be partly heated to avoid ice formation and they are equipped with an arrester.

Hub and point for hub height with **nacelle** and optional helicopter pick up area. The nacelle features dynamo, gear mechanism, monitoring, regulating and control systems as well as and technology of electric supply. The nacelle is fixed on a azimuth-bearing hence it is rotatable to move blades into the wind.

The **tower** holds nacelle and blades. Dependent of place of installation and height it is made of steal, lattice or cement. It shelters a ladder or elevator to reach nacelle.

Jetty. Offshore turbines need a jetty to allow an entrance for attendance, which is placed a couple of meters above sea level. An entrance is possible up to 2m wave height.

Bottom attachment, here **Tripod** as an example for offshore. Monopiles, gravity foundations, Tripiles, Jacket, swimming basements are also in use or test phase for offshore wind turbines.

Figure 2.1.1: Schematic illustration of a typical wind turbine which is used nowadays in offshore (onshore) wind farms. Illustration is based on a schema by Trianel Windkraftwerk Borkum GmbH&Co.KG

As mentioned onshore wind turbines become bigger to catch stronger winds, which are less influenced and weakened by surface friction (through bushes, tress and other surface constitutions), which again supports a higher energy production. In case of offshore wind farming it is not necessary to counteract against wind reduction by surface friction because ocean surface friction is less and no structures disturb the wind filed. Therefore wind is quite consistent in offshore areas as well as strong enough to allow lower towers that provide the same capacity like much higher onshore turbines. Figure 2.1.5 illustrates that context; a capacity of 3000 kW can be reached by 80 m offshore towers while at onshore a hub height of 110 m is required. Whereas dealing here with offshore cases hub heights of used towers are set to 80 m.

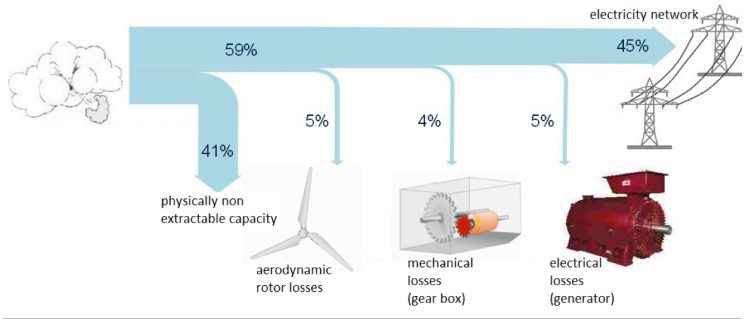

Figure 2.1.2: Energy conversion from wind to electricity. Only 59% of wind energy can be extracted and established to conversion. During transformation process around 14% energy is loosed due to aerodynamic, mechanical and electrical losses. Illustration based on BWE (Bundesverband WindEnergie).

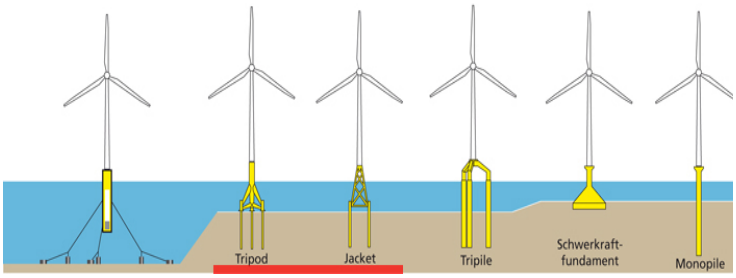

Figure 2.1.3: Fundaments for wind turbines at offshore. From left to right: swimming basement, Tripod, Jacket, Tripile, gravity foundation and Monopile. (Source: Stiftung OFFSHORE WINDENERGIE).

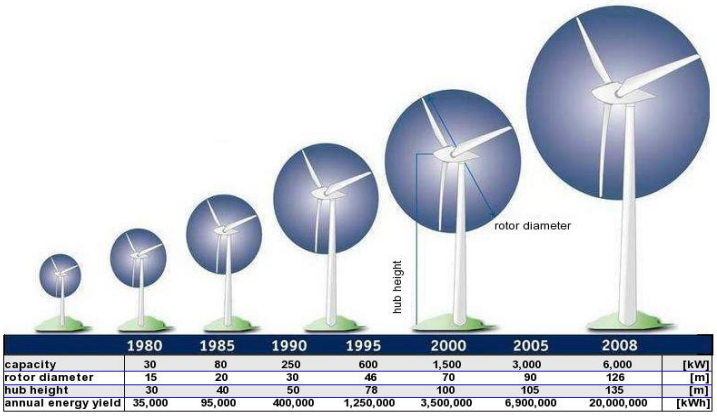

	1980	1985	1990	1995	2000	2005	2008	
capacity	30	80	250	600	1,500	3,000	6,000	[kW]
rotor diameter	15	20	30	46	70	90	126	[m]
hub height	30	40	50	78	100	105	135	[m]
annual energy yield	35,000	95,000	400,000	1,250,000	3,500,000	6,900,000	20,000,000	[kWh]

Figure 2.1.4: Common trend of hub height and rotor diameter. Due to necessary power capacity the evolution of rotor diameter increased with years. Present (year 2013) onshore wind turbines can have a hub height of 200 m accordingly large are rotors. Illustrations based on BWE (Bundesverband WindEnergie)

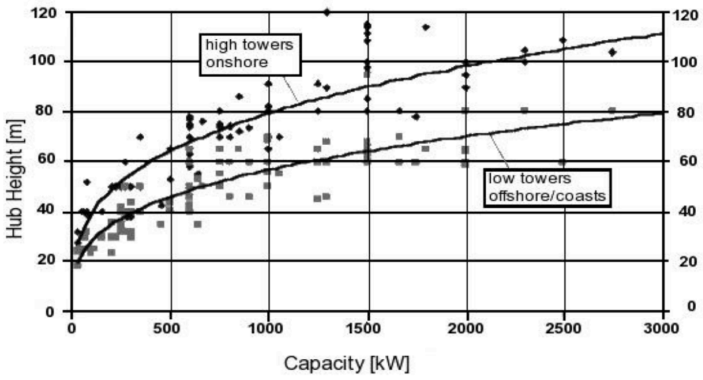

Figure 2.1.5: Common trend of hub height in meter in relation to capacity in kW separated for onshore (black) and offshore (grey). An offshore wind turbine tower is lower than an onshore tower due to stronger wind speeds near ground to that effect higher capacity. Illustrations based on BWE (Bundesverband WindEnergie)

2.2 Wind Farming in the North Sea: Example Germany

The advantages of offshore wind farms regarding space, productivity and minor harassment of humans support constructions of wind turbines in the North Sea. The use of German part of North Sea for wind farming is the only possibility to reach political energy aims mentioned in the introduction of that thesis. Wind farming in the North Sea is used by the United Kingdom, Netherlands, Belgium, Norway and Denmark. Based on statistics of LORC Knowledge, a Danish database collecting all offshore information supervised by **L**indoe **O**ffshore **R**enewable **C**enter, North Sea has the strongest offshore wind farm development beside China. A worldwide map of existing offshore wind farms is placed in appendix B.
Germany cabs tap the potential of offshore wind farming in the North Sea. Following section will shortly define the North Sea and its availability for use of OWFs.

2.2.1 North Sea

The North Sea is located in Europe having coasts to Norway, Great Britain, France, Netherlands, Germany and Denmark. It is defined as a shallow shelf sea with a mean depth of 80 m and a maximum water depth that is in the Norwegian Trench of about 800 m [*Sündermann and Pohlmann*, 2011; *Mathis*, 2013]. The North Sea has got a strong tide and is famous for its Wadden Sea, declared as UESCO world culture heritage.
A summary of synoptically, hydrodynamic and hydrographic conditions of overall North Sea area is given by Mathis [2013] based on Otto et al. [1990], Rodhe [1998], OSPAR [2000], Steele et al. [2009]. Most relevant information of North Sea for this study is its stratification of the area within the so-called Exclusive Economy Zone, which is defined under section 2.2.2. The status reports of the German Federal Maritime and Hydrographic Agency (BSH) provide information about the System North Sea. The results of that reports show a wind statistic of mostly wind directions between southwesterly and westerly winds for the southern part of the North Sea. On average over all seasons the geostrophic wind speed counts around 8.0 m/s since 2005. That value is calculated at position 5º E and 55ºN, which is representative for the area between 0º-10º E and 50º-60ºN [*Loewe*, 2009]. Sea surface temperatures counts in average 10 ºC. Geographically SSTs increases from northwest to southeast. Most areas of the German EEZ are thermal stratified in summer with temperatures of 6-7 ºC at bottom and 15-18ºC, sometimes 20 ºC at surface [*Loewe*, 2009].
Large parts of North Sea are water of Atlantic origin having salinity concentrations greater than 35. Hence highly salty waters of Atlantic origin in the West (35/34 psu) and low-salty waters (lower

than 32 psu) in the East being influenced by Baltic sea waters and continental fresh water input, like from river Rhine and Elbe, characterize distribution of salinity concentration of North Sea.
That information are used to set-up an idealized ocean having North Sea conditions to analyze dynamical changes due to operating offshore wind farms.

2.2.2 Germany's Exclusive Economy Zone (EEZ)

States having access to ocean are able to build offshore wind farms. As a result of UNCLOS (United Nations Convention on the Law of the Sea) states are allowed to build such wind farms only in a special zone near their coasts. This zone is called exclusive economy zone. "The exclusive economic zone is an area beyond and adjacent to the territorial sea, subject to the specific legal regime established in this part, under which the rights and jurisdiction of the coastal state and the rights and freedoms of other states are governed by the relevant provisions of this convention" UNCLOS, Part V, Article 55 (see also appendix B).
Based on this definition Germany's area for offshore wind farms in the North Sea is restricted. Area of Germany's EEZ and its ocean depth is depicted in figure 2.2.1. Germany's EEZ includes important shipping routes whose are indefeasible. Beside these routes a huge area within EEZ is useable for offshore wind farming even in depths of 60 m.

Plans, respectively scenarios, of offshore wind farm demanding within EEZ are listed in LOIZ research and studies number 36 [*Lange et al.*, 2010]. These scenarios deal with different marine management perspectives of EEZ. One of these scenarios, precisely an extreme scenario, is disposed and presented in this thesis in chapter 4.3 to estimate possible changes of North Sea in case of intense offshore wind farming.

Nowadays four offshore wind farms are in operating state [*BMU*, 2013], alpha Ventus with 12 turbines, BARD Offshore 1 with 80 turbines and each with one turbine ENOVA Ofsshore Ems Emden and Hooksiel and several more are approved, under construction and in approval procedure. Figure 2.2.2 marks spaces within EEZ planned and used for OWFs. BARD Offshore 1 lies 90 km westerly of Borkum, ENOVA nearshore, 0.1 km, in industry port Emden and Hooksiel nearshore, 0.5 km, northerly of Wilhelmshaven. Offshore wind farm alpha ventus has a special role in this thesis due to its status as Germany's first offshore wind farm and due to its attribute 'test wind farm' and focus on research. Details of this pregnant wind farm are given in next section.

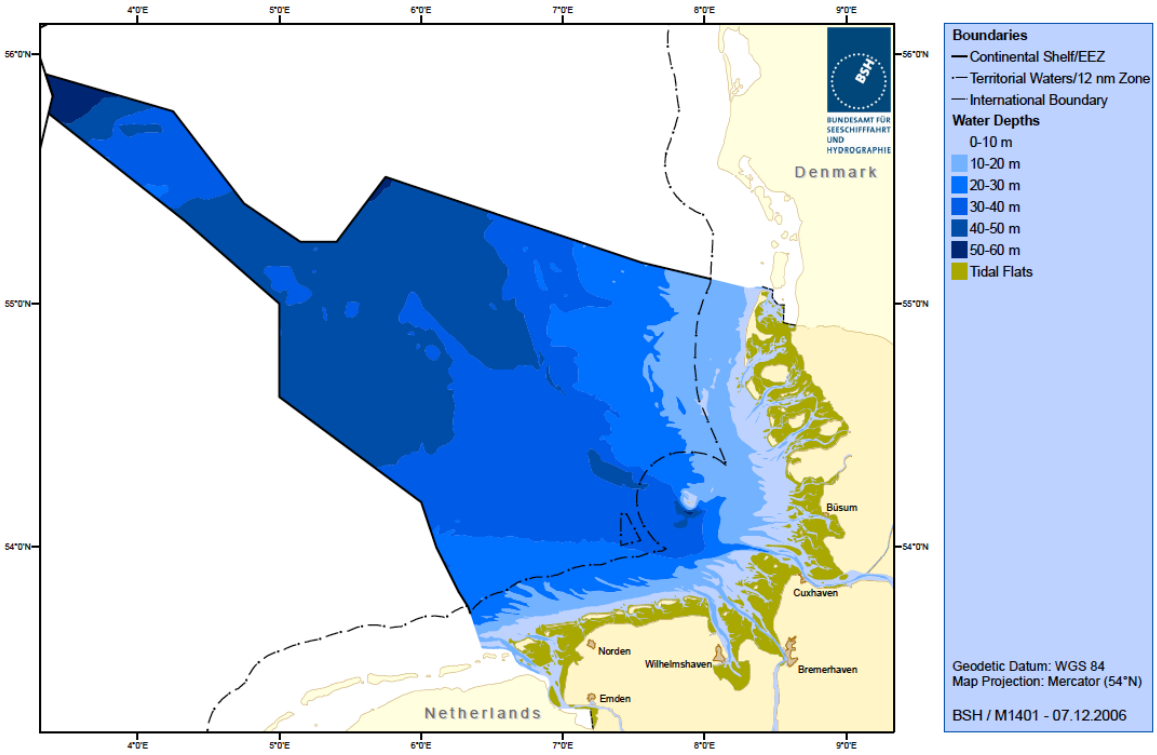

Figure 2.2.1: Germany's part of the North Sea; Continental Shelf, Exclusive Economic Zone. Colors show water depths with a maximum of 60 m. Area of EEZ in the North Sea spans around 28.600 km². Illustration provided from BSH.

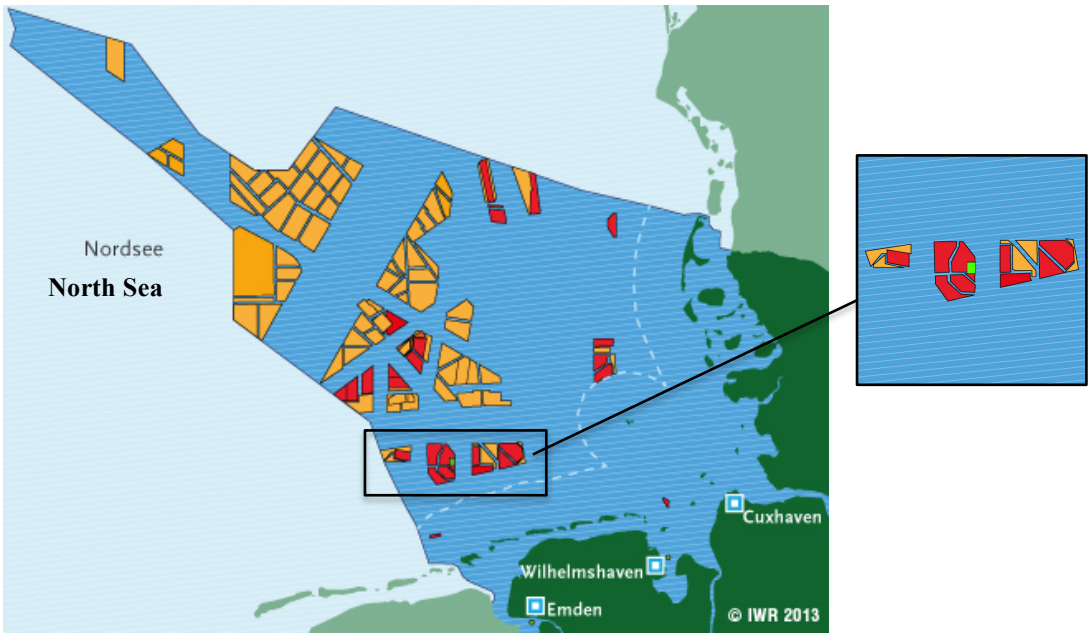

Figure 2.2.2: Offshore wind farm projects in the North Sea, status 2013. Green selection identifies OWF in operating state, red selection marks OWFs, which are approved/under construction and orange areas are in approval procedures. Zoomed area shows a section northerly of island Borkum. Green square presents wind farm alpha ventus. Figure has a copyright by IWR and was taken from BMU[*BMU*, 2013] and only changed by adding and highlighting zoomed area.

2.2.3 alpha ventus

Following information of alpha ventus is based on 'alpha ventus Fact Sheets', whose publishing is supported by BMU (Bundesministerium für Umwelt, Naturschutz und Reaktorsicherheit (engl.: Federal Ministry for the Environment, Nature Conservation and Nuclear Safety).

Alpha ventus is known as Germany's test wind park actuated by the consortium 'Deutsche Offshore-Testfeld und Infrastruktur GmbH&Co.KG (DOTI)" (translation: Germany"s offshore test field and infrastructure GmbH&Co.KG) in June 2006 (FactSheet alpha ventus 2012). *Alpha ventus* was commissioned in April 2010. Hence it was the first offshore wind park in Germany, investment sum of 250 million Euros, 30 million Euros supported by the BMU. The wind park is located 45 kilometer northerly of the island Borkum, where the North Sea has a depth of around 30m, see figure 2.2.2. The test field consists of 12 wind turbines, one research platform, named Fino1, and one relay station. Together all of these wind turbines have got a capacity of 60 MW. Each wind turbine has got a rotor diameter of 116 m with a hub height of 90 m, a capacity of 5 MW and a rated speed of 12.5 m/s. Speed limitations start at 3.5 m/s and ends at 25 m/s. The turbines are fixed on tripods and jackets (figure 2.1.3) and arranged in a 3x4 matrix with three rows in longitude and 4 rows in latitude. The location is mapped and treated in chapter 4.2.4.

Alpha ventus goes along a multiplicity of research projects, which are comprised under the initiative RAVE (**R**eseacrch at ***a****lpha* ***ve****ntus*). Besides developing wind park system and technical optimizing these projects analyze the effect on the close marine surrounding focused on the marine ecosystem. The essential point is that 2 years before demanding research started and is still going on. Experience from *alpha ventus* helped and will help to build further wind farms in the German economic zone.

Here *alpha ventus* is used as a sample of wind farm arrangement in done simulations and provides the possibility of model evaluation due to measurements which are already taken around *alpha ventus* in May 2013. The presence of *alpha ventus* helps to collect information about OWF's influence on ocean and confirms results of this study.

3 MODELS, DATA AND METHODOLOGY

This work comprises two models and a couple of data, which are described here. Finally the chapter will end with a methodology.

3.1 Models

3.1.1 Hamburg Shelf Ocean Model (*HAMSOM)*

The **HAM**burg **S**helf **O**cean **M**odel (HAMSOM) is a numerical three-dimensional baroclinic hydrostatic dynamical model developed by Backhaus in 1985 [*Backhaus*, 1985]. Here a modified version, including improvements by Pohlmann [*Pohlmann*, 2006] is used. HAMSOM is well developed for sea shelf processes and tested in various studies of the North Sea and other shelf seas such as Backhaus et.al [1987], Carbajal [1993], Becker et al. [1999], Hainbucher and Backhaus [1999], Huang [1999] and several more.

Hence HAMSOM is known as an accurate model simulating physical processes well and therefore features the best requirements for this study. Model basics are the primitive equation, a free surface. The horizontal and vertical grid spacing is defined in z-coordinates on the Arakawa C-grid [*Arakawa and Lamb*, 1977]. The model uses a semi-implicit scheme instead of separating the internal and external mode, which largely exempt from the stability criteria usually required for explicit formulations. A more detailed description of the model, its discretization and equations, boundary conditions and model design is given in appendix A.A. Further detailed description of further HAMSOM features is allocated in this study if necessary, for example in section 4.2.2, which deals with a sensitivity study to analyze physical processes in the ocean.

HAMSOM's forcing includes data of wind, pressure, temperature, humidity, precipitation and cloudiness with their origin of ECMWF (European Centre for Medium-Range Weather Forecasts) data on the one hand and on the other hand forcing data also modeled by the atmosphere model METRAS.

3.1.2 MEsoscale TRAnsport and Stream Model (*METRAS)*

The **me**soscale **tra**nsport and **s**tream model METRAS was developed by Schlünzen in 1988 and complemented with a wind turbine parameterization by Linde [*Linde et al.,* n.d.]. Hence METRAS

has implemented wind turbines and so is able to resolve changes due to wind turbines in the atmosphere. This thesis uses METRAS data as a meteorological forcing, which was modeled in collaboration with the Meteorological Institute (MI) of the University of Hamburg based on the need for ocean analysis. The METRAS data are a courtesy of the MI of the University of Hamburg and the METRAS simulations were done by Marita Linde, whose PhD includes atmospheric changes in the North of Germany due to OWFs.
Here only wind turbine parameterization of METRAS is considered. Information of METRAS model design can be found in appendix A.B.

Wind turbine parameterization in METRAS:

Facts about wind parameterization in METRAS are based on Linde et. al. (in progress) and personal correspondence with M. Linde (PhD candidate at MI since 2011).
METRAS uses the actuator disc concept (ADC) for its wind turbine parameterization [*Linde et al.*, n.d.]. This concept is based on Betz [1926a] constitute the rotor as an infinitesimal thin disc with a diameter of rotor diameter and midpoint at hub height and position of wind turbine. A schematic illustration of the concept of the ADC is shown in figure 3.1.1 after Betz [1926b], Mikkelsen [2003] and Linde et. al [in progress].
It is assumed that an air package contains kinetic energy depending on its velocity. Far in front of a wind turbine, the air package is not influenced by the wind turbine and has the velocity v_1. Because of the extraction of kinetic energy, the flow velocity v_2 is reduced behind a wind turbine. This increases the pressure right in front of the rotor disc A' (figure 3.1.1). The parallel streamlines of laminar flow are spreading up. An air package that passes a small area A_1 far in front of the wind turbine passes a larger area A_2 far behind the wind turbine. The maximal thrust T_{max} is reached for v_2=0. Using these assumptions a dimensionless thrust coefficient c_T can be formulated as the percentage of rotor thrust T' to maximum thrust with the air density ρ:

$$c_T = \frac{T'}{T_{max}} = \frac{\frac{1}{2}\rho A'(v_1^2 - v_2^2)}{\frac{1}{2}\rho A' v_1^2} = 1 - \frac{v_2^2}{v_1^2} \qquad \text{EQ 3.1.1}$$

The thrust coefficient c_T is a parameter given for each wind turbine type by manufacture's specifications or it can be determined from field measurements.
The coefficient varies with the speed of wind. According to the definition of the thrust coefficient, the rotor thrust equation (EQ 3.1.2) only depends on the wind speed of the undisturbed flow, the thrust coefficient, and the rotor area. The rotor area depends on the rotor diameter and is easily calculated. But the undisturbed wind speed has to be determined during model simulation.

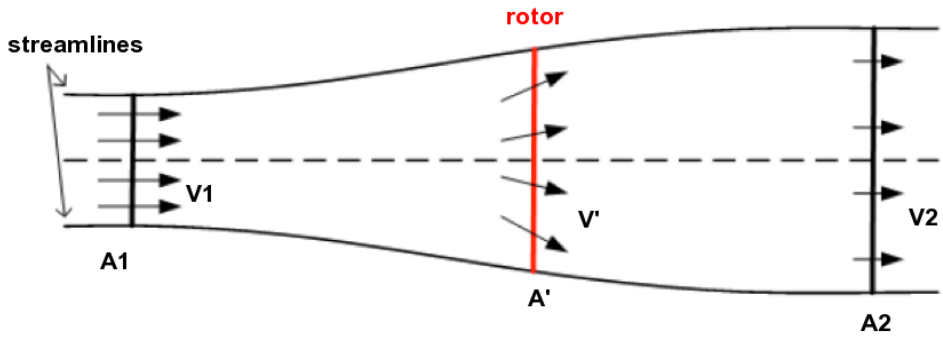

Figure 3.1.1: Schema of actuator disc concept after Betz, 1926, taken from Linde et al. (in progress). Red line marks rotor disc. For further details please see text.

$$T' = \frac{1}{2}\rho A'\left(v_1^2 - v_2^2\right) = c_T T_{max} = \frac{1}{2} c_T \rho A' v_1^2 \qquad \text{EQ 3.1.2}$$

In METRAS, like in all mesoscale models, the horizontal grid size is typically large compared to the size of the wind turbine rotor. It means, for a single wind turbine, the grid cell for the rotor and the reference position is the same. Also several wind turbines might be located within one single grid cell. Therefore a whole wind farm, like *alpha ventus* with 12 turbines, is only located within a few adjacent grid cells. Therefore the wind reduction of several wind turbines superposes to one large wind wake in the model. To adapt that issue the wind counts ratable into affected grid box. That means a preprocessor mask consisted of an auxiliary grid allows calculation of one turbine within a relative bigger grid. Therefore it is necessary to determine the average reference wind speed for each wind farm in METRAS. The reference wind speed is chosen over all grid cells containing the wind farm itself. The area per grid cell covered by a rotor is defined as wind turbine mask.

Multiplying equation EQ 3.1.2 with the wind turbine mask and adding this term to the basic momentum equation leads to the parameterization for wind turbines.

$$\vec{v} = \textit{equation of motion} + \textit{wind turbine mask} * T' \qquad \text{EQ 3.1.3}$$

Due to the wind speed depending thrust coefficient, wind turbines switch on and off autonomously, if wind speed is equal to the cut-in or cut-off velocity. Normally used cut-in and cut-off wind velocities in METRAS are 2.5 m/s – 17 m/s (personal correspondence with M. Linde). Turbines and actuator disc are moveable and are set orthogonal to the wind. The influence of the tower is ignored so far that no real obstacle is implemented. But to have an effect due to friction in case of

less wind, pressure in grid of rotor will increase in case of wind speed is lower than cut-in velocity. With these assumptions and the implementation of the ADC, several large wind farms can be represented in the model domain.
Wind turbines are simulated using an active rotor disc and the changed wind field is parameterized adding a deficit term to the equation of motion.
In this study the height of the tower counts 80 m, like the rotor diameter, which is a normal size of wind turbines in offshore wind parks (compare with figure 2.1.5).

A restriction is the different scale between wind turbine and grid box. Due to ratable consideration of wind change, the effect is ratable projected on the whole grid box the wind turbine is placed within. Although the turbine does not affect the whole box a better solution is currently not available. This adaption leads in turn to an overestimation of the wake size, which has to be considered. Like described in SAR (synthetic aperture radar) data by the work of Li and Lehner [2012] wind farms often lead to one uniform wind wake but under certain conditions single wakes behind each wind turbine can be seen. Such single wind wakes cannot be considered here due to scales.

3.2 Data

Besides using METRAS data as forcing data additional forcing data were necessary. These data are reanalysis data from ECMWF. An additional data set of ocean data comes from ship measurements, which are used to evaluate model results. Further details can be found in following sub chapters.

3.2.1 Climatological and Reanalyze Data

Climatological and reanalyze data were necessary for simulation of the North Sea and German Bight.
METRAS uses ECMWF (European Centre for Medium-Range Weather Forecasts) data as meteorological forcing as well as NOAA (National Oceanic and Atmospheric Administration) Optimum Interpolation Sea Surface temperatures for SST forcing.
HAMSOM uses Era-Interim data and a forcing-mix of METRAS and ECMWF data for meteorological forcing. The mix of meteorological data was necessary because of detriment of METRAS model setup; only atmosphere over investigation area of the German Bight was

simulated by METRAS. Thus atmosphere data over the remaining North Sea area is defined by another, the ECMWF, data set.

Atmospheric forcing includes 10 m wind fields, surface pressure, 2 m and 10 m temperature and humidity fields, precipitation and cloud cover.

Horizontal resolution of atmospheric fields are 1.5º for Era Interim, 1º for ECMWF data, which causes a gridding to HAMSOM horizontal resolution, and METRAS data have a resolution identical with HAMSOM.

Additional necessary for ocean simulation are oceanic forcing at lateral open boundaries for ocean simulation consisting of ocean temperature, salinity concentration, surface elevation and river runoff. Thereby those data are monthly climatological means based on the climatological ocean data set World Ocean Atlas 2001 (WOA-01) by Boyer et al [2005] for salinity and temperature. The river runoff is considered by runoff fluxes of 46 rivers along the North Sea coasts gathered by Damm [1997] and O'Driscoll et al. [2012].

3.2.2 Measurements

The BSH supported hydrographical and hydrological measurements around test wind park *alpha ventus*. The cruise aboard **VWFS** (**V**ermessungs-, **W**racksuch-, und **F**orschungs**s**chiff) WEGA allows the use of Acoustic Doppler Current Profiler (ADCP) and CTD-probe (Conductivity, Temperature, Depth) within 11st to 13rd of May 2013. The data set comprises three ADCP stations, which took measurements over 2 days and 39+3 CTD profiles within one day. Some impressions of WEGA cruise is given in appendix C.1. An explanation of the CTD-probe and the ADCP instruments is documented in appendix C.2 and C.3. Data presentation and evaluation is placed in chapter 4.2.4.

3.3 Methodology

To analyze the effect of OWFs on atmosphere and ocean mainly model data were consulted. As mentioned model results area based on METRAS simulations, which again were used as meteorological forcing for ocean simulation with model HAMSOM. Various simulations were carried out to investigate different factors triggering OWF effect on atmosphere and ocean. To fully capture possible effects the analysis is separated into two main approaches. Hence the analysis is based on two **t**ypes **o**f **s**imulation shortened with **TOS**.

Type of Simulations:
The first type of simulation, TOS-01, serves an idealized approach to analyze physical aspects in theory considering different factors with the aim of providing a common conclusion of OWF effect on atmosphere and ocean. The second simulation type, TOS-02, uses a more realistic approach with simulations concentrating on the OWF effect on the area of the German Bight with the final overall aim of estimating possible impacts for life in that region.
Concepts of TOS-01 and TOS-02 are opposed to each other in table 3.3-I. All simulations for each type of simulations were calculated twice considering case of non-operating wind turbines (reference run REFr) and case with operating wind turbines (OWFr). The difference between OWFr and REFr (OWFr-REFr) emphasizes the effect of the OWF on respective medium.
In the following concepts of TOS-01 and TOS-02 are documented.

3.3.1 Model Box Simulations: TOS-01

Simulations of TOS-01 answer the purpose of the analysis of OWF's effect on atmosphere and especially on ocean under various external conditions like wind speed, size of wind farm, duration of OWF operation, depth of ocean as well of computational issues regarding resolution and used forcing-origin. TOS-01 also comprises the core of this study – a physically process analysis of occurring dynamical changes in ocean due to an OWF of 12 wind turbines.

Model Area in TOS-01 (model box):
TOS-01 uses an idealized model area in the form of a box sizing 240 km by 240 km in the horizontal for both atmosphere and ocean model. The box is located in the German Bight having position of offshore wind farm *alpha ventus* in model center. Figure 3.3.1 shows location and dimension of model area. Offshore wind farm *alpha ventus* is located at 006.60º East and 54.00º North. For ocean simulation a model box (ocean box) is used while for METRAS a similar box is

used but for atmosphere (atmosphere box). Therefore model area in HAMSOM and METRAS differs only by vertical resolution.

But the position of model area on the map (figure 3.3.1) is important for HAMSOM because the ocean model uses an isogonic calculation whereas METRAS is not isogonic but uses a flat area with grid sizes in unit of kilometer. The isogenic approach allows a more precise applying of Rossby Radius due to isogenic dependence of Coriolis parameter *f*. That difference between HAMSOM and METRAS in model design later asks for interpolation and projection of METRAS data to HAMSOM grid (appendix D.1).

Topography in TOS-01 (model box):

In both cases, atmosphere modeling and ocean modeling, the topography and bathymetry, respectively, are flat to elicit the sole effect of induced changes in dynamics by OWFs.

Offshore Wind Farms in TOS-01 (model box):

For analysis different OWFs were used, which all were implemented around the center of the model area. The wind turbines are considered only in METRAS due to the wind turbine parameterization, which is documented in section 3.1.2. In the simulations of the ocean the OWFs are only implemented via meteorological forcing fields that were simulated with METRAS.

The size of the OWFs varies due to different experiments. One OWF, mostly used for analysis, consists of 12 wind turbines with an arrangement based on the German test wind park *alpha ventus*. Additional tested OWFs consist of 48, 80 and 160 turbines arranged in four or rather eight rows, see figure 3.3.2. These different OWFs are used to evaluate changes on the atmospheric wind field and ocean due to different wind park sizes. The number of turbines is based on currently available and planned OWFs in the North Sea (approved wind farm projects within North Sea listed under [*BSH*, 2013]. Each wind turbine, implemented in METRAS, has got a hub height of 80 m and a rotor diameter of 80 m. The rotator disc directly affects in the vertical heights ranging from 40 m up to 120 m. Although *alpha ventus* deals with bigger wind turbines the smaller type of turbine is chosen based on statistics of BWE depict in figure 2.1.4/5.

Model Setup in TOS-01 (model box):

The model setup of the model box differs between simulation of atmosphere and ocean. Thus model setup description is separated into METRAS and HAMSOM. The distinction is a result of an indirect coupling between atmosphere and ocean by using METRAS data as meteorological forcing for HAMSOM and the assumption of idealized model conditions.

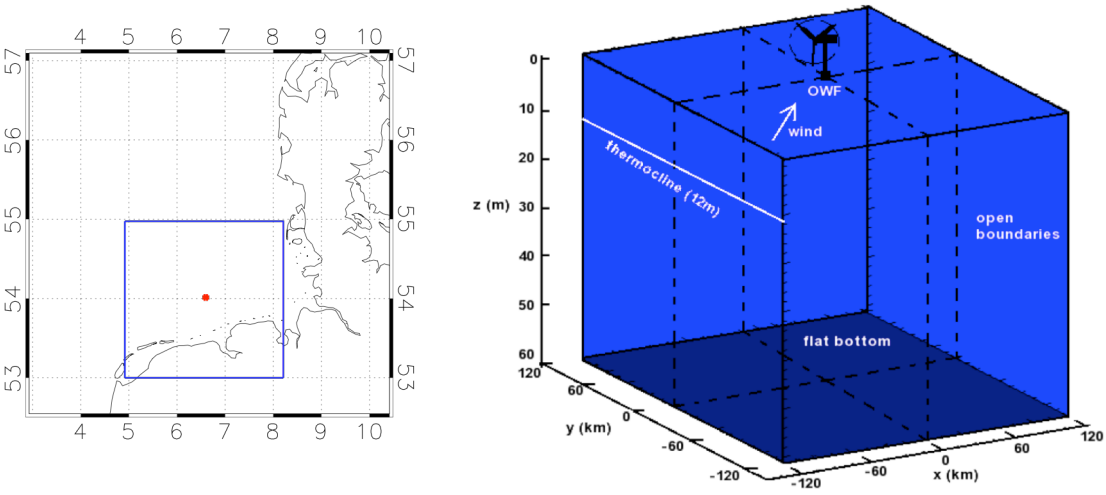

Figure 3.3.1: Geographically location of model area (left) and its arrangement as an idealized ocean box (right). The blue square within the North Sea marks model area having wind farm *alpha ventus* in the middle whose position is given by red point (left). The investigation area contains a box with a horizontal dimension of 240 km x 240 km and a maximal deepness of 60 m. Each grid box sizes 3 km in the horizontal, means a horizontal resolution of 2.5' x 1.5' in HAMSOM, and 2 m in the vertical. Topography, respectively land mass, within box is neglected, the bottom is flat and ocean boundaries are treated as open. Used OWFs are placed in the middle of the box. The atmosphere box in METRAS has the same horizontal dimension and resolution of 3 km 3 km but differs, in comparison with HAMSOM, by the vertical resolution.

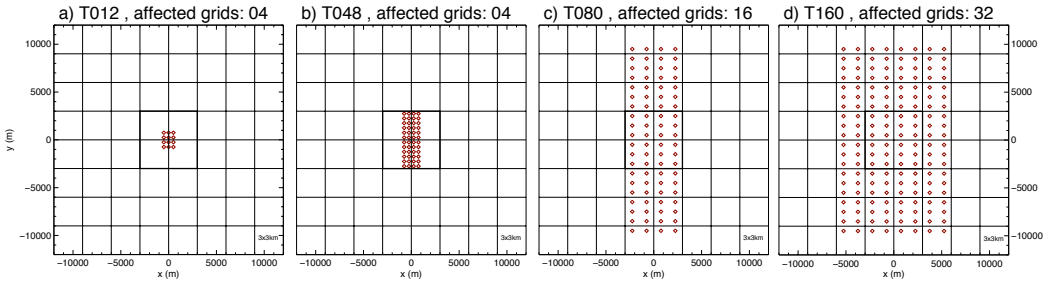

Figure 3.3.2: Arrangement of wind turbines in TOS-01. Wind turbines are placed within grid boxes of 3 km x 3 km dimension and are marked by red diamonds. a) shows arrangement of a small OWF consisting of 12 turbines like *alpha ventus*, b) consists of 48 turbines, c) of 80 turbines and d) of 160 turbines. Effect of each turbine counts ratable into corresponding grid boxes. Spaces between wind towers counts in a) and b) 500 m in x- and y direction, in c) and d) 1500 m in x-direction and 1000 m in y-direction.

METRAS (atmosphere box simulations):

As mentioned, simulations with METRAS were done in collaboration with the Meteorological Institute of the University of Hamburg supported by M.Linde (PhD candidate at MI-Hamburg since 2011). The aim of done simulations with METRAS was the creation of mainly a wind field including OWF information, which can be used as forcing for HAMSOM. Therefore simulation of METRAS differs from HAMSOM especially in time.

METRAS is used with a horizontal resolution of 3 km x 3 km. In the vertical METRAS has an equidistant resolution of 20 m below 100 m and above 100 m the vertical dimension of grid boxes is spread by a factor of 1.175. That vertical resolution is used for all simulations. The top is placed in 9521 m.

As mentioned, the model bottom is flat because of using an ocean landscape type with a constant sea surface temperature (SST) of 15 ºC, over whole simulation time. Additional prescribed variables for simulation are a relative humidity at 10 m of 70%, a one-dimensional start field which is chosen as stable dry and the geostrophic wind field is prescribed as well. The forcing of METRAS only affects directly the upper layers above 1000 m and only at the horizontal boundaries. Therefore METRAS simulates the boundary layer by itself.

The geostrophic wind ug was prescribed with a velocity of ug=8.0 m/s, respectively 5.0 m/s and 16.0 m/s for analysis of OWF's effect based on different wind speeds. The wind direction of the geostrophic wind is West and following the Ekman-Spiral; wind direction in 10 m heights is southwest.

Whole simulation time for METRAS runs counts four hours. After four hours the simulated wind wake was defined as stable in METRAS. Thus the last time step of METRAS result was used as forcing for HAMSOM.

Within atmosphere box simulations METRAS runs comprise ten specified simulations. As mentioned they differ in amount of turbines and predetermined geostrophic wind. The specification of METRAS simulations, which produce forcing for HAMSOM is listed and explained in table 3.3-II. Simulations were done with operating wind turbines (OWFr) and without an OWF (REFr).

Additional, a run including different durations of wind turbine operation was simulated; means turbines are switched off and on. Operating wind turbines means the use of METRAS wind turbines parameterization. Details of operation time are given in chapter 4.1. That simulation is used to determine the evolution of the wind wake. To analyze the alternating OWF-effect on ocean HAMSOM was forced with 10min mean wind fields and not with a constant wind field over time like in all other ocean simulations under TOS-01.

HAMSOM (ocean box simulations):

Like in METRAS, the horizontal resolution of the ocean box in HAMSOM is approximately 3 km x 3 km, more precisely 2.5' x 1.5'. In the vertical **HAMSOM** was run with two different ocean depths of 60 m and 30 m. Vertical resolution is equally spaced from ocean surface to ocean bottom by 2 m. An ocean depth of 60 m is the maximal depth of Germany's EEZ where OWFs can be built. Also 60 m is listed as a limit for OWF constructions (common statement of wind industry [*dena*, 2013]). A depth of 30 m was implemented because offshore wind farm *alpha ventus* is built in such a depth.

Time resolution counts one minute. Simulation times comprises in sum five days with the exception of one run over 30 days. Three days of each simulation are spending to spin-up the ocean and two days, respectively 28 days, to establish OWF's effect (figure 3.3.3).

The spin-up is requested to avoid wind driven waves, Langmuir circulation, strong disruption at borders and other implications initiated by a sudden strong wind forcing on a reposing ocean. During the three days the wind speed increases form 0.0 m/s to 6.0 m/s for wind component u in x-direction and from 0.0 m/s to 2.0 m/s for the wind component v in y-direction following a tangens hyperbolicus function. After three days spin-up time HAMSOM is forced by METRAS over 2 days every 10 minutes.

Boundaries of the ocean box are treated as open, which means that boundaries are defined according to the dynamical boundary equation.

Hydrographic starting conditions, of the temperature and salinity fields, are defined according to different possible North Sea's conditions. Setup for ocean simulations under ocean box simulations comprises three different stratifications of ocean, TS01, TS02 and TS03. All three start fields of temperature and salinity are depict in figure 3.3.4.

Stratification of TS01 is in accordance to the most common North Sea's conditions, which mean warmer and fresher surface layer of 15.0 ºC and 34.0 psu units and a thermocline in 12 m depths. Near bottom temperature are set to 7.0 ºC with a salinity of 35.0 psu.

The second **stratification set-up, TS02,** only consists of two layers and is used to clearly define diffusion and exchange processes at thermocline. Values for the upper layer are 12.0 ºC and a salinity of 34.0 psu, for the lower layer 7.0 ºC and salinity of 35.0. Here the thermocline is even placed in 12 m.

The **third stratification, TS03,** is based on CTD measurements around *alpha ventus* in May 2013 and is used to make the simulation comparable with measurements. In case of TS03 the upper layer has a temperature of 8.0 ºC and 30.5 psu, the lower one has 7.0 ºC and salinity of 32.8 psu. The broad thermocline is located between 5 m and 15 m.

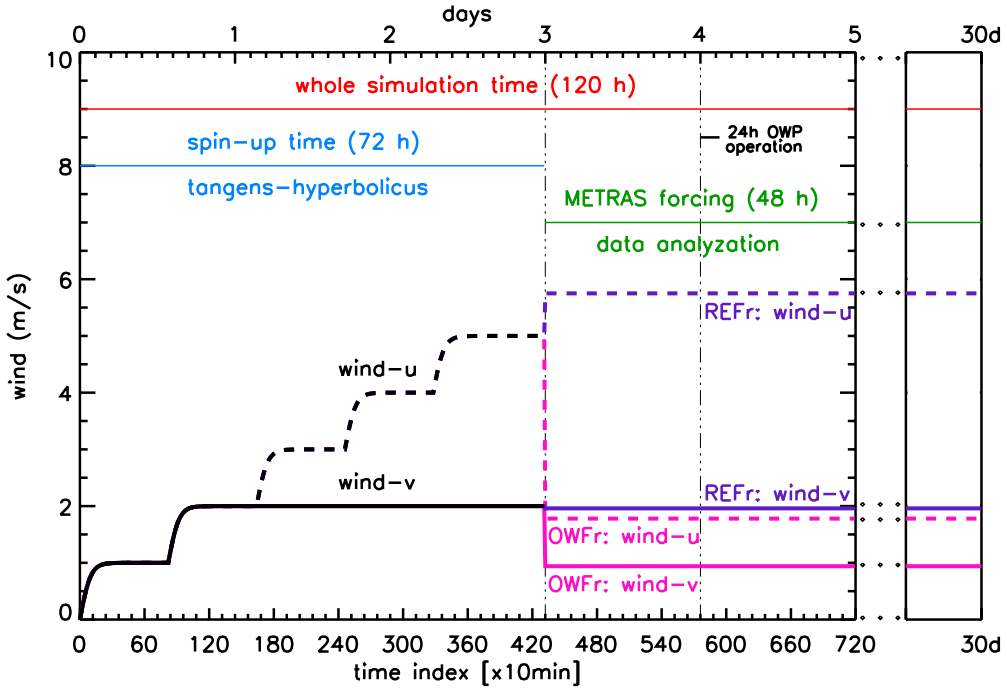

Figure 3.3.3: Time setup of simulation under ocean box. Whole simulation time spans 5, respectively 30 days. Three days of spin-up is required. During spin-up wind forcing is slowly increased to avoid unrequested dynamical effects within the ocean box. Over the last two days a constant wind field of METRAS forces the ocean box. Dashed lines shows wind speed of wind component u, solid lines of component v. Each component is separated into 'ref' (violet) and 'owf' (pink), which stands for different wind forcing fields regarding forcing without OWF signal and with OWF signal. The wind field forces the ocean every 10 minutes (time index of x-axis).

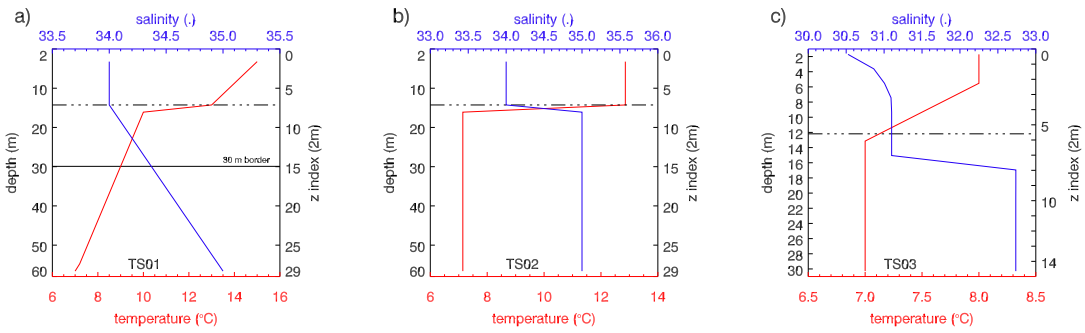

Figure 3.3.4: Setup of temperature (red) and salinity (blue) start fields for whole ocean box. a) For TS01 a linear decreasing/increasing of temperature/salinity is applied with values in accordance to North Sea conditions. b) TS02 is a simplified stratification with only two layers being separated in 12 m depths. c) TS03 is based on CTD measurements taken in May 2013 around test wind farm *alpha ventus*.

Generally HAMSOM is meteorological forced with meteorological fields of 10m-winds, surface pressure, 2m-temperature, 2m-humidity, precipitation and existence of clouds.
One aim of analysis under ocean box simulations is the determination of OWF's effect on ocean due to the knowledge that wind turbines change dominantly the wind field. Therefore in analyses mainly wind forcing and atmosphere surface pressure was used only to detect the single effect of wind change. Two different wind forcing were employed, the one simulated by METRAS including the wind farm's effect based on a disc-rotor-approach and one considering OWFs by using an approach after Broström [*Broström*, 2008] which is explained in chapter 4.1. Broström's approach was applied on METRAS 10 m reference wind field without OWF influence, which was first converted to wind stress.
Full meteorological forcing was used based on METRAS data. But due to METRAS data availability 10 m temperature and humidity fields were implemented instead of the 2 m fields. An interpolation was not reasonable (appendix D.1).
HAMSOM's ocean box is only meteorological forced by METRAS data of last time step where the atmosphere is balanced and wind wake is stable. The approach of using only one constant forcing wind field helps to define occurring processes in the ocean by OWF's wind wake. The forcing acts every ten minutes on the ocean, which is calculated for each minute. Beside last time step of METRAS 10min mean wind values are used for analyzing the effect of OWF operation.

In the end HAMSOM is not forced by the variable wind but by wind stress. Therefore wind values were transformed into wind stress by

$$\vec{\tau} = \boldsymbol{CD} * \frac{\rho_{air}}{\rho_{ref}} * |\vec{v}| * \mathbf{1}.\boldsymbol{e3} \qquad \textbf{EQ 3.3.1}$$

with CD = 0.0016, ρ_{air} = 1,25 kg/m^3, ρ_{ref} = 1026. kg/m^3 , $\vec{v} := wind\ vector$.

Wind forcing incurs into the equation of motion as wind stress acting on the sea surface but the turbulent shear stress is finally the actuating force for motion of the ocean. So the stress is a negative momentum flux into the ocean working as frictional force $\boldsymbol{\mathcal{F}}$ at the sea surface:

$$\left(\boldsymbol{\mathcal{F}}_x, \boldsymbol{\mathcal{F}}_y\right) = \left(\frac{1}{\rho_{ref}}\frac{\partial \tau_x}{\partial z}, \frac{1}{\rho_{ref}}\frac{\partial \tau_y}{\partial z}\right) \qquad \textbf{EQ 3.3.2}$$

Using those stratifications and spin-up of wind forcing the actual effect on ocean is simulated by a run using the baroclinic, prognostic mode of HAMSOM, Smagorinsky diffusion and Lax-Wendroff advection scheme. That simulation is denoted as master simulation. Beside this main setup various setups which differ a little bit from the main setup were considered. These different sensitivity runs

were created to focus on theoretical details activating the occurring circulation pattern. The aim is to understand the physical principle standing behind the occurring ocean dynamic. Especially the analysis of horizontal and vertical momentum exchanges, as well as diffusion and advection processes are important.

All these simulations are listed in table 3.3-III and runs considering OWF are shortly defined here:

- **Master Simulation *T012ug08 TS01HD60F01:*** The master simulation of TOS-01 includes forcing with wind field of 12-turbine OWF and ug=8.0 m/s, temperature and salinity start field TS01, an ocean depth of 60 m and forcing comprises only one balanced METRAS wind and pressure field, which is kept constant over ocean simulation.

- **T012ug05 TS01HD60F01:** Like master simulation but ug=5.0m/s
- **T012ug16 TS01HD60F01:** Like master simulation but ug=16.0m/s
- **T048ug08 TS01HD60F01:** Like master simulation but with OWF consisting of 48 turbines.
- **T080ug08 TS01HD60F01:** Like master simulation but with OWF consisting of 80 turbines.
- **T160ug08 TS01HD60F01:** Like master simulation but with OWF consisting of 160 turbines.

- **T012ug08 TS01HD60F02:** Like master simulation but wind forcing does not persist of one constant wind and pressure field, it includes different fields including the effect of switching on and off wind turbines.
- **T012ug08 TS01HD60F03:** Like master simulation but full meteorological METRAS forcing is used.
- **T012ug08 TS01HD60F04:** Like master simulation but forcing based on Broström approach is used.
- **T012ug08 TS01HD60F01_BTM:** Like master simulation but with manipulated HAMSOM source code to run simulation under barotropic mode.
- **T012ug08 TS02HD60F01_src*:** Like master simulation but with easier temperature and salinity stratification of only two layers (TS02) and manipulated HAMSOM source code to analyze exchange processes.

All simulations were computed twice, with a wind forcing neglecting OWFs - the reference run (REFr) and a wind forcing including the signal of operating wind turbines (OWFr).
The results of meteorological forcing are presented in chapter 4.1, results of these runs for ocean are represented in chapter 4.2, and as well the source code manipulations of HAMSOM are specified there.

3.3.2 North Sea Simulations: TOS-02

The second type of simulations, TOS-02, is used for realistic runs of the North Sea and especially over the German Bight. Simulations of the North Sea are separated into two case studies aiming to estimate possible OWF impacts on the German Bight under more realistic conditions.
Case study I analysis the OWF-effect on the German Bight under a theoretical assumptions of constant wind directions during one-day simulations.
Case study II is an adoption to a real passed meteorological situation of 16th-19th June 2010.

The analyses of the OWF impact on the German Bight consider a strong offshore wind farm demanding within the German EEZ. The here used OWF expansion for the German Bight is called '*B1-2030much*', consists of 8590 wind turbines and is explained in details in chapter 4.3.

Model Area in TOS-02:
Figure 3.3.5 clarifies three model areas for simulations of the North Sea. The green encircled area comprehends the North European Shelf (HAMSOM NES), the red encircled area defines the model area of the finally used HAMSOM North Sea (HAMSOM NS) simulation. The orange marked area shows the model area of METRAS including Germany's EEZ (light blue).

HAMSOM NES (green):
HAMSOM NES comprises ocean simulations of the North Sea and the north European shelf to provide initial data of surface elevation for ocean simulations over the smaller ocean domain HAMSOM NS. HAMSOM NES has a horizontal resolution of 20 x 20 km and in the vertical the resolution counts 5 m from 0-50 m depths, 10 m from 50 -100 meters, 20 m between 100-200 meters and 50 m from 200-700 meters. The topography of the ocean bottom is given in figure 3.3.5. The boundaries are treated as open in case of no coast. The temperature and salinity at the model boundaries are climatological data from WOA-01. HAMSOM NES is meteorological forced with Era Interim data every six hours. Time step of simulations is one minute. Simulations were done for the years 2010 and 2011.

HAMSOM NS (red):
HAMSOM NS comprises ocean simulations of the North Sea with a horizontal resolution of 3 km x 3 km. The vertical resolution is equal to the one of HAMSOM NES. As well the topography is similar but logical only spanned over the model domain of HAMSOM NS. The boundaries are treated as open in case of not any coast. The temperature and salinity at model boundaries are climatological data from WOA-01 and the initial surface elevation is based on

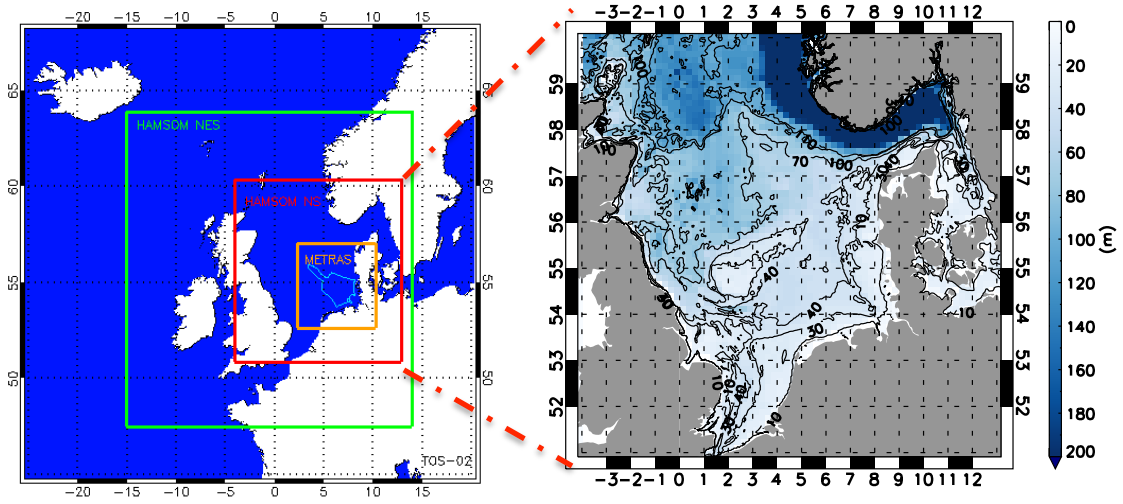

Figure 3.3.5: Left: Overview of model areas in TOS-02. Green area marks the application to the European shelf (HAMSOM NES) with WOA-01 data used at boundaries. This model provides boundary data for the North Sea model (HAMSOM NS), red area. The orange area shows the model area of the atmosphere model METRAS which fully includes the exclusive economic zone (light blue line) of Germany. Right: Bathymetry of HAMSOM model area NS in meters.

calculations by HAMSOM NES. The time step of simulations over HAMSOM NS counts one minute and provide a 10min-mean output.

Simulation time and meteorological forcing differs for simulations of case study I (analysis of OWF-effect related to wind directions) and case study II (OWF-effect under a realistic meteorological situation).

Set-up for case study I: constant wind directions

For case study I 2x8 simulations were done for 1st June 2011; eight runs with operating OWFs and eight runs without OWFs.

The forcing for HAMSOM NS is adopted every 10 minutes and comprises 10m-wind fields, surface pressure, 10m-temperature and 10m-humidity fields. The meteorological forcing consists only of METRAS data. Due to the fact that the model domain of METRAS in figure 3.3.5 (orange square) does not fit with the model domain of HAMSOM NS the METRAS forcing at orange boundary was expanded over the whole HAMSOM NS domain.

Simulations of METRAS forcing data are based on a prescribed geostrophic wind of 8 m/s, meteorological conditions of an early summer day with an initial surface pressure of 1000 hPa, 10m-temperatures of 17 ºC and 10m-humidites of 70 %. The diurnal cycle of the sun is determined by 1st June 2011. METRAS uses a constant SST of 15 ºC and a light stable and neutral moist atmosphere.

This set-up were used for runs of eight different wind directions, which were assumed as constant over the entire simulation time of one day. The constant wind directions at height of the geostrophic wind are:

- N (000º)
- NE (045º)
- E (090º)
- SE (135º)
- S (180º)
- SW (225º)
- W (270º)
- NW (315º)

Based on Ekman spiral the wind directions in 10 m heights vary slightly from the geostrophic ones. Due to this idealized setup of METRAS a combination with other (ECMWF) data was not reasonable. Disadvantages of that procedure are possibly physically abnormalities in North Sea's circulation due the forcing expansion. However such a side effect cannot be detected in the data set.

Set-up for case study II: real meteorological situation

For case study II simulations of the German Bight were done with operating OWFs and without OWFs. The simulations, presented in this thesis, were done for the time range 16th-19th June 2010. This time period is chosen based on meteorological situation and data availability for METRAS runs.

The full meteorological forcing is adopted hourly and includes forcing field of 10m-wind, surface pressure, 10m-temperature, 10m-humidity, total precipitation and cloud-presence. The forcing fields are a hybrid between METRAS data over the orange METRAS-area in figure 3.3.5 and ECMWF data for the rest of the HAMSOM NS domain. At boundaries of the orange METRAS-area (figure 3.3.5) an interpolation was necessary.

Simulations of METRAS forcing data were done for 16th-19th June 2010 as well. As mentioned, the model area of METRAS simulations does not fit with HAMSOM NS and is pictured in figure 3.3.5 by an orange square. Over ocean METRAS sea surface temperature is forced with the NOAA Optimum Interpolation Sea Surface Temperature. The meteorological forcing comprises six hourly fields of temperature, humidity and the horizontal wind from ECMWF. The pressure field is then calculated by METRAS, which simulates its own dynamic.

The meteorological forcing field for simulations under HAMSOM NS needed some preparations. METRAS forcing data over ocean were interpolated and projected to HAMSOM grid and ECMWF data were horizontally interpolated to HAMSOM grid. Also the use of a wind time step of 10 minutes and an hourly residual forcing asked for the need of time interpolation of 6-hourly ECMWF data. Although such strong timely interpolation is normally inappropriate, results show

that only the orange METRAS-area is affected by OWFs and so areas affected by ECMWF interpolation do not influence the OWF-effect analysis.

Simulations in TOS-02:

As mentioned, simulations were done for two case studies. Simulations of case study I with constant wind direction are designated with T8590ug08wd*, while * stands for the wind direction in degree of 000º, 045º, 090º, 135º, 180º, 225º, 270º and 315º.

The more realistic simulations of case study II are designated with T8590S01.

Simulations of TOS-02 are listed in table 3.3-III.

Table 3.3-I: Ocean simulation and analysis concepts at a glance.

main simulation	TOS-01: ocean box simulations	TOS-02: North Sea simulations
description	used for theoretical analysis idealized ocean-box	used for analysis of German Bight real North Sea area
resolution	3 km x 3 km x 2 m	3 km x 3 km x z, with z-indices of 05 m (000-050m), 10 m (050-100m), 20 m (100-200m), 50 m (200-700m)
topography	flat bottom with depths of **30 m and 60 m** no uplift due to bathymetry	North Sea's common topography (figure 3.3.5)
time step (dt)	1min	1min
wind time step	10 min	10 min, hourly
output	10 min mean average	10 min mean average
wind farm	one wind farm with different numbers of turbines (#**12,48,80,160**)	a couple of wind farms in the North Sea, total number of wind turbines is **8590**
wind forcing	**8 m/s** normal test run **5 m/s &16 m/s** to analyze effect of different wind speed	**8m/s** for run with constant wind direction, rest is variable and depends on meteorological forcing
meteorological forcing	Forcing variables (METRAS): • 2 m/10 m-temperature • 2 m/10 m-humidity • precipitation • cloudiness • wind stress • wind speed • surface pressure ➢ mostly only wind (wind stress) and pressure forcing ➢ one simulation with full meteorological forcing including	Forcing variables (METRAS & ECMWF): • 2 m/10 m-temperature • 2 m/10 m-humidity • precipitation • cloudiness • wind stress • wind speed • surface pressure ➢ full meteorological forcing ➢ wind and pressure forcing only
boundaries	open boundaries	open boundaries

Table 3.3-II: Overview of METRAS simulation. Main setup of METRAS under TOS-01 and TOS-02, see text. T000 designates no wind farm and numbers greater than 0 behind T gives number of wind turbines in the simulation.

Type of Simulation	Name	Abbreviation	Description
TOS-01 (BOX MODEL)	M_T000ug05 M_T012ug05	**UG5**	REFr without wind turbines and ug=5m/s OWFr with 12 turbine OWF and ug=5m/s
	M_T012ug08 M_T000ug08	**UG8 / T012**	REFr without wind turbines and ug=8m/s OWFr with 12 turbine OWF and ug=8m/s
	M_T012ug16 M_T000ug16	**UG16**	REFr without wind turbines and ug=16m/s OWFr with 12 turbine OWF and ug=16m/s
	M_T048ug08	**T048**	OWFr with 48 turbine OWF and ug=8m/s
	M_T080ug08	**T080**	OWFr with 80 turbine OWF and ug=8m/s
	M_T160ug08	**T160**	OWFr with 160 turbine OWF and ug=8m/s
	M_T012ug08*onoff	**-**	OWFr with 12 turbine OWF and ug=8m/s and changing OWF operation
TOS-02 (NORTH SEA)	M_T8590ug08**wd000** M_T0000ug08**wd000**	**N**	constant wind direction N
	M_T8590ug08**wd045** M_T0000ug08**wd045**	**NE**	constant wind direction NE
	M_T8590ug08**wd090** M_T0000ug08**wd090**	**E**	constant wind direction E
	M_T8590ug08**wd135** M_T0000ug08**wd135**	**SE**	constant wind direction SE
	M_T8590ug08**wd180** M_T0000ug08**wd180**	**S**	constant wind direction S
	M_T8590ug08**wd225** M_T0000ug08**wd225**	**SW**	constant wind direction SW
	M_T8590ug08**wd270** M_T0000ug08**wd270**	**W**	constant wind direction W
	M_T8590ug08**wd315** M_T0000ug08**wd315**	**NW**	constant wind direction NW
	M_T8590**S01** M_T0000**S01**	**-**	meteorological situation of 16^{th}-19^{th} June 2010

Table 3.3-III: Overview of HAMSOM simulations meteorological forced with METRAS for TOS-01 and TOS-02. Main adjustments are based on number of wind turbines, meteorological forcing and start fields. Each listed simulation here has got its pondo of simulation without wind turbines.

Overview Simulations:	**Abbreviation** **T:** # turbine **ug:** geostrophic wind [m/s] **TS:** 01-common start field, 02-two-layer start field 03-WEGA start field **HD:** HAMSOM ocean depth [m] **F:** METRAS forcing 01-only wind 02-full meteorological forcing 03-on/off forcing 04-Broström run **BTM** barotropic mode **src*** source code manipulation **wd:** wind direction [°] **S01:** summer season	**description, explanation, characteristics, usage**	**Placed in document at page:**
TOS-01	**T012ug08 TS01HD60F01**	Master Simulation	62 et sqq.
	T012**ug05** TS01HD60F01	wind speed analysis	102 et sqq.
	T012**ug16** TS01HD60F01	wind speed analysis	102 et sqq.
	T048ug08 TS01HD60F01	wind farm analysis	109 et sqq.
	T080ug08 TS01HD60F01	wind farm analysis	109 et sqq.
	T160ug08 TS01HD60F01	wind farm analysis	109 et sqq.
	T012ug08 TS01HD60**F02**	consistency analysis	96 et sqq.
	T012ug08 TS01HD60**F03**	effect of met. forcing	120 et sqq.
	T012ug08 TS01HD60**F04**	Broström approach	115 et sqq.
	T012ug08 TS01**HD30**F01	intensity in depth	126 et sqq.
	T012ug08 **TS03HD30**F01	WEGA adaption	131 et sqq.
TOS-01-src	T012ug08 TS01HD60F01**_BTM** T012ug08 **TS02**HD60F01**_src***	physical analysis, different assumptions in source code	74 et sqq.
TOS-02	T8590ug08**wd000**	effect by const. N wind	148 et sqq.
	T8590ug08**wd045**	effect by const. NE wind	148 et sqq.
	T8590ug08**wd090**	effect by const. E wind	148 et sqq.
	T8590ug08**wd135**	effect by const. SE wind	148 et sqq.
	T8590ug08**wd180**	effect by const. S wind	148 et sqq.
	T8590ug08**wd225**	effect by const. SW wind	148 et sqq.
	T8590ug08**wd270**	effect by const. W wind	148 et sqq.
	T8590ug08**wd315**	effect by const. NW wind	148 et sqq.
	T8590**S01**	effect based on real meteorological situation, June 2010	158 et sqq.

4 ANALYSIS

The analysis of OWF's influence on atmosphere and ocean is separated into three parts. Two parts studies the effect of offshore wind farms on the atmosphere (4.1) and on the ocean (4.2) in theory by simulation type TOS-01 based on an idealized model area – the ocean box. Part three (4.3) gives insight into the future of the German Bight regarding plans of wind farm development in 2030.
Before running the ocean model it was necessary to find usable atmospheric forcing data especially wind data considering wind turbines. Here different appendages were chosen.

4.1 Analysis 01: Effect on Atmosphere

As mentioned before wind turbines are used to transform wind energy into electrical energy. The main consequence of this transformation is a reduction of wind speed in the wind field behind wind turbines. This reduction of wind speed is called wake effect. The wake effect is the main component of this study, which drives and controls all following introduced processes and phenomena in ocean. Hence this subchapter analyzes the wake effect with its incidents and conditions. The results are exemplifies in observed and modeled wake effects.

4.1.1 Observed Effects

In the field of observed OWF effects on atmosphere exist a handful of paper in literature. A pioneer position in that field has M. Christiansen. She analyzes wind changes around OWFs using satellite data based on radar methods. An important example is Horns Rev, a Danish wind farm consisting of 80 wind turbines. Figure 4.1.1 depicts examples of studies based on observations around Horns Rev. Hasager et al. [2013] analyzed the occurrence of fog in the wake vortex behind turbines. The fog formation behind turbines uncovers the wind wake of each turbine. Hasager studied the appearance of fog, which appears due to advection of cold humid air over much warmer water surface, the possibility of upward mixing of saturated air from the surface into the cooler layer exist and that can cause super-saturated mixture to develop and condense as fog or sea smoke. In contrast, cold-water advection fog occurs when warm moist air flows across colder water and the dew-point temperature is reached such that fog forms [*Hasager et al.*, 2013]. Such impact of OWF can play an important role for local climates regarding moisture/cloudiness and temperature.

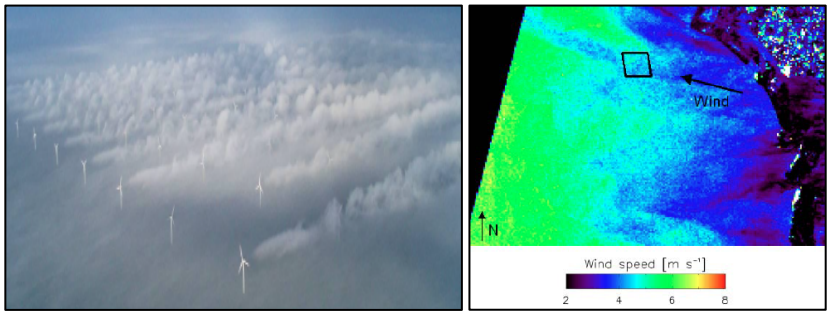

Figure 4.1.1: Wind turbine induced wind wake. Left an photo example of OWF Horns Rev taken from "The Horns Rev photo case" by [*Hasager et al.*, 2013]. Right wind speeds based on ERS-2 SAR around Horns Rev (black square of 5x5km) clarifying wind reduction behind OWF taken from Christiansen [*Christiansen*, 2006].

Christiansen identified the wind wake in evaluated radar images. Figure 4.1.1 illustrates the reduction of wind speed downstream of the wind farm [*Christiansen*, 2006]. While in the surrounding of Horns Rev the wind increases behind coastal area with strong shadowing effect of land, behind the wind farm a long plume of reduced wind speed was detected - the wind wake of the whole wind farm of more than 15 km lengths.

At this juncture it becomes obvious that OWF effects on the wind field are not only a locally phenomenon but impacts an area being much bigger than OWF itself and have to be considered in models.

4.1.2 Modeled Effects

Modeling wind wake of wind turbines is a necessary tool for wind farm planning because wind farm layout depends on the main wind direction and of the size of used rotor. To avoid turbulence from one turbine affecting another wind turbine, wind farms are designated with a minimum distance between individual turbines of around 7 rotor diameters [*Jimenez et al.*, 2007; *Meyers and Meneveau*, 2012] in main wind direction. Wake modeling with high resolution models like Large Eddy Simulations (LES) or Detached Eddy Simulation (DES) is widely in use. LES studies about wind farm wake are done by Jimenez et al. [2007; 2008], Porte-Agel and Wu et al. [2010], *Porté-Agel et al.* [2011], and Hasager et al. [2013], just to name a handful researches. Hasager, for example, did simulation with DES [*Hasager et al.*, 2013]. Such simulations provide a complex view of turbulences behind one ore more turbines. Those details cannot be dissolved with mesoscale models like METRAS. However there exist a trend of implementing wind turbines into mesoscale models to evaluate OWF impact on the climate. The usage of mesoscale models with wind turbine implementation provides the advantage to analyze their impact on weather and climate but one has to deal with disadvantages regarding horizontal resolution.

The impact on the mesoscale are based on a theoretical approach after Broström [2008] and simulated results of the mesoscale model METRAS. Both approaches are adopted to HAMSOM later.

4.1.2.1 Mesoscale 01: Broström

Broström [2008] used a theoretical approach to analyze the influence of large wind farms on the upper ocean circulation by changing wind stress. After Broström a wind stress in x-direction has the strongest disturbance in the y-direction and so he defined the wind stress in two forms. The first is an assumption of a wind stress that is homogenous in the x-direction (EQ 4.2) and the second is a more realistic one (EQ 4.1) with a two-dimensional wind pattern [*Broström*, 2008]. This leads to following formulation of wind stress:

$$\boldsymbol{\tau_x = \tau_{x0} - \Delta\tau_x e^{-\left(\frac{2y}{L}\right)^2}} \qquad \textbf{(EQ 4.1)}$$

$$\boldsymbol{\tau_x = \tau_{x0} - \Delta\tau_x e^{-\left(\frac{2y}{0.8L+0.2x}\right)^2} max\left(e^{-\left(\frac{1-x}{L}\right)}\frac{x}{L}, 0\right)} \qquad \textbf{(EQ 4.2)}$$

with

$$\tau_{x0} := windstress\ outside\ the\ influence\ of\ wind\ farm$$
$$\Delta\tau_x := change\ in\ the\ wind\ stress\ induced\ by\ wind\ farm$$
$$L := characteristic\ size\ of\ wind\ farm$$

Advantage of this description is a cushy application. Here a wind stress field with a mean wind stress of 0.012 N/m^2, which is based on reference wind speed of METRAS wind field simulation without wind farm operation and geostrophic wind speed of ug=8 m/s, is supposed. Investigation area is based on simulation TOS-01 of 240 x 240 km with a wind farm of characteristic size of L=6km in the middle of this area. The changes of such wind stress field due to a wind farm are shown in figure 4.1.2 for two different wind directions, westerly and southwesterly. A westerly flow is even used by Broström while here a southwesterly wind direction is added due to its frequent incidence in the German part of the North Sea [*Loewe*, 2009]. The reduction of wind stress by wind farm impact after Broström has an elliptical form with a maximum at wind farm's end of 0.0054 N/m^2 deficit followed by slightly wind stress increase in flow direction. Minimal values are 0.0064 N/m^2 for westerly flow and 0.0068 N/m^2 for southwesterly flow. Transverse to flow direction the wind farm changes the wind pattern in a symmetric way with the strongest deficit within OWF. The form of the wake is nearly independent of flow direction. Faint aberrations are attributed to the grid and so in flow direction into the front side of wind farm boxes

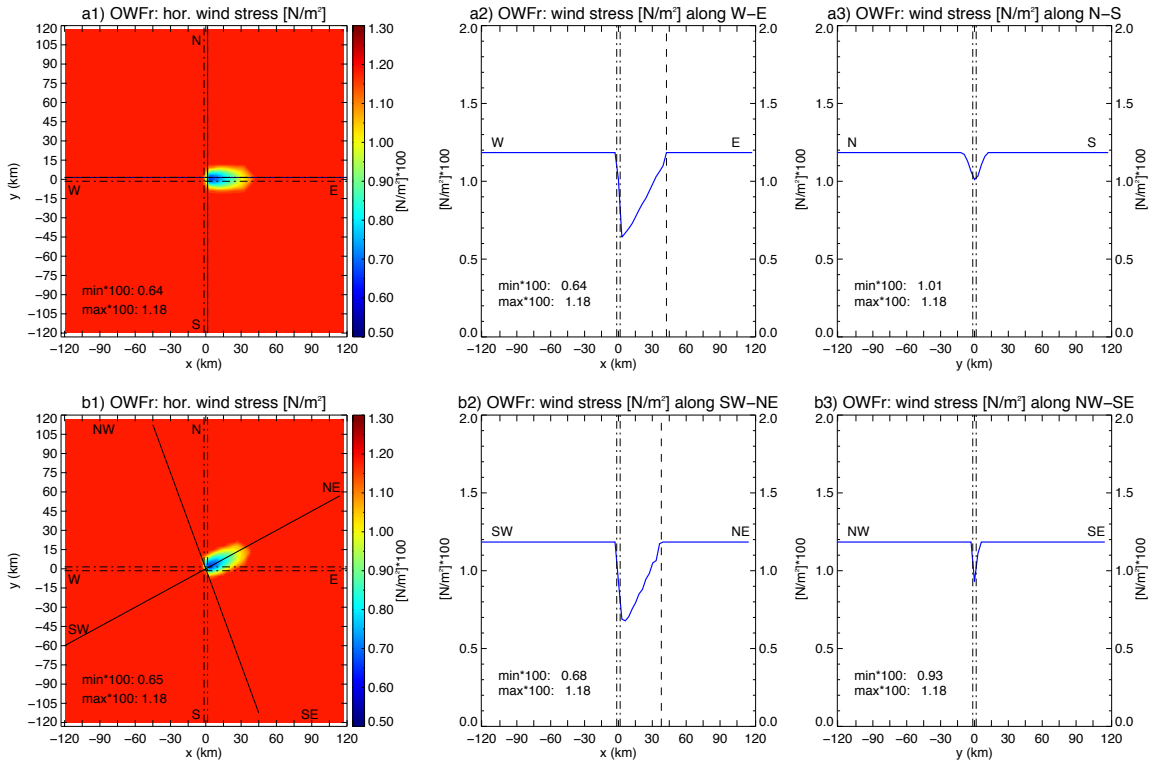

Figure 4.1.2: Adopted Broström wind stress formulation on a reference wind stress field of 0.012 N/m² mean for two different wind stress direction and a characteristic wind farm length L of L=6km. a1-a3) shows result for westerly direction of 270°. b1-b3) shows results for southwesterly direction of 240°. a1/b1) gives the horizontal wind stress field. OWF is placed in the middle, encased by dashed dotted lines, around P(0,0). Horizontal resolution is 3 km x 3 km. Solid lines mark the cross-sections W-E, N-S / SW-NE, NW-SE through the OWF. a2/b2) represents wind stress along the cross section W-E/SE-NE and a3/b3) along cross-section N-S/NW-SE. Dashed dotted lines in the cross-sections plots marks OWF position, the dashed line in a2,b2) clarify the wake dimension in wind direction. The wind stress along cross-sections points up the wake behind and within the wind farm.

Table 4.1-I: Key notes of Broström adoption.

Broström (6x6km² OWF , based on 10 m mean wind by ug=8m/s)	**MAX**		**MIN**	
wind direction	**W**	**SW**	**W**	**SW**
inflow of wind farm	➔■	↗■	➔■	↗■
difference OWFr-REFr [%]	no increase	no increase	-45.88	-44.92
x=const: [N/m²]*100	1.18	1.18	0.64	0.67
y=const: [N/m²]*100	1.18	1.18	1.01	0.93
wake x-dimension [km]	42 (W-E)		38 (SW-NE)	
wake y-dimension [km]	24 (N-S)		18 (NW-SE)	

and into the corner, see illustration at Table 4.1.2-I under line 'inflow of wind farm'. In sum the wake shows a maximal reduction of 45 to 46 % with x-dimension of 39 to 42 km and y-dimension of 18 to 24 km. Here x-dimension means the spread in flow direction and y-dimension orthogonal to flow direction. The impact of the relative small wind farm of an area of 36 km^2 extends to an area of 702 to 1008 km^2, so influences a field, which is 20 to 28 times bigger than OWF it selves. For comparison, the city Hamburg sizes around 755.3 km^2 [*Haffmans*, 2005].

Broström's equations for wind stress changes give an estimation how strong the impact of a wind farm can be. It is a quick test but a pure manipulation of wind stress, not based on physical principles and owing to these limitations this method does not provide an optimal description of wind farm wakes. Considering this method only the impact of the wind field or, more explicitly, of the wind stress field in one special height can be describe. The method cannot be easily adapted to other atmospheric parameters like temperature, humidity and additional forcing fields normally needed for ocean simulations. Even characterized details of wind turbines are ignored, like rotor diameter or turbine power. As well it will be problematic to adopt this approach to non-quadratic wind farm adjustments.

To account for such limitations and to describe such wakes more precise the wind wake is simulated using the mesoscale atmosphere model METRAS.

4.1.2.2 Mesoscale 02: METRAS

This section deals with results of METRAS simulations of TOS-01 (atmosphere box) used for the theoretical analysis. Meteorological forcing for more realistic atmospheric situations, as North Sea simulations, is explained in section 4.3.

METRAS advantage compared to, previously treated, Broström method is its physically based model frame and the employed wind farm parameterization, specified in chapter 3.1.2. The wake is not estimated by an empirical formula but numerical solved. Therefore METRAS' forcing is supposed as the better alternative for simulations of the ocean later due to an expected more realistic wake illustration. On the one hand the commonly used actuator disc approach allows a better definition of the form of the wake as well of its strength and dimension and on the other hand specific details of wind turbines can be considered. Further this way of wind forcing production provides data in the vertical and of all atmospheric parameter as well.

At first OWF's effect on the atmosphere as simulated in METRAS is analyzed followed by an analysis on different wind speeds and wind farms, to estimate the wind wake based on different conditions and by analysis of OWF operation. In the following changes between run with wind turbines (OWFr) and the reference run without wind turbines (REFr) after four hours simulation are considered.

4.1.2.2.1 Analysis of OWF's effect on atmosphere in METRAS

In general atmospheric changes in METRAS are based on a 12-turbine wind farm and geostrophic wind with ug=8m/s (run M_T012ug08 in table 3.3-II). Results for meteorological parameter pressure, wind, temperature and humidity are illustrated in figure 4.1.3.

The main difference in the **wind field** compared to Broström is the form of the wind wake. The change of the wind field can be separated into three areas, a surge zone with weak decreased wind speed in front of the wind farm, the wind wake, a plume of reduced wind speed behind the wind farm and two flanks of increased wind speeds flanking the wind wake. Here the simulated wind wake is more than 120 km long with a width of 30 km and a maximum decrease of 4.42 m/s conforming to a decline of 71.65 %.

In the vertical, the zone being directly affected by the rotor is from 40 m to 120 m. But the wind reduction occurs from ground up to 250 m. In front of the wind farm exists a downwind area reaching into 1100 m heights. Behind the wind farm, above 250 m, wind speeds are increased by maximal 0.62 m/s.

Differences in the horizontal fields in 10 m heights of **pressure, temperature and relative humidity** are poor but show similar formations (figure 4.1.3).

The wind farm district, in the middle of the model area, is in 10 m heights 0.02 ºC warmer and 0.2 % fewer moistly due to operating wind turbines and the pressure is in the OWFr reduced by 1.5 Pa. Outside of the OWF district occurs a circle with plume having opposite changes. There the pressure is maximal 11.33 Pa higher in the run OWFr, temperatures are 0.04 ºC lower and about 0.4 % moister. Within the wind wake district, 15 km northeasterly of the OWF area, temperature increases, while moisture and pressure decreases. Near ground the wind farm leads to very weak changes in temperature and humidity while the pressure field changes at surface at about ±1 Pa. Strongest effects in wind direction of temperature occur around 230 m with a reduction of 0.61 ºC and the positive extreme of 0.22 ºC is located around 130 m. The extreme values for changes in relative humidity are an increase of 7.66 % in 230 m and a decrease of 2.72 % in 130 m. The change of temperature and humidity is linked to up- and downwind in the vertical.

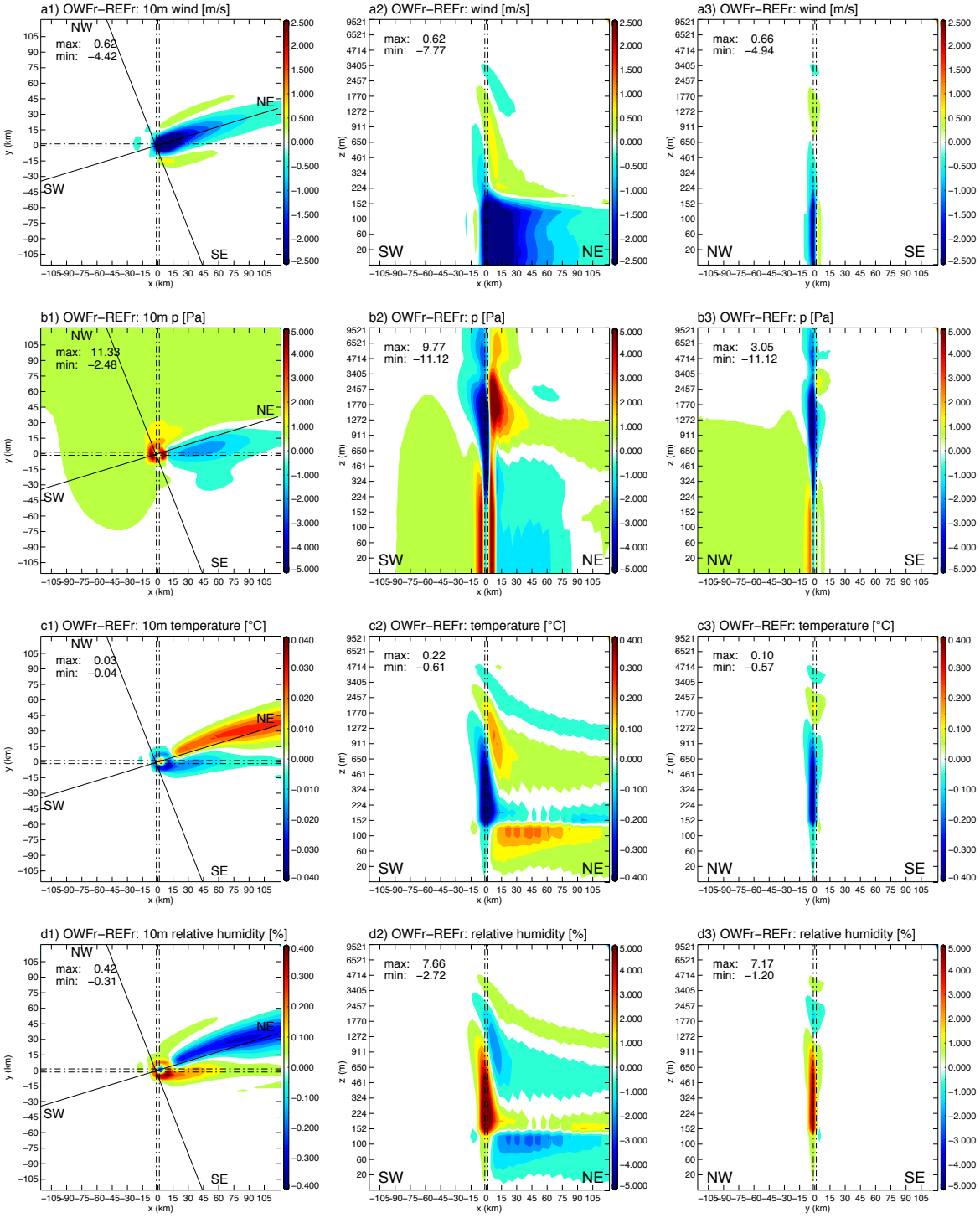

Figure 4.1.3: Changes of meteorological parameter due to an OWF of 12 wind turbines based on a simulation set up of dry and stable atmosphere and a geostrophic wind of 8 m/s after four hours of METRAS simulation. From top to bottom the meteorological parameter are: a1-a3) wind speed (m/s), b1-b3) pressure (Pa), c1-c3) temperature (°C), d1-d3) relative humidity (%). Figures a1-d1) shows horizontal fields in 10 m heights, a2-d2) shows results along SW-NE cross-section through OWF and a3-d3) along the cross-section NW-SE. Dashed-dotted black lines crosses position of the OWF around P(0,0) in the middle of model area. Solid lines in a1-d1) mark cross-sections SW-NE and NW-SE through OWF. The hub height of wind turbines is 80 m, the rotor diameter is 80 m as well.

The warming of lower layers within the OWF and downstream of wind farm is connected with stability conditions and transport of potential temperature θ. In case of stable conditions, like here ($\partial\theta/\partial z \gg 0$), the vertical mixing due to OWF bring warm air down and cold air up, leading to a cooling above hub height, respectively at rotator disc, and a warming below. In case of unstable conditions ($\partial\theta/\partial z \ll 0$) induced turbulence would cause a mixing of cold air downward and warm air upward, producing a cooler surface. The similar process occurs for humidity. Dryer air is mixed down and moist air up, resulting to a frying below hub height and a moistening aloft. In this connection an OWF also triggers surface fluxes. The ocean surface is colder than the above air, leading to a negative ocean-atmosphere thermal gradient, which again means a negative sensible heat flux. An increase of potential temperature due to OWF ends in a more negative sensible heat flux and so more sensible heat is transferred from atmosphere to ground. The drying causes a positive ocean-atmosphere moisture gradient, which positive affects evapotranspiration. That context is also proved in Roy [*Baidya Roy*, 2004].

The combination of changes in pressure and temperature over ocean can favor cloud and fog formation. Here any clouds and precipitation occur perhaps due to stable atmospheric conditions although having moist conditions with 68% relative humidity.

In sum the most important meteorological forcing parameters are the wind speed and pressure, whose drive the upper ocean. Therefore following analysis is concentrated only on changes in the wind field.

4.1.2.2.2 Analysis of different wind speeds

A wind turbine must comply with several safety requirements defined by the international electronic commission (IEC). The IEC Technical Committee 88 prepares standards dealing with safety for wind turbine generator systems and produces standards for design and technical requirements. Hence IEC defined four different turbine classes, which are determined by three parameters, the average wind speed at hub height, extreme 50-year gust and turbulence [*IEC*, 2005]. These parameters, in dependence of location will define the type of wind turbine generator (WTG) in connection with the size of wind turbine. Therefore WTGs and rotors only operate in a limited range of wind speed in dependence of turbine class. Thus a wind wake will be only produced in a certain wind speed range. And the wind speed is taken into account regarding power by the cube. Thereby stronger wind speeds results in higher power and a major energy transformation, which again results in a different strength of wind wakes behind wind farms.

To estimate the effect of wind speeds on the wind wake three wind cases are analyzed. The simulation of these three wind cases differs by the input of geostrophic wind ug, which was set to

ug=5m/s (run **UG5**), ug=8m/s (run **UG8**) and ug=16m/s (run **UG16**) (table 3.3-II). The wind farm consists again of 12 turbines being arranged over 4 grid boxes.

These results are illustrated in figure 4.1.4. The percentage changes of the horizontal wind field clearly show for all three wind-speed cases the three zones of surge, wind wake and flanked flanks. The wind-wakes are larger than 120 km and exceed the model area. But the intensity of the wake is stronger with increasing wind speed.
Extreme values of minima occur within the wind farm. As stronger the prescribed wind field as stronger is the wake. The run of UG5 shows a reduction of 64 %, UG8 72 % and UG16 77% compared to reference run without OWF impact (figure 4.1.4 a1-a3). The impact of the wind speed, respectively wind stress, on the OWF-wake is nearly linear. Figure 4.1.5 pictures that relation between prescribed geostrophic wind ug and the wake given by wind stress in N/m^2. But due to the small data set a linear dependence cannot be generalized. Further simulations with wind speeds between ug=8m/s and ug=16m/s would be necessary for an approved statement.
In case of UG16 the wake is less influenced by geostrophic force compared to the other two wind speed cases, whose wakes are deflected more to the West, due to the stronger mean wind field (figure 4.1.4 a1-a3).

The OWF induced increase at wake's flanks does not follow the positive linkage. Here the lowest increase of 9.01% is given for UG8, the strongest with 9.77% for UG5, which is close to the case UG16 showing a wind speed rise of 9.65%; see also table 4.1.2-II.
Due to these flanks the change in wind speed along the cross-section NW-SE is not symmetric, as it is in case of Broström method. Thus, the wake-flanks do not only vary in intensity, their dimension even differs. While the area of wind reduction downstream the wind farm is quite constant in all three wind-speed cases, the wake-flanks becoming shorter and thinner with increasing wind speed. A reason for this is that in case of higher wind speeds occurring gradients are better balanced, which limits a strengthening of gradients. Therefor it can be said the affected area by OWFs decreases with wind speeds related to the area of the wake-flanks.
Apart from that a comparison of the three wind-speed cases results in a small difference by maximal 10.0 % over the wind wake area and around 0.7 % over the wake-flank zone. However absolute differences results in greater discrepancies. How sensible the ocean reacts to these changes can be seen in chapter 4.2.3.2.

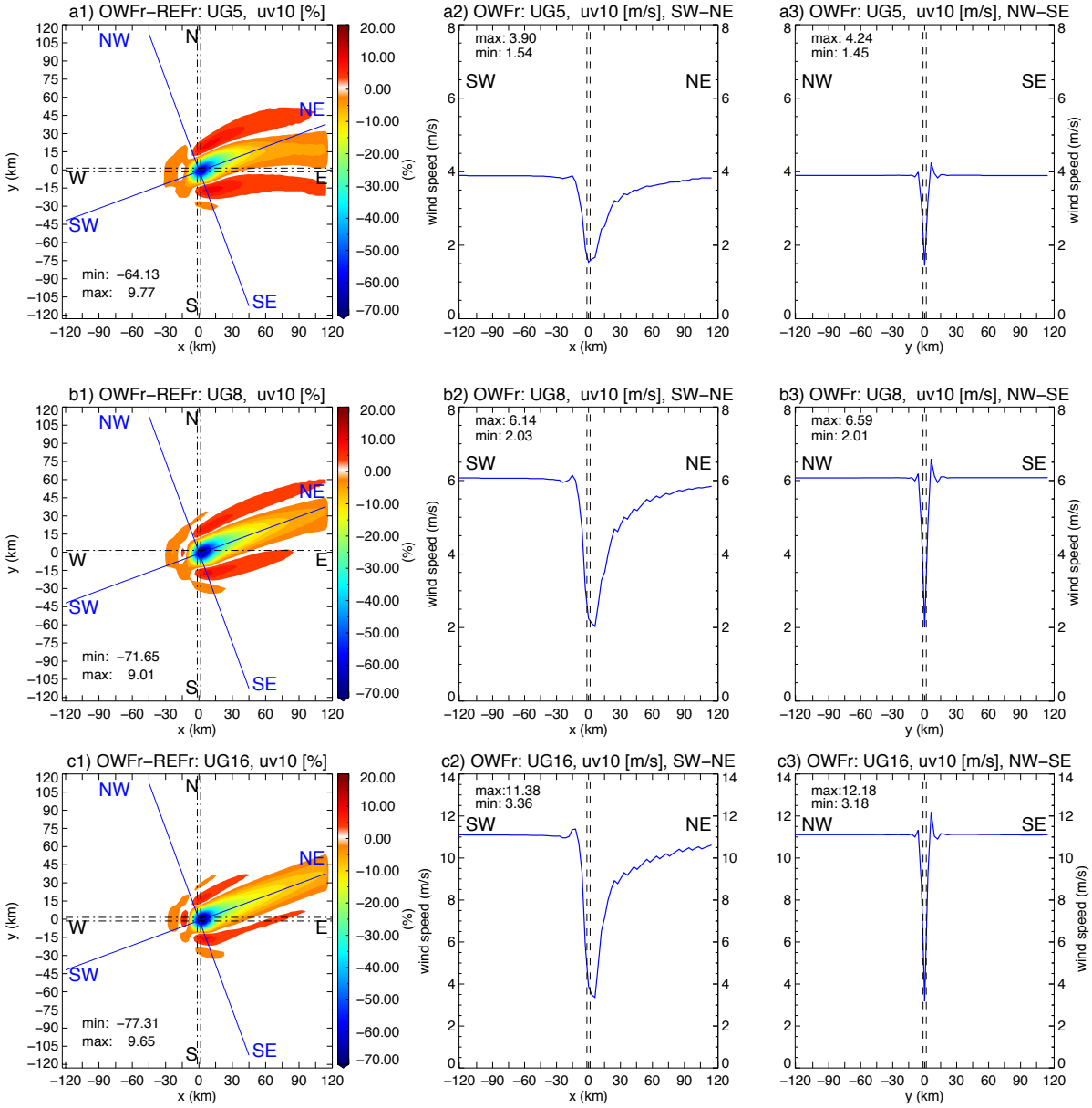

Figure 4.1.4: OWF-effect on wind field due to different prescribed wind speeds. a1-c1) Percentage change of 10m wind field due to 12-wind-turbine OWF. Wind wake reduction a2-c2) in (SW to NE) and a3-c3) orthogonal (NW to SE) to wind direction in case of three different ground wind speeds is presented after 4 hours METRAS simulation; values given in m/s. From top to bottom: Results based on the different prescribed wind fields of ug=5m/s (a1-a3), ug=8m/s (b1-b3) and ug=16m/s (c1-c3).

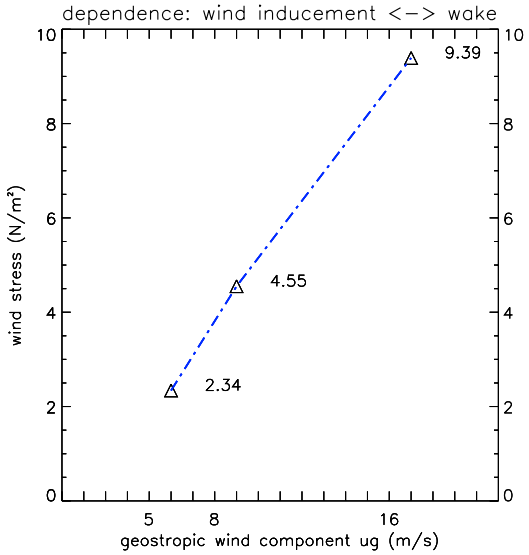

Figure 4.1.5: Dependence of prescribed geostrophic flow (ug in m/s) on wake magnitude (given in N/m² as wind stress being used as forcing for ocean simulations with HAMSOM) after 4 hours METRAS simulation. The relation is nearly linear but due to only three points not to be generalized.

On the basis of cross-sections it is clearly seen that the magnitude of wake depends on the wind speed, figure 4.1.4 b1-b3 and c1-c3). Another occurrence is the weaker the wind the stronger the wind speed within wake plume from NW to SE converges to zero and the wider the wake development from SW to NE is. That means along the section SE-NE until western model edge UG5 has a wake of 135 km, UG8 of 127 km and UG16 of 125 km.

Beside wind speeds also OWF conditions like amount of wind turbines and occupied area can influence the magnitude of the OWF induced wind wake.

4.1.2.2.3 Analysis of different wind farms

Considering political aims, OWFs will be much greater than the here used arrangement of twelve turbines within four grid boxes. This section shows how the wind wake will change due to different amount of wind turbines, including 12 (**T012**), 48 (**T048**), 80 (**T080**) and 160 (**T160**) wind turbines (table 3.3-II).

As mentioned, the wind farm constructions follow the rules of energy production. Due to the fact that each wind turbine produces a wake behind itself, there minimum recommended distances exist between them. Therefore, to be realistic, it is unfeasible to analyze different amount of wind turbines within the four grid cells used before because an amount of 160 turbines cannot be placed

in four grid boxes. That complicates a comparison of OWF-wakes related to wind turbines. Nevertheless keeping a quadratic form close to the middle of model area elects the arrangement. Arrangement of wind turbines over model area is shown in figure 4.1.6 a1-a4). The prescribed geostrophic wind is ug=8m/s for all four wind turbine cases.

The 10 m horizontal wind fields for T012, T048, T080 and T160 are pictured in figure 4.1.6. Independent of the wind-turbine-amount the wind-change formation with the three parts of surge zone, flanks and wake occur. Logically linked to the occupied area by wind turbines, the dimension of the wind wakes varies. Though the range of changes in wind speed are close with a maximal reduction of 80 % for T160, 72% for T012 and T048 and 68% for T080, see Table 4.1.2-II. Spanning the wind turbines over more grid boxes intensifies the wake in magnitude and dimension. Here the wind turbines are distributed along y-direction, almost across wind direction, which defines the wake area.

Comparing OWFs of T012 and T048 they do not show obvious differences (figure 4.1.6) and these points up to the fact that the distribution of wind turbines plays here a more important factor than the amount of turbines. A four times stronger wind farm, related to wind turbines, does not lead to a stronger wind wake. Here the minima are the same (1.72 m/s) and the maxima slightly differ by only 0.02 m/s.

Figure 4.1.7 shows the relation between amount of wind turbines, respectively OWF grid cells, and wind speed based on overall extrema in 10 m heights. T012 and T048 have greater maxima compared to T160 and T080. T080 has a character of an outlayer. The wake in T080 is with 1.93 m/s the strongest and the maximal wind speed of 6.24 m/s is the lowest. In this connection the area in front of the wind farm T080 (between x=-120 km and x=-30km) tends to the smallest mean wind speed of 5.76 m/s compared to T012, T048 and T160. In the case of T160 the mean wind speed in front of the OWF is 5.94 m/s and even smaller as in the case of T012 and T048 but the effect is not as strong as in the case of T080. On the one hand such discrepancies between T080 and T160 lie in a weaker change in the pressure field around OWF for T080. On the other hand the mean wind speed and the wake magnitude is obviously concentrated on the OWF-district and in the case of an OWF over more grid cells, means in the case of a greater OWF, a better model accuracy is provided.

These sensitivity simulations show how difficult a non-modeled parameterization for wind farms is, especially for wake-flanks. There is not a clear linearity between affected grid cells and wind change but the analysis of only three cases does not allow a final statement, for that more cases would be necessary.

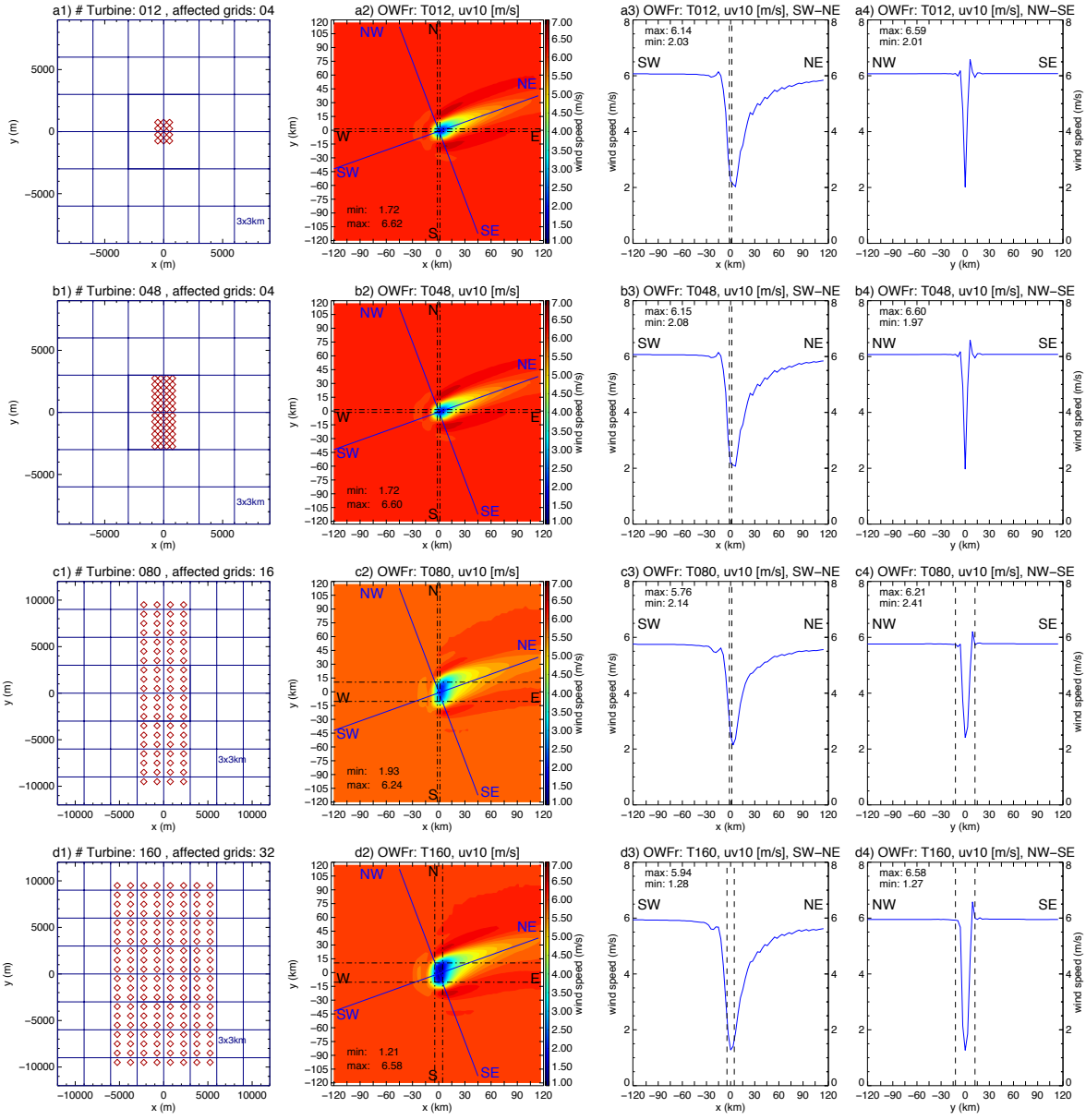

Figure 4.1.6: OWF-effect on the wind field due to different OWF-districts and number of wind turbines. a) Arrangement of wind turbines around center of model area; consider a zooming into model area and distances are given in m. Red little diamonds mark the position of wind turbines for a1) 12 turbines, a2) 48, a3) 80 and a4) 160 turbines. b) 10m horizontal real wind speed field of run OWFr after 4 hours of METRAS simulation. Horizontal black dashed-dotted lines encase OWF district around model center. Black solid lines from SW to NE and NW to SE marks cross sections in and orthogonal to wind direction. c) Shows the 10m-wind speed of OWFr along cross section SW-NE (a3-d3) and along NW-SE (a4-d4).

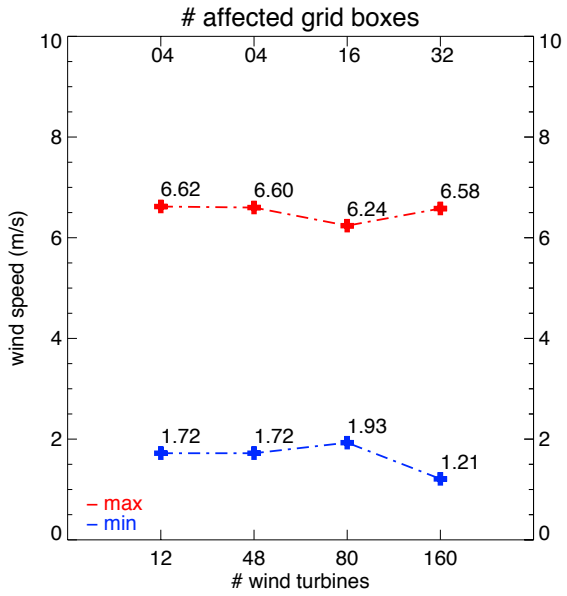

Figure 4.1.7: Dependence of number (#) of wind turbines, respectively grid boxes, on overall wind speed maximum and minimum of 10 m wind field after 4 hours METRAS simulation time. Outliner occurs with 16 affected grid boxes.

But an issue of scale becomes apparent. Because, as explained, the wind farm including 12 turbines results to nearly the similar outcome like a wind farm of 48 wind turbines. Only on the basis of wind speed respectively wind stress one can recognize a difference with a slightly expected stronger minimum in case of 48 turbines. This is explainable by the grid boxes covering the wind turbines. That side effect of modeling hampers a detailed statement of wind farm effects on the wind field. Hence it is not exact to speak here of wind farms of 12, 48 or more wind turbines. A better way would be to specify wind changes based on amount of turbines over an OWF district of for example 4 grid boxes. So in case of here used 12-turbine wind farm the effect is a matter of 12 turbines shared over 4 grid boxes affecting ratable an area of 6x6 km^2. The detected issue of horizontal resolution may overestimate the affected area and has to be considered.

However a tendency of wake intensification with amount of wind turbines, respectively the covered areas, can be supposed in reality. Hence, a bigger wind farm leads to a wider and stronger wind wake with a distinctive core of low wind speed within OWF district and structure of the influence will be mostly the same.

Table 4.1-II: Key notes of METRAS OWF simulation. OWF effect is separated into a positive and negative change over the 10 m horizontal (hor.) field and over whole model area through the vertical layers (vert.).

METRAS (6x6km^2 OWF , 10m wind direction SW)		value horizontal and vertical	max. positive change	max. negative change
Turbine #	ug			
T012	8m/s	**pressure (Pa), hor.10m**	**11.33**	**-2.48**
		pressure (Pa), vert.	**9.77**	**-11.12**
		temperature (ºC), hor. 10m	**0.03**	**-0.04**
		temperature (ºC), vert.	**0.22**	**-0.61**
		humidity (%), hor. 10m	**0.42**	**-0.31**
		humidity (%), vert.	**7.66**	**-2.72**
		wind speed (m/s), hor. 10m	**0.62**	**-4.42**
		wind speed (m/s), vert.	**0.66**	**-7.77**
		wind speed (%), hor. 10m	**9.01**	**-71.65**
	5m/s	**wind speed (%), hor. 10m**	**9.77**	**-64.13**
	16m/s	**wind speed (%), hor. 10m**	**9.65**	**-77.31**
T048	8m/s	**wind speed (%), hor. 10m**	**8.60**	**-71.65**
T080		**wind speed (%), hor. 10m**	**2.66**	**-68.18**
T160		**wind speed (%), hor. 10m**	**8.31**	**-80.05**

4.1.2.2.4 Analysis of consistency of METRAS OWF effect on wind field

Wind turbines only rotate in a limited window of wind speeds. In the case of METRAS, technical data of the wind turbine type NORDEX N80/2500 are considered in the wind turbine parameterization. Hence, the wind turbine parameterization only acts between 2.5 m/s and 17.0 m/s (personal correspondence with M. Linde). This is leading to the question how the wind wake changes in matters of different OWF operation modi. Thereby METRAS provides another advantage compared to using the Broström approach – the possible time analysis of wake development of a wind farm.

Figure 4.1.8 illustrates the 10 m horizontal wind field, simulated by METRAS (run M_T012ug08*onoff), for different time steps and OWF operation cases. The relevant step is on the one hand the time when the OWF is switched off and periods switching on and switching off the OWF. A non-operating OWF in METRAS is still seen in the wind field because frictional

resistance of rotor disc is considered. That leads to an increase within the OWF of 1 m/s. Therefore a non-operating OWF in METRAS is treated like a 'building', which ends in an effect being comparable with a flow around a building.

Due to the dynamic pressure the wind speed increases. In front of OWF the wind speed is reduced, pressure increases based on transformation of kinetic energy. At top and borders a wind flow separation occurs with an increased flow due to depression. Behind the wind farm a lag curl with a depression is expected, that is why even in case of non-operating wind farm a wind wake is simulated behind wind farm.
After turning on wind turbines, means using the rotor disc approach, the wind is suddenly reduced within the OWF district and at the flank the wind is increased due to depression (figure 4.1.8). With time the wake grows and affects an area, which is significantly greater than wind farm itself. With distance to wind farm the wind reduction slowly migrate to the wind speed of the surrounding. The produced wind wake and its flanks by OWF do not suddenly disappear after turning of the wind turbine operation; the main wind field advects wake and flanks.
With time the effect of OWF on the wind field can disappear by switching off the OWF. It can be said that in the ocean the OWF-effect is more dominant and is not erased within few hours after turning off the OWF. However it is important to understand and conceive the OWF-effect on ocean. These signals of OWF on the wind field under different cases of OWF operation will be used as forcing for the ocean in analysis of the OWF effect on ocean.

Summarizing the OWFs dominantly change the wind field in dependence of wind speed and OWF conditions. The wind wake occurs within minutes of simulation time and becomes more intense in the case of greater wind speeds and turbine number. The here presented 10 m wind fields were used as forcing for simulations of OWF-effect on the ocean, which is performed in the following chapter 4.2.

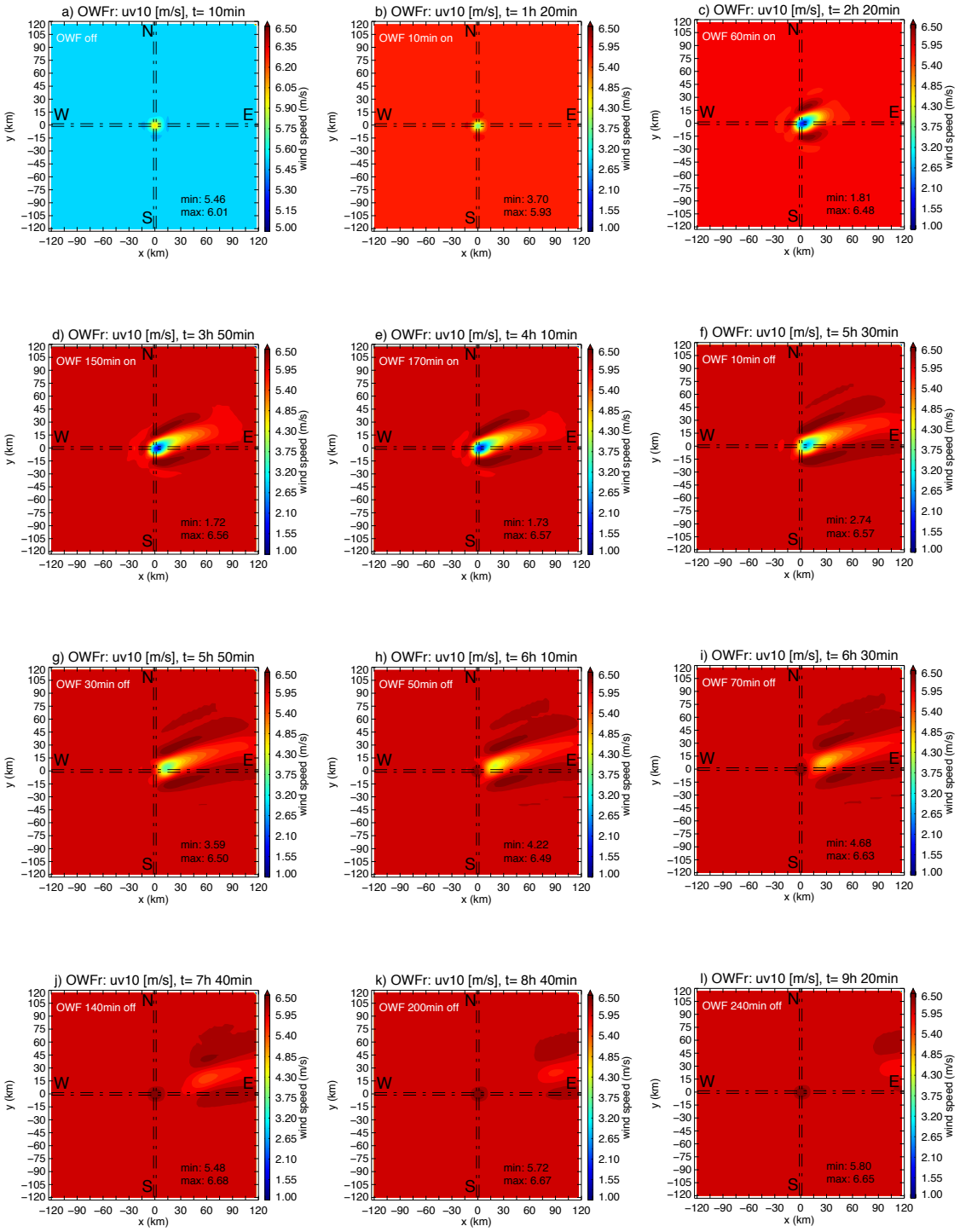

Figure 4.1.8: Variations in the 10m wind field due to different OWF operation mode of a 12-turbine OWF. a-j) shows the development of the real (run OWFr) METRAS 10m horizontal wind field for different time steps and OWF operation cases. First wind farm is off (a) then it is switched on (b) and turbines operate, means METRAS wind turbine parameterization is considered (c-e). Later OWF is switched off again (g). Turning off the OWF ends in advection of wind wake with the man wind field (h-j). Be aware of the different colorbar in a). Shown METRAS simulation times t are listed in the header of each picture.

4.2 Analysis 02: Effect on Ocean

Possible effects of a wind farm on the atmosphere, especially on the atmospheric wind field are summarized in previous chapter 4.1. Based on the fact that wind farms will be heightened construct on the ocean, an analyzing how a changed wind field will affect ocean's dynamics is of special interest in this context. At this juncture different aspects are focused:

First a common description of the impact on ocean is given in sub-item 4.2.1, introducing provoked changes in ocean dynamics and hydrography. Forward a physically analysis explains and derives occurring changes in sub-section 4.2.2. Sub-section 4.2.3 is referred to different METRAS simulations for different wind speeds, amount of wind turbines, consistency of effect and investigations regarding computational assumptions of ocean simulations, like forcing, depth of model area and horizontal resolution to fully capture all sides of the appearing phenomenon. Although HAMSOM is well verified over years the results are compared to measurements in chapter 4.2.4 to estimate the dimension of OWFs impact on ocean and to evaluate the model data.

The main variables that analyzed here are hydrodynamic and hydrological properties. Simulations are based on TOS-01 (box model, chapter 3.3) with a mostly adopted geostrophic flow of 8 m/s; if otherwise than it is explicitly alluded to.
To point out the OWF effect on ocean the results are primarily presented by differences between a run with operating wind farm (OWFr) and without a wind farm, the reference run (REFr). This dodge reflects the clear effect of OWFs because all changes in the dynamics do not occur in REFr.

4.2.1 Common Description of Impact on Ocean

Presentation of this section is based on data of simulation **T012ug08 TS01HD60F01** to primary detect OWFs effect on ocean. Here it is assumed that the change of the wind field is the major effect of the wind farm on the ocean. So only wind forcing is considered to analyze the natural effect of the wind wake on ocean. Additional a forcing beside the wind forcing, like atmospheric temperature, is neglected.

It is known that atmosphere strongly influences surface upper ocean, especially winds directly act with the ocean surface and play a key role for ocean flow [*Wells*, 2012]. Therefore it is awaited that a change in wind field, here induced by a wind farm, influences the ocean system. In particular, since an OWF produces a wind wake of a dimension of several kilometers, as mentioned in 4.1, it is expected to consign a clear signal from atmosphere to ocean. First reflection on this context yields a reduction of upper ocean flow in wind wake region. But the effect of such wind wake on ocean is more complex.
In front of the result presentation it is said that wind's impact on ocean is highly strong and the wake effect can be find in the ocean simulation after a view minutes of simulation time.
For a readily start into subject matter the OWF's effect on ocean is first introduced by a moment analysis after one day of simulation and then the effect evolution over 30 days is documented.

4.2.1.1 Moment analysis of OWF effect on ocean

The moment analysis concentrates on results of simulation **T012ug08 TS01HD60F01** after 24 hours. Here one constant METRAS wind field forces the ocean over the whole simulation time. Although the use of a constant wind forcing field over one day ocean simulation is quite unlikely due to, for example, diurnal variations, that approach helps to clarify magnitudes of possible effects on ocean due to OWF's wind wake. The presentation of the OWF-effect on ocean after one day is chosen as a representative time step to illustrate possible impacts.
The velocity field at surface, which is, in consistent manner, expected to react on wind changes, will be contemplated first. Knowing that wind's u-component dominates the form of wind change, this effect should be also identifiable at ocean flow's u-component at surface. Figure 4.2.1 and figure 4.2.2 presenting OWF effect on ocean by the horizontal velocity field, surface elevation ζ and the velocity components u, v and w.

The **horizontal velocity field** in figure 4.2.1 indicates areas of reduced and increased flow around OWF. Averaged speed over whole model area is 0.1 m/s, which is weak but thoroughly possible for a residual flow in the North Sea. The direction of flow is mostly southeast made up of direction forced by wind and Coriolis effect, which ends in a diversion of theoretical 45 degrees. The change of the horizontal velocity does not agree with the OWF induced change of the horizontal wind field, as might expected, because the velocity component v increases and acts as a result of occurring dynamics due to OWF's wind wake. Nevertheless the main decrease of flow is identified in area of wind wake with -0.058 m/s after one day but also regions of flow increase are produced with a maximal change of 0.067 m/s.

Surface elevation ζ shows a significant change (figure 4.2.1c). Within model area occurs a maximum and a minimum of ζ with division along wind wake axis in wind direction. That dipole structure of ζ has its increase north of the wind farm and wind wake while its minimum is placed south of the OWF. The change induced by the OWF is in order of several millimeters; here ζ counts an increase of 5.86×10^{-3} m and a decrease of 9.16×10^{-3} m compared to reference run after one day simulation. Such formation of dipole is also postulated by [*Broström*, 2008] as one main effect OWFs have on the ocean. Also Paskyabi and Fer [*Paskyabi and Fer*, 2012] whose adopt Broström's approach to analyze the response of the upper ocean on large wind farms in the presence of gravity waves identified the disturbance in thickness of the upper ocean layer having a form of a dipole. The imbalance of dipole's extrema is responsived later on but is correlated with additional occurring dynamical effects including circulations.

Having a look on each component of velocity, pictured in figure 4.2.2, the **u-component** clearly contains the wind wake information and is like a fingerprint of the wind's u-component, respectively the wind field. The zone of wind wake, the raised flanks and a distinct surge zone is clear seen at surface in the horizontal. After 24 hours the wind wake affects the entire ocean strength of 60 m depths and reduces speeds up to 0.14 m/s. The increasing of the u-component due to the wake-flanks counts 0.08 m/s.
Especially in front of the wind farm and in wake-flank's areas the **v-component** is reduced by 0.04 m/s, respectively increased by 0.05 m/s. Even here the whole model depth of 60 m is affected while changes of v-component due to wind farm has its extremes around depth of the thermocline, in 12 m. Above this layer the effect of the velocity component u counts stronger. The magnitude of v-component depends on the wake-flanks as well as surface elevation and induced vertical motion.

Therefore the most interesting velocity component is the vertical one. On the basis of the **vertical component w** a triggered change in ocean dynamics due to wind turbine is evident. In the horizontal at the sea surface a wind farm provokes two main cells of positive and negative vertical velocity, spanning an area around the OWF of at least 10x10 grid cells, which means more than 900 km^2. These numbers underline a strong impact of wind changes induced within four grid cells, so an area of 36 km^2 where OWF is placed. The cross section through the model area from West to East and South to North of component w shows that vertical cells have been established within 24 hours. In average the cells have a size of around 30 km x 15 km and affecting all ocean layers, especially the upper 30 meters. These upwelling and downwelling cells, with speeds of 0.04 mm/s, results in an overturning after 15 to 16 days. Even if that duration seems quite long, considering that in such time range the wind and the number of operating turbines can change, the induced vertical motion is an important phenomenon, which may also have an impact on the ecosystem. Beforehand these vertical cells are durable which will be discussed later under 4.2.3.

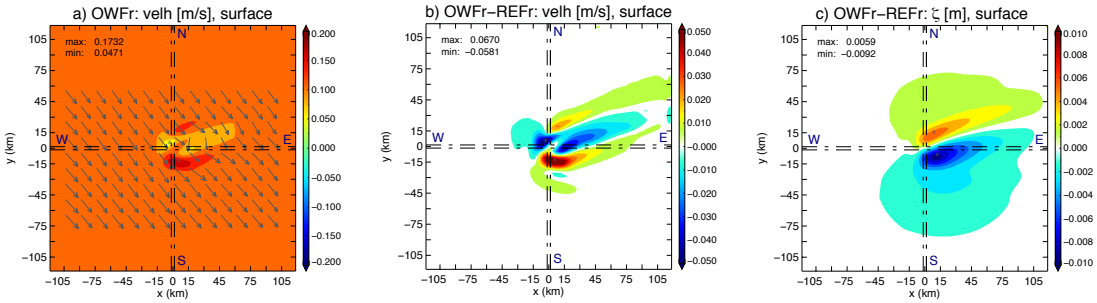

Figure 4.2.1: 12-turbine OWF-effect on the ocean system at surface after 24 hours of operating wind turbines. Shown variables are a) the real horizontal velocity field (OWFr) and direction of flow and the OWF-effect (OWFr-REFr) on b) horizontal velocity field and c) on surface elevation ζ. OWF is placed in the middle of the model area where dashed dotted lines are crossing. The horizontal velocity field has a main wake behind the wind farm in wind direction, which was southwest. The velocity wake is flanked by an increase in velocities. Surface elevation ξ shows a dipole structure.

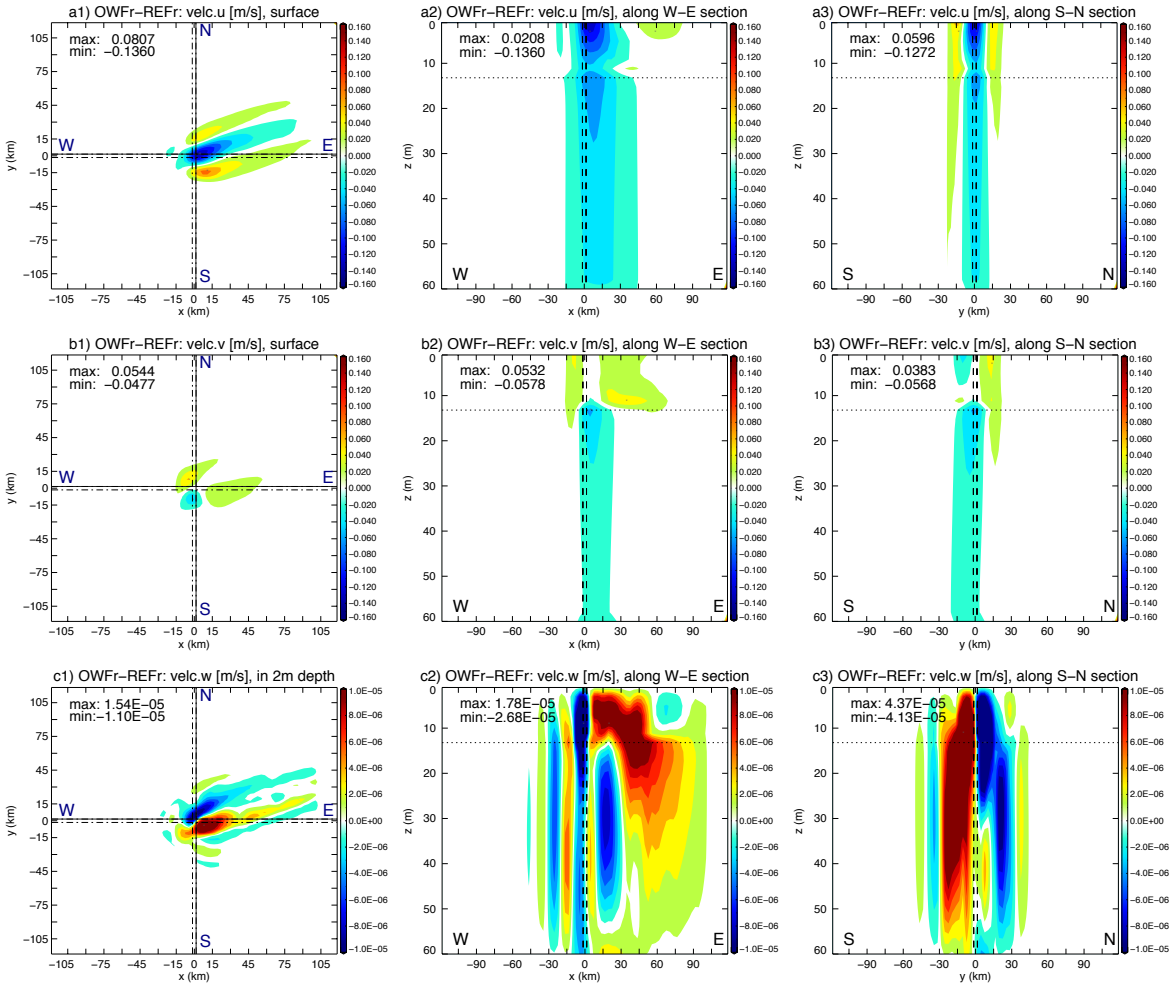

Figure 4.2.2: 12-turbine OWF-effect on ocean velocity components after 24 hours operating wind turbines. Effect is presented for a1-3) u-component, b1-3) v-component, c1-3) w-component in the horizontal at surface (a1,b1) and in 2m depths (c1) and along W-E (a2-c2) and S-N (a3-c3) cross-sections through OWF which are marked with solid lines in first domain. The dimension of the vertical component w is here 3.78m/d, which leads to an overturning after 15.89 days. Thermocline is defined in 12 m depths (dotted line in a2/3-c2/3) and the OWF is placed in the middle of model domain around x=y=0.

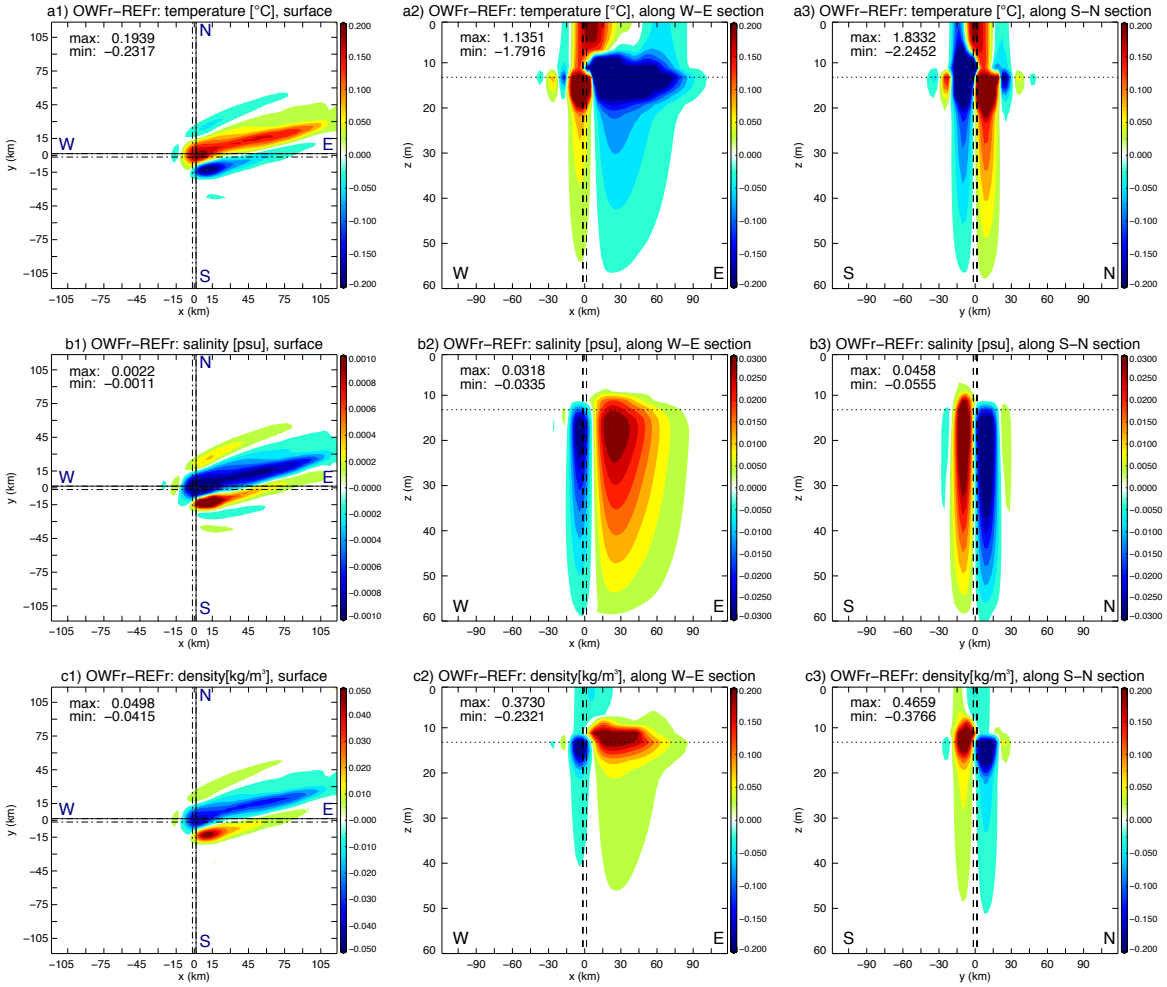

Figure 4.2.3: 12-turbine OWF-effect (OWFr-REFr) on hydrographic conditions after 24 hours operating wind turbines. Effect is presented for a1-3) temperature, b1-3) salinity, c1-3) density in the horizontal at surface (a1-c1) and along W-E (a2-c2) and S-N (a3-c3) cross-sections through OWF which are marked with solid lines in first domain. Thermocline is defined in 12 m depths (dotted line in a2/3-c2/3) and the OWF is placed in the middle of model domain around x=y=0.

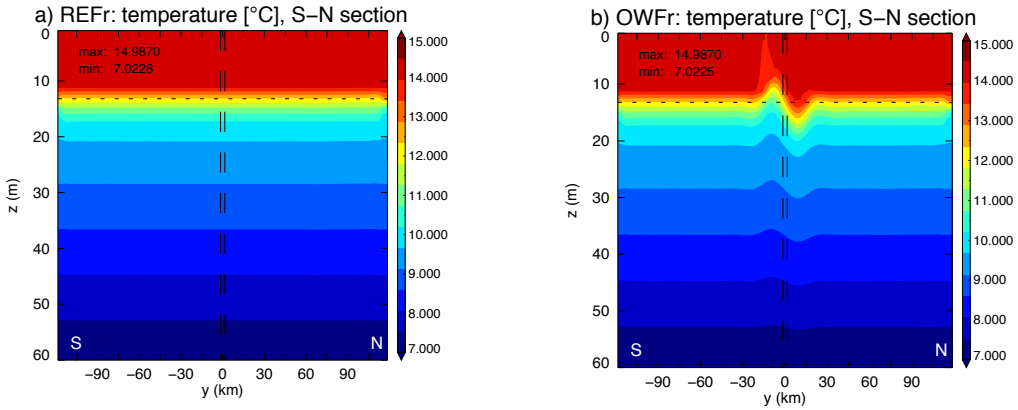

Figure 4.2.4: Temperature stratification of run a) without OWF (REFr) and b) run with operating wind turbines (OWFr) along cross-section from S to N through the OWF after 24 hours simulation with operating wind turbines. Values are given in °C. Operating OWF induces excursion of thermocline of about 10 m. That distortion is drawn through all layers. Thermocline is defined in 12 m depths.

Beside hydrodynamic changes the **hydrographic parameters** are affected, too. Figure 4.2.3 summarizes results of **temperature, salinity and density** after 24 hours operating wind turbines are aware of different color bars. At surface these variables depict the wind field.
Here an increased sea surface temperature (SST) in the wake zone of 0.2 degrees Celsius is recorded. The increase is adhered with a subsidence of surface elevation in the reference run which result in little cooler reference SST compared to OWF-run. The northern flank-area is about 0.06 ºC cooler while in the southern flank-area, where the main upwelling cell is located, a stronger decrease of 0.2 ºC appears. Respectively in those areas the ocean becomes more/less salty with extreme changes of 1-2 $x10^{-3}$ psu. Therefore the wake area becomes less dense of 0.04 kg/m^3 and denser of around 0.05 kg/m^3 in the upwelling zone. Extreme changes are located around 12 m where the thermocline was set at the beginning but still the whole ocean depth from surface to bottom is affected. In the vertical the dependence on vertical motion is obvious because hydrographic changes occur in the region of up- and down-welling cells. Although along x-section from West to East vertical motion shows a more turbulent structure with several cells of opposite velocity directions, the change in the hydrographic fields are more homogeneous due to stronger vertical motion in the cross-section from South to North.

Summarizing an operating OWF induces a new oceanic dynamic around the OWF district. The important effect is the generation of up- and downwelling cells connected with changed hydrographic conditions, especially at thermocline, compared to reference run. Operating OWF induces an excursion of thermocline of about 10 m (figure 4.2.4). This distortion affects all layers but weakens with depth having an exclusion of 4 m in 54 m depth.
The presented phenomenon of OWF on ocean forms the subject of further examination in this thesis. Questions of analysis are what exactly drive vertical motion, which processes control hydrographic conditions, how durable are those up- and downwelling cells, what magnitude is expected and what conditions occur in reality?

4.2.1.2 Temporal Analysis of OWF effect on ocean

So far theoretical effect of OWF on ocean after 24 hours is investigated. With the help of temporal analysis first principle of the physics describing the phenomenon can be established. That time analysis comprises a run of one month (30 days) with operating wind turbines. Again here used assumption for ocean simulation is a constant wind field (last time step of METRAS run) forcing the ocean every 10 minutes by wind speed and direction for each time step. In reality meteorological conditions will be never as constant as used here but that proceeding allows an

estimation of possible OWF effect on ocean by reaching a equilibrium ocean change. Also the approach is used to avoid additional effects due to wind veering and gusts, for example. As well such proceeding allows the best analysis of development of the effect.

Changes in the **horizontal velocity field (VELH)** due to wind are referred to the wind forcing that incurs into the equation of motion as wind stress acting on the sea surface and pictured in figure 4.2.5 a). The area of wind wake downstream of wind farm is projected on sea surface in form of flow reduction from first time step on (first time step is given after 10 minutes of simulation including a 10 minute mean) with minimal speed of 0.01 m/s. With time the wake flanks are even identifiable resulting in an increase of horizontal velocity of 0.07 m/s and more, figure 4.2.5.
The direction of the horizontal velocity field at surface is veered by around 45 degrees compared to the wind direction due to friction and Coriolis force; so a southwesterly wind direction in 10 m heights leads to a nearly westerly (NWW) ocean flow in accordance with the Ekman-theory. Although wind direction is constant with time, the direction of VELH varies from west more to northwest close to OWF. That is connected with changes in the magnitude of velocity components, especially of the v-component. While during the first hours of operating wind turbines the horizontal velocity field looks like a fingerprint of the wind field, including a wake area, a surge zone and flanks, the structure slightly changes with time. Hence the u-component indicates the wind field, including an increase of magnitude with time. The change at velocity component is smaller compared to the u-component. With time the v-component shows a similar structure to the u-component but intensified changes are stronger located around the OWF. Beside the horizontal velocities another indicator for a change in ocean dynamics is the change in surface elevation.

The reduction of the horizontal velocity field in the wake area affects the **surface elevation ζ** in a way that ζ increases easterly of OWF first, figure 4.2.5. Physically the reduced ocean flow ends in a reduced transport of water masses in the wake area, which again results in a slack flow and so in an increase of surface elevation. Due to law of conservation of mass a counter reaction to that is recognized westerly of OWF; here ζ decreases. So OWF leads to a dipole formation of surface elevation. The positive and negative cores of ζ-changes moves with time counter clockwise till the final dipole position is reached having an increase of surface elevation north of the wind farm and a decrease south of the wind farm. ζ-changes are spread over whole model area. A separation of the model area into increase and decrease of ζ is defined by the separation line y=0.25x-30 by setting zero point within the OWF. The positions of ζ-extrema at beginning of the simulation (figure 4.2.5 d1) are supported by the atmospheric pressure, presented in section 4.1.2.2, and the velocity wake.

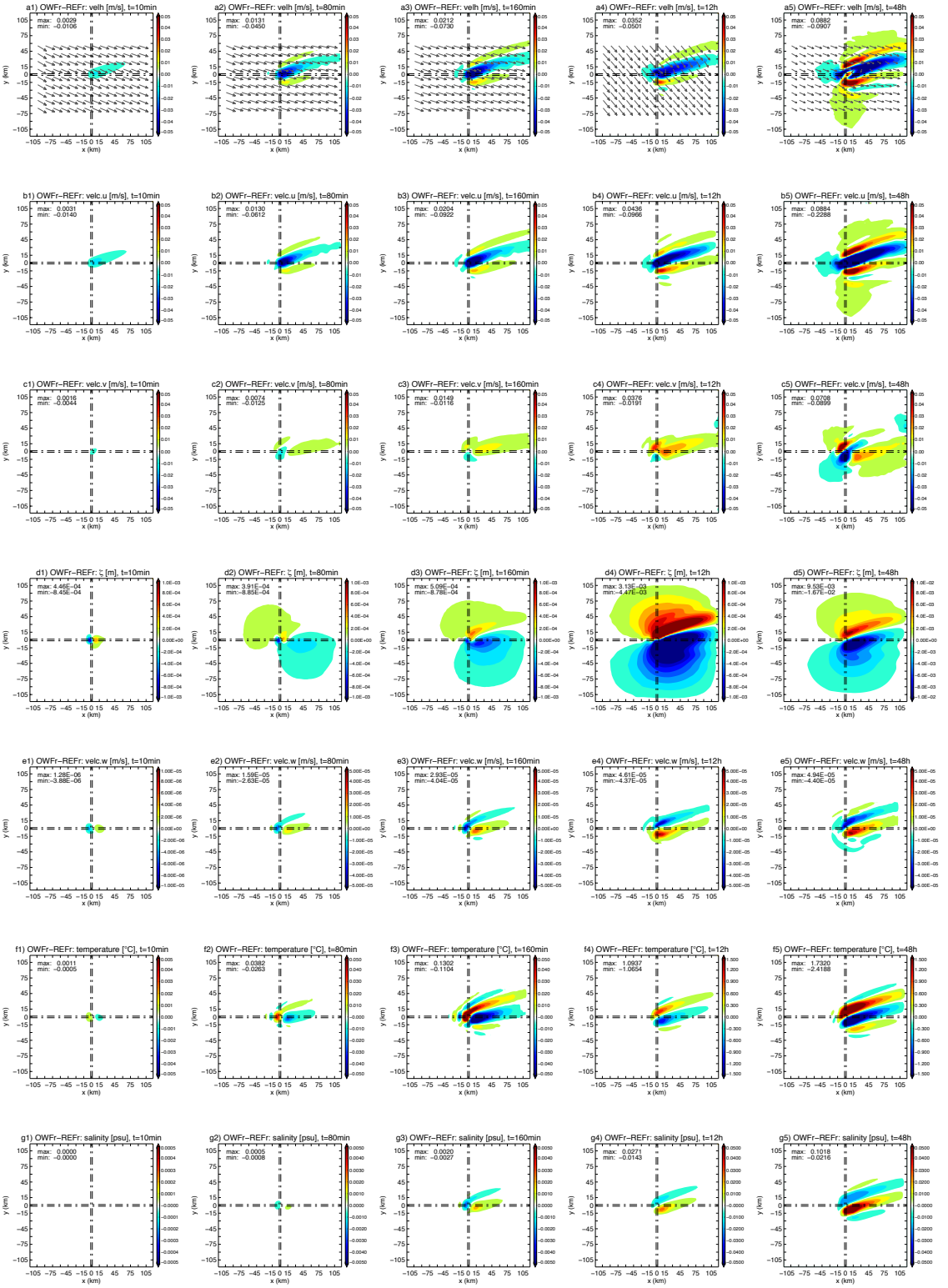

Figure 4.2.5: 12-turbine OWF-effect (OWFr-REFr) on ocean at five different time steps of ocean simulation at surface for horizontal velocity field (a1-5), velocity component u (b1-5) and v (c1-5) and surface elevation ζ (d1-5) and at 12 m depths for velocity component w (e1-5), temperature (f1-5) and salinity (g1-5). Results after 10min (a1-g1), 80min (a2-g2), 160min (a3-g3), 12h (a4-g4) and 48h (a5-g5) of operating wind turbines are presented. The OWF is placed in the middle of model area where dashed-dotted lines are crossing. Take aware of different color bars at later time steps. Black arrows give direction of horizontal velocity field of run OWFr. Units of variables are listed in header of each figure.

The final distribution of the positive and negative ζ-change depends on the increase of the velocity wake under geostrophic conditions and the Ekman transport, which is explained later in section 4.2.2.3.

Connected with changes in the surface elevation **vertical motion w** occurs following the same formation process around the OWF, figure 4.2.5. Two main cells of opposite vertical velocities increase by time with showing downward speeds in the South of the OWF and an upward pointed w-component in the North. Reason for the of up- and downwelling will be later examined, in section 4.2.2. After two days additional areas are affected by vertical motion beside two main cells. Here especially the area southwesterly of OWF shows belts of vertical motion at depths of thermocline.

Changes in **temperature and salinity**, representative for density, occur slower than changes in hydrodynamics, figure 4.2.5. Strongest changes are detected at depth of thermocline, while at surface effects are weaker. An increase/decrease of temperature/salinity at surface in the area of the wake is related to a change in surface elevation and wind forcing. The effect on surface grows by time first, but the mostly warmer/less salty conditions are only a temporary effect. At the depth of the thermocline the OWF-effect on temperature and salinity is caused by vertical velocities. A cooling and salinization dominates model area downstream of the OWF after one day.

Although changes are variable within the first 48 hours of simulation, formation of change is relative constant after two days. Figure 4.2.6 and Figure 4.2.7 illustrate changes during a time period of 30 days along y-section as representative.

The **surface elevation** increases quite consistence with time, figure 4.2.6 a). The analysis clarifies that maxima and minima stays stable after 27 days. The magnitude of negative tilt is stronger with 33.22 mm change while the positive change only counts 18.22 mm. The combination of horizontal and vertical compensation motion avoids a symmetric dipole.

The trend of **horizontal velocity** field and **components** is not as smooth as in case of surface elevation. Over the first two days a projection of wind field can be identified in the change of ocean flow but within OWF the flow shows an increase from day three onward, see figure 4.2.6 b). The velocity wake, formed in the beginning, is shifted more to the North and becomes weaker and horizontally thinner with time. Hereby an additional second region of flow reduction occurs 20 km south of OWF from day 10 on. Therefore the area of a southerly wake-flank spreads more to the South. Maximum changes in the flow are 0.18 m/s increase and 0.09 m/s decrease at beginning and 0.08 m/s from day 14 on. The upcoming second flow-wake is a result of an intensified positive v-

component south of the OWF, figure 4.2.6 d), as reaction on changed surface elevation. Within the OWF the v-component is more negative in the run OWFr than in REFr, while the u-component is positive in both cases with the exception of the OWF and wake area in OWFr. That leads to a higher horizontal velocity within OWF-area in case of OWFr compared to REFr. However the u-component and v-component reach their constant level earlier than the surface elevation. After 5 days they have within the OWF a reduction of -0.32 m/s for u-component and -0.12 m/s for v-component, see figure 4.2.6 c-d). A maximum increase counts 0.08 m/s and 0.05 m/s for u- and v-component.

The magnitude of the **vertical velocity** cells increases with time and is shown in figured 4.2.6 e-f). The dimension of the cells leads to a diameter of 15 km along y-section for both. At surface their increase stops and the magnitude of cells pulsing a little bit due to the horizontal velocity field. In 12 m depths at thermocline the cells become nearly symmetric with maximal velocities of around $6.0x10^{-5}$ m/s, which is in accordance with 5.18 m/d, which again would end in an overturning after 11.57 days. Beside the two main cells additional areas of mostly downwelling occur from day 6 on.

While vertical cells appear to be symmetric after 20 days of simulation, changes in the **hydrographic conditions** are dominated by cooling of the southern area at surface, which becomes saltier and so denser, figure 4.2.7. A cooling is expected due to transportation of warmer water into the depth and cooler water to the top. At the thermocline the warming is more distinct and the decrease with time is clear visible, even its dispersion in the horizontal. The warming in the south is connected with an additional vertical downward motion between day 9 and 20. At surface a maximal decrease of -1.8 ºC is simulated, at the thermocline of -2.95 ºC and the warming starts at the thermocline with 1.75 ºC., figure 4.2.7. While temperature/salinity maxima are first concentrated at the vertical motion cells, horizontal processes seem to support exchange by time over model area, which first affects surface.

If different time steps are compared at the beginning of the simulation, it is apparent that the upwelling cell has faster vertical velocities than the downwelling cell. Due to that cooling is slightly faster than the warming. Therefore it also takes longer to warm lower ocean layers.
Figure 4.2.8 shows temperature profiles for different time steps of the ocean simulation at two points 6 km south and north to the OWF center along S-N cross section. In the case of downwelling the thermocline drops from 12 m to 20 m depths. In the area of upwelling the thermocline rises by more than 10. The change in thermocline depth grows with time; its magnitude depends on location.

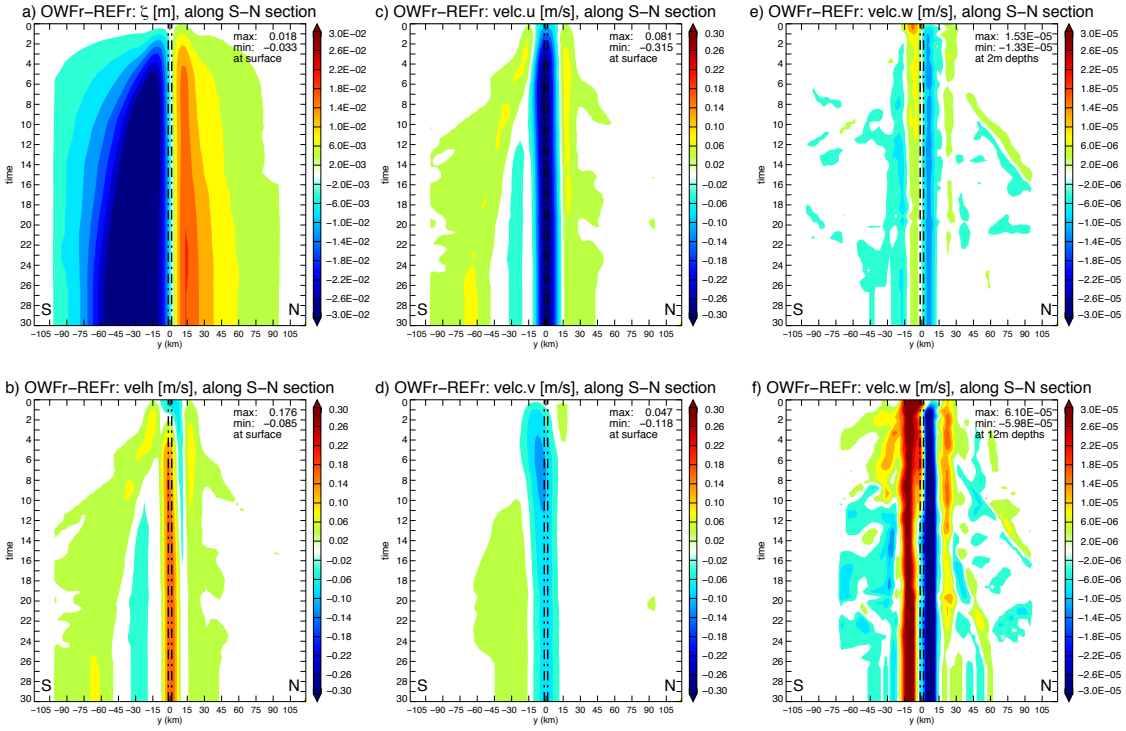

Figure 4.2.6: Development of 12-turbine OWF-effect (OWFr-REFr) with time along S-N cross-section through the OWF at surface for a) surface elevation ζ, b) horizontal velocity field, c) velocity component u, d) velocity component v, e) at 2 m depths and f) at 12 m depths for velocity component w. Time range comprises 30 days of constant operating wind turbines. OWF-district is marked with dashed-dotted lines.

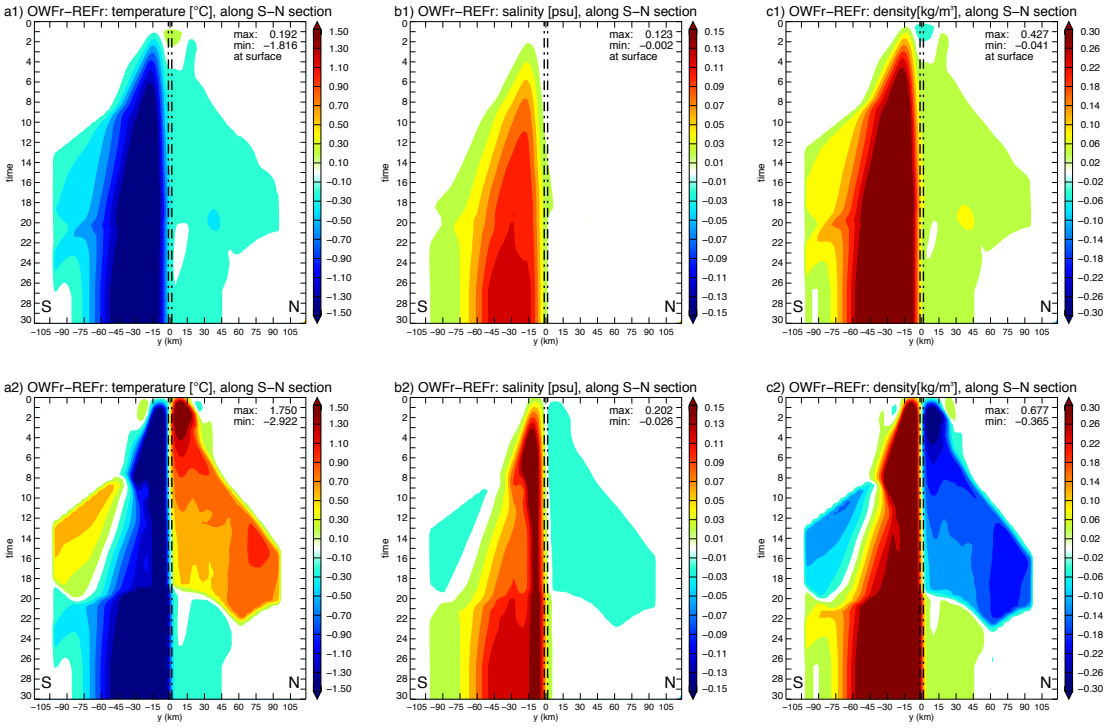

Figure 4.2.7: Development of 12–turbine OWF-effect (OWFr-REFr) with time along S-N cross section through the OWF at surface (a1-c1) and at 12 m depths (a2-c2) for temperature (a1-2), salinity (b1-2) and density (c1-c2). Time range comprises 30 days of constant operating wind turbines. OWF-district is marked with dashed-dotted lines.

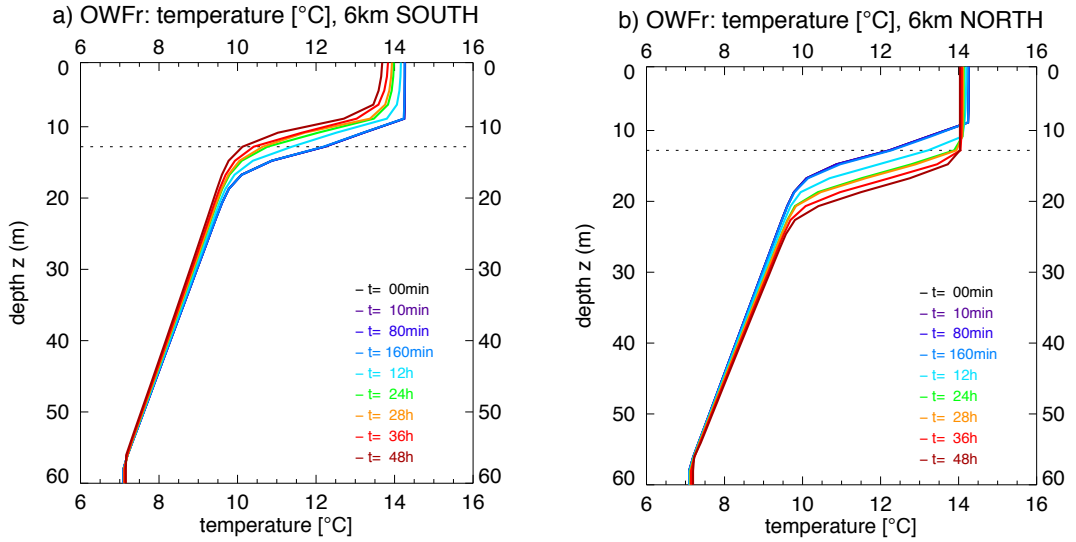

Figure 4.2.8: Temperature profiles of run OWFr considering 12 wind turbines for different time steps t at two representative positions along S-N section. a) Temperature profiles at 6 km south to OWF center. b) Temperature profiles 6 km north to OWF center. Hence a) is placed in upwelling region and b) in downwelling region. Thermocline is pushed with time up and down in dependence on sign of vertical velocity component w. The different time steps of OWF operation are 0min, 10min, 80min, 160min, 12h, 24h, 28h, 36h, 48h starting with a coloring from black to red.

Due to the stable distribution at beginning, the thermocline cannot be fully eroded but in case of a more realistic temperature distribution the ocean would be stronger mixed as realistic runs which is shown in chapter 4.2. Compared to beginning of the simulation the temperature at upper layer undergoes a decrease of averaged 1.5 ºC within 30 days southerly of OWF and leads to a temperature gradient between south and north of approximately 2 ºC.

Details of physically processes linking and triggering the OWF induced phenomenon on the ocean system are analyzed in next sections.

4.2.2 Theoretical Analyze of arising OWF-Effect on Ocean

The effect of an offshore wind farm on ocean includes modifications in ocean dynamics and hydrography, as documented in 4.2.1. The cause of vertical mixing, indicated as upwelling and downwelling, is associated with changes of the hydrographic components temperature, salinity and density. An induced change of ocean's stratification is of special relevance. Thereto this section aims to understand the impact on ocean due to operating wind turbines by analyzing the physical conditions, especially influencing vertical processes, step by step with the help of a sensitivity study.

The preparation of the sensitivity study accounts the following facts and orientations:

i) An OWF results in up- and downwelling cells around OWF-district.
In common, local mixing of the upper ocean is predominantly forced from the state of the atmosphere directly above it [*Moum and Smyth,* 2001]. Main processes for mixing are convection, wind forces, precipitation and ice on the upper ocean [*Moum and Smyth,* 2001]. Here the variable wind can be identified as the main impulse of OWF-effect on the ocean so far. The wind is the most important atmosphere component of this analysis because an intensified vertical motion occurs by using a forcing covering wind as meteorological forcing only. Additional, topographic irregularities can be excluded as a mechanism for incipient vertical velocities because of using a flat ground in simulations. But what exactly triggers changes in the vertical?
On the basis of the OWF induced wind change and related changes of surface elevation and considering time analysis we can assume that vertical motion is driven by these horizontal changes at surface, whose affects the barotropic pressure field. To review, the importance of stratification under barotropic conditions is presented in 4.2.2.1.

ii) An OWF results in an increase and decrease of hydrographic values (around thermocline).
Main processes supporting changes in the hydrography on short time scales are diffusion and advection of temperature, respectively salinity. The question is now whether horizontal gradients dominantly impact the OWF-effect on hydrography or whether vertical advection mainly causes such changes? Hence the impact factor of diffusion and advection and exchange of momentum in the vertical and as well in the horizontal are analyzed in section 4.2.2.2.

Sensitivity Analysis:
On these grounds the physically analysis comprises various sensitivity runs, which are listed in table 4.2.2.-I. All runs underlie the main setup of TOS-01 (BOX-MODEL) with a 12-turbine wind

farm over grid cells in the middle of the model domain and a prescribed geostrophic wind of ug=8m/s. To analyze the physics of the emerging phenomenon HAMSOM's equation within the source code (src) were prepared so far to receive the impact of different physical processes.

Simulation name for simulation under barotropic conditions is **T012ug08 TS01HD60F01_BTM** (BTM). Corresponding effect-reference simulation is **T012ug08 TS01HD60F01** (BC). BC is the master simulation presented in previous chapter considering the full HAMSOM code with 3D baroclinic primitive equations and an undisturbed diffusion and advection scheme.

Simulations considering vertical and horizontal exchanges are designated with **T012ug08 TS02HD60F01_src*** ('*' stands for modification listed in table 4.2.2-I) and are explained in context. Corresponding effect-reference simulation is **T012ug08 TS02HD60F01**. That effect-reference run differs from master run BC by temperature and salinity stratification. Here temperature and salinity start field TS02 (figure 3.3.4 b) is used. That TS-stratification consists only of two layers. The reason for another TS-description is the fact that the vertical exchange processes affects layers above and around the thermocline. Those layers can become indistinct due to the fact that such processes leads to a vertical mixing and so to a change on the conditions of the TS-stratification. Hence the impact of each process at the thermocline is not clear identifiable. Therefore the temperature and salinity field was simplified to two main layers, which allows an distinctive detection and analyses of the influence of exchange processes via and around the thermocline.

All setups listed in table Table 4.2.2-I were simulated in case of OWF and in case of no OWF to picture the sole effect after one day of simulation.

Table 4.2-I: Overview of runs for sensitivity study; common based on TOS-01 (BOX-MODEL). T000= no OWF, T012=12-turbine OWF | ug08=8m/s prescribed geostrophic wind | TS01 & TS02 prescribed temperature and salinity field | HD60= ocean depth of 60m | F01=only wind and atmospheric surface pressure forcing

Main Run	Description
i) Analyze of Barotropic Cause [temperature and salinity start field: TS01]	
T000ug08 TS01HD60F01 **T012ug08 TS01HD60F01**	Full HAMSOM model code with 3d baroclinic primitive equations and diffusion, advection scheme, called **master run**
T000ug08 TS01HD60F01_BTM T012ug08 TS01HD60F01_BTM	master simulation but no baroclinic pressure component, TS changes barotrop, **abbreviation BTM**
ii) Analyze of Barotropic Cause [temperature and salinity start field: TS02]	
T000ug08 TS02HD60F01_src50 **T012ug08 TS02HD60F01_src50**	like master simulation but with TS02, no exchange limitation; called **normal run**
T000ug08 TS02HD60F01_**src51** T012ug08 TS02HD60F01_**src51**	no vertical exchange of momentum
T000ug08 TS02HD60F01_**src52** T012ug08 TS02HD60F01_**src52**	no vertical TS diffusion
T000ug08 TS02HD60F01_**src53** T012ug08 TS02HD60F01_**src53**	no horizontal TS diffusion
T000ug08 TS02HD60F01_**src54** T012ug08 TS02HD60F01_**src54**	no vertical TS advection
T000ug08 TS02HD60F01_**src55** T012ug08 TS02HD60F01_**src55**	no horizontal TS advection
T000ug08 TS02HD60F01_**src56** T012ug08 TS02HD60F01_**src56**	no vertical TS advection & diffusion
T000ug08 TS02HD60F01_**src57** T012ug08 TS02HD60F01_**src57**	no horizontal TS advection & diffusion
T000ug08 TS02HD60F01_**src58** T012ug08 TS02HD60F01_**src58**	no horizontal exchange of momentum, no Smagorinsky diffusion
T000ug08 TS02HD60F01_**src60** T012ug08 TS02HD60F01_**src60**	no vertical exchange
T000ug08 TS02HD60F01_**src61** T012ug08 TS02HD60F01_**src61**	no horizontal exchange

4.2.2.1 Analysis of Dynamical Pattern under Barotropic Conditions

Investigation of ocean's reaction on operating OWF under barotropic conditions helps to strike a statement of the trigger of the vertical motion.

Generally barotropic conditions of an ocean system are mostly identified in the relative homogeneous deep layer. Physically a barotropic ocean means parallelism of isopycnic and isobar surfaces having a constant slope with depth. The horizontal pressure gradient, as well as the geostrophic flow is constant with the depth.

The 'simplification' of baroclinic model to barotropic model is done by negligence baroclinic components. In case of here used HAMSOM simulation **T012ug08 TS01HD60F01_BT (BT)** barotropic means the negligence of the baroclinic pressure component and the non-prognostic calculation of temperature and salinity. A better treatment of temperature and salinity and further eliminations of baroclinic components is not possible due to model design.

In this context is must be mentioned that HAMSOM uses a semi-implicit numerical scheme. The pressure component only is separated into the internal (baroclinic) and the external (barotropic) components. Referred to Backhaus [*Backhaus,* 1985], the separation of barotropic and baroclinic pressure component is indicated in following relation:

$$\boldsymbol{P(z) = (g\varrho_1\zeta)_{ext} + (P'(\zeta) + g\int_z^0 \varrho' dz)_{int}} \qquad \textbf{EQ 4.2.1}$$

with

P(ζ) := atmospheric pressure at sea level ; P'(ζ) := atmospheric pressure anomaly at sea level

ρ_1 := actual density of layer

ρ' := ρ_1-ρ_0 , ρ_0 as reference density

g := acceleration due to gravity

ζ := surface elevation

ext := external component (barotropic)

int := internal component (baroclinic)

Based on explanations by Backhaus [1985] the atmospheric pressure P(ζ) is put into the internal pressure component, because it does not need to enter the implicit scheme for the external pressure variations, which is involving the sea surface elevation at the first layer. In case of the internal component the atmospheric pressure enters as a pressure anomaly P(ζ') due to the approximation of the internal pressure gradients. That approximation obtains a high accuracy when it depends entirely upon anomalies [*Backhaus,* 1985].

The variations in the temperature and salinity field and thus in the density field occur at much lower frequencies than the oscillation of the free surface. Hence they are solved by means of an explicit scheme and therefore HAMSOM can only simulate temporal and spatial changes of the

large baroclinic fields. But the use of implicit and explicit system components ends in the fact that a barotropic mode during the implicit scheme strongly influences the temperature and the salinity being treated in the explicit scheme. This means the advection velocities derived from the solution of the primitive equations are centered in time between the adjacent time-levels for heat and salinity, because they are defined half a time step apart from these. Finally a constant temperature and salinity field gives the barotropic conditions for the hydrography.

The pressure is incurred in the equation of motion. Vertical integrated over a depth range h, according to a computational model layer thickness h, the equation of motion can be formulated like in Backhaus [1985] as

$$\frac{\partial}{\partial t}\begin{pmatrix}U\\V\end{pmatrix}+\begin{pmatrix}0 & -f\\ f & 0\end{pmatrix}\begin{pmatrix}U\\V\end{pmatrix}+\frac{h}{\varrho}\begin{pmatrix}\partial p/\partial x\\ \partial p/\partial y\end{pmatrix}=\begin{pmatrix}X\\Y\end{pmatrix}+\begin{pmatrix}\Delta\tau^{x}\\ \Delta\tau^{y}\end{pmatrix} \qquad \text{EQ 4.2.2}$$

with

f := Coriolis Parameter

$\begin{pmatrix}X\\Y\end{pmatrix}$ **:= for example advective terms, horizontal diffusion term**

Δ **:= vertical difference**

τ **:= shear stress term**

U,V := components of transport averaged over depth h

p := pressure

Finally the barotropic HAMSOM run BP is adjusted by neglecting the baroclinic pressure gradient within the equation of motion (EQ 4.2.2.2).

Based on this adjustment HAMSOM run BP provides following **results in case of barotropic conditions**:

In figure 4.2.9 the difference between OWFr and REFr of barotropic simulations BTM is depicted for ocean variables surface elevation ζ, the vertical velocity component w in 3.0 m depth and the SST field after 24 hours operating wind turbines.

In case of barotropic mode the change of surface elevation ζ and the vertical velocity component shows similar structures like the master run (baroclinic mode). As expected the temperature field does not show an effect due to an OWF in the case of barotropic conditions.
The maximal difference in **surface elevation ζ** is $+3.65 \times 10^{-3}$ m, the minimal counts -6.16×10^{-3} m, which is slightly lesser than the master run, which shows $+5.86\ 10^{-3}$ m and -9.16×10^{-3} m. Here the

comparison of the extreme values of ζ results in an about 35% weaker ζ-effect in the case of BTM but related to the mean ζ-effect the BTM simulation is 4.54 % weaker than the master simulation.

The weaker effect on surface elevation can be explained using the **vertical velocity component.** The existence of the OWF-effect on the vertical velocity component indicates that the vertical motion occurs as a cause of ζ-dipole formation. The wind wake causes a wake in ocean flow, which provokes congestion of mass and the downwelling is a compensating reaction.
The impact on vertical velocity component w by BTM has a maximum of $1.0x10^{-5}$ m/s and a minimum speed of $-1.2x10^{-5}$ m/s in 3.0 m depth, figure 4.2.10. While here the minimum, downwelling, is nearly equal with the master run, having $-1.1x10^{-5}$ m/s, the maximum, upwelling, of the barotropic run is 34.29 % lower than the master run.
The effect of the barotropic run compared to the baroclinic master run is under barotropic conditions stronger at thermocline by around $3.0x10^{-5}$ m/s, which is equivalent to a 45 % stronger effect for upwelling and downwelling by BTM, figure 4.2.10. Stronger vertical mixing over time in the barotropic case results in a slightly faster compensation of the surface elevation. Thus run BTM shows lower values after one day at surface.

The vertical velocity component of the barotropic run has its maxima in 27.00 m depth with values of $5.0x10^{-5}$ m/s up to $7.0x10^{-5}$ m/s (~6 m/d). Here the vertical cells around the OWF are more intensified with the depth than in the master run but their horizontal dimension are restricted to 15 km compared to the 30 km in the master run along S-N cross section through the OWF, figure 4.2.10. The cells in BTM are smoother and more symmetric than the one in the master run, especially along the W-E cross-section through the OWF. Therefore the positions of extrema in the horizontal are not equal for both cases. At surface, the positions of the extrema have discrepancies only of one grid box, so 3 km in x-direction but with depth the positions of the positive/negative maximal change switches more to the North/South in the barotropic mode with difference to the master run of three kilometer (one grid box). Hence under barotropic conditions the extreme changes occur closer to the OWF.

Finally, the physics behind the vertical motion can be identified as a barotropic effect caused by changes in the surface elevation and not as an impulse of OWF induced hydrographic changes.
Overall the barotropic mode boost maximal changes of ocean system over whole ocean box by averaged 65 %, thus the impact due to the baroclinic mode counts 35 %.
The start of upwelling and downwelling at all is independent of hydrographic OWF-changes but differences in the simulation of BTM and BCM link to additional processes triggering the dimension and magnitude of the OWF-effect on ocean dynamics.

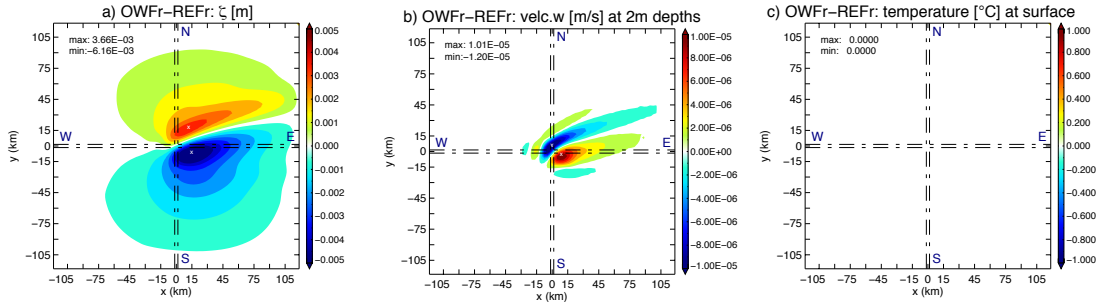

Figure 4.2.9: 12 –turbine OWF-effect (OWFr-REFr) on ocean under barotropic conditions. Ocean variables are a) surface elevation ζ, b) vertical velocity component w at 2m depths and c) SST. The existence of vertical motion in model area and no reaction in the temperature field, respectively in the salinity and density field, due to OWF under barotropic conditions leads to the assumption that vertical motion is a result of changed barotropic pressure implicated by surface disturbance of ζ due to operating wind turbines.

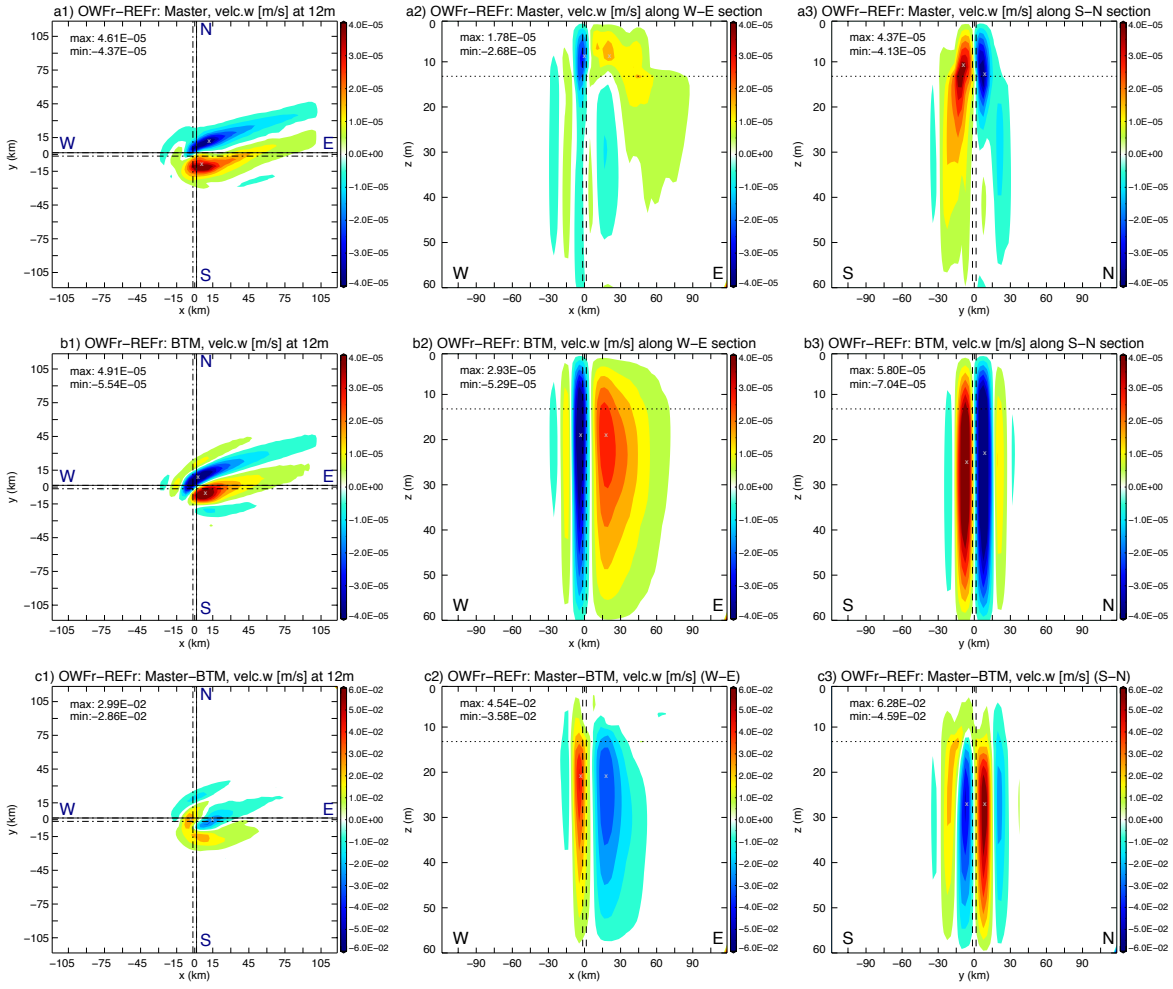

Figure 4.2.10: 12-turbine OWF-effect (OWFr-REFr) on the vertical velocity component w for a1-3) master run, means barotropic mode (Master), for b1-3) run under barotropic conditions (BTM) and c1-3) the difference between Master and BTM. Results are presented in the horizontal at 12 m depths (a1-c1) and along the cross-sections W-E (a2-c2) and S-N (a3-c3) through the OWF. OWF is placed around x=y=0. BTM results in a smoother and intensified vertical velocity especially in deeper depths but even in 12 m depths. In the case of Master maximal changes are concentrated around the 12 m layer.

Such processes are supposed to be mainly vertical transports due to diffusion and advection of temperature and salinity as well as the exchange of momentum, which in turn influences the diffusivities.

4.2.2.2 Analysis of Vertical and Horizontal Exchanges

Reflection of the OWF-effect on ocean under barotropic conditions yields to the result of vertical motion being a requirement of mass re-disturbance based on wind wake and reduced surface flow. But beside the barotropic factor additional processes have to be considered to describe the final phenomenon on ocean impacted by OWF.
Such processes are defined for horizontal and vertical exchanges comprising the exchange of momentum, heat, mass and salinity. They can be summarized under advection and diffusion. The exchange processes are based on local gradients, which are strengthened by turbulent motion.
In hydrology advection means the transport of solved or suspended material in water with the flow, so with the mean speed and direction of the ocean flow [*Rubin and Atkinson*, 2001]. In the vertical the salinity and heat transport, as well as the one of momentum, is related to the vertical velocity component w.
Diffusion is defined as a transport of molecules along a concentration gradient [*Jones*, 2010]; as intensified the gradient is as stronger is diffusion.

The different terms regarding advection and diffusion in HAMSOM were switched on and off by manipulating the source code to evaluate their impact factor. Therefore some explanations about HAMSOM details are necessary. The following description is in according to Backhaus [1985] and Pohlmann [2006].

HAMSOM's diffusion and advection terms are bounded in the equation of motion, the transport equation of temperature, respectively salinity. While the diffusion terms, the vertical shear stress and the terms determining the surface gravity waves are formulated implicitly, all other terms are formulated explicitly [*Pohlmann*, 2006]. The advective terms in the momentum equation and the transport equation for temperature and salinity are solved explicitly with the exception of the vertical advective term. Advection and diffusion of temperature and salinity in HAMSOM follows a method related to the difference scheme of second order accuracy from Lax and Wendroff [1960,1964]. That second order advective scheme was implemented to HAMSOM in combination with a Superbee-flux-limiter [*Roe*, 1986] by Hein [2013] and is able to simulate the diffusion more realistic and the mixing processes are fully controlled by physical processes. The use of the flux-

limiter avoids spurious oscillation due to shock waves, the contact with surfaces or discontinuous derivatives across any characteristics [*Roe*, 1986]. Fick's laws describe the diffusion itself.

At this point two important coefficients of the model HAMSOM must be introduced – the vertical eddy viscosity coefficient A_{vc} and the vertical eddy diffusion coefficient A_{dc}.

The coefficient A_{vc} is used because small scale vortices or eddies in the motion cannot be resolved at the mesoscale. To consider such vortices the large scale motion is calculated with and eddy viscosity that characterizes the transport and dissipation of energy in the smaller scale flow. So A_{vc} is linked with the transfer of momentum caused by turbulent eddies and is linked to the molecular exchange in the vertical because the vertical eddy diffusion coefficient A_{dc} in the prognostic equation of temperature is calculated via A_{vc}. In an equation this subject matter is describe as follows:

A_{vc} can be separated into different applications, into the usage in surface mixed layer, the bottom mixed layer and the interior, which is under laminar conditions. In the case of the laminar part the coefficient A_{vc} is defined as 0.0134 cm^2/s. In the case of the turbulent part the coefficient A_{vc} is defined by

$$\mathbf{A_{vc} = (c_{ML} * h_{ML})^2 * \sqrt{\left(\frac{\partial u}{\partial z}\right)^2 + \left(\frac{\partial v}{\partial z}\right)^2 + \frac{1}{S_M}\frac{g}{\rho}\frac{\partial \rho}{\partial z}}} \qquad \textbf{EQ 4.2.3}$$

with

c_{ML}:=0.05

h_{ML} := thickness of mixed layer

S_M := turbulent Schmidt-Prandtl number ~ 1.3

The vertical eddy diffusion coefficient A_{dc} is described through the generally accepted linear relation [*Pohlmann*, 2006]

$$\mathbf{A_{dc} = \frac{A_{vc}}{S_M}} \qquad \textbf{EQ 4.2.4}$$

Both parameters, the vertical eddy viscosity and diffusion coefficient, are necessary to parameterize the Reynolds stress terms in the shallow water equations and in the transport equation for heat [*Pohlmann*, 2006]. So A_{vc} impacts the vertical exchange. Due to that it was possible necessary to examine the influence of this coefficient on the influenced ocean by keeping A_{vc} minimal. Minimal means the usage of a laminar A_{vc}. That procedure helps to define its impact on the vertical velocity component and the distribution of temperature and salinity through the vertical diffusion.

In the following the analysis of the vertical exchange is presented followed by analysis of horizontal exchanges:

Vertical Exchange:

This sensitivity study aims to estimate the impact of vertical and horizontal diffusion and advection on the new state of system after one day.
The analysis of the vertical exchange comprises, next to the normal run used as a reference (**src50**), five simulations, labeled with **src60, src51, src52, src54** and **src56**, including different adjustments regarding vertical exchange. These adjustments consider the before mentioned parameters vertical eddy viscosity coefficient A_{vc}, vertical eddy diffusion coefficient A_{dc} and the vertical advection term of temperature and salinity (labled here as TSVA) in their prognostic equations.

Three options regarding vertical exchange were applied:

- **Setting A_{vc}** to a minimum of 0.0134 cm^2/s nearly avoids vertical exchange of momentum. Subsequent, the momentum at surface increases, so the horizontal velocity increases because lower layers will not be forced by momentum of surface layer. The surface motion due to shear stress triggers the lower layers.
- **Setting A_{dc}** to zero avoids vertical diffusion of temperature and salinity (TS). A_{dc} is zero in case of a minimal A_{vc} due to its definition. That means no vertical mass transport of TS.
- **Setting TSVA** to zero avoids vertical transport of temperature and salinity with the vertical flow, so with w-component.

In the following these three options were applied to HAMSOM in different combinations. In the first sensitivity run, **src60**, all three options are set to minimum/zero. In a second step, in the sensitivity run **src51**, only A_{vc} is set to minimum, vertical advection and diffusion are treated as normal. In the sensitivity run **src52** consequences of vertical diffusion are carved out by setting A_{dc} to zero; in **src54** TSVA is neglected and in **src56** TSVA and vertical TS diffusion is set to zero.
For analysis extrema of variables along the N-S cross-section after one day of simulation are used as the representative data set. The maximal effect on ocean due to an operating OWF is illustrated separated into a positive effect, means an increase of variable compared to reference run without wind turbines, and the opposite – the negative effect. Based on the asymmetric surface elevation the maxima and minima are not symmetric. An overview of changes in the OWF-effect on ocean by vertical exchange processes is pictured in figure 4.2.11

The sensitivity run, src60, preventing vertical exchange of momentum, vertical advection and diffusion of temperature and salinity (TS), shows a weaker effect in surface elevation due to a stronger impact on velocities but does not show an effect in the hydrographic stratification and the thermocline does not form an excursion around the OWF. Higher velocities are based on a constant hydrographic field unpersuaded by additional changes in the density and so the pressure field.
Figure 4.2.12 illustrates the difference in temperature along the cross-section from S to N through the OWF for the normal simulation src50 and the run src60 without vertical exchange processes. Runs without vertical TS exchange processes have a warmer upper layer because the exchange of heat is forbidden; while in the normal run the upper layers become cooler due to the exchange via the thermocline. The other way around is also explained by the exchange via the thermocline, which ends in warmer layers close below the thermocline.

Ignoring vertical diffusion, src52, the vertical exchange of temperature and salinity (TS) is connected with vertical advection. Results show that the negligence of the diffusion increases the effect on hydrographic conditions compared to normal run (figure 4.2.11). On the one hand that leads to the assumption that vertical advection plays an important role for the exclusion of the thermocline and on the other hand the vertical diffusion seems to break the development of the hydrographic effect. Having a look on the distribution of the temperature in comparison with the normal run in figure 4.2.13, then less obvious changes are identifiable. The examination of the OWF-effect illustrates that a cooling occurs at and above the thermocline southerly of the OWF and the warming occurs only below the thermocline northerly of OWF. The change is sharp in form of small ‘arrows’, linked in the direction of the vertical velocity component w, and it is stronger vertical limited than in normal run. So the diffusion supports reduction of the gradients over the vertical layers. Therefore in the normal run the effect has a more oval form blurred over more layers. Hence differences between the run src52 (no vertical diffusion) and the normal run are located at thermocline ±30 km around the OWF along the S-N section. Here we can say that the diffusion does not causes the exclusion of the thermocline but triggers the form and therewith the extrema of the OWF-effect on temperature.
The vertical dimension is halved and the effect-magnitude of the hydrographical variables is increased by averaged 45.82 % compared to the normal run.

In a third step the **vertical TS advection is set to zero, src54**, which prevents the exchange of heat with the vertical motion w. The effect on the hydrographic values is minimal but exalt in the upwelling regions, which means a decrease of temperature and increase of salinity (figure 4.2.14.
Compared to the normal run the effect is around 95.0 % smaller for the hydrographic variables, means nearly no change in TS is registered. So the vertical advection plays a dominant role for the development of the thermocline exclusion.

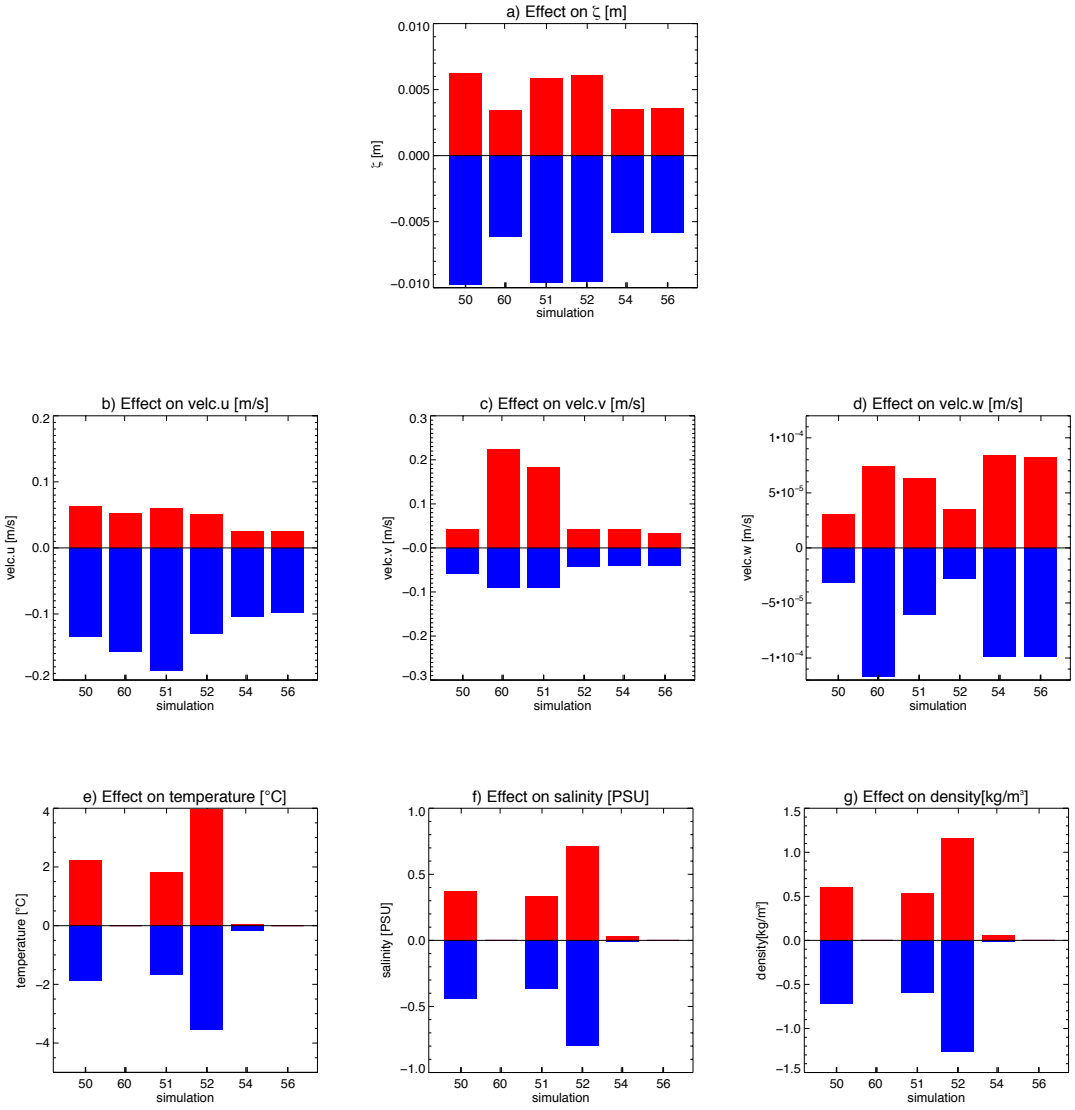

Figure 4.2.11: Overview of maximal OWF-effect (OWFr-REFr) on ocean after one day of simulation along cross-section S-N in comparison of sensitivity runs regarding the vertical exchange. Y-axis gives the change of the variables a) surface elevation, b) velocity component u, c) velocity component v, d) velocity component w, e) temperature, d) salinity and e) density. X-axis comprises simulations of sensitivity study, src*: 50 denotes 'normal run'. 60 is run without vertical exchange of momentum, advection and diffusion. 51 ignores vertical exchange of momentum in simulation, 52 ignores vertical diffusion and 54 vertical advection. 56 denotes run ignoring vertical diffusion as well as vertical advection but vertical exchange of momentum is treated as normal.

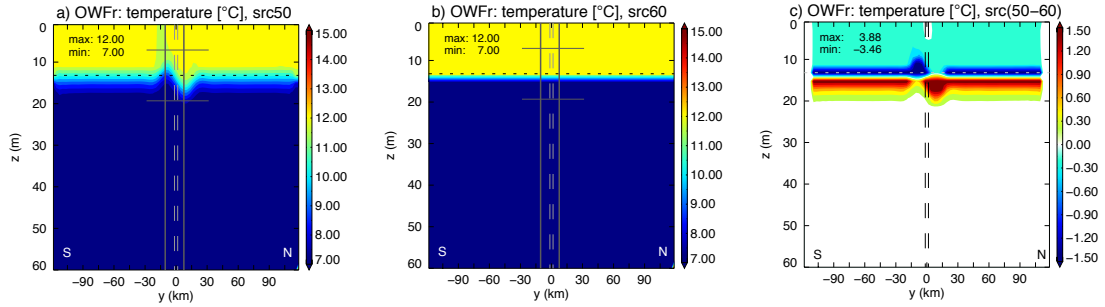

Figure 4.2.12: Comparison of the OWFr temperature stratification along the S-N cross-section through 12-turbine OWF around P(0,0) between a) the normal run (src50) and b) the sensitivity run avoiding the vertical exchange of momentum, vertical diffusion and advection (src60) after one day OWF operation. The Vertical changes in the hydrographic conditions are forbidden in src60. c) shows the difference between src50 and src60. The dashed horizontal line marks the depth of thermocline, the dashed-dotted lines mark the OWF area and solid lines accent the effect-dimension.

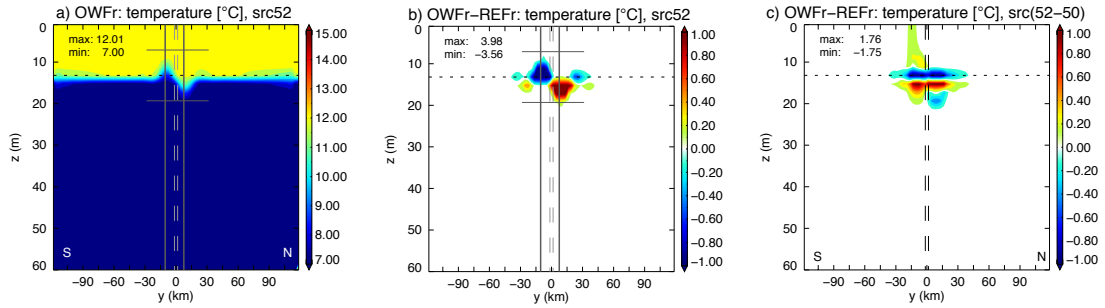

Figure 4.2.13: OWF-effect on ocean's temperature stratification based on sensitivity run without diffusion (src52) for a) OWFr and b) difference between OWFr and REFr and c) comparison of the effect to the normal run (src50) after one day OWF operation. No vertical diffusion means that the occurred changes regards to the vertical advection. The dashed horizontal line marks the depth of thermocline, the dashed-dotted lines mark the OWF area and solid lines accent the effect-dimension.

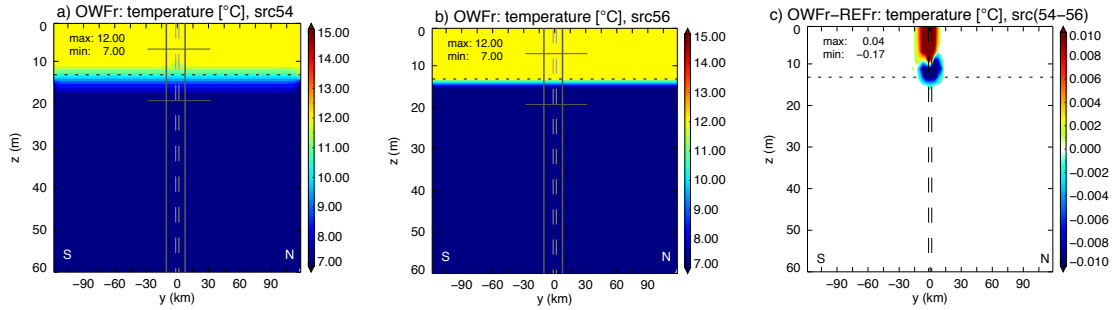

Figure 4.2.14: Impact of the vertical diffusion (run src54: neglecting vertical advection) on the a) OWFr temperature stratification compared to b) the sensitivity run without advection and diffusion (src56 after one day OWF operation; the difference is pictured in c). The Diffusion leads to a diffusive transition at the thermocline but without a sharper thermocline. The heat transport is supported by diffusion within OWF. Sensitivity run src54 in comparison with src56 depicts the single effect of vertical diffusion. The dashed horizontal line marks the depth of thermocline, the dashed-dotted lines mark the OWF area and solid lines accent the effect-dimension.

A comparison of src54 (no vertical advection) with the **simulation, without vertical advection and without vertical diffusion,** (src56) shows, that the diffusion ends in a diffusive thermocline with a linear transition between upper and lower water layers (figure 4.2.14). Without vertical advection and diffusion a sharp transition exists. Hereby it becomes apparent that the diffusion supports changes within the OWF in upwelling direction via the thermocline. Therefore the diffusion also supports a temperature increase from surface down to the thermocline following the gradient of concentration; as known, diffusion acts again concentration gradients.
For this reason the vertical advection dominates the TS-effect based on the velocity component w. But with time the temperature/density gradient around the thermocline within the up- and downwelling cells becomes weaker due to intensified vertical advection, which leads to reduced vertical velocities in the normal run (figure 4.2.11). Without vertical TS advection the up- and downwelling cells have intensified magnitudes of extrema, which are in average three times stronger than in the case of the normal simulation.
Figure 4.2.15 illustrates the single impact of the vertical TS-diffusion and the vertical TS-advection on the vertical velocity component w. As mentioned, the vertical advection reduces up- and downwelling by an average of 64.38 %, while diffusion only support the vertical motion by around 1.21% in relation to src56 (no vertical TS advection and diffusion)
Summarized the OWF-effect on the hydrography based on vertical advection and diffusion acts by the same means but different on the velocity field, mostly contradictory.

The last vertical exchange mode here, simulation run **src51**, considers HAMSOM vertical eddy viscosity coefficient A_{vc} and so the **vertical exchange of momentum**.
Regarding the hydrography the coefficient A_{vc} increases the OWF-effect by 10.94 % for the negative effect and by 17.51 % for the positive effect, means an averaged impact of 14.23 % (figure 4.2.11). The vertical velocity component w is greater in that sensitivity run than in the normal run, exactly by 49.45%, as well as the v-component with a 77.03 % greater increase and the u-component with a wake-increase of 28.25 % (figure 4.2.11). Generally A_{vc} supports changes in hydrographic fields due to stronger vertical motion and triggers the dimension of the wake in the velocity field. These results here also strengthen the thesis of the vertical motion having its origin in changed barotropic conditions. Minimizing the vertical eddy viscosity coefficient A_{vc} almost neglects the vertical exchange of momentum, which dominantly influences the upper layers. Based on the definition of the vertical eddy diffusion coefficient, depending on A_{vc} , the vertical diffusion of TS is avoided in the case of a minimal A_{vc}. But due to a less impact of the diffusion on the final OWF-effect on ocean that side effect will not much influence the manner of A_{vc}-impact.

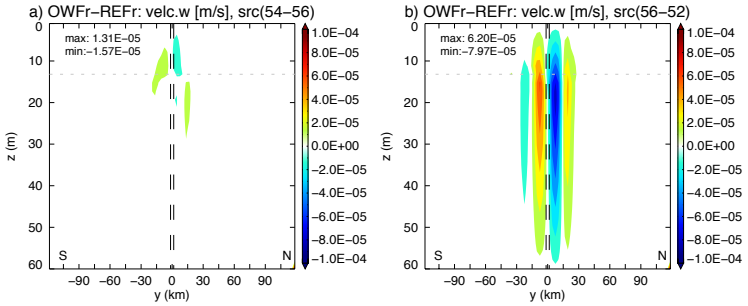

Figure 4.2.15 : Impact of diffusion (left) on velocity component w and impact of advection (right) on the velocity component w after one day OWF operation by taking differences between src54 (no vertical TS advection), src52 (no vertical TS diffusion) with src56 (no vertical TS advection/diffusion). The diffusion supports up- and downwelling a little bit while advection leads to control vertical motion and reduces magnitudes. The OWF-effect on w is stronger in the case of no advection, in the case of diffusion the effect is similar compared to normal run.

The sensitivity run src51 (no vertical exchange of momentum) leads to an increased reduction of the velocity component u, while the velocity component v is strengthened compared to the normal run. The strong change in the horizontal velocity is explained on the one hand by a reduced Ekman transport due to the wake and by a neglected transmission of momentum from surface layer to below layers. Therefore the velocity-wake area becomes more intensified and the wake-flank area as well. A more intense wake leads to a stronger effect in surface elevation, which triggers change in the v-component because of a reduction in the Ekman transport (see explanations to Ekman transport in section 4.2.2.3).

Figure 4.2.16 pictures the horizontal velocity components, the direction of the horizontal velocity field at surface and the vertical velocity component w along the cross-section from S to N through the OWF for sensitivity run src60 (no vertical TS diffusion & advection and no vertical exchange of momentum), src56 (no vertical TS diffusion & advection) and the difference between the two to capture the single impact of a normal handled A_{vc} coefficient after one day.

The direction of flow differs due to difference in the velocity components and hence in the Ekman transport. The horizontal velocity field in run without vertical exchanges (src60) causes a more intense vertical velocity component due to a more dominant gradient in the horizontal velocity field.

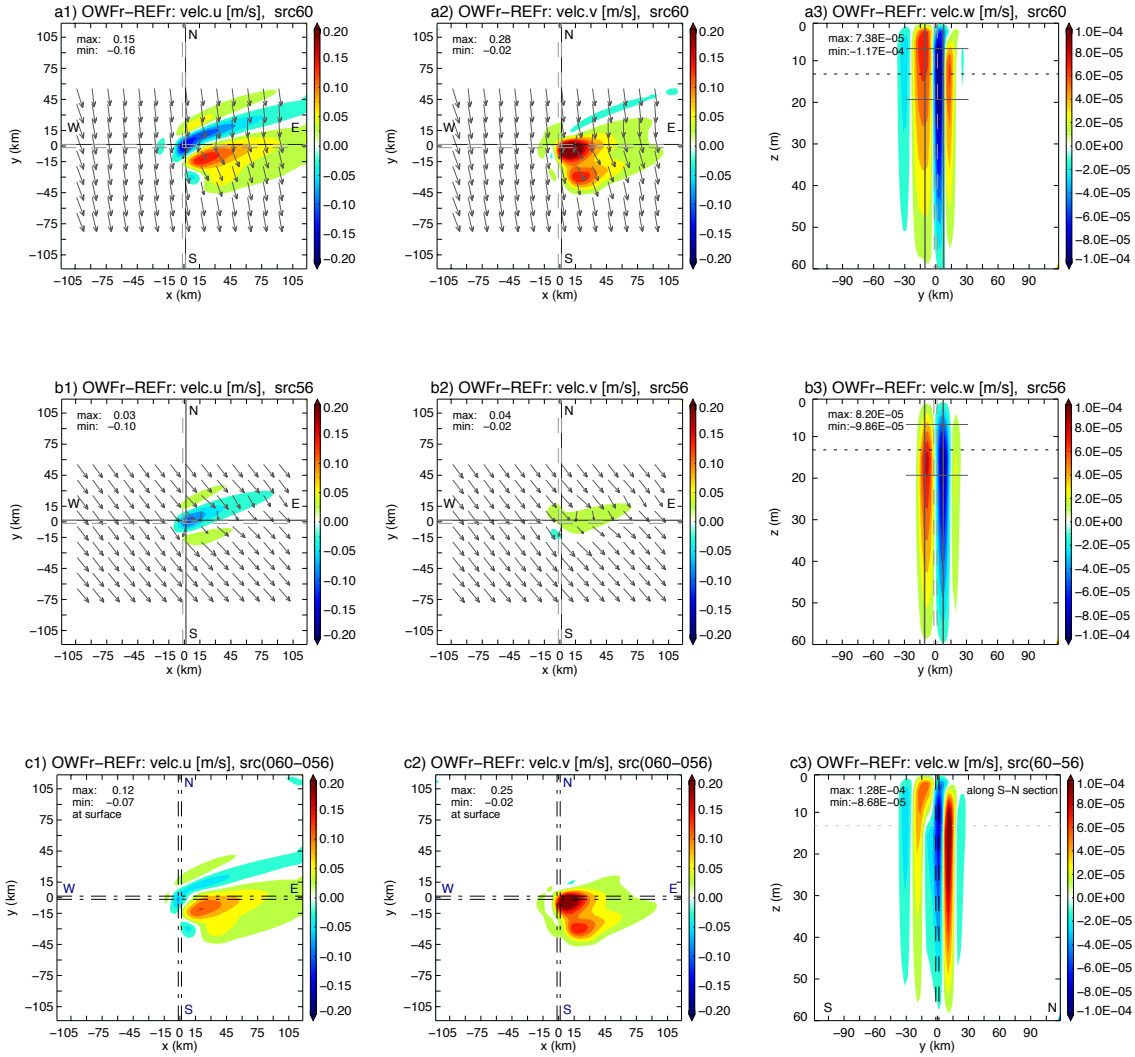

Figure 4.2.16: Single impact of A_{vc} on velocity components independent of vertical diffusion and advection, after one day OWF operation, at 2m depths. a1-3) shows results for run src60 (nor vertical exchange, A_{vc}=min, no TS advection/diffusion), b1-3) for run src50.56 (no vertical TS advection/diffusion) and c1-3) shows the difference between src60 and src56. Variables are the a1-c1) velocity component u, a2-c2) velocity component v in the horizontal and a3-d3) velocity component w over the vertical along cross-section S-N through OWF. Arrows define direction of horizontal velocity field. A_{vc} controls horizontal dimension of OWF-effect. Therefore a clear defined wake with flanks is adopted from the wind field and therefore the vertical motion is limited to two main cells. Additional vertical cells are suppressed due to a weaker gradient at surface.

Using a **minimal A_{vc} and also ignoring the vertical TS diffusion and advection (src60),** then the vertical component w ends in the strongest downwelling of all sensitivity runs (figure 4.2.16). Whereas the vertical motion cannot have an effect on temperature due to negligence of vertical TS advection/diffusion. Differences to the normal run count 72.82 % for downwelling and an increase for upwelling of 58.53 %.

Considering the run **without diffusion and especially advection, src56,** (advection stronger triggers w), the magnitudes of up- and downwelling cells are more symmetric by maximal averaged changes to the normal run of a 49.44 % increase.
If we prohibit a vertical exchange of the momentum then the vertical motion, which is triggered by the surface elevation and the horizontal velocity, can affect lower layers more easily, because the effect at upper layers run faster due to a stronger gradient in momentum. The stronger gradient and an intense horizontal velocity depend on the fact that the momentum cannot be transferred from top to the below layers. While advection triggers the magnitude of w, A_{vc} also controls the number of vertical cells. Additional the vertical cells, beside the two main cells around OWF, are caused by velocity gradients at surface and they are suppressed in the case of normal vertical eddy viscosity coefficient A_{vc}.

Summarized, the vertical exchange triggers dimension and magnitude of the up- and downwelling cells. The hydrographic conditions are influenced by the vertical advection, which again affects the vertical motion. The vertical diffusion acts especially at the thermocline and support an exchange within the OWF-district. The vertical eddy viscosity coefficient A_{vc} affects the vertical exchange of momentum and the vertical velocity component w due to variations in the form and the magnitude of the wake in the velocity field. The flanks of the wake become more important and the v-component increases in direction from north to south. Also the wake is intensified and even the vertical velocity component w. As higher A_{vc} as stronger the velocity components are reduced at surface.

Horizontal Exchange:

The horizontal exchange plays a secondary role for the OWF-effect on the ocean system in the vertical. The sensitivity runs regarding horizontal exchanges are listed in table 4.2.2-I.
Figure 4.2.17 illustrates the extrema along the cross-section S-N through the OWF for each sensitivity run regarding horizontal exchanges like diffusion, advection, momentum and their combination. Overall differences between the various horizontal exchange modes exist but the extrema does not vary strong with maximal discrepancies of ±10% compared to the normal run

(src50) with the exception of src53 and additional src58 for the velocity components. Sensitivity run src53 avoids horizontal TS-diffusion, while src58 avoids Smagorinsky diffusion and exchange of momentum.

The Smagorinsky diffusion describes a non-linear diffusion acting horizontally depending on u- and v-component. The Smagorinsky diffusion coefficient K_{smg} includes the horizontal tension strain T_{hs} and the horizontal shearing strain S_{hs}.
In Cartesian coordinates it can be written as follows:

$$\frac{\partial \mathbf{u}}{\partial \mathbf{t}} + \vec{\mathbf{v}}\,\Delta\mathbf{u} = \cdots + \mathbf{K_{smag}}\Delta\mathbf{u} \qquad \textbf{EQ 4.2.5}$$

$$\frac{\partial \mathbf{v}}{\partial \mathbf{t}} + \vec{\mathbf{v}}\,\Delta\mathbf{v} = \cdots + \mathbf{K_{smag}}\Delta\mathbf{v} \qquad \textbf{EQ 4.2.6}$$

$$\frac{\partial \mathbf{w}}{\partial \mathbf{t}} + \vec{\mathbf{v}}\,\Delta\mathbf{w} = \cdots + \mathbf{0} \qquad \textbf{EQ 4.2.7}$$

with $K_{smag} = l_s^2\sqrt{T_{hs}^2+S_{hs}^2}$ and $T = \frac{\partial u}{\partial x} - \frac{\partial v}{\partial y}$, $S = \frac{\partial u}{\partial y} + \frac{\partial v}{\partial x}$.

The use of the Smagorinsky horizontal diffusion stabilizes the dynamical core against horizontal shear instabilities.
Therefore the negligence of Smagorsinky diffusion leads to a stronger wake and hence stronger changes in the velocity components in src58 compared to normal run (figure 4.2.17). Changes in the horizontal velocity field again affect the vertical eddy viscosity coefficient A_{vc}, which impacts the vertical velocity component and the hydrographic variables.

The reduction of the hydrographic conditions in the case of no horizontal TS-diffusion (src53) shows that the horizontal diffusion intensifies the gradients in the density field and thereby impacts velocity field and the surface elevation. Here (in src53) the effect on the surface elevation develops very slow compared to the normal run and so the gradient is weaker from beginning on, which again weakens all changes in the ocean. Without horizontal diffusion the rise in surface elevation due to the velocity wake is more locally limited and not spread over the whole area and is controlled by the horizontal advection.

Summarized horizontal exchanges balance the OWF-effect and the vertical structure of the ocean system. Horizontal exchanges controls gradients in the horizontal, which affects vertical changes. Especially the horizontal diffusion (TS-diffusion and Smagorinsky diffusion) influences the final magnitude of OWF-effect but dominantly the vertical processes trigger the OWF-effect on the ocean system.

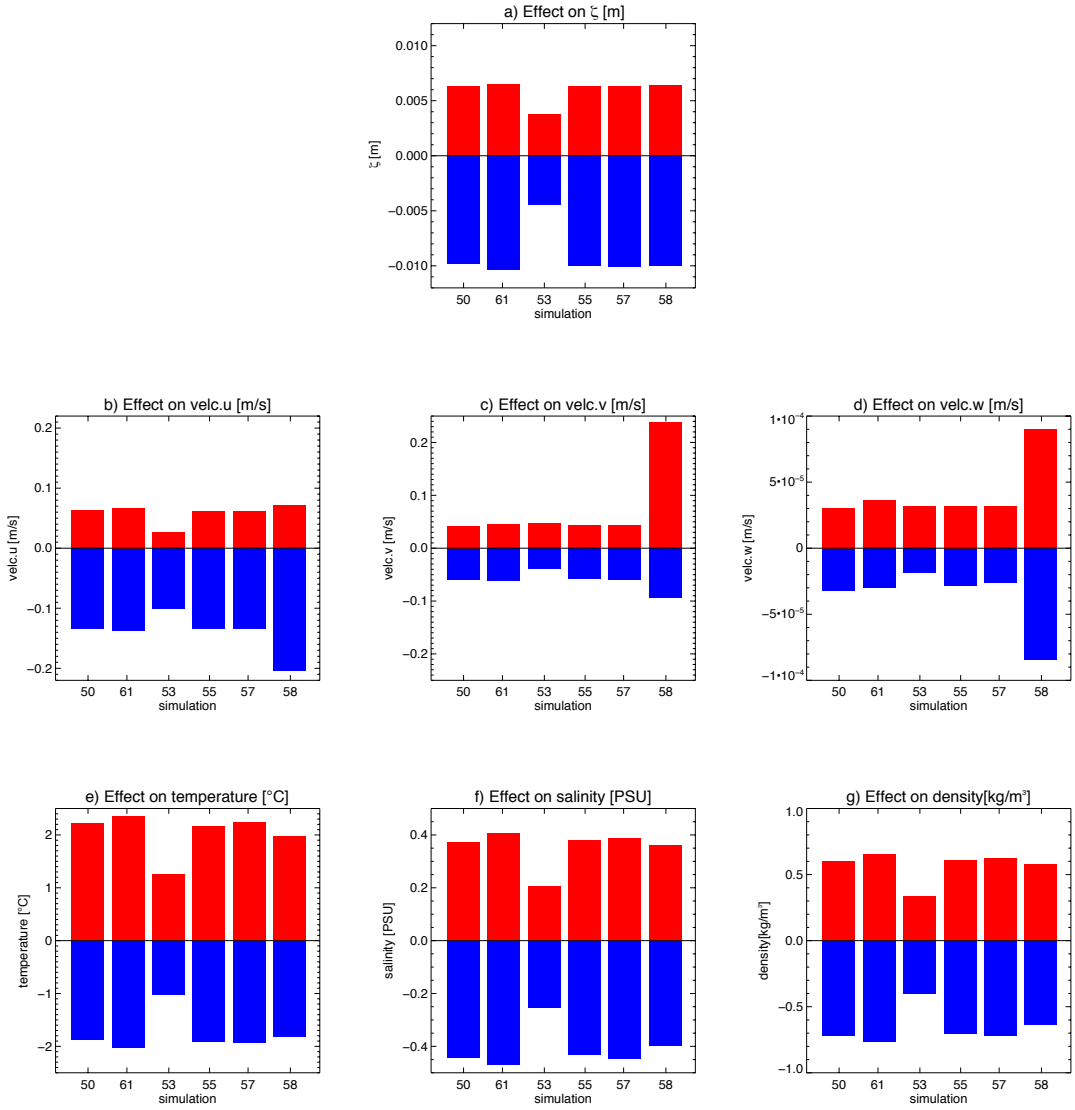

Figure 4.2.17: Overview of maximalOWF-effect on ocean after one day OWF operation along cross-section S-N in comparison of sensitivity runs regarding the horizontal exchange. Y-axis gives the change of the variables a) surface elevation, b) velocity component u c) velocity component v, d) velocity component w, e) temperature, f) salinity and g) density. X-axis comprises simulations of sensitivity study src.*: 50 denotes 'normal run'. 61 is run without horizontal exchange of momentum, advection and diffusion. 53 ignores horizontal diffusion, 55 ignores horizontal advection, 57 avoids horizontal advection and diffusion, 58 is no use of Smagorinsky (HAMSOM parameter horcon=0).

4.2.2.3 Assessment and Integration of Effect Analysis

Previous documented analyses deal with the OWF-effect on the ocean system under barotropic and baroclinic conditions and in the case of various exchange-process combinations. The manner of the vertical motion is related to changes in the barotropic pressure due to the change in the surface elevation released by the flow reduction due to the wind wake. The treatment of the exchange analysis results in the statement that especially vertical advection with vertical motion triggers the change in the hydrographic conditions. Partly betoken during prior explanations this section illustrates the main physical principle behind the occurred changes on the ocean system.

Starting once more from initial situation then our ocean system is forced by a constant wind field, which is affected by a wind farm. The wind turbines of the wind farm detract the atmosphere energy by transforming wind energy into mechanical one. That energy detraction means a reduction of wind speed downstream of wind farm. So a wind wake is formed by OWFs. That wind field acts with the ocean surface and creates a surface stress.
Under undisturbed conditions the constant wind field causes an Ekman transport. The Ekman transport is known as the net motion of water as a result of balance between the Coriolis and turbulent drag forces. The net sum of the water column is theoretically ~90º directed to the movement of the wind (in the northern hemisphere), at least partly for real conditions.
Under operating OWF conditions the wind wake causes a wake in ocean flow and the locally reduced surface stress results in a reduced Ekman transport. This again causes a convergence of water masses within the wake and to the left of the wake and a divergence at the right side of the wake (looking into wind direction). The convergence/divergence of the water masses are associated with an increase/reduction of the sea level, respectively which in turn induces downwelling/upwelling.
Common known connection between up- and downwelling and Ekman transport is in relation to coasts. An up- and downwelling also occur, beside coats, in the open ocean where winds causes surface water to diverge from a region or to converge toward some region. The last one is on hand here. Figure 4.2.18 schematic illustrates that term of conditions. Here the horizontal velocity and Ekman transport is reduced within the area of the wake and increased surface elevation. The area of the velocity wake can be treated as a barricade or ‘coast’ and now downwelling occurs where Ekman transport moves surface waters towards the region of velocity wake (‘coast’), the water must pile up and sinks. On the other side of the velocity wake upwelling occurs where Ekman transport moves surface water away from the wake area (‘coast’); surface water is then replaced by water that wells up from below. Upwelling and downwelling illustrate mass continuity in the ocean; that is, the change in distribution of water in ocean area is accompanied by a compensating change in water distribution in another area. And those two areas are the dipole formation of the

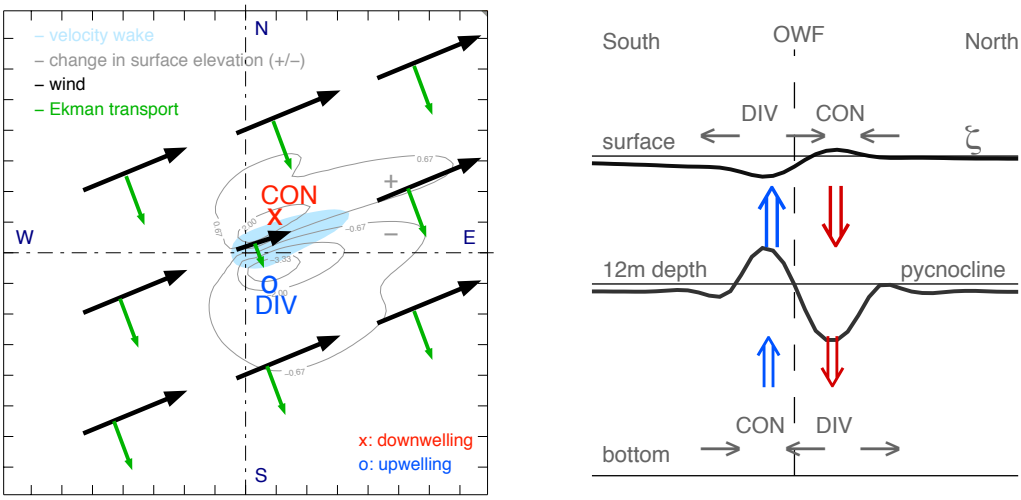

Figure 4.2.18: Left: Schema of adjustment of Ekman transport resulting in up- and downwelling. Ekman transport (green arrows) is detracted to wind direction by theoretical ~90º to the wind (black arrows). Due to velocity wake (light blue area) Ekman transport is reduced, which causes convergence/divergence of water masses (change in surface elevation ζ is light grey) and downwelling 'x' and upwelling 'o'. Right: Schema of conditions of OWF-affected ocean system along cross-section S-N through OWF. Constraint for downwelling is a positive decline in surface elevation ζ and convergence. The opposite is essential for upwelling. The pycnocline shows the opposite change of surface elevation.

surface elevation northerly and southerly of OWF. The formation and dimension of surface elevation's dipole is a result of the Coriolis effect and the wind wake due to geostrophic conditions.

Finally the vertical motion is a mandatory constraint of the wind driven change in pressure (barotropic effect), in the velocity field and so in the Ekman transport and can be defined as a wind driven but coastal independent upwelling/downwelling. The final dynamical situation of model area around OWF is illustrated in figure 4.2.18. A positive change in surface elevation means a lowered pycnocline, respectively the opposite for negative surface elevation. The zone where the upper part of the water column has a lower density is characterized by an increased sea surface height and a deepened pycnocline. At surface convergence is incurred which support downwelling while divergence occurs at low surface elevation with upwelling. Due to divergences and convergences the change in the horizontal velocity field at surface varies from the wind field by time.

Based on exchange study changes of hydrographic is then a result of vertical motion, divergence and convergence, dominantly supported by vertical advection.

External impact-factors triggering the intensity of wind wake and so of ocean's answer are considered in the analyses of next section.

4.2.3 Analyzing OWF's effect on ocean under various assumptions

Analysis of OWF's effect on ocean under various assumptions aims to capture possible comprehensive impacts triggering wind wake and so effect on ocean.
On the one hand an exalted impact on OWF's effect on ocean considering aspects of influences due to duration of operating wind turbines, magnitude of wind speed and size of OWF are documented.
On the other hand different computation assumptions for ocean's simulation are considered focusing on additional aspects based on assumptions regarding forcing and design of ocean box.

In this connection focus is more precisely the analysis

- **4.2.3.1:** of ocean effect's consistency due to duration of operation
- **4.2.3.2:** of wind speeds triggering wind wake magnitude
- **4.2.3.3:** of wind park power regarding amount and arrangement of wind turbines
- **4.2.3.4/5:** of influence by forcing comprehending inducement by Broström approach (4.2.3.4) and full possible meteorological forcing (4.2.3.5), which can be applied in HAMSOM
- **4.2.3.6:** of design of ocean box dealing with a reduction of ocean depth from 60 m to 30 m water depth

The results are based on simulation under TOS-01 (model ocean box) considering above-mentioned modifications using temperature and salinity start field TS01. Modifications are usage of forcing (F01, F02, F03, F04), of wind speeds (UG05, UG08, UG16), of number of wind turbines (T12, T48, T80, T160), of ocean depth (HD60, HD30) and of horizontal resolution (HR3, HR1).
Tables of statistics including information of extrema are listed in appendix E.

4.2.3.1 Analyzing consistency of OWF effect on ocean

During the description of common effect of a wind farm wake on ocean it was shown that the effect on the ocean appears immediately after using wind forcing with operating wind turbines. The theoretical analysis underlines that first vertical cells come up triggering changes of hydrographic parameters. Therefore it is analyzed what happens to the vertical velocity due to wind farm operation. Offshore wind farms need special services, which can be only done in case of stagnancy of the rotor blades. Additional the wind turbines having an operating limit based on wind speed. Depending on the machine a normal operating turbine is working between 5 m/s up to 25 m/s [*Vestas Wind Systems*, 2013], in case of METRAS simulation between 2.5 m/s and 17 m/s. The limited operation is caused by technical limitation. Therefore we can assume that a wind farm or single wind turbine are not always in operating state. What will happen if we switching of turbines for relative short time duration, what happens in case of weak or strong wind speeds and what differences can we estimate between different wind park sizes? Corresponding simulation for result presentation is **T012ug08 TS01HD60F03**.
The aim of this sub chapter is it to make a statement how we can trigger ocean dynamics by switching on and off wind farms. Does the effect suddenly disappear or is it slowly disappearing over longer time? How long will it take to bring ocean dynamics back to reference conditions?

Therefore three OWF operation cases are used for this analysis. An overview of cases is given in figure 4.2.19 including different durations of turbine rotation. Thereby ‘on’ means the usage of rotor disc approach in METRAS, ‘off’ means no use of the rotor disc approach but as mentioned in section 4.1.3 the wind field is affected because the frictional resistance of rotor disc is considered. Additional ‘off_ref’ is implemented which fully ignores the OWF existence.
Forcing is based on **M_T012ug08*onoff**, whose results are introduced in section 4.1.3. The importances of forcing are these three options:
During ‘on’ the wake is developed and increases, at ‘off’ the wake is advected with the main wind field and at ‘off_ref’ the wind field is set to the reference run.

Operation case 01 (**opc01**) starts with 4.2 hours operating wind turbine, followed by 7.8 hours ‘off’, 4.2 hours ‘on’, 4.2 hours ‘off’ and finally 26 hours ‘off_ref’.
Operations case 02 (**opc02**) starts with 4.2 hours ‘on’, 6.1 hours ‘off’ and finally 36.5 hours ‘off_ref’.
Operation case 03 (**opc03**) starts with 2.6 hours operating wind turbines, is then switched off and uses 44.1 hours ‘off_ref’.

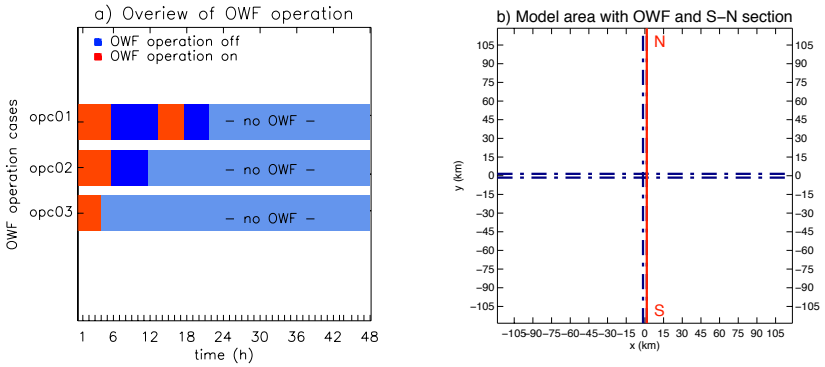

Figure 4.2.19: a) Operation cases opc01, opc02, opc03 and their operating time. Blue is non-operating wind turbines, red is operating wind turbines and cornflower-blue marks simulation where OWF is ignored completely. b) shows y-section (S-N cross-section) through OWF for analysis (red line).

The analysis concentrates on the cross-section from South to North through the OWF, see figure 4.2.19.

Figure 4.2.20/21 and figure 4.2.22 summarize the development of the OWF-effect based on the three operation cases opc01, opc02 and opc03 for velocity field and hydrographic conditions along cross-section S-N through OWF.

Overall the Hovmöller diagrams of the three operation cases strongly differ from previous long-time analysis (section 4.2.1.2), which is based on a constant wind forcing per time step. Due to turning on and off the OWF an additional side effect occurs – an inertial oscillation.

In all three cases it was not possible to bring ocean back to dynamical conditions comparable with reference run. Even in case of absolutely ignoring OWF for more than 44 hours, so after 1.8 days, ocean response on OWF does not fully disappear. In comparison of the three operation cases it can be said that as stronger and longer OWF acts on atmosphere and ocean as longer and stronger ocean is affected.

Whereat changes in hydrographic, figure 4.2.21, do not end up in surprising physically differences, the velocity field, figure 4.2.20, leads to horizontal circulation, which strongly affects the vertical component.

First the **velocities at surface** are analyzed. As expected, with turning on OWF and with it an increase of wind wake, the ocean velocity field is affected by speed reduction in the wake area. Maximal decrease is reached till point of turning off OWF. Although first operation time is quite short, with 4.2 hours for opc01&opc02, respectively 2.6 hours for opc03, the reduction counts around -0.1 m/s for opc01&opc02 and 0.07 m/s for opc03. As indicated in section 4.2.1 the v-component of velocity encroach in the dynamical system by strong changes close to the OWF. The change of v-component compared to the reference run is dominant at the end of the first OWF operation duration.

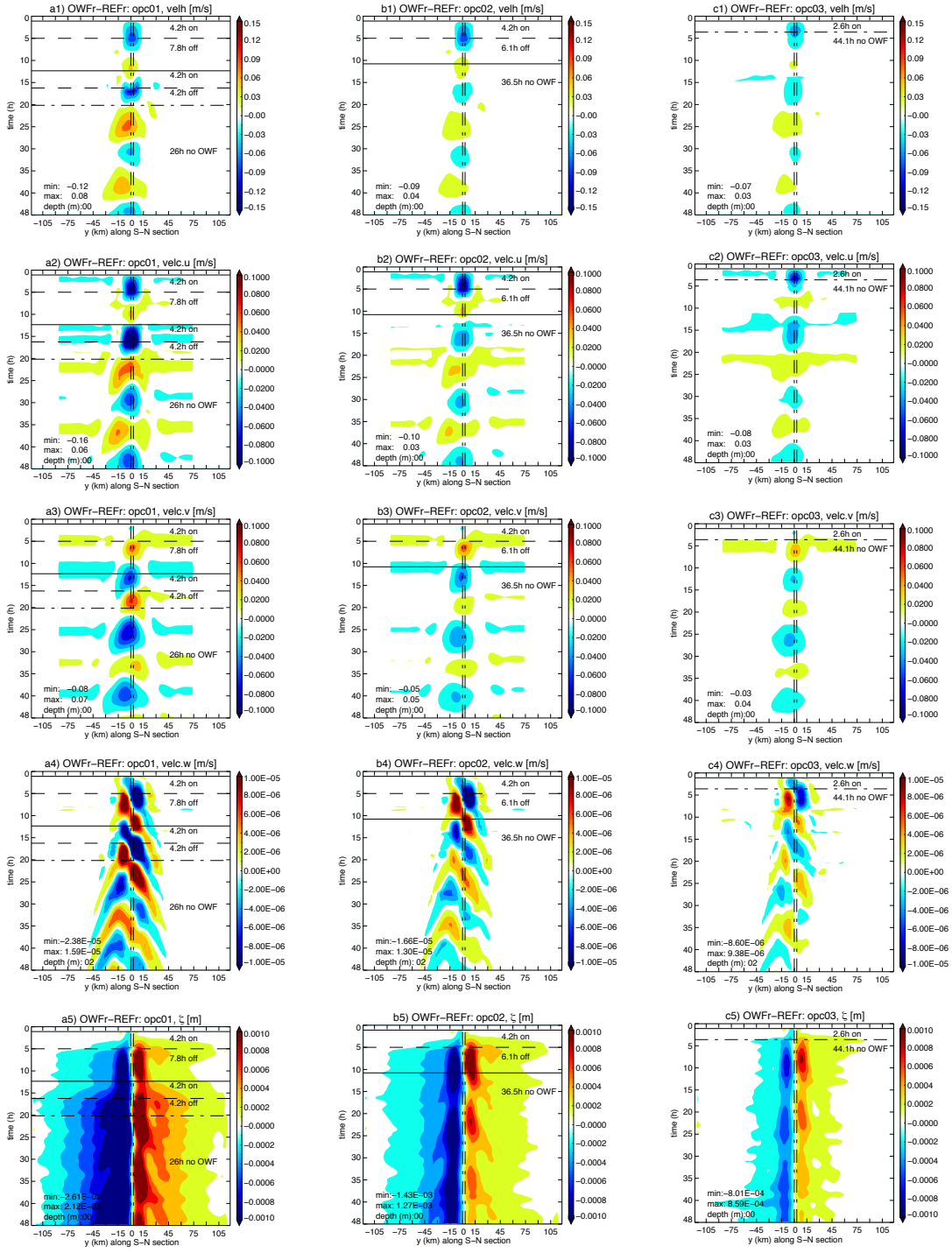

Figure 4.2.20: Hovmöller diagrams of OWF-effect (OWFr-REFr) of hydrodynamics depending on three different cases of OWF operation opc01 (a1-5), opc02 (b1-b5) and opc03 (c1-c5) along S-N cross-section. a1-c1) show results of horizontal velocity field at surface, a2-c2) of velocity component u at surface, a3-c3) of velocity component v at surface, a4-c4) of velocity component w at 2m depths, a5-c5) of surface elevation. Horizontal black lines clarify mode of OWF operation. Here the solid lines shows the start of OWF-operation mode, while dashed horizontal lines stands for switching off/ignoring the OWF. The OWF-district is around y=0km and counts 12 wind turbines. While horizontal velocity component u acts in step with wind forcing, maximum changes of the residual dynamical variables occur time-shifted. After 1.8 days of without OWF signal the OWF signal on ocean still exist, albeit weaker.

V-component increases by 0.04 m/s up to 0.07 m/s at surface. It is a horizontal effect to counteract against wake in u-component and so produced dipole of ζ. At the point of turbine shut down the u-component increases again while v-component is reduced and additional w changes to keep equation of motion.

During that time the dipole structure of **surface elevation** is built in factual connection - as stronger wake is as stronger tilt of ζ is. Formation of extrema for ζ is delayed compared to the velocity wake by more than 5 hours for all three cases. Furthermore it is recognized that surface elevation ζ does not consequently decrease by time during 'off' phase of OWF. It decreases by pulsing. In time differences of 14 hours a weaker extrema of ζ exists, weaken over 7 more hours followed by an increase again to a little weaker extrema than before. Extrema are placed close to OWF but depending on first 'on' duration the horizontal is different affected in the three operation cases. The pulsing of ζ is connected with the vertical cells. Changes in surface elevation and velocity field are concentrated at OWF region, only surface elevation affects more horizontal area by time.

As mentioned, the strongest difference compared to theoretical run with constant forcing over time is detected at vertical **velocity component w** (figure 4.2.20). Turning on and off wind turbines lets expect that the horizontal velocity field varies which affect surface elevation and so vertical motion. But the dynamic is not only pulsing, related to OWF operation, an additional side effect occurs.

Shifted by time the velocity component relative strongly increases by turning of the OWF after 4.2 hours in all three-operation cases.

The diversity between increase and decrease of horizontal velocity components due to the OWF-operation ends in an pulsing of vertical cells, which rotates counter-clockwise around the OWF. With time the core of upwelling/downwelling rotates around the OWF, which leads to the alternating trend with time. The rotating effect only strongly affects an area ±30 kilometers around the OWF center and affects all depths. Such alternating of velocity triggers the increase and decrease of the surface elevation. The rotation of the vertical cells occurs due to a provoked inertial oscillation by turning on and off wind turbines. Movement of vertical cells is counterclockwise with a period of 13-15 hours, which agree with a mean inertial oscillation T around latitude 55.00º of 14 hours based on

$$\boldsymbol{T = \frac{2\pi}{2\Omega sin\varphi}} \qquad \textbf{EQ 4.2.8}$$

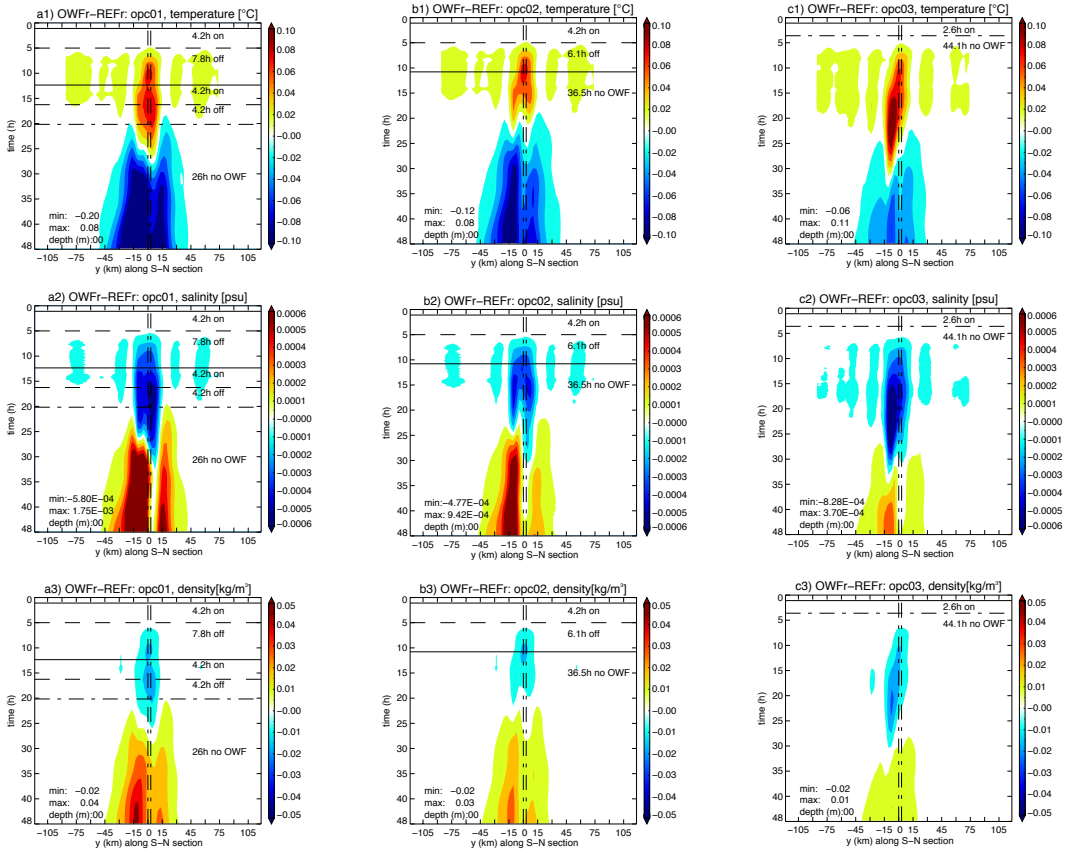

Figure 4.2.21: Hovmöller diagrams of OWF-effect (OWFr-REFr) of hydrographic depending on three different cases of OWF operation opc01 (a1-3), opc02 (b1-b3) and opc03 (c1-c3) along S-N cross-section. a1-c1) show results of SST, a2-c2) salinity at surface a3-c3) of density at surface. Horizontal black lines clarify mode of OWF operation. Here the solid lines shows the start of OWF-operation mode, while dashed horizontal lines stands for switching off/ignoring the OWF. The OWF-district is around y=0km and counts 12 wind turbines. Maximal changes occur parallel to extreme changes of surface elevation.

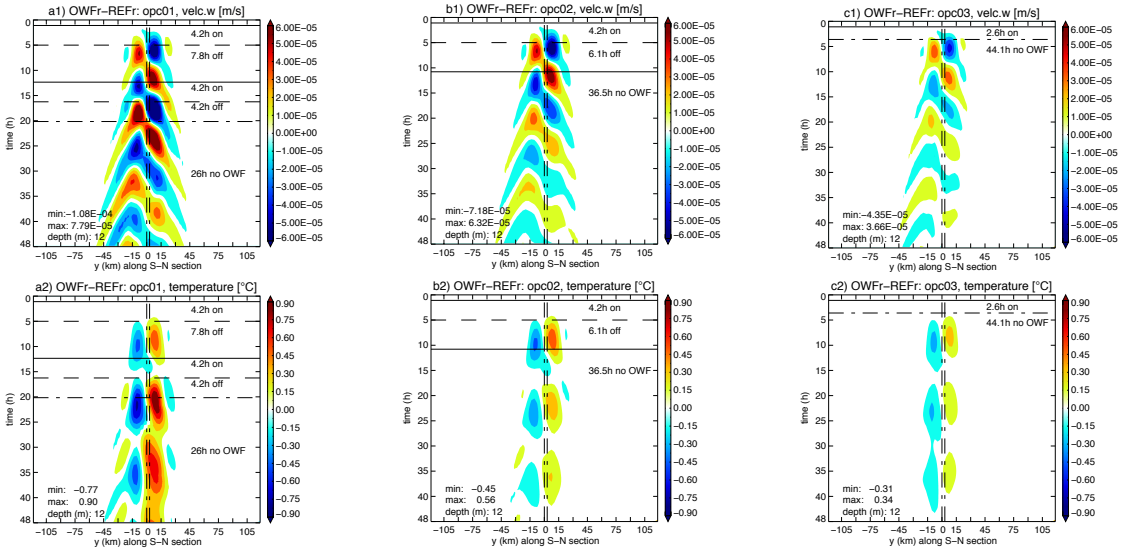

Figure 4.2.22: Hovmöller diagrams of OWF-effect (OWFr-REFr) in 12 m depths of vertical velocity component w (a1-c1) and temperature (a2-c2) along S-N section for the three OWF operation cases opc01 (a1-2), opc02 (b1-b2) and opc03 (c1-c2). Inertial oscillation is obvious seen at w-component.

Due to no coasts and no tides in the model-ocean-box the inertial oscillation cannot be suppressed like in nature.

In the **hydrographic fields** that alternating effect cannot be observed at the surface, see figure 4.2.21. Here it is clearly seen that the OWF-effect on ocean's SST acts delayed becoming obvious after turning of OWF. The OWF leads to a stronger and longer increase of SST than in the operation case opc01 and opc02 after the first power on period. Here the cooling occur around 5 hours earlier due to stronger vertical velocities supported by stronger start-wake and switching on turbines one more time.

Operation case opc02, where the OWF is turned on only once, ends faster in cooling but not as strong as opc01, figure 4.2.21. In case of opc01, where the OWF is turned on again after 7 hours, a SST-warming is longer kept within the OWF influenced area. Similarities occur for salinity and density, see figure 4.2.21. The rotation of vertical cells around OWF affects temperature not at the surface but in the depth. Figure 4.2.22 depicts the evolution of the vertical velocity component w and the temperature at thermocline in 12 m depth. With a delay to the vertical velocity component a significantly temperature reaction occurs but the warming/cooling does not rotate around OWF like the cells of vertical motion. The warming (north of the OWF) and the cooling (south of OWF) only vary due to the rotation of the vertical cells. Due to the inertial oscillation the effect on temperature can be nearly reduced at the turning point from positive vertical motion to negative vertical motion (figure 4.2.22) but the effect on the temperature field is strengthened again when the downwelling/upwelling cell takes effect in north/south of the OWF.

That inertial oscillation avoids a quick re-establishment of starting conditions. It also shows how sensible ocean dynamics are related to a wind field. Hence even a short operation of OWF can induce a mixing, which is connected with temperature changes of 0.5 ºC up to 1.0 ºC within a couple of hours.

4.2.3.2 Analyzing OWF effect on ocean depending on wind speed

The OWF induced wind wake depends beside size and power of the wind farm on the wind speed. Stronger wind speeds result in different strength of wind wakes behind wind farm, which again leads to variation on ocean effect.
To evaluate the wake effect on ocean related to wind speeds three wind speed cases were analyzed. As so far only the wake effect in case of one wind speed based on ug=8m/s has been discussed. In case of METRAS wind turbines operate in case of wind speeds at hub height of 2.5 m/s up to 17.0 m/s (personal correspondence with M. Linde). Thus choice of wind speeds for analysis comprises ug=5m/s (UG5), ug=8m/s (UG8) and ug=16m/s (UG16). The wind forcing shows, that in all three cases the affected area is similar, but stronger wind speed leads to a more intensified effect, section 4.1.2.2.2.

Simulations are based on TOS-01 with the wind farm of 12 turbines directly impacting an area of 36 km^2. Corresponding simulations for result presentation are **T012ug05 TS01HD60F01, T012ug08 TS01HD60F01** and **T012ug16 TS01HD60F01.**

Because of the similar structure of effect on ocean this analysis concentrates on a single point-comparison. The chosen points mark the middle of the model area, so wind farm itself, as well as areas of extreme changes due to OWF. In sum eleven positions at different levels, which are surface, 12 m (depth of thermocline), 30 m (half of model depths) and 60 m (bottom) are included into this analysis. These positions are pictured in figure 4.2.23.
A single point analysis is chosen to accent discrepancies over whole OWF-affected area. Independent of wind speed velocity wake, dipole in surface elevation and vertical cells occur. In case of UG 5/8/16 m/s vertical cells have a dimension of 15/30/30-40 km width and clearly affect depths till 30/60/60 m. Therefore difference in simulations at investigation positions dominantly varies between P-3 and P+3 for all variables.

Correlation (COR) of results along the single points and the root mean square difference (RMSD) are used as a statistical tool to analyze accuracy of simulation results based on forcing of three different wind speeds. Here RMSD is used as a measure of the discrepancy among the three different model samples to compare values due to different forcing cases. In the following the effect on ocean due to wind farm is examined.

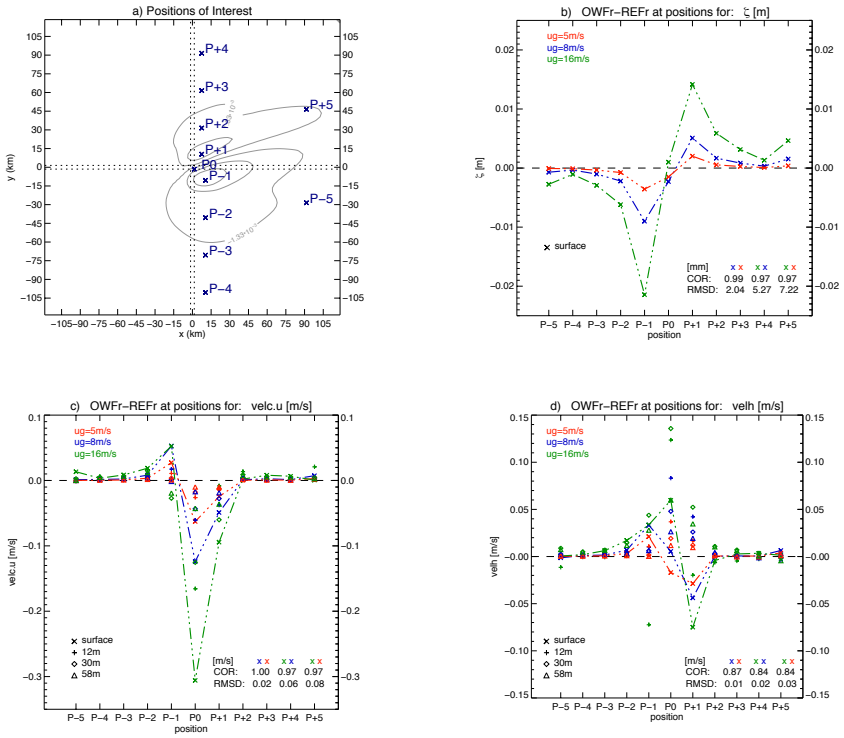

Figure 4.2.23: a) Positions of interest for analyze of different wind speed conditions chosen by effect's extreme (here clarifies by grey contour lines of surface elevation in m) x-position. P0 points the OWF center, P+ is 6 km , P- 9 km easterly. b)-c) show OWF's effect after one day of simulation by surface elevation ζ (b), velocity component u (c) and horizontal velocity field (d) forced by ug=5 m/s (red), ug=8m/s (blue) and ug=16 m/s (green). Different symbols stand for different depths; 'x' surface, '+' 12 m, '◊' 30 m and 'Δ' 58 m close to bottom. COR gives correlation and RMSD the root mean square for corresponding values and depths.

At all the analysis of the three sets of wind speed forcing in section 4.1.2.2.2 shows that a relative stronger wind field means already a more intense wind wake. Considering METRAS' wind turbine parameterization the rotor thrust grows with the cube of velocity, so in case of higher wind speeds turbines are able to detract more energy out of atmosphere and therefore wind reduction behind OWF is intensified. An intense wind wake results in an intense velocity wake of the ocean velocity u-component. Figure 4.2.23 documents that fact. Overall extrema of variables mostly increases with increasing wind speeds. The strongest effect is identified at thermocline in 12 m depth while at surface, 30 m or at bottom effects are consequently smaller.

The effect of **velocity component u** along investigations point P-5 to P+5 over area, based on different UG-speeds, has its wake at position P0 within the OWF and is high correlated by 1.00 between forcing UG5 and UG8 and 0.97 between UG5, respectively UG8, and UG16. By means of the correlation of the three different **horizontal velocity fields** it becomes clear that velocity component v exerts a diverse impact on the velocity field. The stronger the wind forcing is the higher are the discrepancies. Correlations along investigation points with UG16 are only of 0.84 at

surface. Between UG5 and UG8 forcing exist little fewer differences, 0.87 correlates them. Wake magnitudes at surface have a linear character and RMSD increases with wind speed difference.
The effect of **surface elevation** ζ shows a similar distribution; having a maximum at P+1 and a minimum at P-1, with a high correlation between UG5, UG8 and UG16, see figure 4.2.23. Results for ζ at investigation points have a weak root mean square difference between the runs of different wind speeds. The stronger the wind forcing the more distinctive is the extreme of ζ dipole structure. The growth of extreme leads to an exponential character but cannot be specified due to only three wind cases.

The fact that a stronger wind results in a stronger effect on ocean surface, the effects on vertical velocity and temperature must be consequently intensified. Effect on **vertical velocity component** and **hydrographic parameter** compared by different forced wind speeds are pictured in figure 4.2.24. The maximal upwelling along investigation points occurs at point P-1 for all three wind cases through all layers. The strongest downwelling is placed at P+1 for wind case UG5 and UG8, while for UG16 the maximal downwelling can be find at P0.
Figure 4.2.25 illustrates that maximal upwelling velocity at 12 m nearly fits the same position, only the run based on UG16 forcing has its maximal upwelling one grid box (~3km) easterly of result based on UG5 and UG8 forcing. Regarding to maximal downwelling, the effect at 12m of run with UG16 forcing has its extreme within the OWF, while extremes of UG5 and UG8 forced runs are placed more northeasterly. It seems that with increased wind forcing the position of downwelling switches more towards midpoint of OWF but only based on three cases it is not possible to make a statistical fundamental statement. Nevertheless it can be underlined the stronger the wind speed forcing is the stronger vertical motion will be, especially in deeper layers. The strongest upwelling at 2 m, at position P-1, is identified by simulation with forcing UG8, figure 4.2.24 a). This does not enervate the termed relation because at surface extrema are also affected by horizontal flow and so positions of extrema are not defined at same location, which also causes a bad correlation. That is why here run, forced with UG16, gives only the lowest upwelling. However maxima/minima of vertical velocity w is 1.04×10^{-5}/-0.77×10^{-5} m/s (for forcing UG5), 1.54×10^{-5}/-1.10×10^{-5} m/s (for UG8) and (for UG16) 0.0246/-0.0194 mm/s over whole area and within first 2m depths.

Further an increase in wind speed forcing results in a swift of positions of maximal and minimal vertical velocity into higher depths. Figure 4.2.25 clarifies the dependence between induced wind speed, depth and extrema. Additional, it can be said that the upwelling effect is a little bit more dominant than the downwelling one and that the discrepancy between these two motions increases with wind speed.

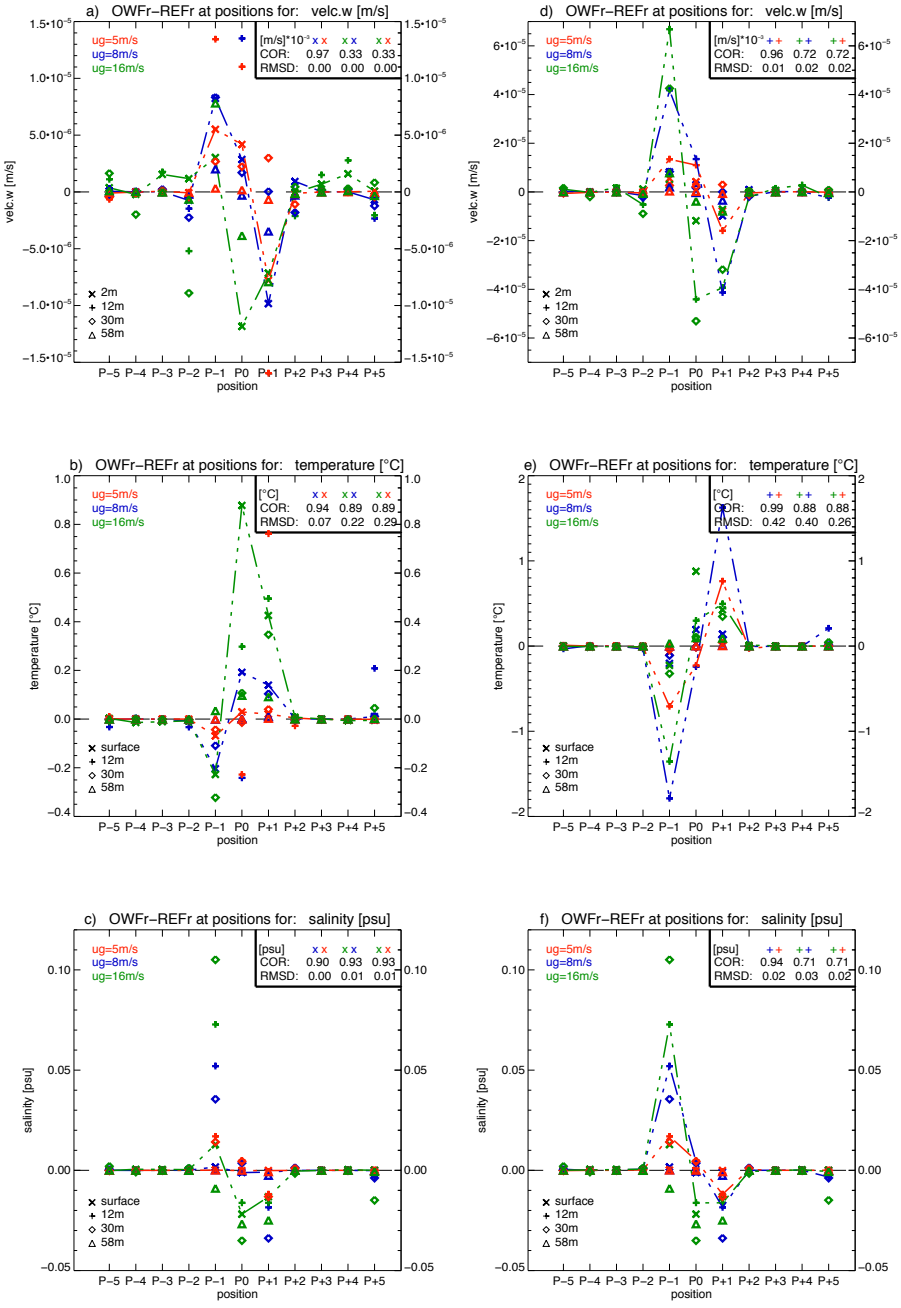

Figure 4.2.24: OWF's effect on ocean due to three different wind forcings after one day of simulation at positions given in figure 4.2.23a). a-c) focuses on surface, respctively 2m for velocity component, d-f) on 12m depth. Rows show from top to bottom a,d) velocity component w, b,e) temperature and c,f) salinity forced by ug=5 m/s (red), ug=8m/s (blue) and ug=16 m/s (green). P0 points the OWF center, P+ is 6 km , P- 9 km easterly of N-S cross section. Different symbols stand for different depths; 'x' surface (respectively 2 m for velc.w), '+' 12 m, '◊' 30 m and 'Δ' 58 m close to bottom. CORR gives correlation and RMSD the root mean square for corresponding depths marked with a-c) symbol 'x' and d-f) symbol '+'.

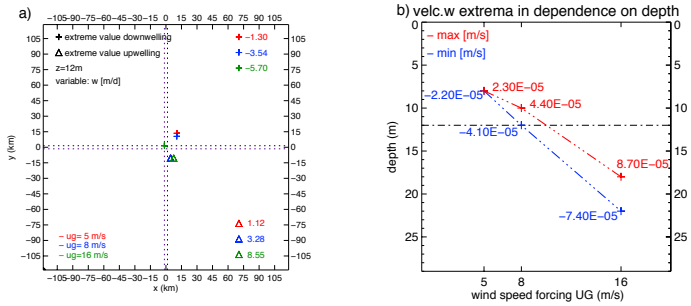

Figure 4.2.25: a) Position of extremes of variable w in 12 m depth and b) extremes of w in the vertical along y-section based on different wind speed forcing. In the depth of thermocline, so 12m, the position of positive extreme is comparable between different wind speeds, while the negative extreme swift into OWF with increased wind forcing. Negative maxima are slightly higher than the positive ones and positioned in deeper layers.

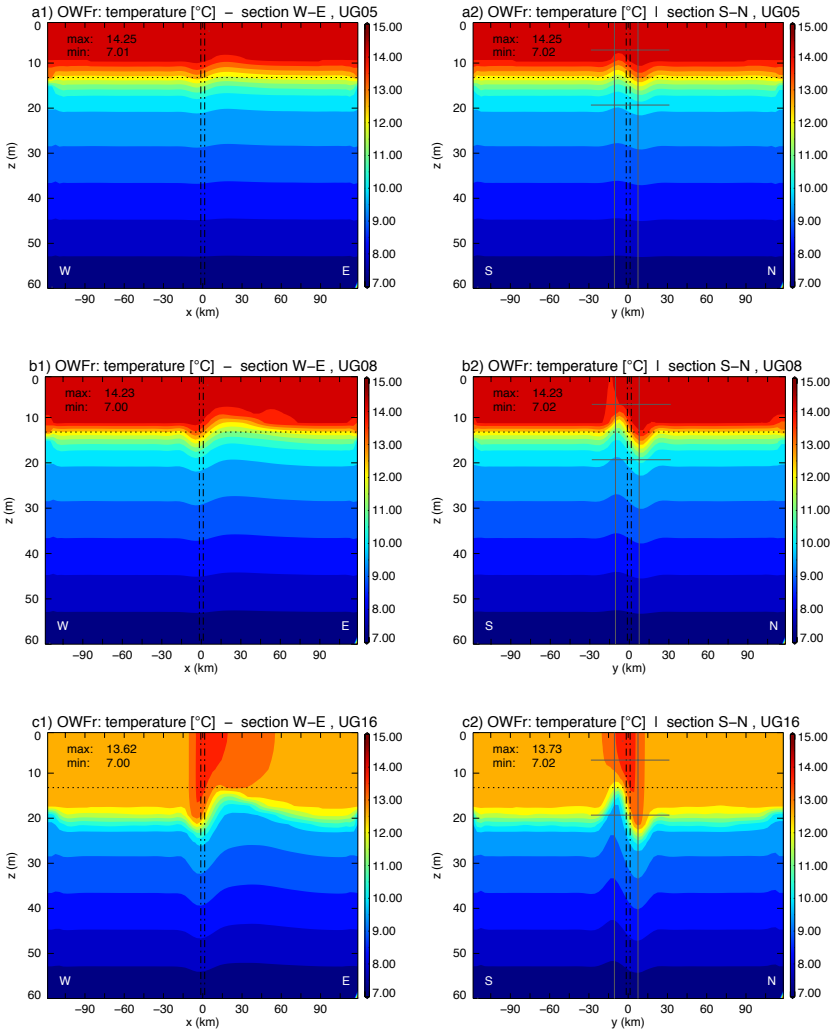

Figure 4.2.26: Temperature profiles along a1-c1) W-E and a2-c2) S-N sections through OWF based on different wind speed forcings of a1-a2) 5 m/s (UG5), b1-b2) 8 m/s (UG8) and c1-c2) 16 m/s (UG16) Excursion of thermocline around OWF based on UG08 is marked by solid black horizontal lines. Excursion increases with stronger wind speed. Additional, thermocline is shifted to deeper layers.

The effect of the forcing of 16 m/s wind speed ends in a **temperature** increase at surface of 0.88 ºC at position P0 and a decrease of 0.23 ºC at position P-1, figure 4.2.24 b). Maximal temperature decrease at P-1 due to forcing of UG8 is slightly weaker, -0.20 ºC and for UG5 forcing only -0.07 ºC. The temperatures are higher than in the reference run at the downwelling area. At this forcing of UG16 has the strongest effect of 0.88 ºC increase, compared to 0.19 ºC/ 0.03 ºC for UG8/5. Although the vertical velocity component w at the thermocline is more intense for UG16 forcing than for UG8, the temperature extrema at thermocline are maximal in the case of forcing UG8. This underlines the previous analysis that vertical mixing is not single driven by the vertical velocity component w but also by additional exchange processes. Additional a stronger wind forcing quickens processes; that is also a reason for weaker temperature effects by UG16 because upper layers are faster mixed, which originate one abundant upper layer. In turn the thermocline is pushed into deeper depths

The shift of the **thermocline** position is pictured in figure 4.2.26. The change from UG5 to UG16 forcing at thermocline is clearly seen. Excursion increases with wind speed forcing from two (UG5) over four (UG8) up to eight (UG16) meters. In case of UG16 the thermocline is switched from beginning 12 meters to 20 meters depths. Correlations of temperatures with forcing UG16 are around 0.15 higher than for the vertical velocity component w at thermocline. Correlations between UG5 and UG8 are high with 0.94 at surface and 0.99 at thermocline.

The effect on **salinity** forced by the three different wind speeds has a weak variability in comparison due to goof correlations of around 0.9 at surface, figure 4.2.24 c) and f). Differences of the effect mostly occur in the downwelling region at positions P0 and P+1, especially in the thermocline depth. However the OWF-effect on salinity increases with wind speed forcing.

Upshot

Summarized the effect of an OWF on the ocean, considering different wind speeds, does not impacts strong on horizontal dimensions. Dipole structure, up- and downwelling cells have similar dimension because they depends more on the OWF arrangement. Positions of maxima and minima vary due to differences in the horizontal velocity field, which depends on the wake intensity. Here a trend of extrema moving towards the OWF grid boxes with higher wind speed forcing was detected. That behavior is based on the fact that the maximum decrease in wind is placed close to the OWF and so affects here stronger on the ocean. The cells of vertical motion become more intense with higher wind speeds and cell's extrema occur in deeper layers, which stronger affects vertical layers again. Stronger OWF induced wind wakes support the vertical mixing and leads to a stronger exchange of temperature via the thermocline. Hence the depth of the thermocline increases with wake intensity. The variation of the OWF-effect due to different wake intensity in temperature is in order of tenths of a degree, even for the horizontal velocity component u and variations of the surface elevations counts several millimeters, for the vertical motion hundredths of mm/s.

Overall an increase in wind speed leads to an intensification of OWF-effect and accelerates ocean's reaction on wind wake in order of tenths and hundredths. If we consider that shown results after one day of simulation are based on runs forced by a constant wind field we can assume that slightly changes over a day in the wind field will not strong affect ocean's reaction on the wind wake but will impact the magnitude of changes on ocean variables and especially the depth of thermocline.

4.2.3.3 Analyzing OWF effect on ocean depending on wind park power

So far presented effects on ocean are based on a wind farm of 12 turbines spanning 4 grid cells, so an area of 36 km^2. Compared to the international interurban offshore wind farm program such a wind farm is very small. In future one wind farm will embrace a much higher amount of wind turbines starting from 50 up to 160 turbines. This section illustrates ocean's effect due to different wind wakes based on various wind farm sizes. Simulations are based on TOS-01 (ocean box) with an induced wind speed of ug = 8 m/s. Detailed explanations of wind forcing are given in section 4.1.2. There it is perceived that due to model setup and model resolution distinctions between wind-wakes are rare and due to big grid cells of 3 x 3 km the affected areas are similar. Corresponding simulations for result presentation are **T012ug08 TS01HD60F01, T048ug08 TS01HD60F01, T080ug08 TS01HD60F01, T160ug08 TS01HD60F01.** Simulations are based on forcing sets including OWF of 12 turbines (T012), 48 turbines (T048), 80 turbines (T080) and 160 turbines (T160). Affected grid cells are 4 for 12T and 48T, 16 for 80T and 32 for 160T. Results here are again focused on one day simulation time step.

Figure 4.2.27 summarizes the four different wakes in velocity component u based on different OWFs, which were identified as a fingerprint of the wind field.
Comparing the effect on the u-component at surface the runs with different numbers of wind turbines leads to a similar structure of the OWF induced change, which mostly depends on the OWF-area. In run with 80 wind turbines a stronger exhaustive change between OWFr and REFr occurs, especially a northerly increased wake-flank, figure 4.2.27 c1), due to stronger wake-flanks in the wind forcing.
The affected area of run T012 and T048 is identical due to same number of grid cells comprising wind turbines but the velocity wake in the u-component is little more intense by T048 with a minimum at surface of -0.139 m/s compared to -0.136 m/s for T012. A reason for difference rests in a different magnitude of the wind field due to the considered power and amount of wind turbines in METRAS wind turbine parameterization. In the case of T080 and T160 the wake is deformed by the OWF-area and therefore the wake width in y-direction is bigger for T080 and T160 compared to T012 and T048. As in case of the wind field the ocean's u-wake grows with numbers of wind turbines, means with the OWF-area. Depending on the affected area by the wind-wake the u-component and already the velocity field implicates a disturbance which is more addicted to the wind wake district. In all four cases the minimal u-velocities occur within the OWF or in case of a wider OWF a more northerly. Wake flanks are more intense in case of a bigger OWF and so the wake-flanks of increased velocities stronger impacts deeper layers than T012.

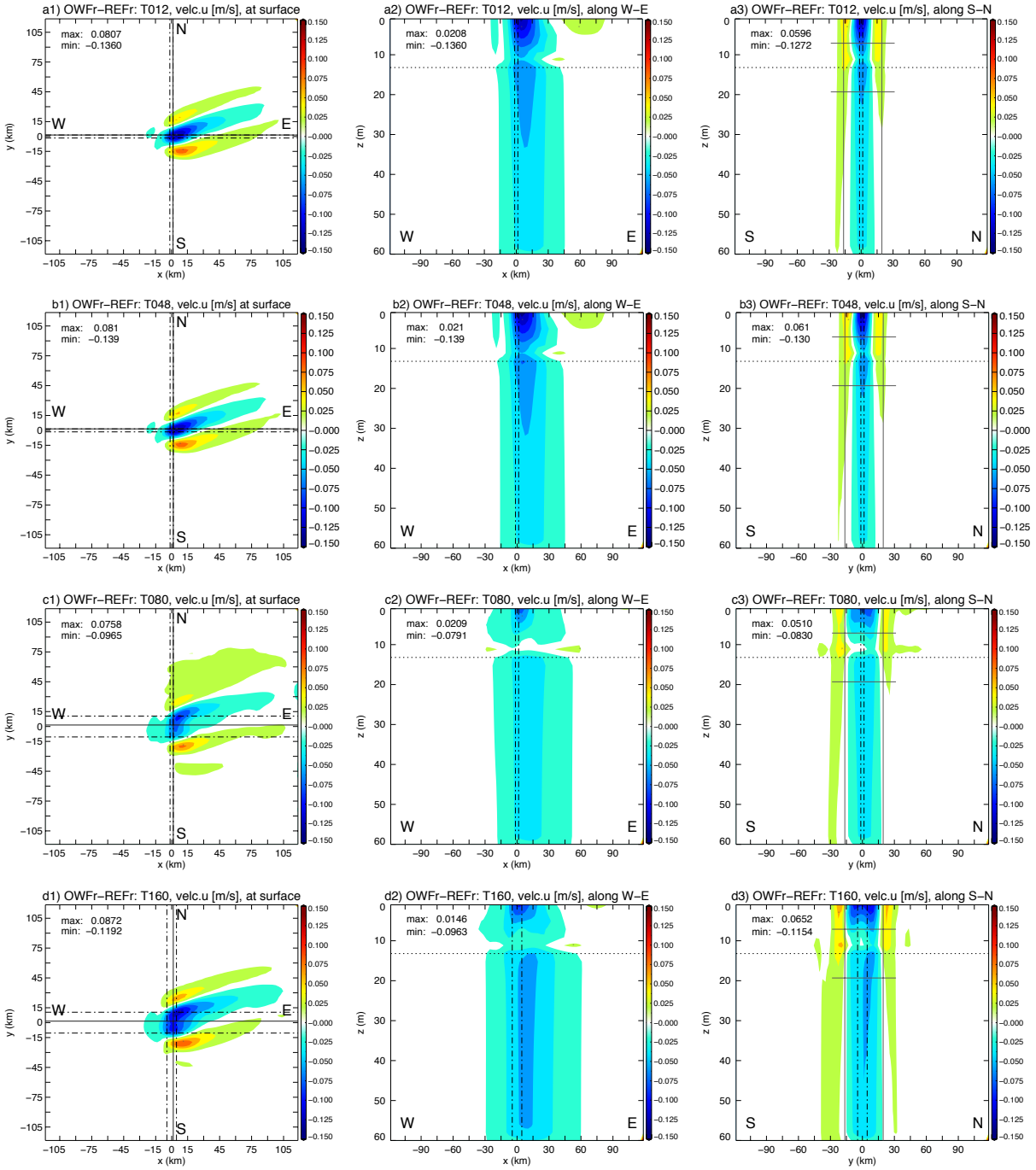

Figure 4.2.27: Change of velocity component u (velc.u) due to different amounts of wind turbines. a1-a3) illustrated velc.u in case or T012, b1-b3) T048, c1-c3) T080, d1-d3) T0160 at a1-d1) surface, a2-d2) along W-E section and a3-d3) along S-N section through OWF. Dashed dotted lines encase OWF district. Solid lines denote cross-section through OWF and dotted lines in section plots marks depth of thermocline based on T012. Units are given in m/s.

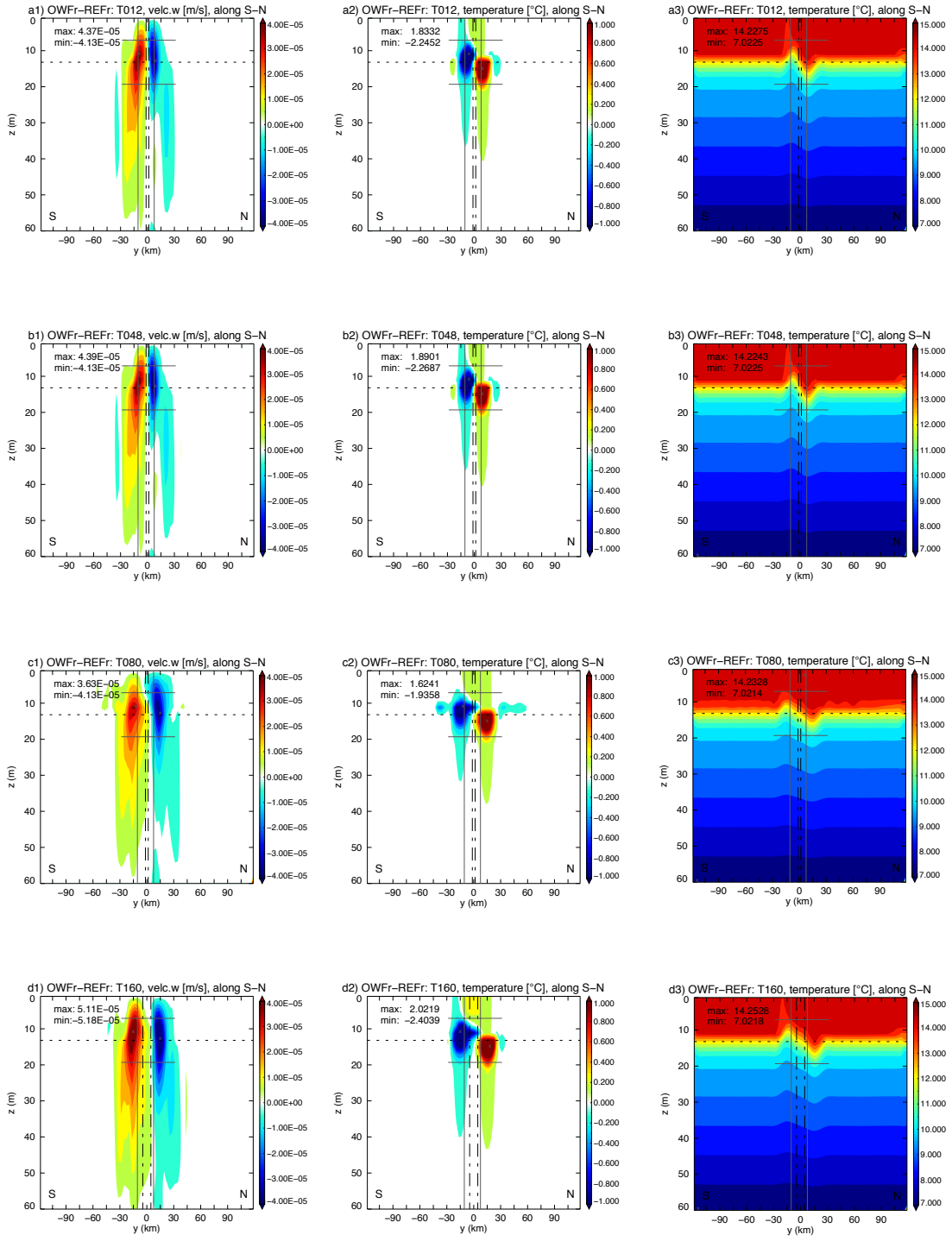

Figure 4.2.28: Effect of a1-d1) vertical velocity component w and a2-d2) temperature and a3-d3) temperature stratification of OWF run based on 12 turbine (a), 48 turbine (b), 80 turbine (c) and 160 turbine (d) OWF along y-section through OWF from S to N. Crosses marks position of maxima and minima, dashed line illustrates depth of thermocline and limits of thermocline exclusion is mark by short black solid lines based on T012.

The maximal wake magnitude is given by T048, as mentioned in 4.1.2 reasons for that context is that in T080 and T160 more grid cells, filled with fewer wind turbines, are astonished by the wind turbines.

Although the wind-wakes, based on various amounts of turbines, do not show strong difference in magnitude, the influence of more grid cells by wind turbines indicates variations in ocean conditions. In all four cases the changes occur in the vertical, with two main vertical cells, and consequently in the temperature field, illustrated in figure 4.2.28. The more grid cells are affected by the wind reduction the more intense are the vertical velocity cells with a maximal global mean of downwelling and upwelling for T160 of -1.68E-06 m/s and +1.83E-06 m/s. The extrema along S-N cross-section through OWF are in order of 10^{-5} m/s and as bigger the OWF is as stronger is the intensification of the vertical motion, especially for downwelling. While upwelling varies stronger between the simulations the downwelling is constant with a minima of -4.13E-05 m/s.

The vertical effect is also quite consistent. The extrema of velocity component w in 12 m depth have the same maxima/minima location for T012 and T048, respectively T080 and T160, figure 4.2.29 a). The extrema of the vertical cells along S-N section are also located in same depths for all turbine assumption apart from T48 having maximal upwelling in 12 m and not in 10 m, figure 4.2.29 b). A maximal downwelling is registered along the S-N cross-section in 12 m depth for all OWF sizes.

Figure 4.2.28 also represents the effect of wind turbine amount on the temperature in the vertical. Thermocline stays at 12 m depths for all four simulations. In space of intense vertical mixing temperature variations occur with maxima beneath and minima above thermocline.

Among run T080 the temperature stratification is only affected around the OWF. Simulation run T080 shows a little cooling at thermocline along S-N cross-section due to the different wind field and therefore a diffuser surface elevation. It can be said that a different number of turbines operative affect the excursion of thermocline around the OWF. The excursion of the thermocline is more horizontally distorted in the case of greater OWF-districts, figure 4.2.28 a3-d3). But the horizontally distortion has hardly influence on the vertical dimension of excursion in contrast to wind speed effects. Neglecting T080 the change in the temperature increases with the OWF sizes due to temperature advection by vertical motion and is supported by wider vertical cells of changes and horizontal diffusion.

Figure 4.2.30 clarifies the fact that affected grid cells play a much more important role for the effect on the ocean than the number of turbines. Extrema of the surface elevation increases with OWF-size and number turbines. A comparison of the surface elevation along S-N cross-section results in a good correlation of 0.90 up to 1.00 with an RMSD in order of 10^{-3} m and 10^{-4} m for run

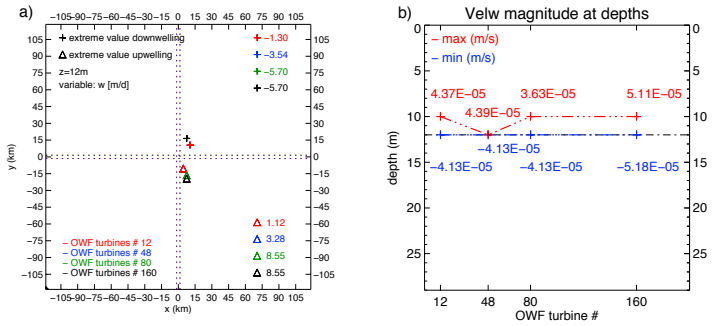

Figure 4.2.29: a) Location of extremes of variable w in 12 m depth and b) variations of overall maxima and minima along y-section from S to N in dependence of depth.

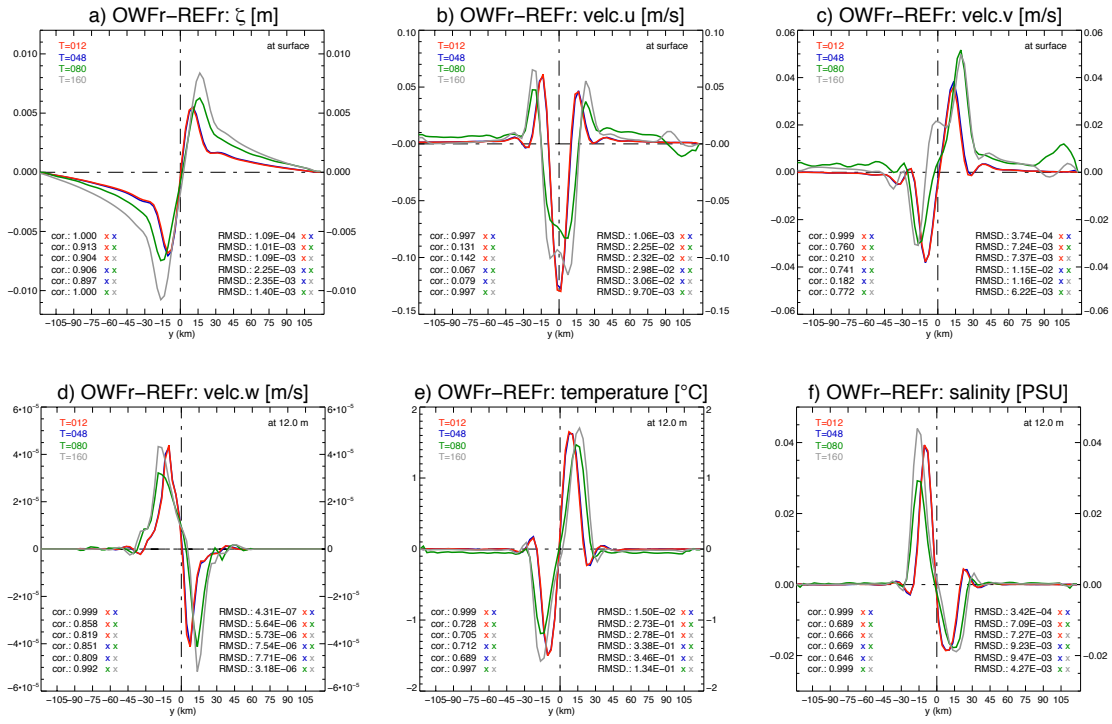

Figure 4.2.30: Comparison of ocean variables changes due to OWFs. a) surface elevation, b/s) velocity component u/v at surface, d) velocity component w at 12 m, e) temperature at 12 m and f) salinity at 12 m. Results are colored for T012 in red, T048 in blue, T080 in green and T160 in grey. Blue and red curves strongly fit each other. Corr, gives correlation and RMSD root mean square difference between lines corresponding to colors of symbol 'x'.

T012 and T048, figure 4.2.30 a). The runs T012 and T048 (wind turbines are scattered over four grid cells) show along y-cross-section from S to N at surface and as well in 12 m depth a high correlation of 0.99 and better for the velocity components u, v and w as well as for hydrographic variables, figure 4.2.30 b-f).

Independent of v-component T080 and T160 are even well correlated for almost all ocean variables by 0.99 and better. Discrepancies between T080 and T160 in the velocity v-component (correlation of 0.77) relate to the difference of affected grids (16 and 32) and discrepancies in the wind forcing field.

The important factor of the OWF-size regarding grid cells is highlighted by the comparison of runs with OWFs over four grid cells (T012&T048) to runs with OWFs over more grid cells (T080&T160). Here correlations, along representative S-N cross-section, are almost bad for velocity components u and v and tends often to the statement of not being correlated. Horizontal variations due to the OWFs along the cross-section S-N impact the correlation value in figure 4.2.30 a-b). The simulations of different OWFs result in good correlations for the variables velocity component w, temperature and salinity at 12 m depths along cross-section S-N (figure 4.2.30 d-f)). Here the stronger agreement underlines the connection of formation of up- and downwelling to surface elevation. The change of the ζ-dipoles more to the north for ζ-increase and to the south for ζ-decrease is also identified in w-component and hydrographic conditions. The distortion of thermocline in dependence to the OWF-area is also documented in figure 4.2.30 e) based on the horizontal dimension of the temperature excursion.

Upshot

The comparison of the effect on ocean due to different wind farm sizes results in the assumption that the wind farm size does not impacts vertical mixing in a direct way. Different wind speed forcing cases stronger impacts on the vertical stratification. But the wind farm size amplifies the effect in the horizontal. The magnitude of vertical mixing slightly varies due to the different amount of affected grid cells and the maximal anomaly between T012 and T160 in the temperature counts 0.25 ºC. The results of that analysis come in force that greater OWFs have a comparable effect on ocean to smaller wind farms. But based on issues of the horizontal resolution and wind-wake presentation it must be considered that a finer grid in case of T012 will may result in a horizontally smaller wake dimension orthogonal to the wind direction. Hence the effect on ocean would be weaker.

Therefore the outcome of that analysis cannot be generalized at this point. A more detailed wake illustration simulated by higher resolution would be necessary for a final statement.

But results can be generalized for velocity wakes at ocean surface. A slightly wider wake does not change stratification in the vertical but triggers impact in the horizontal. Although vertical cells become slightly wider the magnitude of vertical mixing stays nearly stable.

4.2.3.4 Analyzing OWF effect due to wind forcing based on Broström approach

Section 4.1.2.1 introduces a simple approach to describe wind reduction behind one cubic wind farm developed by Broström [*Broström*, 2008]. That approach can be used for relative big wind farms. The here used wind farm located over four grid cells, thus comprising an area of 6 km x 6 km, almost complies with a large wind farm compared to used wind farm of 0.15 ºE (~9.56 km at 55ºN) in LOIZ report 2010 [*Lange et al.*, 2010], where Broström approach is employed. Although effect on ocean using Broström approach for wake description is documented, the approach is not fully evaluated so far. A comparison between wind forcing considering OWF effect by METRAS approach and Broström approach enables the identification of contrasts. Simulations considered for that analysis are the master simulation using METRAS forcing **T012ug08 TS01HD60F01**, here abbreviated and denoted as F01, and the run **T012ug08 TS01HD60F04**, denoted as F04. Thus ocean conditions are the same and only forcing differs in dimension, formation and intensification of wind wake.

The difference between run OWFr and REFr of ocean variables, surface elevation ζ, velocity component u and w and temperature, due to the two different wind wake approaches after one day simulation are documented in figure 4.2.31. It is apparent that the Broström forcing (F04) also results in the common OWF-effect on ocean. In the case of F04 the ocean shows the velocity wake, the dipole structure of surface elevation ζ and the up- and downwelling cells connected with cooling, respectively warming. But the formation and dimension of the occurred OWF impact on the ocean system differs obviously in comparison to the METRAS forcing (F01).

In case of velocity **u-component** the velocity wake by F04 is 0.092 m/s deeper than in F01 based on extrema at surface but the wake is spanned nearly along W-E cross-section through the OWF (figure 4.2.31). A maximum reduction of the u-component by F04 is placed within the OWF at the southeasterly grid box (OWF consist of four grid boxes) but the wake trail is totally dislocated compared to F01, which has its maximum reduction in the northeasterly grid box of the OWF-district. In case of F04 wake slightly tends to SW direction, but geostrophic effect is limited due to the short wake length downstream of the wind farm. Based on satellite data, mentioned in chapter 4.1, Broström approach underestimates the wake dimension. The stronger wake magnitude after one day of simulation is explainable by the compact and locally more limited effect on the ocean.

A more detailed view of the **surface elevation** reveals that the formation of ζ, in case of F04, varies in dimension compared to F01, which is connected to the dependency of the velocity wake and ζ.

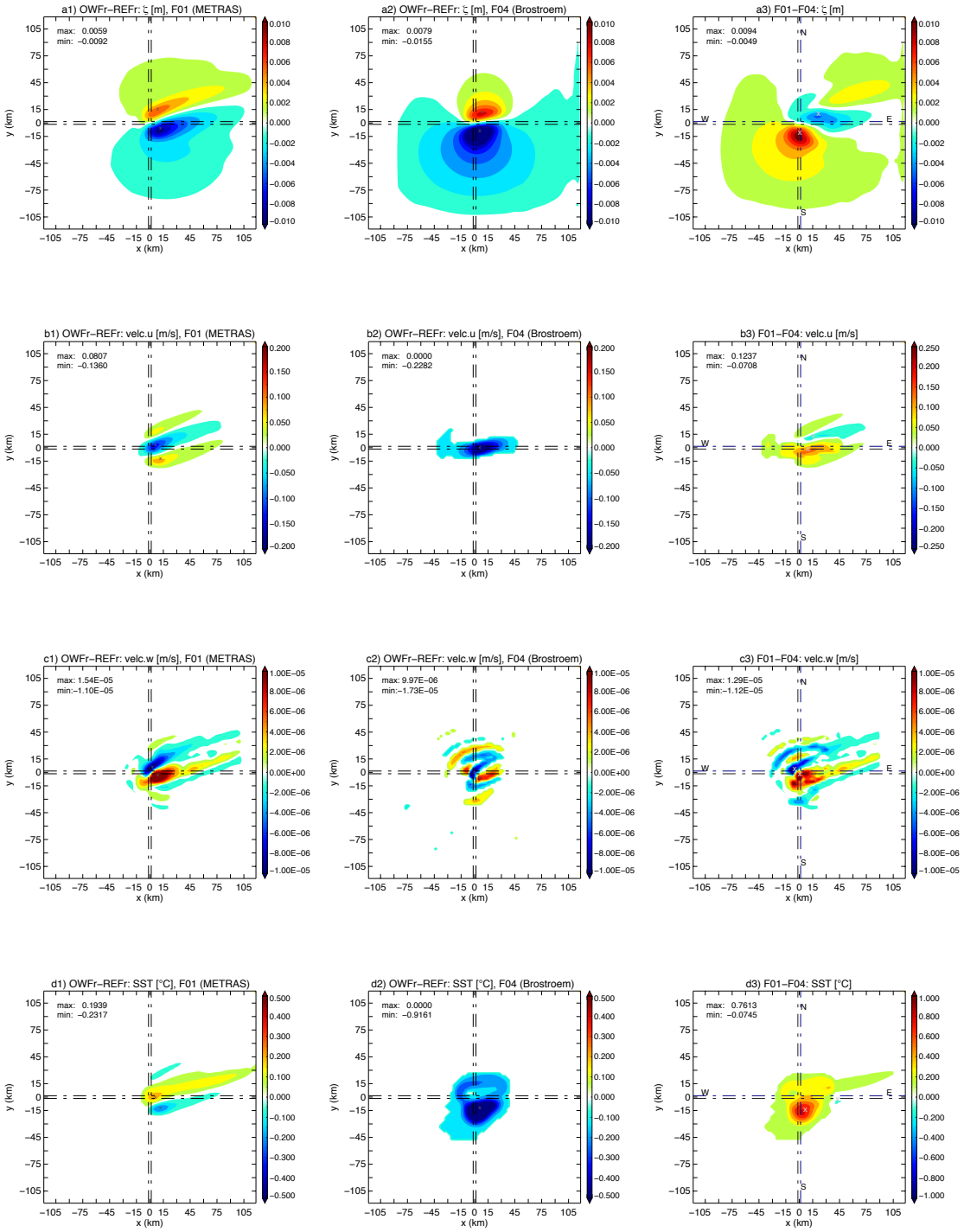

Figure 4.2.31: Comparison of simulated OWF effect on ocean using a1-d1) forcing F01 (METRAS approach) and a2-d2) forcing F04 (Broström approach). a3-d3) gives difference between F01 and F02. Ocean variables are a1-a3) surface elevation ζ, b1-b3) velocity component u at surface, c1-c3) velocity component w at 3 m depth and d1-d3) sea surface temperature SST.

Considering the whole model area the significant positive effect on ζ is spread over a smaller area in the case of F04, even though the affected area comprises a greater uniform/denser spaced increase than F01 shows. However the location of ζ-extrema differs by maximal two grid boxes, so 6 km distance (compare positions of extreme in tables 1 and 7 in appendix E).
The ζ-maximum of F02 and F04 is biased by 2.7E-4 m, while F04 has the stronger increase. In opposite to the positive part of the ζ-dipole the area of lower surface elevation stronger affects a wider area, so nearly the whole model area southerly of the OWF, while changes in F01 are more concentrated at the southeasterly part of model area, Figure 4.2.31 a1-a3). Again F04 also dominates the effect on the negative ζ-dipole with -0.016 m compared to F01 with -0.009 m changes. The impact of the wind direction on the ζ-formation is stronger by F01 due to a longer wake trail downstream behind the OWF. In the case of Broström approach (F04) that effect is more or less neglected, which leads to a ζ-formation being nearly parallel to the cross-section W-E, only having an inclination to it of 13.50º.

The occurrence of **vertical motion** is identified in both forcing cases but in the case of F04 the downwelling and upwelling is not described by two main cells – a blurred transition of three downwelling zones and three to four upwelling zones around the OWF is established after one day of simulation (Figure 4.2.31 c1-c3). The induced downwelling by the OWF in the area of the positive ζ-dipole results in flanked upwelling and hence again in downwelling zones. The downwelling is with -1.73E-05 m/s stronger for F04 than in the case of F01 having -1.1E-05 m/s. But the upwelling is about 5.43E-06 m/s weaker by F04. Due to that the difference in the velocity component w between F01 and F04 (Figure 4.2.31 c3), the dominant upwelling cell of F01 and the dominant downwelling areas of F04 can be explained. In the vertical along S-N cross-section, in figure 4.2.32, the impact on the vertical motion in case F04 significantly includes more intensive affected vertical layers, especially within the OWF than F01 due to horizontal distribution of ζ, the u-velocity wake and thus the distribution of vertical motion in the horizontal. Therefore the extrema of the w-component are placed in lower layers, so below the thermocline for upwelling, which is for F01 above the thermocline. Maximal differences in the w-component between F01 and F04 are in order of 5E-06 m/s for downwelling and 2E-05 m/s for upwelling, with the dominant effect given by F01. Again upwelling is stronger influenced by changed external model assumption than downwelling.

Although upwelling is weaker in case F04, in 12 m depth and hence in layers above, the **SST** pictured in Figure 4.2.31 d1-d2) shows a cooling of -0.92 ºC. Here the SST is not triggered by vertical motion because the cooling is an effect of the declination in the surface elevation.

Though the METRAS approach yields to a greater vertical motion but the effect on **temperature** is overall stronger influenced by F04. Besides, the cooling of SST the use of F04 results in typical warming and cooling formation around the OWF along the S-N cross-section (Figure 4.2.32 b1).
The horizontal dimension of the cells of temperature changing is wider (along S-N section) in case of F04. But the location of cell's extrema nearly fits with run F01. The temperature extrema of cooling are located at 10 m depths, of warming at 14 m depths in both forcing cases. The discrepancies in the horizontal count more than 3 km (tables 1 and 7 in appendix E).

The more intense warming in F04 is related to a continuous downwelling cell from surface to bottom with continuous high vertical velocities within the OWF than in case F01. Continuous vertical velocity cells support temperature advection over the entire ocean depth, which explains stronger changes at the thermocline.

Figure 4.2.33 illustrates the impact of run F01 and run F04 on the excursion of thermocline. Finally the Broström approach leads to a more significant effect at upper layers with a slightly stronger excursion at the thermocline than the METRAS approach. At depths below 40 m the excursion is stronger by F04, hence F04 fortifies the OWF-effect over the vertical layers. Du to this analysis it can be assumed that a stronger effect on surface elevation forwards temperature changes in the vertical. Hence the Broström approach helps to identify the impact of an OWF on ocean but tends to an overestimation of the OWF-effect especially for temperature changes.

Upshot:

The Broström approach (F04) was defined for theoretical analysis of wind farm effects on ocean surface having a quadrate, cubic arrangement. Nevertheless, as mentioned, here the produced OWF wind wake is too small compared to the METRAS approach (F01) and satellite data. However the Broström approach is considered here to elucidate that especially the wind wake plays an important role, due to physically reasons given in 4.2.2, and triggers the ocean system. The flanks of the wind wake, being simulated by METRAS, have a secondary role on ocean's reaction and mainly support an upwelling zone. Anyhow the use of the Broström approach is restricted and not as realistic as the METRAS approach. As mentioned in 4.1.2.2 the METRAS approach has a substantial advantage over turbine specifications are considered and OWF formation is arbitrary, which ends in a more realistic wind field and therefore into a more realistic change in surface elevation. Thus the Broström approach cannot be adapted in case of a complex OWF-arrangement. Hence for studies of the North Sea under planned OWF construction in 2030 METRAS wind farm approach is necessary.

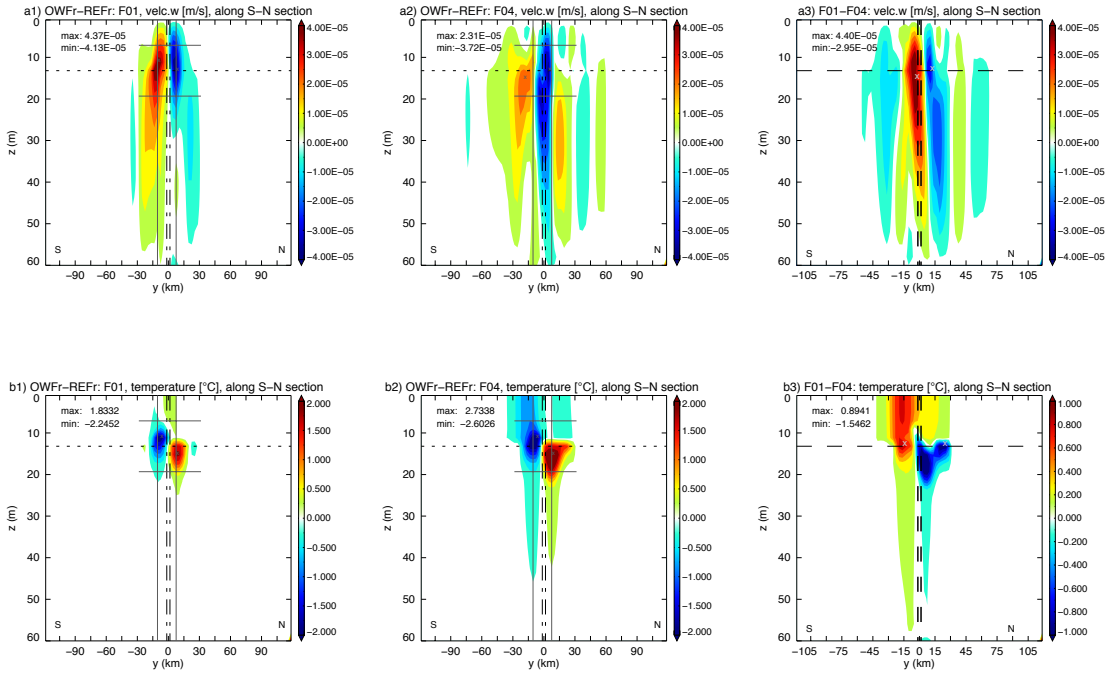

Figure 4.2.32: Comparison of simulated OWF effect of a1-3) velocity component w and b1-3) temperature along S-N section through OWF using a1-b1) forcing F01 (METRAS approach) and a2-b2) forcing F04 (Broström approach). a3-b3) gives difference between F01 and F02. Ocean variables are a1-a3) surface elevation ζ, b1-b3) velocity component u at surface, c1-c3) velocity component w at 3 m depth and d1-d3) sea surface temperature SST.

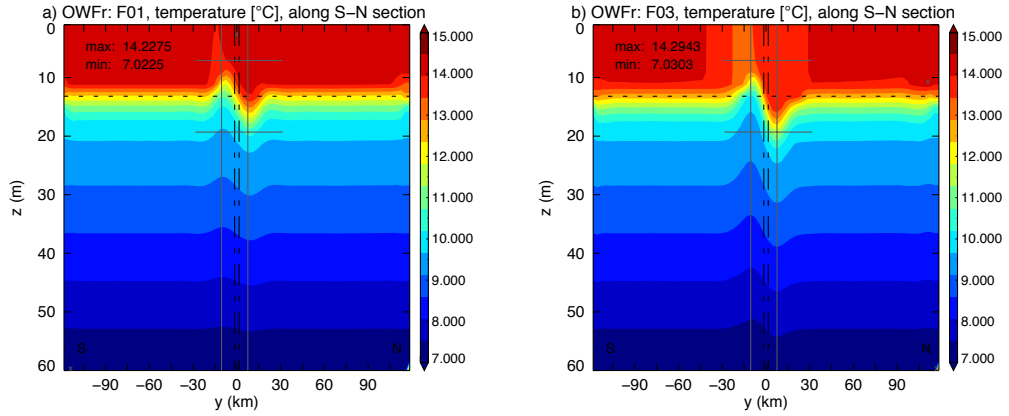

Figure 4.2.33: Stratification of temperature along y-section from S to N through OWF for a) F01-METRAS approach and b) F04-Broström approach. The Broström approach leads to a more significant effect at upper layer with slightly stronger excursion at thermocline.

4.2.3.5 Analyzing OWF effect in case of full meteorological forcing

Previous exposures of simulations dealing with wind farm's impact on ocean only consider effects of the forcing variables wind and pressure indicated as the most important variables for analysis of the OWF-effect on ocean. But whole atmosphere influences ocean in reality and based on the fact that wind turbines even influences temperature and humidity fields of atmosphere it will be investigated here how strong these additional forcing components affects the final phenomenon. But it must be noticed that the indirect forcing only allows influences of the atmosphere on the ocean and not the backward feedback. Due to the eminent change of sea surface temperature (SST), a grand question is raising and already not outstanding at all, how strong the back coupling would affect the atmosphere, especially the interaction between ocean and atmosphere. Based on model construction, useable infrastructure and time scope, only analysis of atmosphere impacts on ocean is treated here. Full meteorological forcing for HAMSOM comprises wind speed, surface pressure, temperature and humidity in 10 m height, cloudiness and precipitation. Here METRAS simulation results of forcing were chosen to be cloud free without precipitation. Therefore only temperature and humidity will have an additional impact on ocean in that analysis. Corresponding simulations for the presentation are the master simulation **T012ug08 TS01HD60F01**, including only pressure and wind forcing and is abbreviated to F01, and the simulation **T012ug08 TS01HD60F03** including full forcing being denounced to F03.

METRAS simulations are based on a SST of 15ºC and temperature at bottom of 15.59 ºC. Figure 4.1.3, in capter 4.1, shows that a wind farm not only changes the wind but also temperature distribution as well as humidity. As mentioned, previous results are only based on induced changes in the wind field which mainly drives the effects in ocean but changed temperature and humidity conditions also impact ocean's evaporation and heat exchange as an interaction between ocean and atmosphere. Such interaction won't result in a new dynamic pattern but can influence the temperature and salinity field in the upper layers.

Heat and fresh waters enters into HAMSOM through the source terms in the transport equation of temperature, respectively salinity. The source term of temperature consists of the total heat flux, which acts into ocean at surface (into the first model layer) and from there the effect of insolation at surface can penetrate into ocean depths. Due to those deeper layers can also indirect gain heat from the atmosphere. The source term of salinity is calculated by the different between evaporation and precipitation while evaporation is calculated from the turbulent flux of water vapor.

In METRAS the atmospheric boundary layer cools within the OWF due to the advection of cooler air from higher atmosphere layers to layers below the turbine rotation disc of METRAS wind turbine parameterization.

A comparison of the ocean's temperature stratification built without (F01) and with (F03) full meteorological forcing after one day of operating wind turbines is given in figure 4.2.34. That cooling can be finally pursued in upper ocean layers. Here the difference between the simulation with full meteorological forcing (F03) and without (F01) along W-E and S-N cross-section through the OWF shows that the use of the full meteorological forcing ends in a cooling down to the thermocline round -1.30 ºC. That cooling results in a drop of the thermocline from 12 m to 14 m depths. Due to that the differences between F03 and F01 in figure 4.2.34 c), show positive values around 12 m. The nearly homogeneous upper layer of temperature in F03 (figure 4.2.34 b)) with a mean value of 12.5 ºC spreads from top to 14 m depths, while in F01 the upper layer of averaged 14.0 ºC ends above the thermocline and in 12 m depths the temperature is 12 ºC. The warmer region within OWF above thermocline in case of F03 is a result of the velocity wake. The use of F03 stamps mightiness of upper temperature layer. That fact and the cooling involve a shift of OWF effects extrema.

Figure 4.2.35 illustrates the velocity component u and w, temperature and salinity at three/two points within the OWF, 12 km southerly and 6 km northerly to the OWF along S-N cross-section over depth. Especially in the downwelling region that switch is apparent. The minimum of velocity component w is placed at thermocline in 12 m depth for F01 and in case of F03 minimum it is located at 14 m. The same behavior is given for temperature, figure 4.2.35 c).

At position P1, within the upwelling region, maximal vertical velocities are placed at 11 m for F01 and at 13 m for F03 but the corresponding temperature minima are both in 10 m due to the temperature exclusion of same intensity at this point. Simulations with F01 and F03 are correlated with 0.70 for temperature, 0.96 for w-component, 0.7-0.9 for u-component and 0.57/0.80 for salinity. Differences at u-component occur at the wake-flanks biased by 0.001 m/s, vertical velocity component is biased by 10^{-6}-10^{-7} m/s, temperature has a bias of -0.13/0.19 ºC and salinity of 0.008, especially in upper layer. As mentioned changes of ocean's temperature are connected to the forcing air temperature and due to the humidity forcing, which influences ocean's evaporation, the salinity concentration changes, although there is no precipitation.

Based on that statistics at reference positions the effect of run F03 on the hydrodynamics is weak in comparison with the effect on the hydrographic conditions, especially for upper layers.

Analysis of values in the horizontal at different depths, pictured in figure 4.2.36, underlines that statement. Figure 4.2.36 illustrates the condition of the ocean system at investigation positions through the model area chosen by considering extrema.

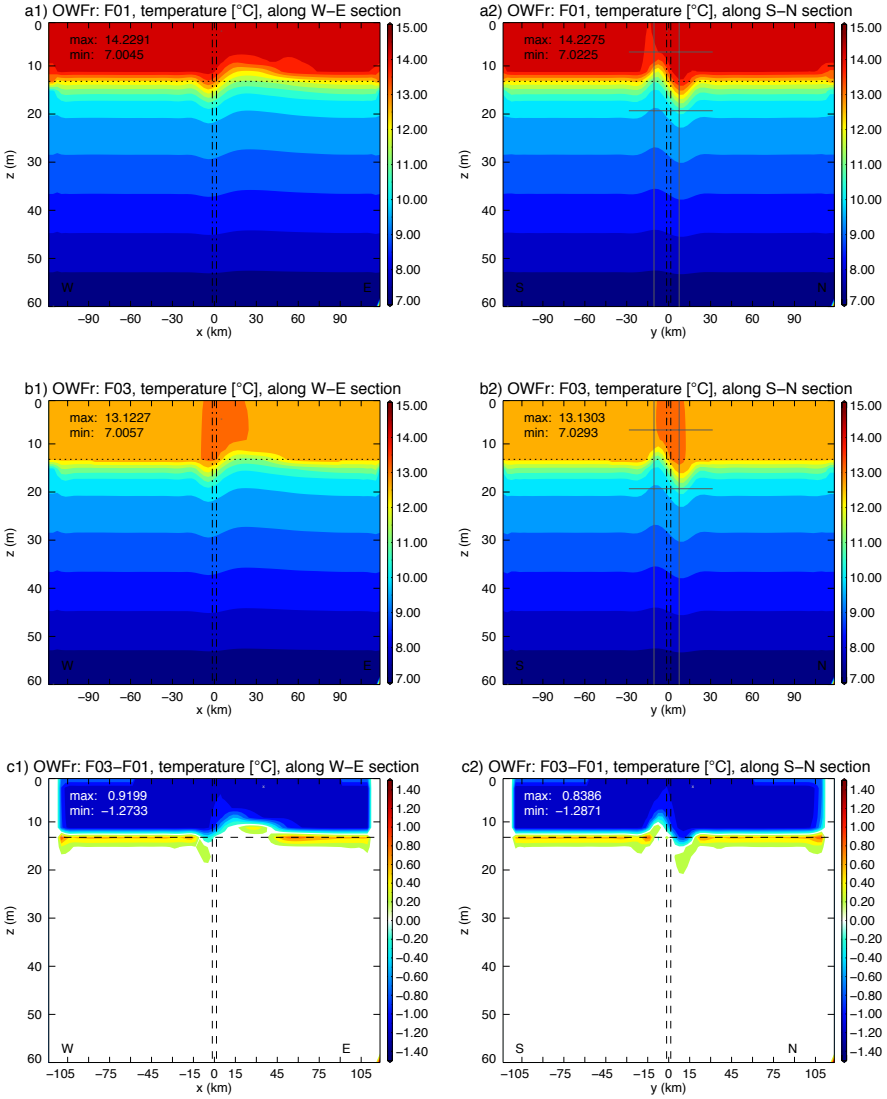

Figure 4.2.34: Temperature profiles along x-section from a1-c1) W to E and along y-section from a2-c2) S to N of restricted forcing F01 (a), full meteorological forcing F03 (b) and the difference of both (c). Considering full forcing the upper layers become cooler by around 1.2 ºC, while close to the thermocline the layers are warmer by 0.8-0.9 ºC.

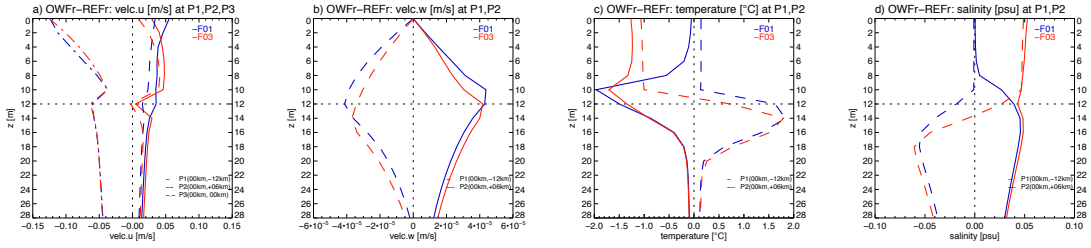

Figure 4.2.35: Comparison of OWF effect on velocity component a) u and b) w, c) temperature and d) salinity based on forcing F01 (blue) and F03 (red) over depth at two, respectively for u-component three, positions. P1(0,-12) (solid lines) is placed 12 km southerly of OWF, P2(0,6) (dashed lines) 6 km northerly. P3(0,0) (dashed-dotted lines) for u-component is positioned within OWF. Horizontal dotted line marks depth of thermocline, vertical one separates positive and negative values.

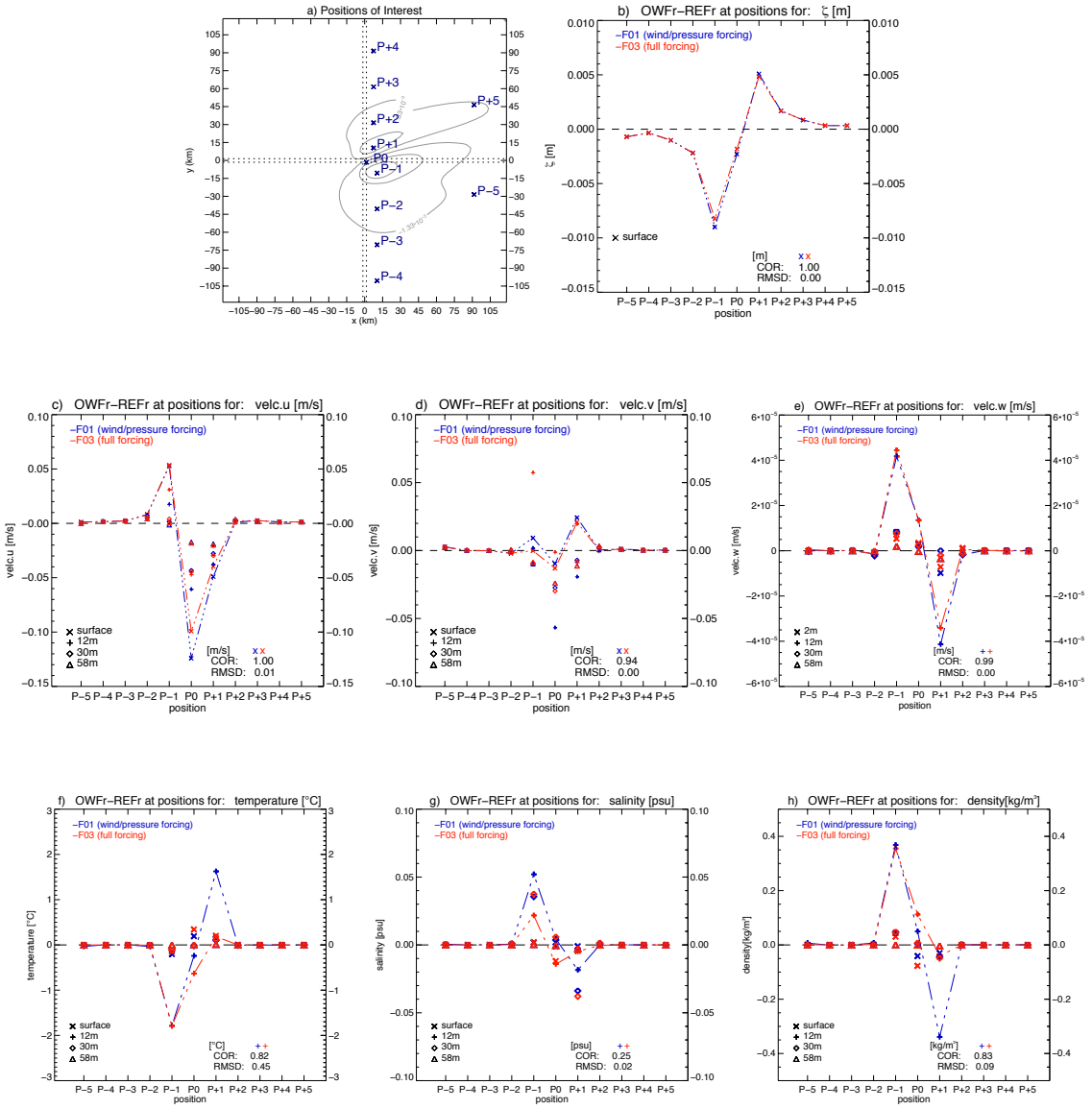

Figure 4.2.36: a) Location of investigation positions of interest, contour show surface elevation of simulation with F01. b-h) Horizontal analysis of OWF effect on ocean variables (b) surface elevation c/d/e) velocity components u/v/w, f) temperature, g) salinity and d) density) after 24h operating turbines at positions marked at left top. Results at surface (respectively at 2m for w-component) 'x', 12 m depths '+' and bottom '◊'. Correlation and RMSD is given at surface for b-d) and e-h) for 12m depths. Analysis shows values for simulation with forcing F01 (blue) and F03 (red).

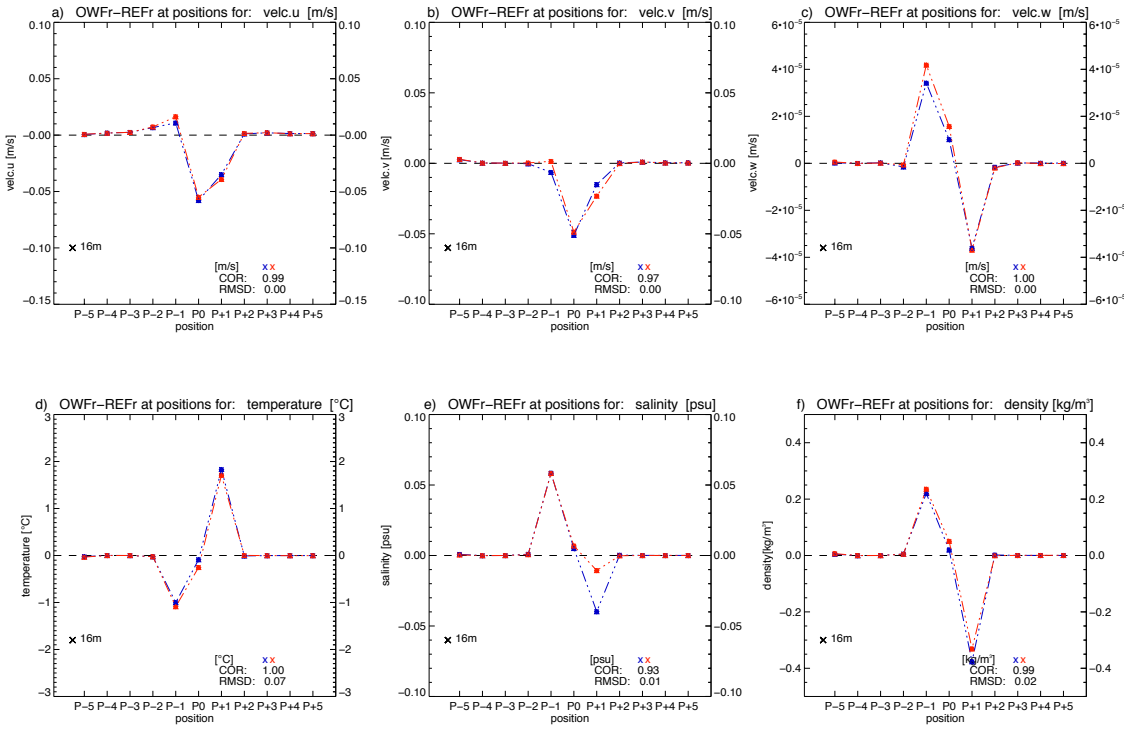

Figure 4.2.37: Comparison of OWF induced changes on ocean variables based on F01 (blue) and F03 (red) over positions defined in figure 4.2.38 at 16 m depths. Ocean variables are the a/b/c) velocity components u/v/w, d) temperature, e) salinity and f) density. COR gives correlation and RMSD the root mean square differences along positions.

Surface elevation an u-component at surface correlates run F01 and run F03 with 1.00, v-component of run F01 and run F03 is correlated by 0.94 with RMSD in order of 10^{-3} m/s.

The vertical velocity component w in 12 m depth is high correlated by 0.99 and show RMSD along the positions of 2.43E-06 m/s. The contrasts in the horizontal velocity components, obviously in v-component, with depth are a result of changes in the temperature, salinity field and the desnity field in run F03.

The cooling of upper layers dominates the differences in hydrographics of F01 and F03 at 12 m depth. Here the temperature is correlated by 0.83, salinity only by 0.25 due to disrepancies within the OWF and at P+1 in 4.2.36 g). Accordingly high are the RMSD of 0.45 ºC and 0.017 psu along the positions of investigation. Below 12 m the full forcing has only a weak impact on ocean systems.

Figure 4.2.37 documents that ocean variables at 16 m over investigated positions are highly correlated by 0.93 to 1.00, while w-component and temperature have the best correlations, salinity

gives the worst one. But from 18 m depths down to bottom the OWF-effect of run F03 on salinity adjusts to the OWF-effect of run F01.

Upshot:

As expected meteorological forcing mainly affects the upper layer of the ocean. While the impact on dynamics is very weak with the exception at depth of thermocline, the impact on temperature and especially on salinity is dominant. While temperature discrepancies occur till 12m depths, the effect on salinity is stronger and includes layers till 18 m depths in the downwelling area. The use of forcing F03 finally decreases upper temperatures, which reduces gradients and weaken vertical exchange, while the drop of thermocline from 12 m to 14 m increases vertical exchange in layers below. F03 has no impact on the spatial dimension of OWF's effect on ocean mainly because the surface elevation is equal to F01. Merely the drop of thermocline also drops extrema of vertical cells.

4.2.3.6 Analyzing OWF effect in dependence on Depth of Ocean

Variations in ocean depth constitute a barrier for offshore wind farm construction regarding fundaments and under water installations. Engineering tests of swimming fundaments for wind turbines like the Hywind-Project 2009 of the Norwegian oil combine StatoilHydro, the Windfloat-Project 2011 at the coast of Portugal, the Windflow-Project 2012/13 in France, the Sway-concept of Inocean, Shell and Statkraft and other will result in offshore wind farms being independent of ocean depth in future but such construction are still in testing phase. However companies yet prefer non-swimming fundaments and so they are restricted to shallow waters [*BWE*, 2014]. Considering possible construction in the German EEZ a maximum depth of 60 m, which was used in previous analysis, must be negotiated. Common depths of areas being selected for wind farming counts around 30 m like the area of OWF *alpha ventus* has.
Keeping in mind that in case of 60 m ocean depth the OWF impacts the whole ocean this section will clarify whether a shallower water of 30 m depth will strengthen the OWF-effect on hydrographic conditions and vertical mixing or not. The idea behind this analysis is that a smaller vertical extent supports a stronger vertical temperature excursion.
Analysis covers the master simulation **T012ug08 TS01HD60F01**, here denoted as HD60, and the HAMSOM run **T012ug08 TS01HD30F01**, denoted as HD30. To compare simulations based on 60 m (HD60) and 30 m (HD30) depths the start field of temperature-salinity stratification in case of HD30 is in accordance with the upper layers of run with 60 m because the TS start field is just cut at 30 m. So distribution from top to bottom till 30 m is the same in both cases.

A comparison of the OWF-effect on surface elevation in dependence on HD60 and HD30 after one day of simulation is pictured in Figure 4.2.38. The simulation of HD30 results in a stronger growth of the dipole effect with a difference by $+2.10 \times 10^{-3}$ m and -3.94×10^{-3} m. The stronger stamped dipole in HD30 is connected with the shallower model box setup and a more intensified wake in the flow through all ocean layers, displayed at the velocity component u in Figure 4.2.39 a1-a3). The reduced effect at u-component between 10 m and 12 m is based on a weak reverse flow in REFr as well as in OWFr due to exchange processes at the thermocline. The whole ocean depth in HD30 undergoes on an average 16.14 % stronger reduction of the flow than HD60, considering only the upper 30 m for HD60. Thus wake in the velocity component u is formed quicker which supports an accommodation of speed between top and bottom layer and so a reinforcement of the wake.

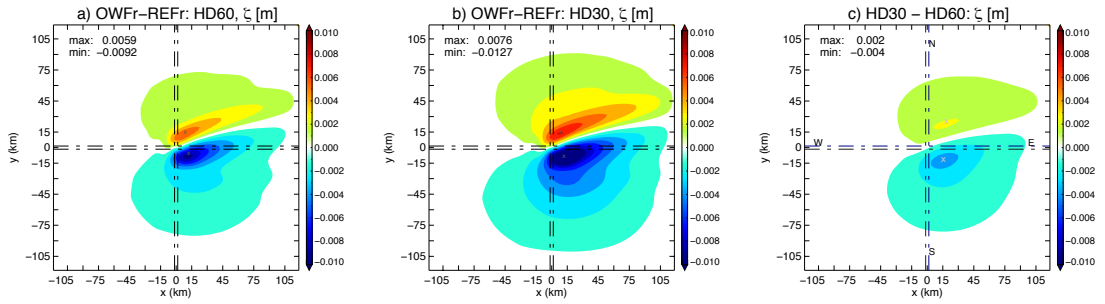

Figure 4.2.38: Effect of 12-turbine OWF on surface elevation of simulation with 60 m (a), 30 m (b) and difference 30m-60m (c). A stronger reaction of shallower waters is illustrated. Crosses mark position of extrema. Horizontal black lines encase OWF district.

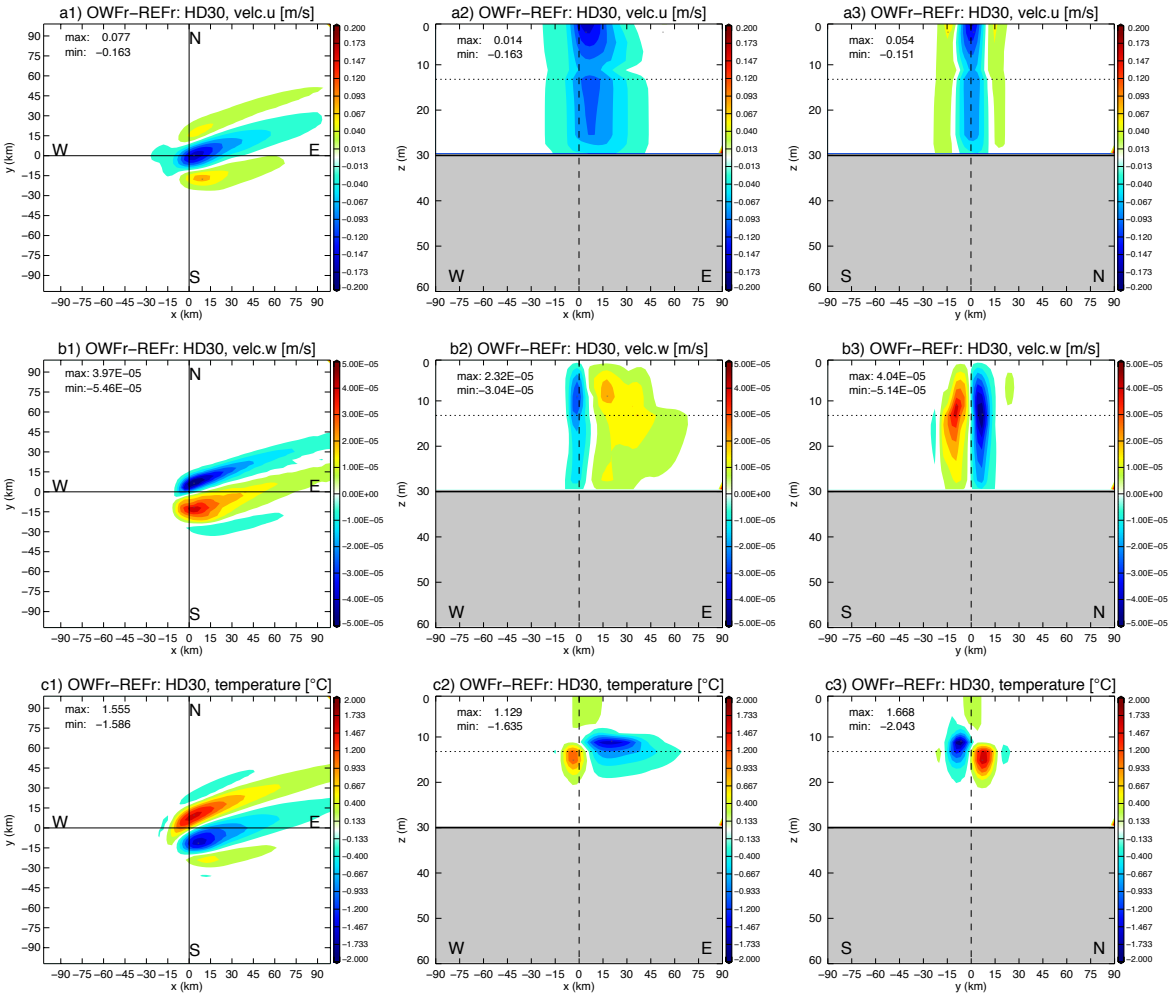

Figure 4.2.39: Effect of 12-turbine wind farm on ocean with depth of 30 m. Shown variables are velocity component u surface (a1-a3), velocity component w (b1-b3) and temperature (c1-c3). a1-c1) pictures horizontal effect at surface, respectively 2m for velocity component w, a2-c2) gives x-section from W to E and a3-c3) y-section from S to N through OWF along solid lines in horizontal plot. OWF is places around P(0,0)

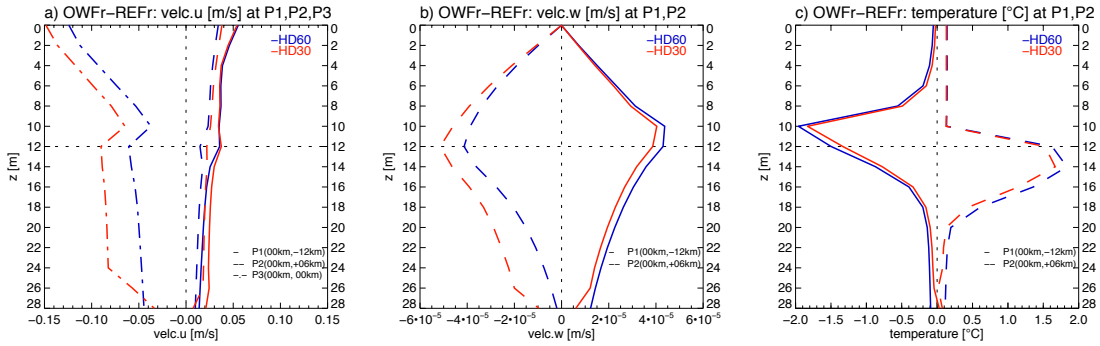

Figure 4.2.40: Comparison over depths of velocity component a) u and b) w and c) temperature for simulation based on 60 m (blue) and 30 m (red) depths at positions in km P1(0,-12), P2(0,6) and for velocity component u additional P3(0,0). Horizontal dotted line marks depth of thermocline, vertical one separates positive and negative values.

Figure 4.2.40 a) illustrates discrepancies of the u-component between simulation HD60 and HD30 at three points, within the OWF (P3), South (P1) and North (P2) of OWF along cross-section S-N through the OWF (exact positions of P1, P2, P3 are illustrated in appendix D.2). The points are chosen based on the position of extrema. At the wake-flanks the two simulations are highly correlated by around 0.97 with low biases of 0.009 m/s at P1 and 0.003 m/s at P2. Within the OWF in the wake area, at P3, the correlations are weaker, as expected due to Figure 4.2.39 a1-a3). Here 0.898 correlates HD60 with HD30, biased by 0.013 m/s while HD30 shows a stronger wake. Above thermocline (above 12 m) runs HD60 and HD30 agree well, below thermocline a shallower water strengths the vertical motion. The OWF-effect in case HD30 is reduced at the bottom due to friction, while HD60 is unpersuaded by bottom friction in that depth.

The occurrence of vertical motion has the same distribution in the horizontal for both ocean depth cases. As well the vertical cells ranges from surface to bottom in both cases but in run HD30 the vertical cells are smoother in the vertical and clearly results in two dominant up- and downwelling cells around the OWF. Especially along W-E section through the OWF (Figure 4.2.39 b2), the upwelling is undisturbed with depth and more consistent in HD30 than in HD60. In case HD60 occurs after one day simulation a zone of downwelling below the thermocline and eastward of the OWF. In case HD30 the effect shown at 12 m depth (fFigure 4.2.39 a), can be broaden from surface to bottom. Simulation HD30 has got a more intensive downwelling of maximal -5.46×10^{-5} m/s compared to HD60 with -4.37×10^{-5} m/s over the whole model box and also the mean of downwelling over the affected area leads to a stronger effect by HD30 with -1.27×10^{-6} m/s than HD60 with -1.09×10^{-6} m/s, see also tables 1 and 9 in appendix E. The depth where the extrema occur is 12 m in both cases. The maximal upwelling occurs in depth of 10 m for both cases and

again the run HD30 shows here a stronger value being $0.11x10^{-6}$ m/s higher than in case HD60. Below 10 m the upwelling is weaker than in 10 m depth for both simulations but the run HD60 becomes here more intensified due to bottom friction affecting results in run HD30. In the horizontal HD30 tend to location of extrema through layers being closer to OWF grid boxes with maximal differences to HD60 by 6 km in x-direction, so 2 grid boxes, and 3 km in y-direction; location of extrema of H60 are slightly more easterly positioned after one day simulation. Inspection of distribution of w-component at Point P1 and P2, Figure 4.2.40 b), shows that downwelling at P2 is weaker in HD60 while upwelling at P1 is nearly identical till 4 m depth. Below 4 m and especially from 10 m on HD30 gives a lower upwelling. One must note that position of investigation P2 does not fit with position of overall maximal upwelling; that is why run HD60 dominates here in the upper layers. The dominant downwelling for HD30 is registered for the whole 30 m ocean depth. Correlations of w-component of run HD60 and HD30 are 0.98 in P1 and 0.95 in P2, while again main discrepancies occur below the thermocline due to different defined depths of the model bottom. The two simulations are higher biased for downwelling by $9.15x10^{-6}$ m/s, while upwelling only is biased by $4.5x10^{-7}$ m/s.

In dependence of vertical motion two zones of changes in the temperature field are obvious (Figure 4.2.39 c1-c3)). Although the vertical velocity component w in run HD30 is greater for downwelling and mostly for upwelling the maximal effect of the temperature within the model box is more dominant in case HD60 but discrepancies in the global mean change between run HD30 and over the upper 30m of HD60 counts only -0.0024ºC/+0.004ºC for cooling/warming. The vertical position of extrema occurs in both cases around the thermocline in 10 m depths for cooling and in 14 m depths for warming. A global maximal change in temperature is -2.70ºC/+1.92ºC for run HD60 and -2.36ºC/+1.68ºC for run HD30 (documented in tables 1 and 9 in appendix E). In case HD30 the effect on temperature in the vertical is stronger located around the thermocline due to a decrease of w-component with depths below 12 m. Due to smoother vertical cells in HD30 the change of temperature is more uniform over the affected areas than in case HD60, which leads to a smaller global mean over whole ocean depth for HD60 compared to HD30. However a change in the temperature over the vertical at position P1 and P2 (Figure 4.2.40 c), shows the little more dominant effect on the temperature field by HD60. Temperatures at both positions are stronger correlated, with 0.99, than velocities' w-component. In the upwelling region occurs the highest bias of 0.060 ºC compared to 0.004 ºC for the downwelling position due to the fact that in case HD60 advection of cooler water, below 30 m depths, cools upper layers.

Upshot:

Summarizing, shallower water depths strengthen the wake in the u-velocity, and hence a stronger dipole structure of surface elevation occurs. Therefore we can expect a stronger downwelling and also a stronger upwelling above the thermocline in shallow waters. Here, the vertical positions of w-component extrema are independent of the ocean depth but strongly depend on ocean stratification. Also a shallower water leads to stronger distinct vertical cells from top to bottom while in the case of deeper ocean the formation of the vertical cells vary more in the horizontal. Nevertheless the ocean depth plays a secondary factor for the common OWF-impact on the ocean system. Like in previous analysis it becomes clear that the distribution of hydrographic conditions and position of thermocline are more significant for the OWF-effect because at the thermocline the OWF induced dynamical change effectively impacts the ocean system.

4.2.4 Evaluation of modeled OWF Effect on Ocean

The theoretical approach of using HAMSOM over an ocean box to determine the effect of an OWF on ocean's dynamic gives possible dynamical changes. Although HAMSOM is a well physically proofed model the here used restrictions of a model box and its forcing lead to the question how realistic the dimension of arising phenomenon, treated in the last subchapters, is. Hence a snap-shot of conditions around offshore wind farm *alpha ventus* was taken owing to BSH's support, which supports to put model results and measurements of temperature and velocity into relation to each other.

The area around wind farm *alpha ventus* with measurement stations, time and position of data collection are represented in figure 4.2.41. The measurements comprise 39+3 CTD stations and three ADCP mooring stations only taken for this analysis. The time frame was May 11st to 13th, 2013, at which CTD measurements were taken on May 12 and the ADCP instruments collected data over two days from May 11-13. Additional temperature and dynamical data were and are retrieved permanently by instruments of the station Fino1, relay station and swell buoy located in the area of *alpha ventus* (figure 4.2.41).
A separation of ADCP-measured velocity data into its component was deemed as the easiest way to detect upwelling and downwelling as shown in the model data. But the residual velocity signal in the North Sea is strongly disturbed by the tide, which makes the analysis of velocity components difficult as well as the fact that changes of the vertical velocity component are small and hard to detect, even after subtracting the tidal signals. Hence the ADCP-data taken at three positions (North, East and South to *alpha ventus*) does not result in a distinct, with model data comparable, signal and thus they are only documented in appendix C.3, for the sake of completeness.

Based on, the analysis will be concentrated on the CTD-data taken along four sections westerly, northerly, easterly and southerly of the wind farm *alpha ventus* (figure 4.2.41). The northern and southern sections are around 12.80 km long, the western and eastern ones around 10.90 km. The distance to *alpha ventus'* center counts in longitude direction around 5.5 km in latitude direction 6.4 km because of bordering prohibited zones based on wind farms constructions. The arrangement of investigated locations was chosen based on previous model results with focus on catching modeled OWF-effects.

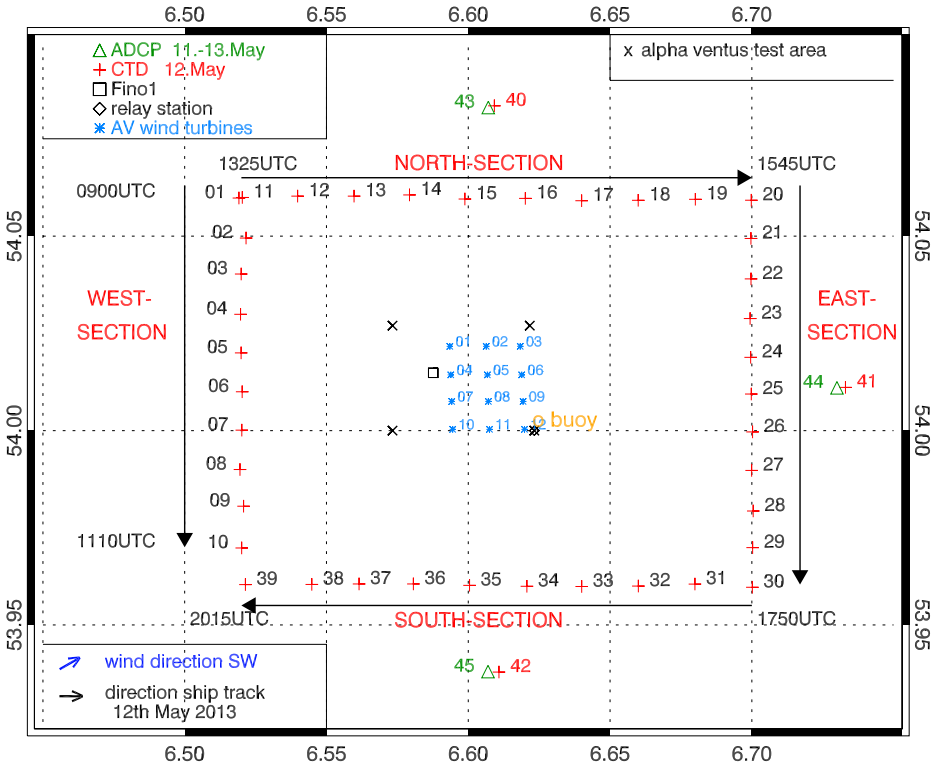

Figure 4.2.41: Map of investigation area around test wind farm *alpha ventus* (black '+'). Wind turbines are marked blue, CTD measurements are red marked with '+', ADCP measurements green marked with 'Δ', the sign for the Fino1 platform is '□' and for the relay station '◆', which is close to turbine 12 and the swell buoy (orange 'o buoy'). Black arrows mark direction of ship track for CTD measurements. The CTD-sections (West, North, East, South) are defined along the CTD-stations.

The used model simulation for the evaluation is the run **T012ug08 TS03HD30F01** of the model set-up TOS-01 (ocean box), which means a wind farm of 12 wind turbines (T012) within 4 grid cells, a wind forcing based on a prescribed geostrophic wind of 8 m/s (ug08), a temperature and salinity start field based on the measured profiles during the ship cruise (denoted as TS03), a model depth of 30 m (HD30) and only a forcing being established by METRAS 10m-wind field and surface pressure (denoted as F01).

Hence the main differences been simulation assumptions and nature conditions existing during the measuring campaign are the use of a simplified meteorological forcing, not exact same wind turbines (hub height difference of 10 m, rotor diameter difference of 36 m and different technical parameters), a homogeneous water depth of 30 m, an averaged initial conditions for temperature and salinity based on taken CTD measurements and in the model simulations the tide is neglected.

Considering only **meteorological** pressure and wind forcing is justified to the fact that there was no possibility to get an area-wide realistic meteorological forcing (for example satellite data) and due

to the fact that dynamical oceanic changes are dominantly driven by wind (result of section 4.2.3.5). The decision of using wind forcing based on a prescribed geostrophic wind of 8 m/s is leaned on to be the closest description of wind situation discovered on-site.

The wind turbine parameters were not changed for the comparison-simulation due to computation time and costs as well as that the used model resolution tends to overestimate the wind wake dimension orthogonal to the wind direction. Additionally, it must be said that during the measuring period not even all of the twelve turbines were running all the time due to planned maintenance and regarding *alpha ventus'* power plan the turbines were not running with full power. Based on these facts it is supposed that the used smaller turbine may balance the later listed issue of horizontal resolution and that the used wind turbine adjustment fits reasonably with reality.

The **bathymetry of model** is flat which is not a big limitation since the investigation area around *alpha ventus* is known as flat and sandy with an averaged depth of 30 meters in marine charts. Such a bottom-topography was chosen because the dependence of OWF-effect on the water depth is relatively low as shown in section 4.2.3.6.

It must be clear that this section provides an evidence of physically accuracy of model results and gives an estimation of OWF-effect's dimension by means of temperature analysis.

Prior doing a description of the evaluation between measurements and model results, the situation in May before and during data collection around *alpha ventus* is presented using data of research platform Fino1. The important data here are information about the wind situation, which is depicted in figure 4.2.42. The wind often veers between south and west over the days before measuring period. Especially from May 8, 2013 on, wind directions ply between 175º and 250º fairly constant over heights between 33 m up to 90 m. An averaged wind direction of 205.51º predominates during measuring period, which nicely accords with wind direction of used METRAS 10 m wind forcing field. Even the wind speed, measured at Fino1, is 8.50 m/s, averaged over heights and campaign time. Considering METRAS 10 m wind field of 6.5 m/s - 7.0 m/s (based on prescribed ug=8m/s), we can say that the wind forcing for HAMSOM is close to the realistic wind situation. Discrepancies are kept in mind for the evaluation.

Oceanic conditions of the North Sea on May 2013 show a continuous increase of temperature as expected in springtime based on solar radiation, figure 4.2.43. During the measuring period, there occur values averages over depth (3m-25m for temperature and 6m-25m for salinity) and time of 7.42 ºC for temperature and 32.77 psu for salinity (figure 4.2.43). The mean flow velocity over depth and time was 0.44 m/s and at 2m depths around 0.85 m/s.

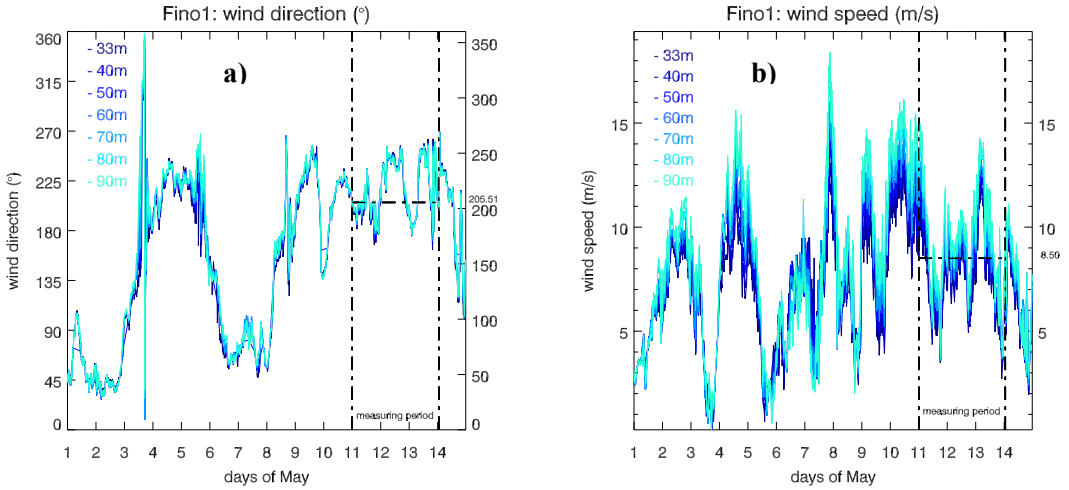

Figure 4.2.42: Wind situation in May 2013 at Fino1, including measuring period from 11-13 May. Left shows wind direction, right wind speed. During measuring period wind direction was mainly SW with a mean wind speed of 8.10m/s above 33m. Horizontal dashed-dotted line gives median of shown variable.

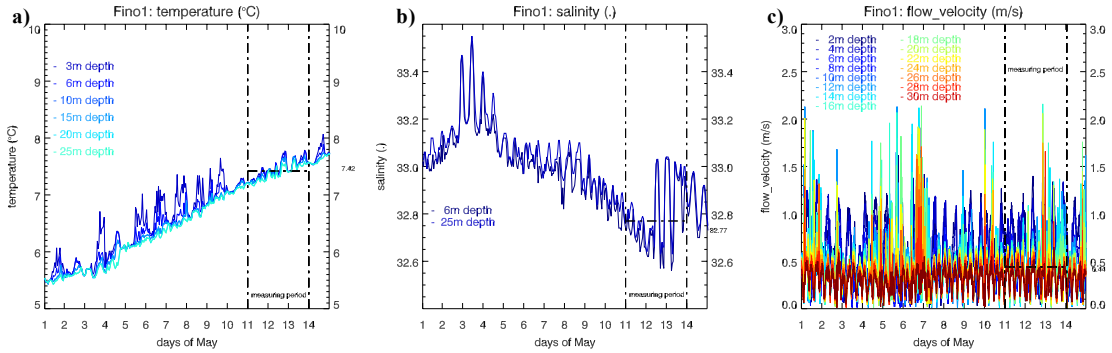

Figure 4.2.43: Temperature (a), salinity (b) and flow velocity (c) of May 2013 at Fino1, including measuring period 11-13 May at various available depths. Horizontal dashed-dotted line gives median of shown variable.

As mentioned the strong tides in the North Sea hampers the measurements of the vertical velocity component w via the used ADCP instruments, therefore the CTD measurements play a key role in the presentation of evaluation. An advantage of the CTD-data is that the temperature is not strongly affected by the tide and is expected to represents the vertical stratification with an evidence of the vertical mixing, vertical exchange and the vertical motion as defined in the model results. Variations of the CTD-measurements, especially at surface, based on alternating cloudy conditions (no precipitation) and slightly varying swell during measuring period is considered in following analysis of the temperature.

Supposing the offshore wind farm *alpha ventus* has no effect on ocean dynamics we would expect standard temperature stratification with higher temperature in the upper layers, a more or less clear thermocline (no excursion) and cooler layers below. Also, and that's important, we would expect that such a stratification occurs over the whole area and is quite constant. The investigation area is placed in shallow water strongly affected by wind. Therefore the sea around the wind farm *alpha ventus* is expected as well mixed with mostly no or very weak thermocline although solar radiation would support a formation of thermocline.

The CTD measurements result in a maximum SST of 8.0 ºC and 7.0 ºC at bottom on May 12, 2013. Though the weak temperature difference of 1.0 ºC from top to bottom the CTD measurements show complex structures, which are illustrated in figure 4.2.44.
Precise structures in the vertical occur along the four section of CTD in the West, North, South and East of *alpha ventus*. Zones of cooler and warmer temperatures were observed along the tracks, which looks like an undulating formation clarified by black dashed lines in figure 4.2.44, which is an evident of the excursion of the thermocline. All sections have in common that cooler temperature-ridges border on a trough of warmer temperature values. Such a zone of slightly raised temperatures is mostly placed along the sections at the sector of *alpha ventus* between longitude/latitude positions 54ºN 6.57ºE, 54.03ºN 6.57ºE, 54.03ºN 6.62ºE and 54ºN 6.62ºE (district of *alpha ventus* test wind farm area 'x' in figure 4.2.41).
These zones, 'bubbles' from bottom to surface or surface to bottom were measured in all sections with various intensities. The western and northern sections comprise cooler temperatures than the eastern and southern one, with differences of tenths of degree.

Along the western section from South to North a cooler ridge was formed with values of 7.28 ºC blurring at 9 m depths (figure 4.2.44). Another cooler ridge occurred at the most northern part of this section with 7.25 ºC. A slightly warmer temperature column disconnects these ridges beginning at the northern projected corner of *alpha ventus*. **At the northern section** warmer temperatures transported to depth could be seen in latitude of *alpha ventus*. A maximum was observed at the eastern part of this section, which is a part being defined to be in the wind wake of the wind farm (figure 4.2.44). Moving from North to South **along the eastern section**, temperatures increased with a maximum drop in the zone behind the wind farm *alpha ventus* of 7.76 ºC. **Along the southern section** highest temperature values occurred with a maximum of 7.97 ºC close to surface in the more eastern range of the wind farm. Temperature values of 7.8 ºC reached the bottom forming a funnel at latitude of *alpha ventus.* West and east of the wind farm local extreme 'bubble's of cooler water were observed influencing the surface at both ends of that section. A zone of around 7.90 ºC dominates down to 10 m depths (figure 4.2.44).

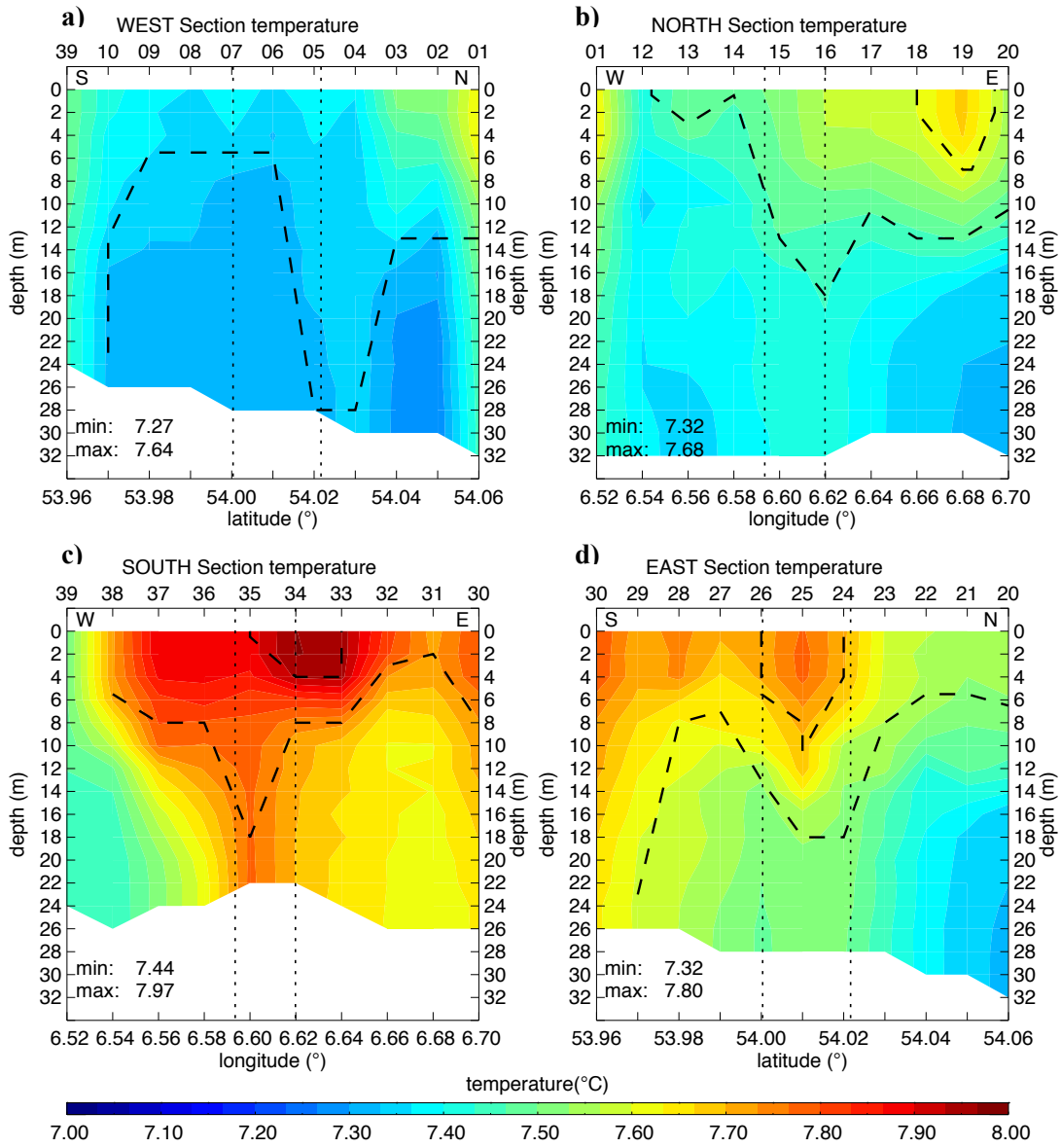

Figure 4.2.44: CTD-temperature sections (a-d) around wind farm alpha ventus from May 12. a) gives West-Section, b) North-Section, c) South-Section and d) the Eas-Section. Black dotted vertical lines mark abreast with the wind farm. Black dashed lines accent temperature formation comparable with HAMSOM model results. Temperature structure shows evidence of vertical mixing due to wind farm's wind wake. Superior x-axis gives number of CTD position. Distance of sections to wind farm counts 5.5-6.5 km. Length of latitude-sections is 12.8 km, of longitude-section 10.9 km. In the horizontal CTD were allocated without any interpolation. In the vertical data were averaged over 2m, which is consistent with used vertical resolution of HAMSOM.

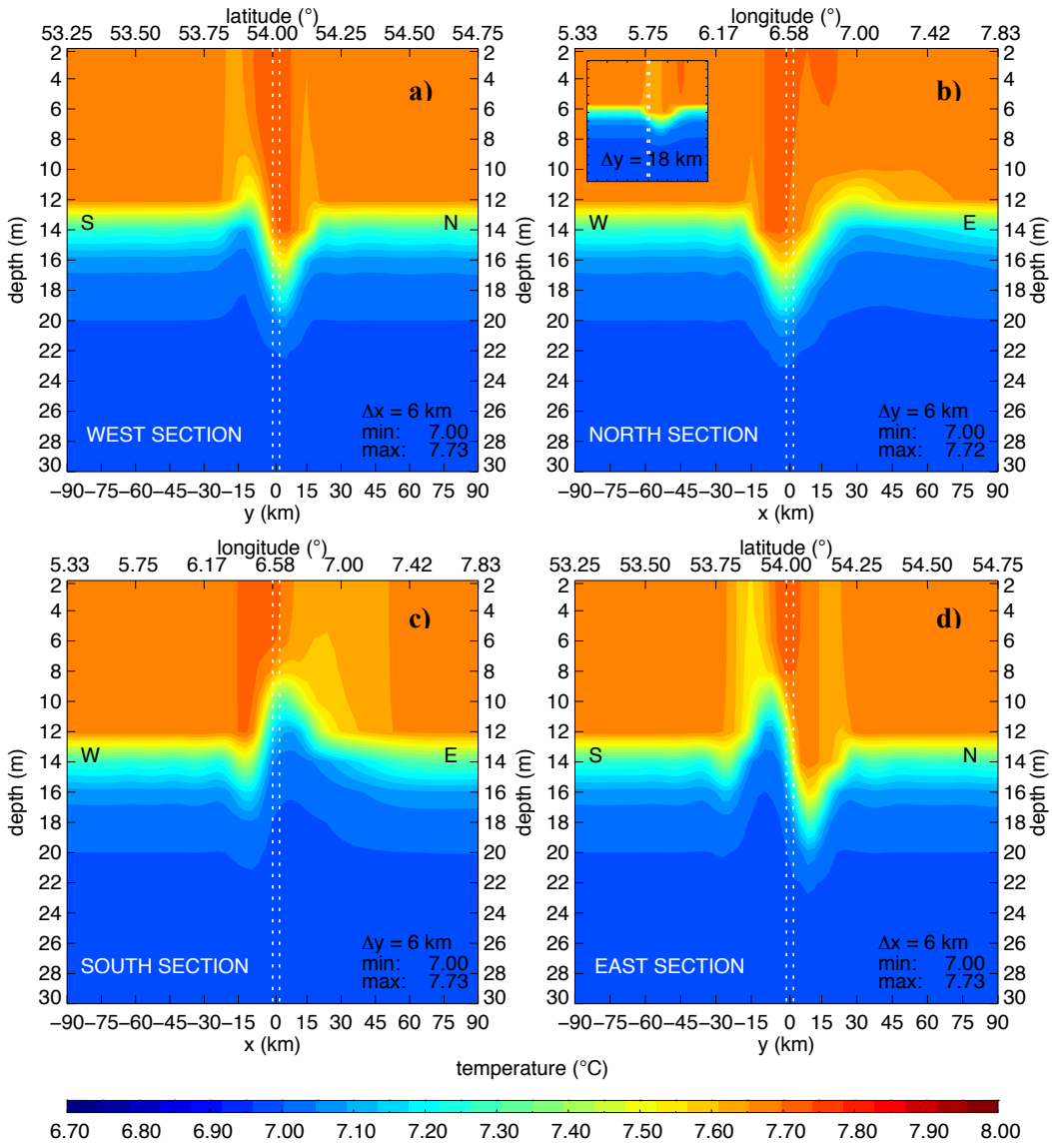

Figure 4.2.45: HAMSOM's result for temperature distribution against depth along a) West-, b) North- c) South- and d) East-section around the 12-turbine wind farm. Distance Δx and Δy of each section to wind farm is 6 km (big figures). Small figure in North-section (b) shows result for Δy=18km. Result after 3 days of simulation T012ug08TS02HD30F01. Projection of wind farm position is marked with white dotted lines.

These measured results can be reasonable well reproduced by the HAMSOM simulations. Despite divergences between model and reality, the model results after three days of simulation are used for comparison. This time step is based on the fact that on May 10, 11 and 12 similar wind conditions were discovered, so till the CTD measurements, the ocean system had around 2.5-3 days to react on the OWF-influence under nearly constant wind conditions.

Simulated temperature distributions within a distance of six kilometers to the wind farm are displayed in figure 4.2.45 along each section (West, North, East, South) through the whole model area. While measurements show a clear temperature transition from surface to bottom, the model results are blocked by a too strong thermocline as a separation frontier, which leads to nearly two main ocean layers although the starting TS profile is based on the CTD-data. A layer of mostly 7.65 ºC exists above 12 m, a dominant layer of 7 ºC below 20 m. The discrepancies are a result of tidal mixing. In the here used model simulation of the ocean box tides are neglected. Tides would support vertical mixing in the lower layers due to bottom friction. But still a strong agreement of temperature distribution between model and measurements can be identified between 10 m and 22 m, especially around the OWF area. The realistic used distance to the OWF of 6 km shows a temperature distribution comparable with measurements although the 3 km horizontal resolution of model is quite coarse. The model also provides little details depending on warmer zones within the wind farm sector. These zones having temperatures of 7.73 ºC, which means a difference of 0.1 ºC compared to the not OWF affected areas (between -45 km and -90 km and 45 km and 90km) and is of the same dimension like for the CTD.

Especially in the **northern section** (figure 4.2.45) the model simulates the warmer extrema easterly displaced from wind farm sector, which was also measured. That extremum can be identified in the model by 6 km distance to OWF but at 18 km distance the structure is closer to measure (figure 4.2.45 b, north section)

In the case of the **south-section** (figure 4.2.45) the maximum with depth is shifted to the front of the wind farm zone, while CTD data shows a maximum within the wind farm sector. The overall maximum occurred close to surface, east of the OWF zone, which can also be found in simulations. The wave formation in sections with peaks and troughs is overestimated along the sections by the model, while the structure gives a comprehensive agreement.

The **west-section** (figure 4.2.45) shows a wave formation with one minimum and two peaks at whereby the maximum peak in the south is wider and stronger then the northern one. The model results a horizontal width of the southern peak of 15 km to 20 km, the horizontal dimension by measurements leads to around 5 km.

At the **north-section** (figure 4.2.45) one trough is easily observably, followed by a rudiment of a long persistent peak, between 20 km and 75 km, where colder water is upwelling. Over that peak,

at and close to the surface, the mentioned warmer extreme is located. Here the model gives a horizontal dimension of the trough with 30 km, measurements only with 3 km. The local field of extrema at surface has a horizontal dimension of 7-10 km in the model, around 2 km in case of CTD measurements.

The warmer region, at the **south-section** (figure 4.2.45) spans a horizontal length of around 14 km, the model 15 km to 45 km. The maximum within the wind farm corridor at the **east-section** has similar dimensions in the horizontal for both data sets. But the southern peak has a horizontal resolution of 4-5 km for CTD data, 20 km for the model results

The model depicts the OWF-effect quite well but due to the model restriction, the thermocline disturbance is overestimated in the horizontal and underestimated in the vertical. On the one hand discrepancies between the modeled and observed ocean occur due to the simplified meteorological forcing (no temperature, humidity forcing, etc.) and the negligence of tides in the simulations. On the other hand the wind wake itself results in differences in the OWF-impact on the ocean. The discrepancies in the technical wind turbine parameters (thrust coefficient, rotor diameter, hub height, etc.) and in the operation mode of the wind turbines can affect the wind wake description. The used forcing of a constant 10 m wind field prescribed by a geostrophic wind of 8 m/s and constant wind direction can affect the wind wake. And the horizontal model resolution of 3 km x 3 km can affect the dimension of the wind wake as well. For example satellite analyses of the wind wake behind *alpha ventus* show that the wind reduction can occur as several wind wakes behind each turbine and not as one big wind wake [*Li and Lehner*, 2012] downstream of the wind farm, like simulated by METRAS.

These mentioned model restrictions could result in a different wind wake behind the OWF compared to the actually predominating wind wake of May 12, 2013, behind *alpha ventus*. Considering the horizontal resolution of the wind wake we can assume that the OWF-effect on ocean varies in dependence of the wind wake dimension as the analysis of the Broström approach in section 4.2.3.4 shows. Hence the simulation can overestimate the horizontal dimension of the affected areas in the ocean.

On the basis of a comparison between modeled SSTs and measured SSTs the issue of the horizontal resolution can be clarified. In the case of measurements the square around the OWF along the West-, North-, East- and South-section has a distance to the OWF center of averaged six kilometers. In assumption that the model overestimates the horizontal dimension of the OWF effect on the temperature field compared to the CTD measurements, the modeled SSTs along that square around the OWF, in six kilometers distance to the OWF center, cannot fit the measurements. Considering the horizontal resolution, the modeled SSTs along another square around the OWF having a greater distance to the OWF center is provided.

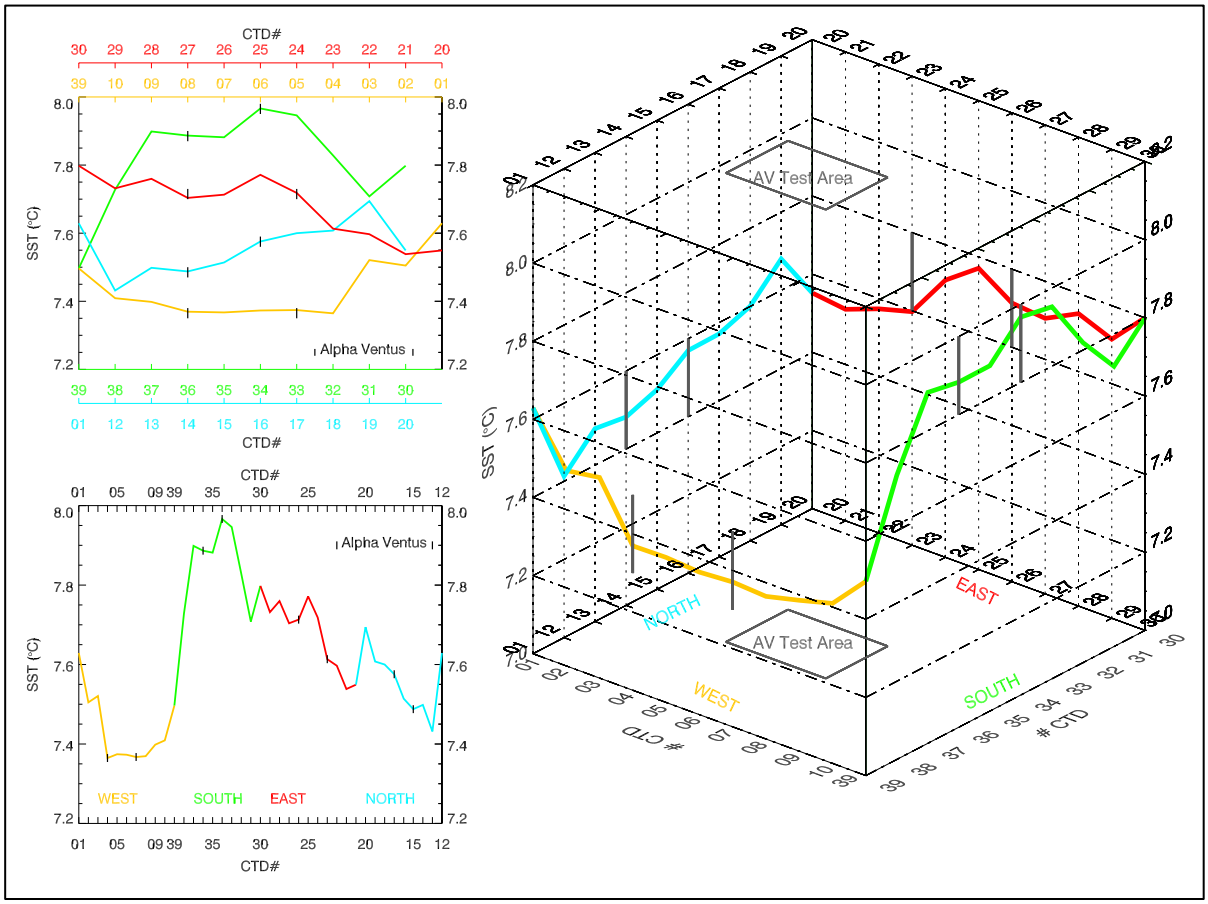

Figure 4.2.46: CTD-SST around wind farm *alpha ventus* in three different presentations to exemplify surface temperature field along section 'West' (yellow), 'South' (green), 'East' (red), 'North' (blue). Grey bars mark section of wind farm's position. Upper left figure illustrates SST for each section. Lower left figure accent temperature differences around wind farm. The right figure helps to get a spatial idea of SST distribution. The cube's z-axis gives temperature in °C starting with 7 °C and ending with 8.2 °C. X- and y-axis reflects CTD numbers, respectively position.

Figure 4.2.46 exemplifies the situation of measured SSTs around the wind farm *alpha ventus* along the mentioned 6km-distance-square on May 12, 2013. The line plots summarize that the highest SST values were measured along the southern and eastern section and the lowest values were detected at the west section. The cube-illustration helps to get a spatial idea of the SST along the square around the wind farm.

The counterpart, the modeled SSTs around the OWF, is pictured in figure 4.2.47. Figure 4.2.47 a) shows the modeled sea surface temperature of the whole model area. In the middle the OWF-district (4 grid boxes) is marked with a solid black square. The modeled SST along the corresponding square around the OWF with a distance of 6 km to the OWF center, shown in figure 4.2.46, illustrates that the modeled SSTs strongly differ from the measured one.

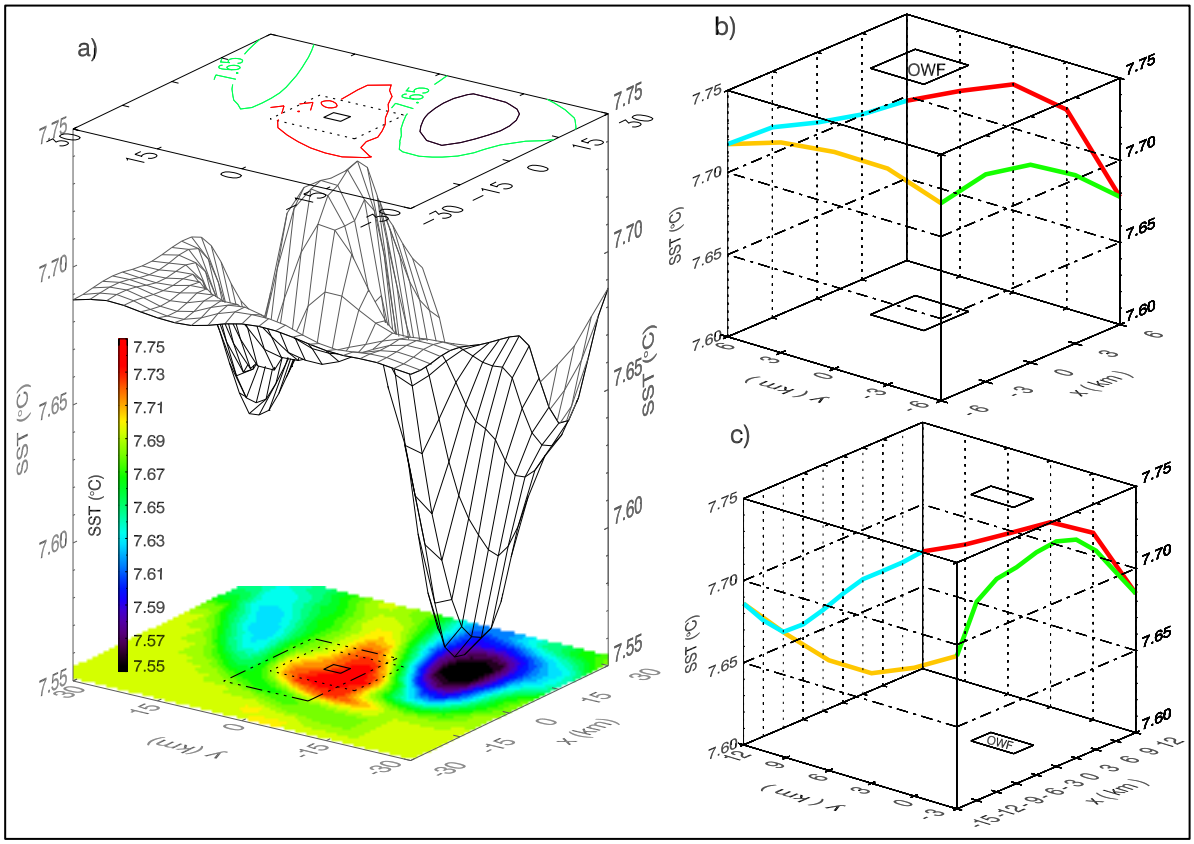

Figure 4.2.47: a) HAMSOM SST in three-dimensional illustration. Square of solid lines marks OWF in the middle of the area, which is surrounded by dotted square indicating sections by 6km difference to OWF. Additional a square of dashed-dotted lines highlights closest SST compared to CTD measurements. b) and c) picture HAMSOM SST along squares of a). b) HAMSOM SST along section in 6 km distance to OWF. c) HAMSOM SST along section with a distance of Δy=12 km from OWF to northern, Δy = 3 km to southern section and Δx = 15 km to western, Δx = 12 km to eastern section. Little black squares mark OWF position in b) and c). Results are based on three days operating wind turbine simulation.

Using a greater square provides a better agreement; moving the original ‘6km-distance square’ more to the North and expand it to the West and slightly into the East then the modeled SSTs along that square, in figure 4.2.47 c), fits quite well the measured SSTs in figure 4.2.46. Along that new square the modeled SSTs show a drop in SST along the west-section, common lower SSTs in the North, higher values in the section of the OWF at east-section and the maximum of increased SSTs along the south-section. The new square (figure 4.2.47 c)) counts in the North and East a distance to the OWF center of 12 km, in the south only 3 km, in the West 15 km and comprises a 2.8 times greater area than the ‘6km-distance square’, means in x-direction the dimension of the simulated temperature effect is overestimated by factor 1.75, in y-direction by factor 1.25 compared to observations. In average the differences between observed SST along ‘6km-distance square’ and simulated SST along the greater square counts 0.20 ºC.

The modification of the square around the OWF for comparison is not performed arbitrarily but is based on known computational restrictions – here the horizontal resolution of the wake presentation. Apart from that the model captures the observed temperature structures.

To integrate the temperature disparity related to vertical motion then a warming is connected with downwelling and a cooling with upwelling. Hence along the sections of CTD-measurements at zones of the OWF a warming is detected dominantly from top to bottom which links to downwelling in these regions and possibly also within the '6km-distance square' and so within the OWF. At the corners of that square a cooling is observed with the exception of the southeast corner. The fact that the corners show a cooling, result in the assumption that these corners are outside of the main downwelling cell, where the model shows weak positive vertical velocities.
With using the '6km-distance square' it appears to be too small to detect the upwelling cell being expected south/southeast of the wind farm as model results show.

Overall the agreement between simulation and measurements is impressive considering the theoretical model setup and computational restriction and the observed temperature profiles link to downwelling within and around *alpha ventus*.

4.3 Analysis 03: Future Scenario – German EEZ 2030

Political commitment regarding the offshore wind energy supply asks for the offshore demanding in the German North Sea, precisely within Germany's exclusive economic zone (EEZ). There exist different scenarios for the EEZ utilization in future, summarized in LOICZ report 2010 [*Lange et al.*, 2010]. At this juncture the so-called scenario ***B1*** is the most interesting one for this study here. Scenario B1 defines the EEZ as an energy park separated into different stages of expansion of offshore wind turbines. An energy supply of 30 GW is political planned till 2030 but that amount is not limited and it cannot be excluded that further OWF expansion will commission. Regarding available areas within the EEZ, it is concentrated on one of the strongest possible realizable expansion called ***'B1-2030much'***. Such an expansion shall supply around 90 GWs energy. The North Sea areas covered by wind turbines based on the scenario B1 and the expansion '2030much' is illustrated in figure 4.3.1. The specified area equates to 8590 10MW-wind turbines in the atmosphere model METRAS, being set in a horizontal distance to each other by 1990m. Hence the wind turbines are evenly spread over the OWF-district.

This chapter shows the effect of such extreme amount of wind turbines in the North Sea and its dynamical and hydrographical conditions. Simulations are based on the setup North Sea simulations (TOS-02 in chapter 3.3.2) and include two different ways of case studies. Case study I focus on the effect of different wind directions, case study II considers the effect of OWFs under real meteorological conditions of June 2010. Anticipatory, the model results based on expansion scenario *B1-2030much* does not simulate changes of the generally North Sea circulation that is why result presentation and analysis is focused on the area close to the OWFs where the OWF-effects are identified (figure 4.3.1.)

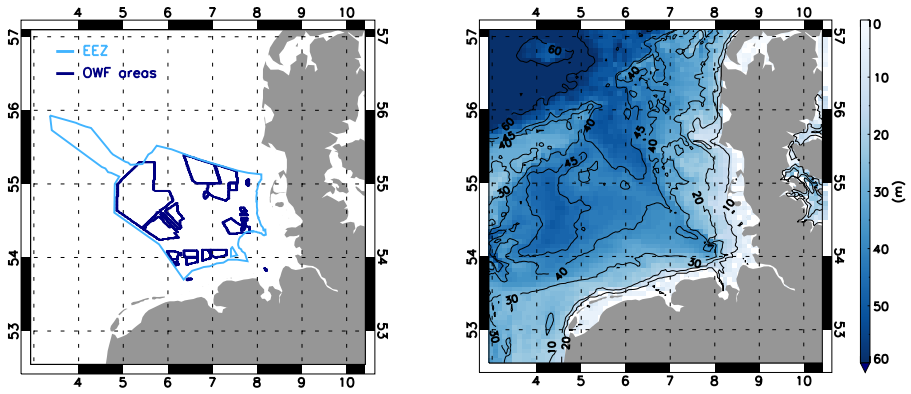

Figure 4.3.1: Left: German EEZ (surrounded by light blue lines) and areas covered by wind turbines (surrounded by dark blue lines) based on scenario *B1-2030much*. Such expansion will supply 90 GWs energy which equates to 8590 wind turbines in the atmospheric model METRAS. Right: Bathymetry of German Bight in meters. Maximal depth in EEZ counts 60 meters.

4.3.1 Case Study I: Estimation of OWFs impact by different wind directions

Case study I concentrate on the effect of OWF under scenario *B1-2030much* in matters of different wind directions. Under realistic meteorological conditions wind speed and direction can vary with time, which again results in variations of ocean dynamics and can constrain constant formation of ocean dynamics. An approach of constant wind speed and direction is applied for better analyzing the possible effect the scenario *B1-2030much* can have on the German Bight. As mentioned common wind direction within the German EEZ is southwest to west but conditioned by the particular weather situation other wind directions are possible. Thus eight wind directions around wind rose are implemented distinguished into N, SE, E, NE, S, SW, W and NW. Simulation time for each wind direction counts one day. Again runs without wind turbines and with operating wind turbines were necessary and finally results after one day of simulation are of interest.

4.3.1.1 Effect on atmosphere in German Bight of Case Study I

This section provides atmospheric changes of the variables wind, temperature and humidity over the German Bight simulated with METRAS for case study I. Figure 4.3.2 shows a representative collection of 10 m temperature, 10 m humidity fields and 10 m horizontal wind field of reference run without wind turbines. The important point of that representation is that over ocean the 10 m fields of temperature, humidity and wind are homogenies. Hence changes in those fields only occur due to operating OWFs.

After 24 hours of simulation the reference runs have a 10 m temperature of 14-15 ºC over ocean, humidity is of 90 % and wind speeds are of 3 m/s. Cut-in of wind turbines is set to 2.5 m/s, cut-off is set to 17.0 m/s in hub height. The wind field at hub height does not reach velocities being greater than 17.0 m/s, thus it is assumed that the wind turbine parameterization is never avoided. In the following difference between OWFr and REFr are presented for each defined wind direction after one day of simulation.

The changes of the horizontal wind velocity are shown in figure 4.3.3. Most of the EEZ area is influenced by a reduction of wind speed between 10 % up to 60 %. An intensified wake is formed especially within OWF-areas. An increased wind speed of around 17 % up to 26 % occurs at the constraints of the wind farms depending on the wind direction. So also in the more realistic case of scenario *B1-2030much* the structure of wake and wake's flanks can be identified. While the wind wake is strong locally limited over the OWF-district, the wind increase also influences coasts and land depending on wind direction. In case of a wind coming from the coasts, so in case of south, southeast and east directions, the wake length in wind direction is longer broad over the ocean.

As mentioned in 4.1, here the use of the METRAS approach for wind wake simulation is necessary because obviously Broström approach cannot cover such special formation for OWFs.

The changes of temperatures in 10 m are depicted in figure 4.3.4. Here the temperature increases by about 3 % - 5 %, partly also decreases by about 1 % - 3 %, 4%. The rise in the temperature is especially located in lee of wind farm areas but also within OWFs and comprises a bigger zone than cooled areas are. A cooling is located in luv of OWFs, so in wind direction in front of the OWFs and mostly connected with land. With the exception of case East wind, the temperature increase is slightly more dominant than the reduction.

The changes of the humidity in 10 m are shown in figure 4.3.5. The formation of the changes is similar with the one of the temperature. In the case of warming the humidity is reduced by 11 % - 15 %. In the case of cooling the humidity increases by 3% - 4%, 11% in the case of north-wind, and around 9 % in the case of east-wind.

Precipitation and cloudiness was not formed within these simulation runs for all wind cases.

Over ocean the OWFs normally leads to a cooling by around one K [*Linde et al.*, n.d.], while onshore farms leads to opposite effect [*Baidya Roy*, 2004], [*Baidya Roy and Traiteur*, 2010], [*Zhou et al.*, 2012]. Here listed changes become quite constant after 8 hours of simulation. Therefore the warming cannot be caused by the diurnal cycle. The cooling and the increase of humidity are connected with warmer dryer air coming from land, which flows over ocean and advects moisture. The SST in METRAS is constant during the whole simulation time and is set to 15 ºC. The 10 m temperature fields do not reach temperatures below that value. The warming in the area of wind reduction downstream of the OWFs is connected with vertical mixing and thus changes in the surface fluxes as explained in chapter 4.1 (section 4.1.2.2.1). In reality a more unstable stratification is expected during night over water, supporting vertical mixing and a cooling in 10 m. During day, the more stable stratification over water keeps the OWF induced cooling [*Linde et al.*, n.d.]. The overall cooling, documented in Linde [*Linde et al.*, n.d.], is a result of a stronger impact during night than during day.
However here conditions do not really change with time causes only a warming and drying of lower layers.

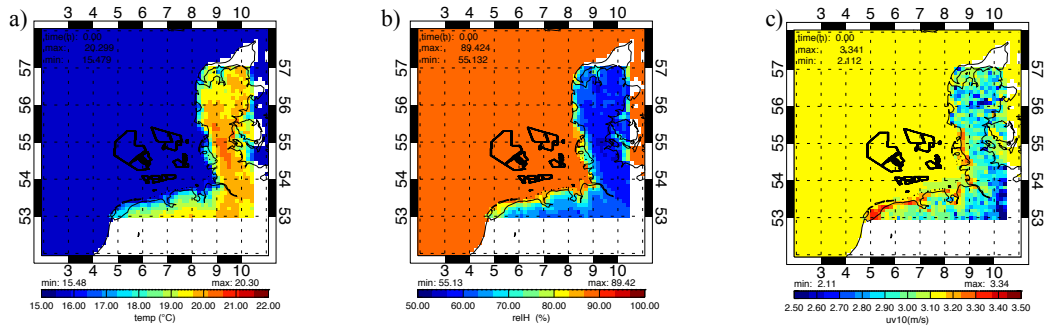

Figure 4.3.2: Fields of 10m a) temperature, b) humidity and c) wind speed after one day of METRAS simulation. Results belong to run with constant wind direction N as representative example for all wind directions. Due to wind direction the extrema can vary slightly; the important point is that in 10m heights the conditions are nearly homogeny over ocean. Outside of METRAS model area (figure 3.3.5) the METRAS data at boundaries were expanded over ocean.

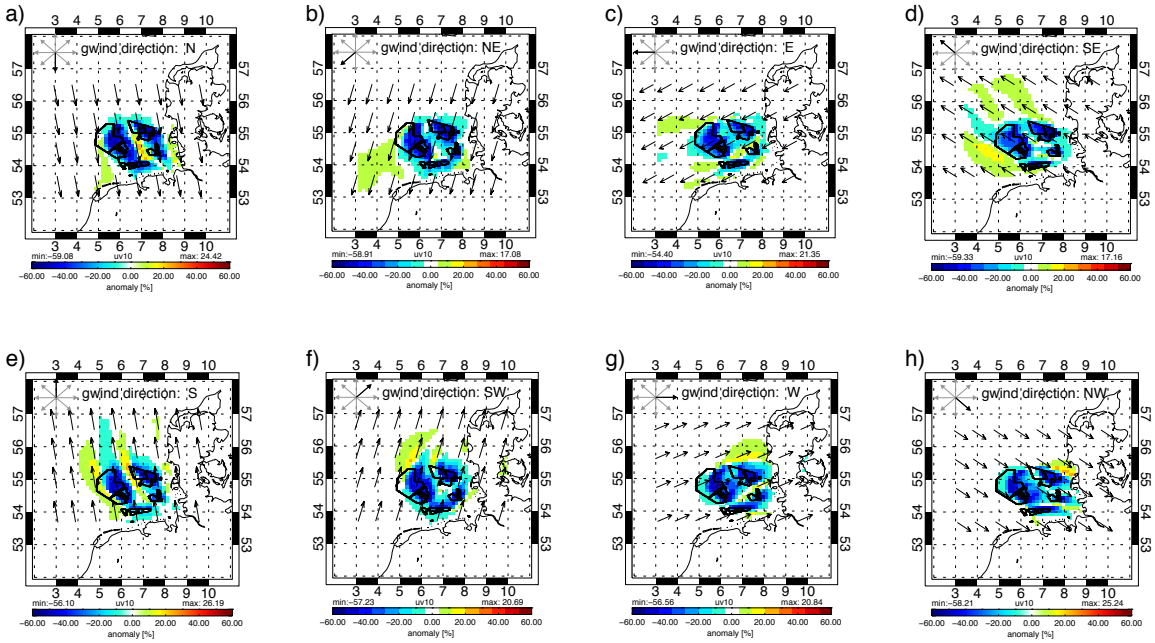

Figure 4.3.3: Changes of 10m horizontal wind field due to operating OWFs after one day of METRAS simulations for different wind direction cases. The change (OWFr-REFr) is given in percent. The prescribed constant wind directions at height of geostrophic wind are N (a), NE (b), E (c), SE (d), S (e), SW (f), W (g) and NW (h). Surrounded areas by black solid lines within German Bight are OWF areas comprising 8590 wind turbines. Arrows define real wind direction (OWFr) in 10 m heights. Maximal changes of 60% are located at OWF-districts. In sum changes are regional located within Germany's EEZ.

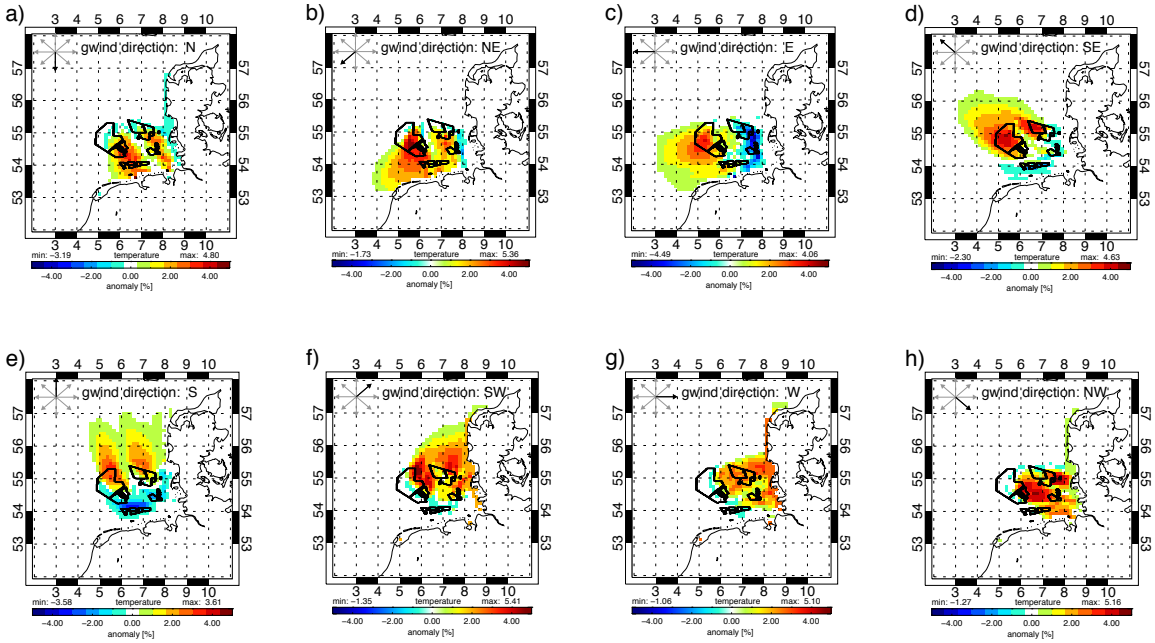

Figure 4.3.4: Changes of 10m temperature field due to operating OWFs after one day of METRAS simulations for different wind direction cases. The change (OWFr-REFr) is given in percent. The prescribed constant wind directions at height of geostrophic wind are N (a), NE (b), E (c), SE (d), S (e), SW (f), W (g) and NW (h). Surrounded areas by black solid lines within German Bight are OWF areas comprising 8590 wind turbines.

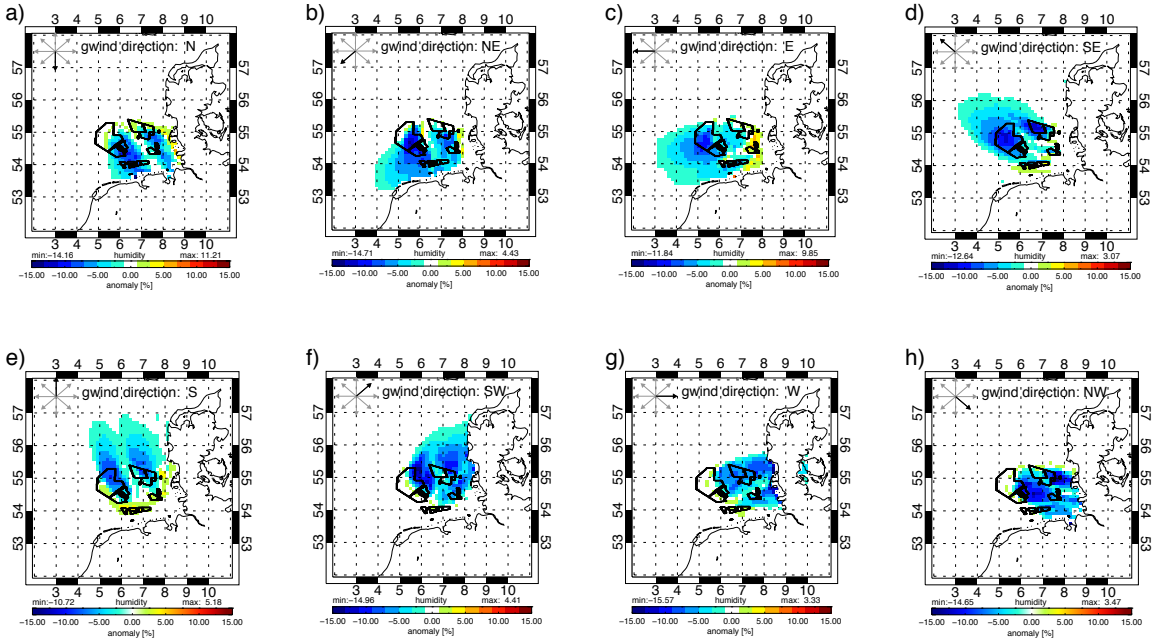

Figure 4.3.5: Changes of 10m relative humidity field due to operating OWFs after one day of METRAS simulations for different wind direction cases. The change (OWFr-REFr) is given in percent. The prescribed constant wind directions at height of geostrophic wind are N (a), NE (b), E (c), SE (d), S (e), SW (f), W (g) and NW (h). Surrounded areas by black solid lines within German Bight are OWF areas comprising 8590 wind turbines.

4.3.1.2 Effect on ocean in German EEZ of Case Study I

This section provides dynamical and hydrographical changes of the ocean over the German Bight simulated with HAMSOM for case study I (constant wind direction over one day). Figure 4.3.6 shows the representative temperature stratification of the North Sea along the latitude 54.62º through the model area after 24 hours simulation of REFr based on June 2011. Alike an important point of that representation is that stratification over simulation time of one day does not vary in REFr. Hence changes only occur due to the operating OWFs in OWFr. The maximal SSTs are around 13.0 ºC in coastal areas and at bottom temperatures reaches 7.63 ºC.

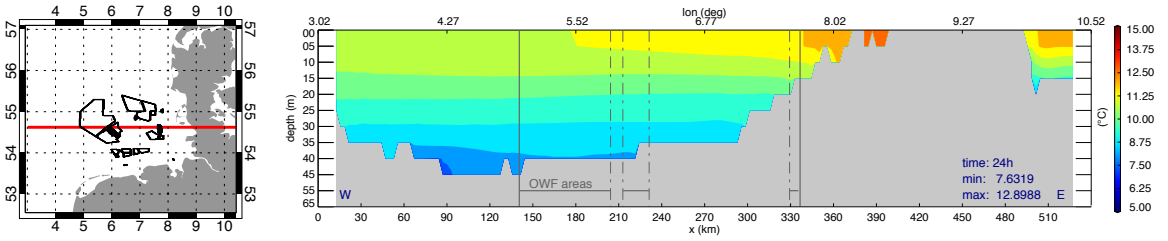

Figure 4.3.6: Left: Latitude 54.62º (red line) through model area with scenario *B-2030much.* Black surrounded areas mark fields of offshore wind farms. Right: Reference temperature stratification along latitude 54.62º based on June 2011 and SW wind direction as example. Grey shaded area is land, respectively bathymetry. Horizontal and vertical grey lines mark position of areas including wind turbines. Values are given in degrees Celsius. SST for other wind directions varies slightly in coastal regions.

In the following difference fields between OWFr and REFr are presented for each defined wind direction after one day of simulation for surface elevation, vertical velocity component w, horizontal velocity components u and v, temperature and salinity. Shown results of the surface elevation, the velocity components are based on run with full meteorological forcing. The presentation of temperature and salinity is distinguished into wind and pressure forcing only and full meteorological forcing. That is necessary because here the OWF-effect on the temperature indicates a warming, which is in opposition to the general OWF cooling over ocean being found in literature. As analyzed in section 4.2.3.5 the meteorological forcing including temperature and humidity mainly affects the hydrographic conditions of the ocean's upper layers, especially at the sea surface. The surface elevation and the vertical velocity component are in average independent of the OWF-effect on atmospheric temperature and humidity forcing fields in 10 m height. The horizontal velocity varies only in order of ±0.001 m/s due to gradients in density fields triggered by determined temperature and salinity changes based on the forcing but do not affect vertical motion.

Changes in the surface elevation ζ in the case of scenario *B1-2030much* are illustrated in figure 4.3.8 for all eight wind direction cases. As the theoretical analysis implies a dipole of ζ is even

formed in the more realistic simulation of the German Bight. The magnitude of dipole's extrema are similar for each wind direction case in the range of -0.382 m to 0.0308 m. Mostly the minima results in a stronger effect than the increase with the exception of wind direction cases SE, S and SW. The positions of dipole's extrema depend on wind direction. Downstream behind and within the OWF (lee of OWF) often a minimal in ζ is identified and in front of OWF, so in luv/windward of OWF, the maximum is detected. Changes in the surface elevation are connected with greatest wind stress and so the wake in velocity components. Having u-component the strongest content of wake then the wake areas leads to an increase of ζ, having v-component the strongest wake then the ζ-maximum occurs in the area of the v-component-wake. That fits with the explanations of Ekman transport and divergence and convergence in chapter 4.2.2.3.

Therefore two positive extrema of the ζ-change exist in the case of wind direction S because over the OWF-district the v-component show two areas of flow-reduction see figure 4.3.11. As well in the case of wind direction W the u-component show in figure 4.3.10 a wake over the OWF-district with three local minima which ends in three local minima at surface elevation between latitude 54º and 55º. Although changes in surface elevation are in order of maximal 0.04 m such a less amending can have an economic relevance for the Elbe estuary regarding shipping and harbor industry. Here changes of the surface elevation due to the OWF-expansion should be considered beside tides for bigger ships leaving and entering Elbe and Hamburg harbor because for those a water-level change of a few centimeters play an important role not to run aground. Such a change can also play a role in the case of storm surges.

The theoretical analysis in chapter 4.2 underlines the formation of up- and downwelling cells due to the change in surface elevation. Such cells also occur in the German Bight (figure 4.3.7). Figure 4.3.9 illustrates the **change of the vertical velocity component w** at 12.5 m depth. In contrast to the two main vertical cells in theory, here belts of up- and downwelling occur in dependence on arrangement of wind farms within the EEZ.

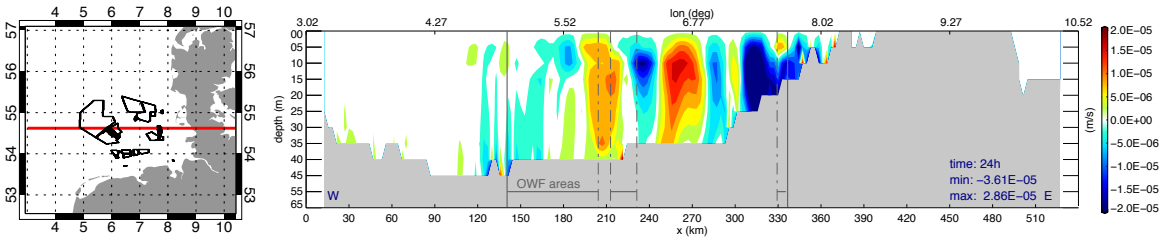

Figure 4.3.7: Left: Latitude 54.62º (red line) through model area with scenario *B1_2030much.* Black surrounded areas mark fields of offshore wind farms. Right: Change of vertical velocity component w due to operating wind turbines along 54.62º for wind direction case SW as example to show that vertical cells affect whole ocean depth. Grey shaded area is land, respectively bathymetry. Horizontal and vertical grey lines mark position of areas including wind turbines. Values are given in m/s. Here minimal/maximal vertical motion equates to -3.11/2.47 m/d.

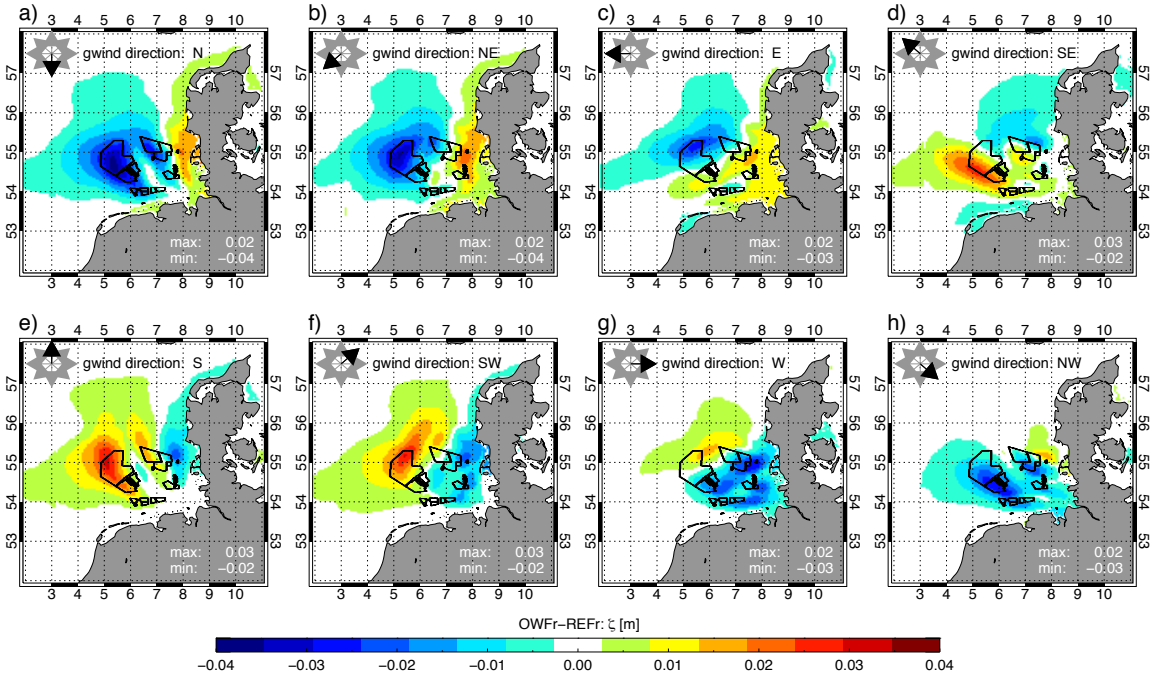

Figure 4.3.8: Change in surface elevation due to OWFs in case of different wind direction cases (gwind direction a)-h) from N-NW) after one day of simulation. The wind direction is defined at height of geostrophic wind. Units given in m. Dark grey shaded area marks land, black lines illustrate OWF-districts. Results are for full forcing.

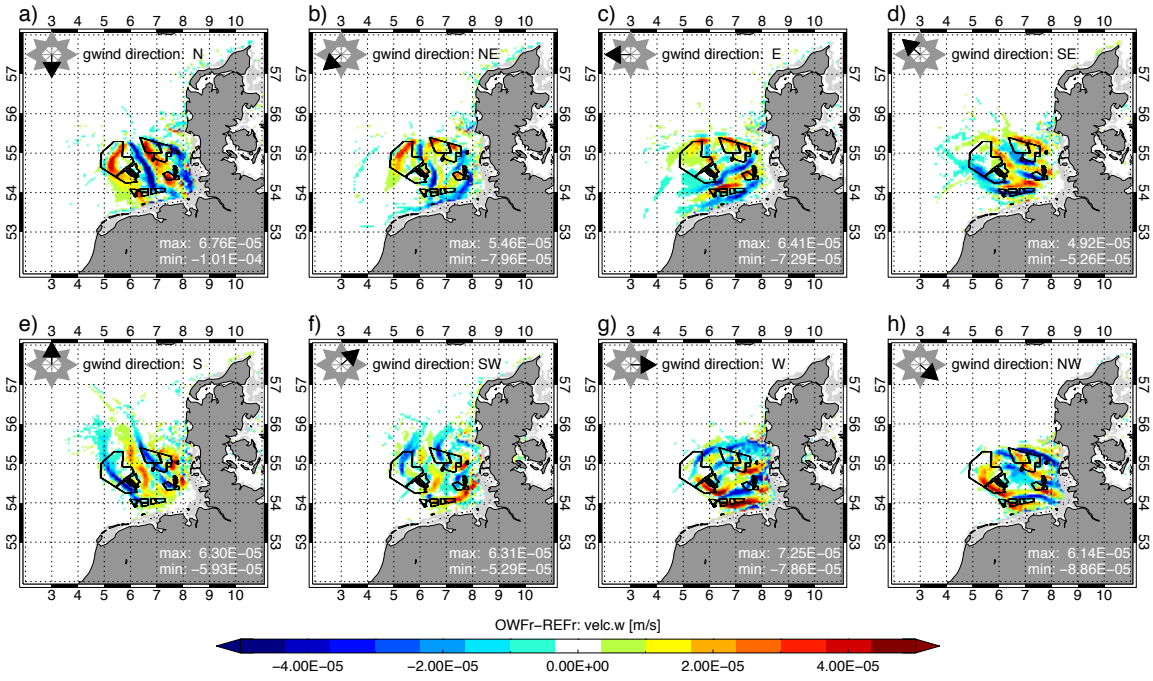

Figure 4.3.9: Change in velocity component w at 12.5 m depth due to OWFs in case of different wind direction cases (gwind direction a)-h) from N-NW) after one day of simulation. The wind direction is defined at height of geostrophic wind. Units given in m/s. Dark grey shaded area marks land, light grey shaded area marks bathymetry and black solid lines illustrate OWF-districts. Minimum counts -6.05m/d, maximum 8.64 m/d, which means an overturning after 3.5-4.9 days in areas of 30 meters water depth. Results are for full forcing.

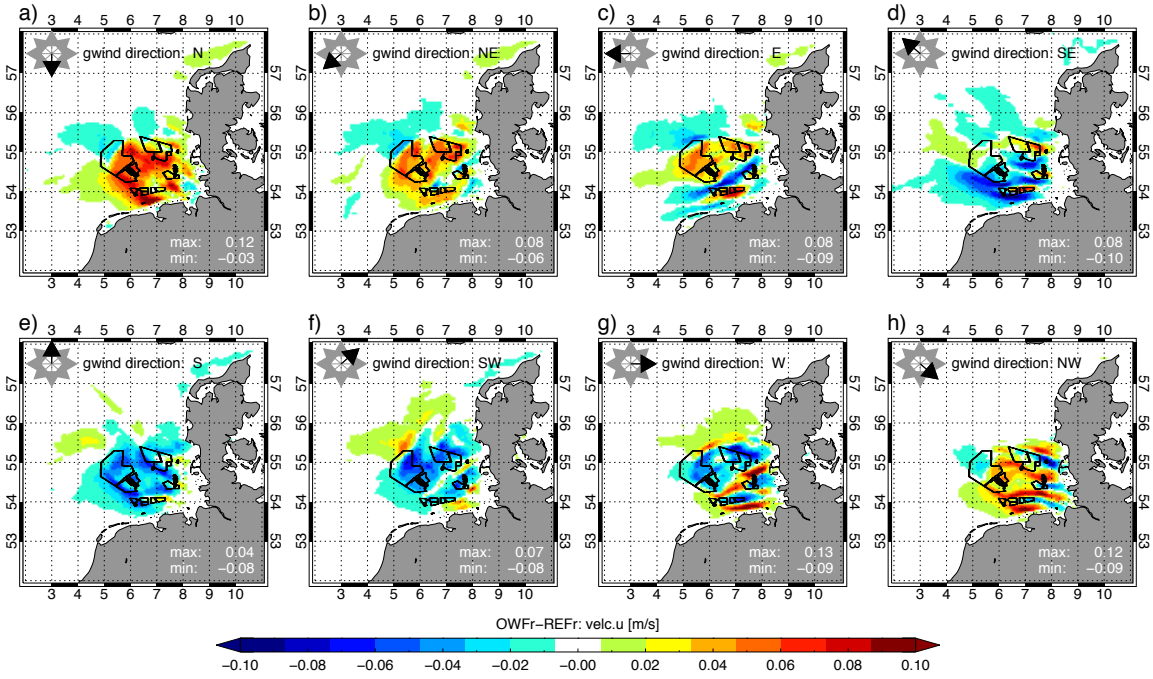

Figure 4.3.10: Change in velocity component u at surface due to OWFs in case of different wind direction cases (gwind direction a)-h) from N-NW) after one day of simulation. The wind direction is defined at height of geostrophic wind. Units given in m/s. Dark grey shaded area marks land, black lines illustrate OWF-districts. Results are for full forcing.

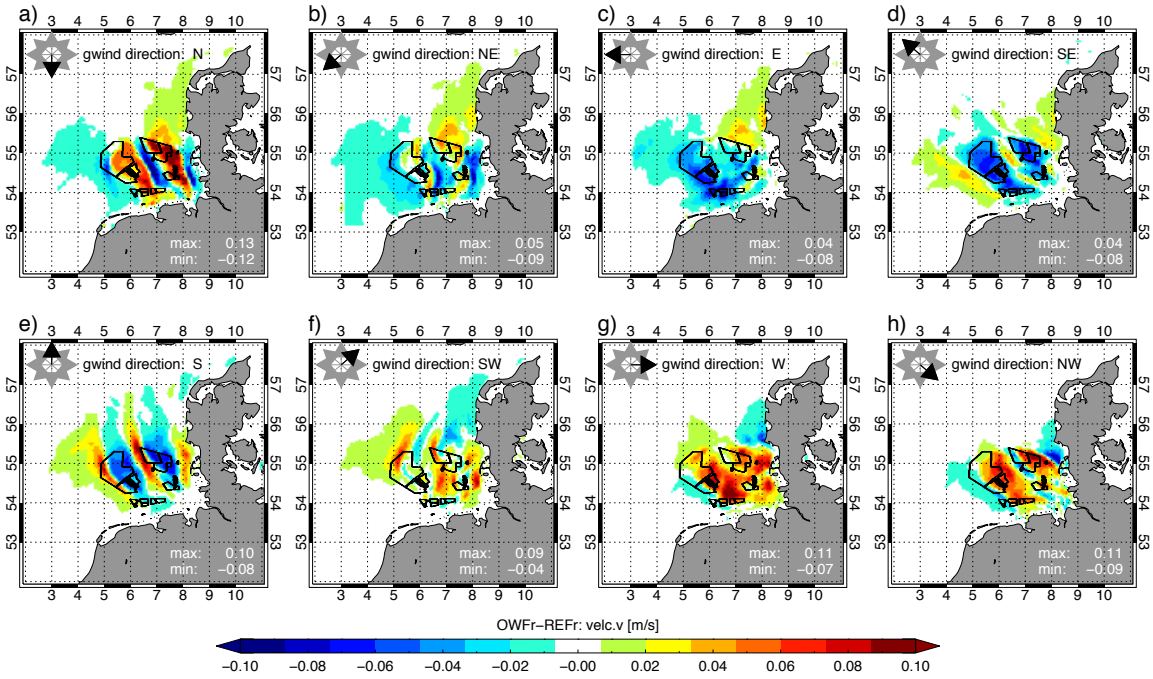

Figure 4.3.11: Change in velocity component v at surface due to OWFs in case of different wind direction cases (gwind direction a)-h) from N-NW) after one day of simulation. The wind direction is defined at height of geostrophic wind. Units given in m/s. Dark grey shaded area marks land, black lines illustrate OWF-districts. Results are for full forcing.

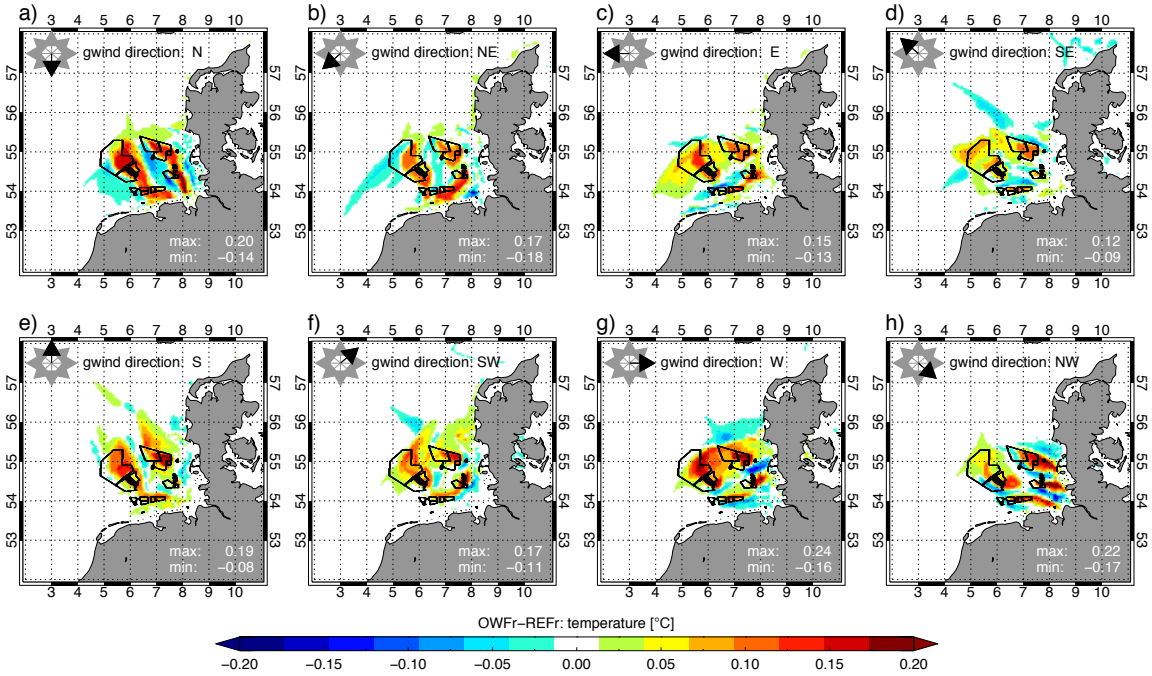

Figure 4.3.12: Change in SST due to OWFs in case of different wind direction cases (gwind direction a)-h) from N-NW) after one day of simulation. The wind direction is defined at height of geostrophic wind. Dark grey shaded area marks land, black lines illustrate OWF-districts. Results are only for wind and pressure forcing.

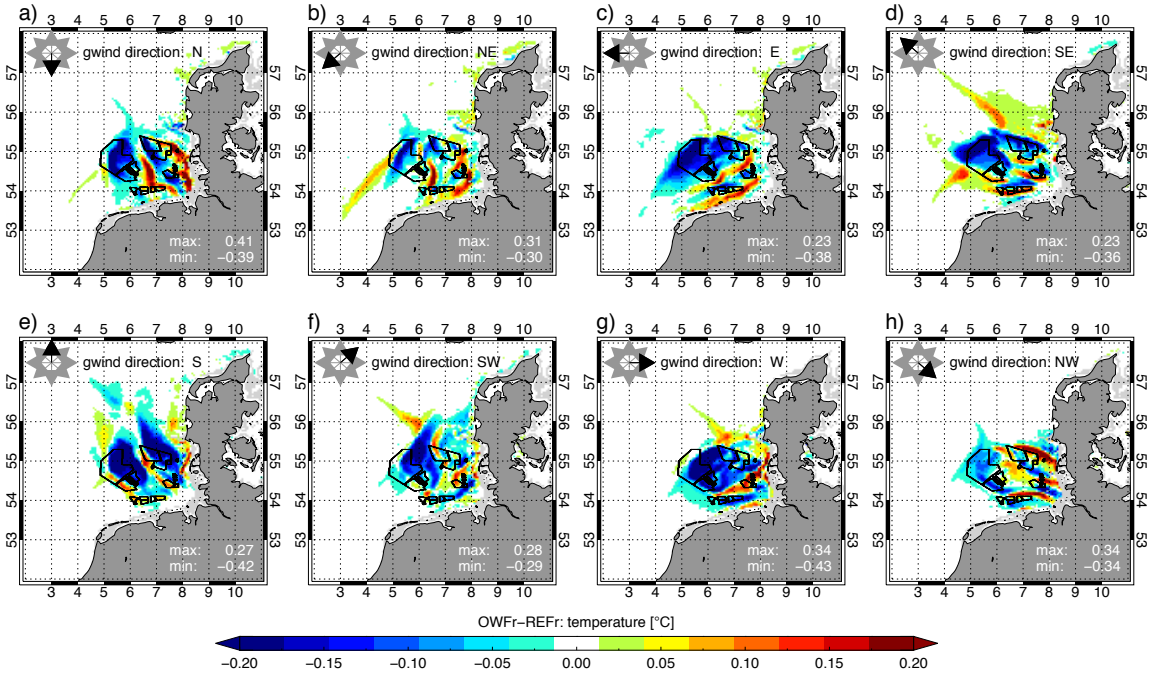

Figure 4.3.13: Change in temperature at 12.5 m depth due to OWFs in case of different wind direction cases (gwind direction a)-h) from N-NW) after one day of simulation. The wind direction is defined at height of geostrophic wind. Units are given in degrees Celsius. . Dark grey shaded area marks land, light grey shaded area marks bathymetry and black solid lines illustrate OWF-districts. Results are only for wind and pressure forcing.

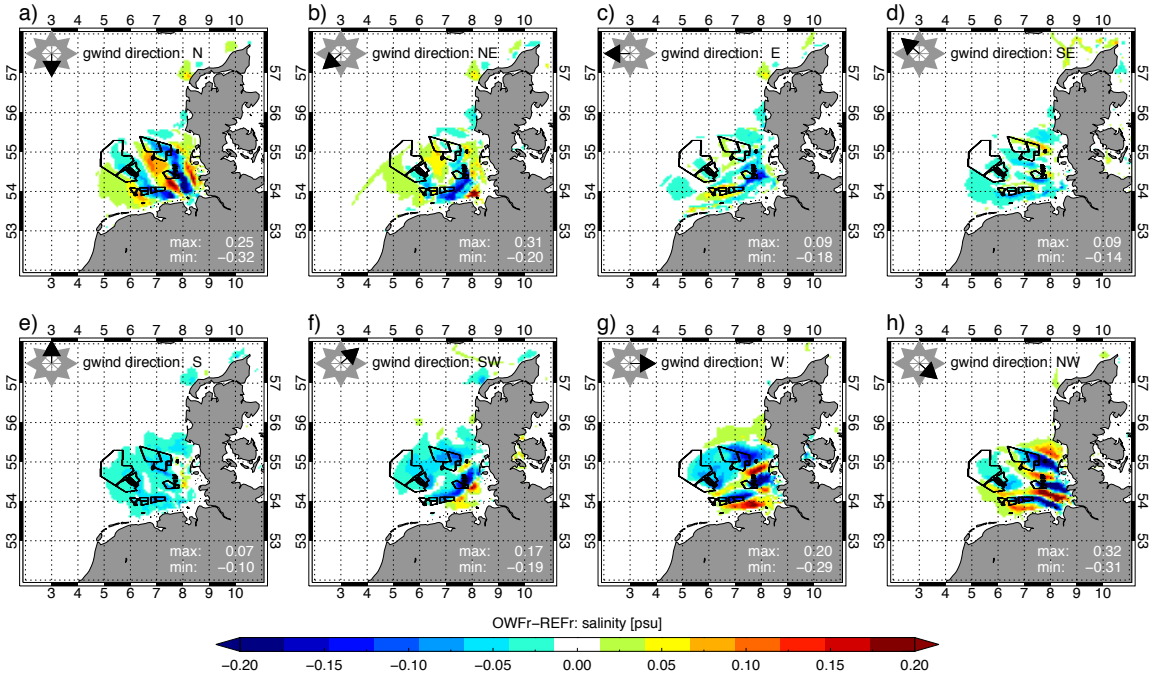

figure 4.3.14: Change in salinity concentration at surface due to OWFs in case of different wind direction cases (gwind direction a)-h) from N-NW) after one day of simulation. The wind direction is defined at height of geostrophic wind.. Units are given ins PSU. Dark grey shaded area marks land, light grey shaded area marks bathymetry. Results are only for wind and pressure forcing.

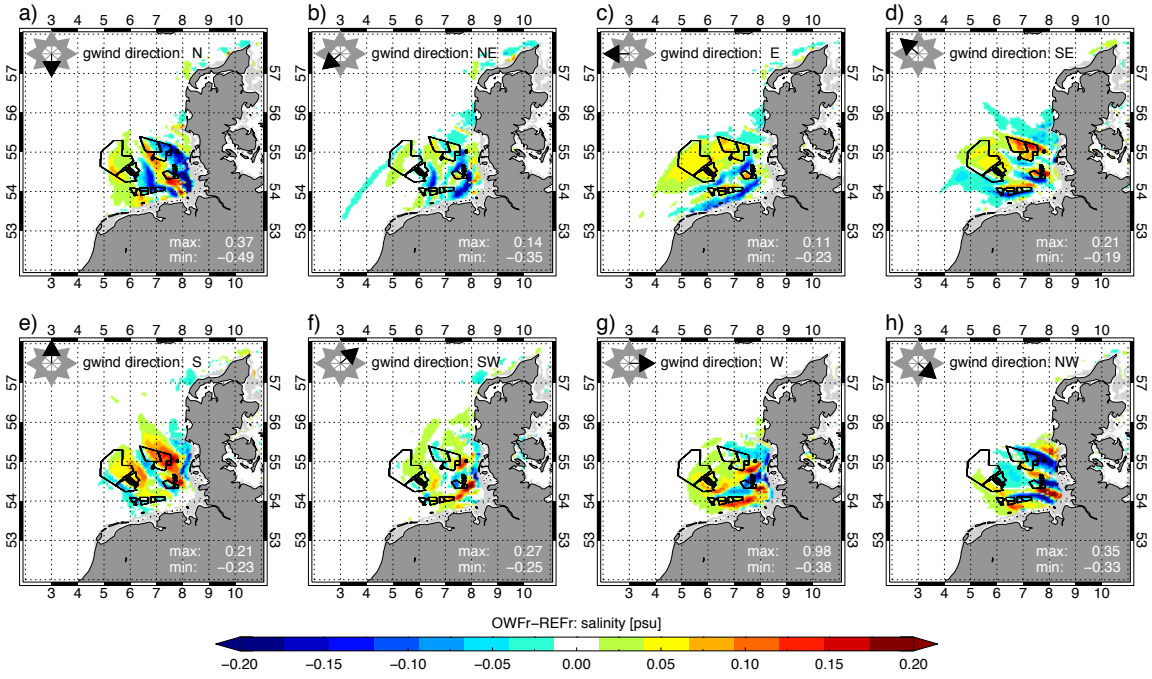

Figure 4.3.15: Change in salinity concentration at 12 m depth due to OWFs in case of different wind direction cases (gwind direction a)-h) from N-NW) after one day of simulation. The wind direction is defined at height of geostrophic wind. Units are given in PSU. Dark grey shaded area marks land, light grey shaded area marks bathymetry and black solid lines illustrate OWF-districts. Results are only for wind and pressure forcing.

The belts of maximal changes are in dependence on surface elevation. In the case of a negative change in ζ upwelling and in the case of a positive ζ downwelling is simulated, which agrees with the theoretical results. The magnitude of vertical motion is independent of the wind direction due to a high agreement of extrema between wind direction cases. Maximal upwelling is $7.0*10^{-5}$ m/s (6.05 m/d) and the maximal downwelling has speeds of $-1.0*10^{-4}$ m/s (8.64 m/d). In waters with depths of 30 m such motion means an overturning within 3.5 to 5 days. Figure 4.3.7 exemplary specifies at the case of wind direction SW that the vertical motion affects whole model depths with maximal changes between 10 m and 15 m. The intensity of the OWF induced vertical velocity w is stronger over the whole depth towards the coasts, especially for downwelling. As the analysis of the OWF-effect on the ocean system in section 4.2.3.6 shows that intensification is supported by shallower water.

Changes of the velocity components u and v at surface due to OWFs are illustrated in figure 4.3.10 and figure 4.3.11. In dependence on the wind direction the velocity wake is stronger dominated by the u- or the v-component. At surface the changes are in order of ± 0.10 m/s, which means an increase/decrease of 20 % compared to the reference run with averaged horizontal velocities at surface of 0.5 m/s.

The effect in temperature and salinity fields due to the OWFs in scenario *B1-2030much* is depicted in figure 4.3.12 and figure 4.3.14 at surface and in figure 4.3.13 and figure 4.3.15 at 12.5 m depths. The figures show the results for the ocean simulations with forcing neglecting full meteorological forcing and clarify hydrographic changes due to dynamical changes.

The OWF effect on temperature are scattered over the areas of the OWF induced vertical motion. In case of upwelling/downwelling a decrease/increase of the temperature is registered. In 12.5 m depth the cooling within the OWF area dominates the warming by averaged 0.36 ºC over all wind direction cases, figure 4.3.12. The strongest cooling is given in the case of wind direction S with -0.42 ºC. On average the warming counts 0.30 ºC with a maximal temperature increase in the case of wind direction N with 0.41 ºC. While in the depth changes in the temperature are in coherency with the vertical motion, at sea surface the SST leads more to a warming then to a cooling. Here the warming of maximal 0.24 ºC (in case of West wind) is an effect due to the velocity wake, which shifts the temperature front. That effect is pointed up in figure 4.3.16, exemplify for wind direction N. SSTs are shown for reference run REFr and run with operating wind turbines OWFr separated for simulation with wind and pressure forcing only and full meteorological forcing after one day. The differences between run OWFr and REFr in SST relies to a deformation of the temperature front, visible at the 9 ºC and 10 ºC contour line, which is deformed by the velocity wake. The shift in the case of full forcing is superposed by the impact on the temperature forcing on SST.

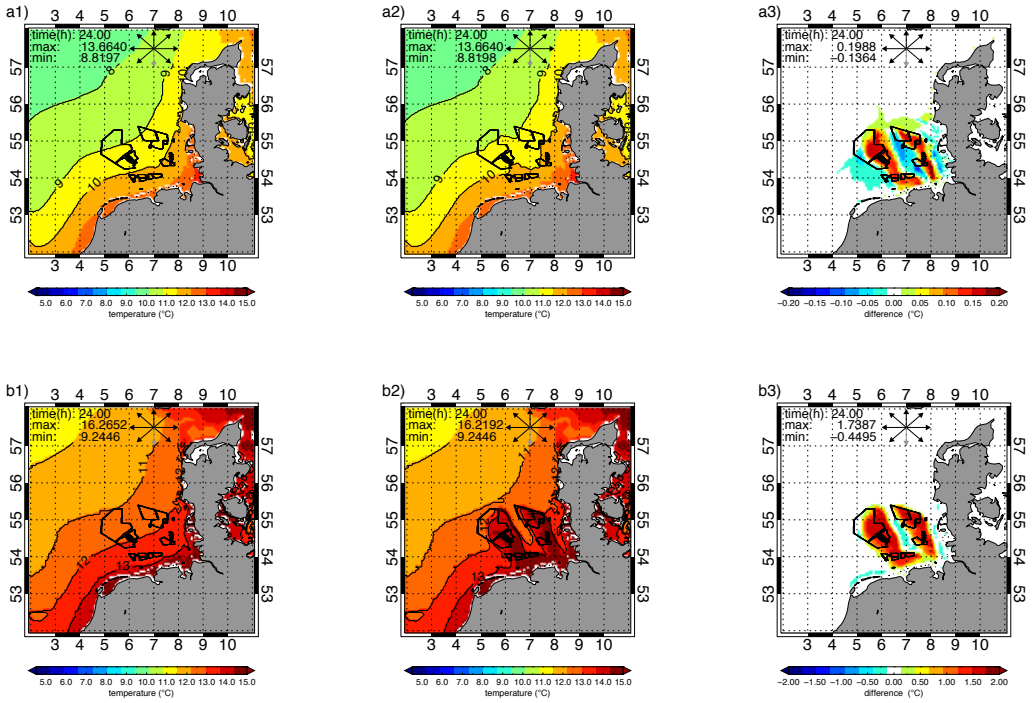

Figure 4.3.16: SST within German Bight for REFr (left), OWFr (middle) and difference between OWFr and REFr (right). Upper row presents results for SST in case of wind and pressure forcing, second row pictures SSTs in case of unrestrained forcing. Results show exemplary OWF effect on SST for wind direction case N wind. OWF affect ocean flow, which leads to shift in temperature front causing warming/cooling at surface compared to reference run.

While dynamics only end in a temperature effect, due to the OWF by ±0.20 ºC, the full meteorological forcing leads to an averaged SST-warming of 1.68 ºC and a cooling of 0.72 ºC. Considering the full forcing and the here OWF induced warming at 10 m heights, the SST and the upper ocean is significantly warmer than in case of wind and pressure forcing only. A wind and pressure forcing only represent only 12-29% of the OWF-effect on ocean temperature related to simulation results under full forcing. But considering now that under more realistic meteorological conditions the atmosphere will cool, as mentioned before, and bearing in mind that simulations show dominantly an upwelling in the OWF-district, it must be expected that the German Bight would suffer an overall cooling.

The OWF-effect on salinity gives a change in order of 0.2 psu, particularly 0.3 psu. At surface the salinity concentration decreases for the wind direction clockwise from East to West (figure 4.3.14). The wind directions having a northern component also results in a slightly increase of 0.3 psu. In 12.5 m depth (figure 4.3.15) the increase and decrease of salinity concentration is mostly balanced as a result of the vertical motion. In average over all wind direction cases the increase of salinity concentration counts 0.33 psu, which equates to a change of 0.95 %, and the

salinity decrease counts 0.31 psu, a change of 0.88 %. A maximal increase of salinity concentration of 0.98 psu is registered in the wind case direction W, the maximal decrease of -0.49 psu is found in the wind case direction N.

Summarized the analysis of the OWF-effect on German Bight, under constant wind directions, gives an idea of possible dynamical and hydrographical variations due to produced wind wake. Important here is a change in the surface elevation in order of centimeters; the change into belts of vertical up- and downwelling is in order of three to five meters per days giving the German Bight a 'whirlpool' character. Related to the hydrographic changes are significant for the temperature/salinity in order of ±0.2 ºC and ±0.3 psu. But hydrographic variations can increase based on atmospheric boundary layer resulting in a warming of more than one degree Celsius, respectively cooling.

4.3.2 Case Study II: OWFs impact based on real meteorological situation

Various theoretical assumptions were analyzed to estimate OWFs effect on atmosphere and especially on ocean. For a better estimation of the OWF effect under daily wind variabilities the simulations of scenario *B1-2030much* consider realistic meteorological conditions. Therefore a meteorological situation in June 2010 is chosen as realistic example.
Simulations of June 2010 were done over the days 16th-19th again for operating wind turbines (OWFr) and for no wind turbines (REFr). The wind turbines only operate at wind speeds between 2.5 m/s and 17 m/s at hub height. The ocean runs are based on North Sea simulations (TOS-02) described in section 3.3.1.2. The result presentation focuses on daily means calculated by a 10min-mean model output.

The mid of June 2010 denotes an interesting weather situation with a strong cooling effect over Europe with strong precipitation events including snow in the Alps. Synoptic inspection shows that Germany was in sphere of a long-wave trough with an expansion from Scandinavia till Mediterranean Sea. The activity focus was placed over Scandinavia connected with a ground low-pressure over mid-Scandinavia. During the days from 16th to 19th June 2010 the frontal system crossed Germany from NW to SE, which results especially over the Alps in extensive rainfall. To easily integrate that meteorological situation over the four days figure 4.3.17 shows 500 hPa Geopotential for each day.

4.3.2.1 Effect on Atmosphere for Case Study II

The mean **wind direction** over the German Bight in 10 m height was NE to N. Figure 4.3.18 summarizes effect of OWFs based on scenario *B1-2030much*:

The **formation of the wind wake** is similar to the wind direction case N and NE described in previous section. The daily means of 10 m wind fields are more or less equal for day 16th and 17th with wind speeds of 10 m/s. Here the maximal wind reduction of 5.35 m/s and an increase of 1.40 m/s occur especially towards coasts. Only the daily mean of the wind direction slightly varies between those two days. At 18th of June 2010 the OWF-effect is weaker due to lesser wind speeds over the German Bight of below 10 m/s. But at 19th June the wind reduction counts up to 9.03 m/s. The 10 m wind speeds on that day simulated in run OWFr are in average 11m/s. The wind turbines operate over the whole time of simulation.

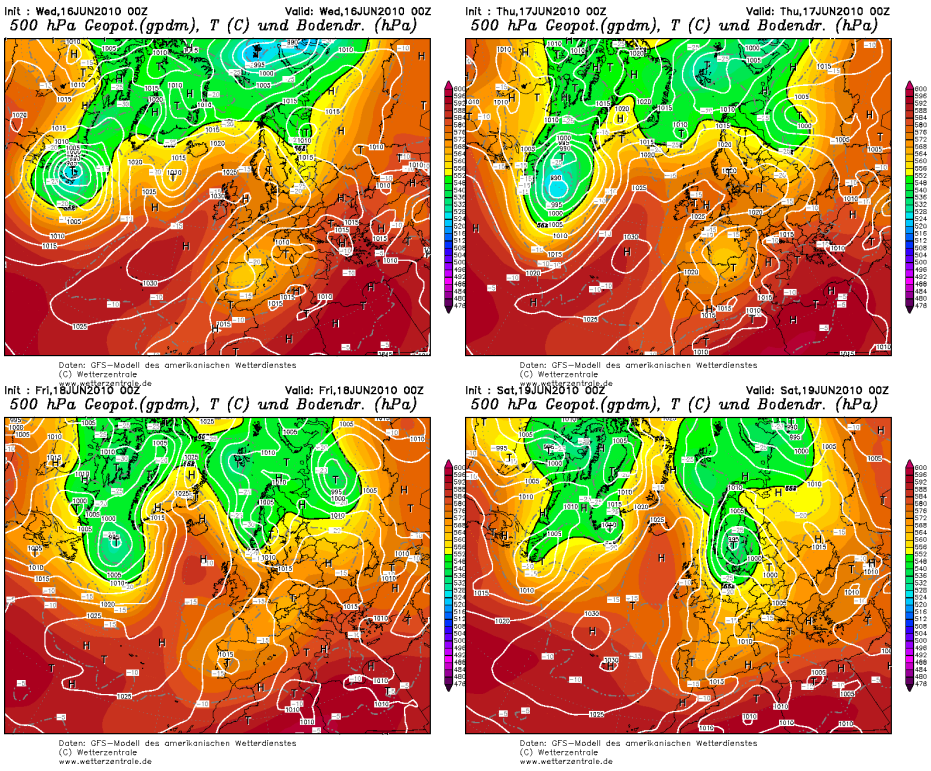

Figure 4.3.17: 500 hPa Geopotential from 16th-19th June 2010. Over the four days a long-wave trough affects meteorological situation of northern Europe and Germany. Maps are taken from www.wetterzentrale.de.

The effect of the OWFs on the **10 m temperature field** obviously shows the previous mentioned generally detected cooling of around 0.5 ºC over ocean. Particularly a warming is identified of maximal 0.72 ºC at day 18th connected with offshore wind. At 19th of June the cooling dominates due to a strong wind wake.

The effect of the OWFs on the **10 m humidity field** consists of a drying of around 5 % and a reduction of total **precipitation** by averaged 0.005 kg/kg. Due to that in case of the run OWFr the **presence of clouds** southerly of the wind farm areas and northerly of the German coast at 16th and 19th June 2010 was not detected like in REFr. On the other hand OWFr leads to some cloudy spaces within the OWF-district on 19th June northerly of latitude 54.00º, which are not given in REFr.

4.3.2.2 Effect on German Bight for Case Study II

Even for the ocean simulations results for days in June 2010 are comparable with the theoretical approach of wind direction N/NE in previous section. The daily means of the OWF-effect on the ocean in June 2010 are documented in figure 4.3.19:

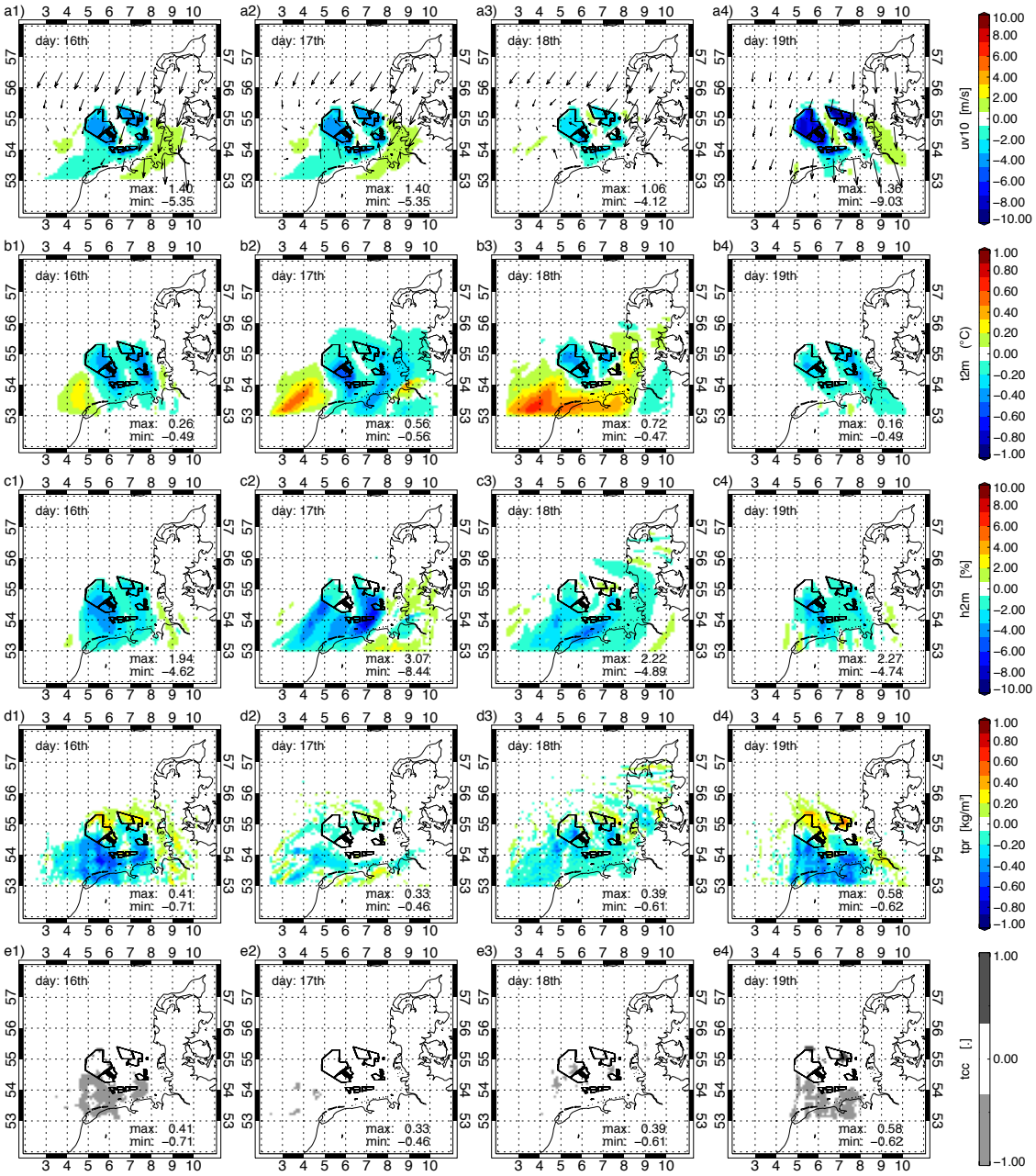

Figure 4.3.18: Daily mean change (OWFr-REFr) of meteorological forcing due to OWF for 16th (a1-e1), 17th (a2-e2), 18th (a3-e3) and 19th (a4-e4) of June 2010. From top to bottom: 10 m horizontal wind field (a1-a4), 10 m temperature (b1-b4), 10 m humidity (c1-c4), total precipitation (d1-d4) and presence of clouds (e1-e4). In case of cloudiness means dark grey (1) OWFr has clouds and REFr not, leight grey (-1) means OWFr has no cloud but REFr, white (0) means presence of clouds is similar for OWFr and REFr. Arrows in figures of the horizontal wind field show wind direction of OWFr. Solid black lines illustrate OWF-districts of expansion szenario *B1-2030much*.

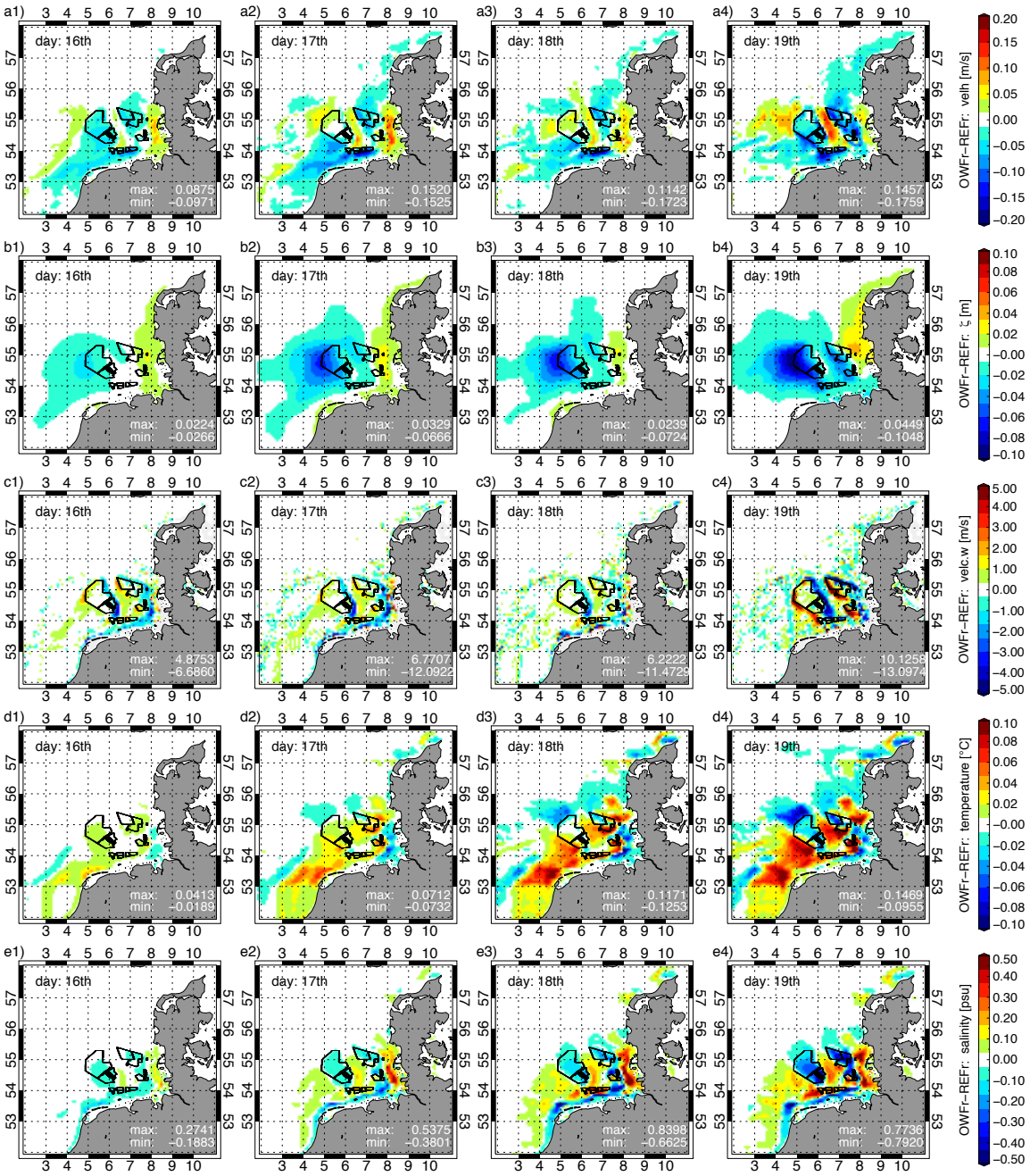

Figure 4.3.19: Daily mean change (OWFr-REFr) of ocean conditions due to OWF for 16th (a1-e1), 17th (a2-e2), 18th (a3-e3) and 19th (a4-e4) of June 2010. From top to bottom: horizontal velocity field at surface (a1-a4), surface elevation (b1-b4), vertical velocity component w at 12.5 m depth (c1-c4), SST (d1-d4) and salinity concentration at surface (e1-e4). Dark grey shaded areas are land, light grey (at velocity w) marks bathymetry and solid black lines illustrate OWF-districts of expansion szenario *B1-2030much*.

The **horizontal velocity** wake-areas are more connected to the wind wake with reductions in order of 0.15 m/s. The **surface elevation** has a dipole with a minimum at the ocean in area of OWFs and a maximum in coastal regions easterly of the OWF-districts of -0.1048 m and 0.0449 m.
The extrema of the dipole grows with the time and reaches higher values than under the theoretical conditions due to higher wind speeds.

The **vertical component w** at 12m depth shows an intensification of up- and downwelling with time. The positions of the belts correspond to the theoretical wind direction case N with upwelling belts at western edge of the OWF-district and downwelling at the eastern edge of the OWF-district. At 19th June the vertical motion has values of -13.10 m/d and 10.13 m/d. Connected with the velocity wake the triggered shift in temperature front and the increase in temperature forcing, the **SST** shows areas of a temperature increase along the coast from west to east, which is connected with the velocity wake, the triggered shift in temperature front and the increase in temperature forcing. Again that effect dominates the field of SST and with the depth cooling/warming corresponds to up-/downwelling. At 19th of June the daily mean change of SST counts around +1.5 ºC and −0.1 ºC. In dependence on the SST the **salinity** concentration at surface shows a decrease of -0.18 PSU at 16th June up to -0.79 psu at 19th June and an increase of 0.77 psu. Decreases obviously occur in the OWF-districts and along the coasts southerly of OWFs from West to East towards the Elbe estuary.

Summarized the OWF expansion scenario *B1-2030much* leads to an intensified modification of the North Sea within the area of the German Bight. Due to an extensive vertical motion of several meters per days, triggered by wind speed and change in surface elevation, the hydrographic conditions are strong affected. Special consideration to the development of the OWF-effect on the ocean must bear in mind. In dependence of the wind direction and the wind speed ocean conditions will easily varies within the German Bight due to OWFs with currently unknown and not assessable effect on the ecosystem.

5 SUMMARY, CONCLUSION AND OUTLOOK

With the objective of evaluation the influences offshore wind farms can possibly have on the atmosphere and the ocean this study deals with the analysis of physically OWF-effect. At his juncture model simulations were consulted and set into relation with measurements. Thereby one focus is the physically, theoretical coverage of the OWF-effect and the other one obtains the determination of especially oceanic changes of the North Sea within the German Bight in future due to the politically planed OWF expansion.

The theoretical analysis of the OWF-effect on atmosphere show that wind turbines produces a wind wake downstream of wind farm. Depending on the wind speed, the amount of turbines, their arrangement and spanned area, the wind wake consists of a maximal simulated wind speed reduction of 70 %; as stronger wind is as intensive the wake is. The wake maximum is located within the wind farms and behind wind farms wind again increases with distance to OWF-center. A change from the operating mode into non-operating wind turbines results in advection of the provoked wind wake by the mean wind. Depending on atmospheric conditions and surface fuxes an OWF can cool or warm atmospheric boundary by ±1K, which also affects the humidity. The dimension of the wake-tail counts more than 120 km downstream of the OWF and the wake dimension orthogonal to wind direction is determined by OWF configurations.
The here used description of wake is based on two approaches by Broström [2008] and the wind turbine parameterization of atmospheric model METRAS. METRAS leads to more realistic results compared to satellite data than Broström and has more advantages in matters of turbine types and atmospheric simulations. Hence results of the OWF-effect on the atmosphere are based on METRAS simulations. A technical simplification of the wake description can be the use of statistical description and analysis of the OWF induced variations of the atmosphere like the example analysis of the impact of wind direction on the wake over the German Bight placed in chapter 4.3. Model simulations can only develop such statistics but they can be applied to ocean simulation by manipulating forcing fields due to OWF-effect statistics.

The consequences in atmosphere due to operating OWFs, significantly affects the ocean system. The wind wake causes a wake in the ocean velocity field within and behind the wind farm, which is connected with a reduced Ekman transport causing divergence and convergence of the water masses. That ends in a change of the surface elevation and the barotropic pressure field in form of a dipole structure having an increase of surface elevation at and north to the wind wake and a

decrease south to the wind wake. These effects on the ocean surface again cause vertical motion in order of several meters per day. Vertical motions means cells around the OWF of upwelling and downwelling advecting the temperature field which results in an excursion of the thermocline around the OWF in the vertical of possible ten meters, in dependence on ocean's stratification. Respectively the salinity and density field are affected.
Analyses of external impacts triggering the OWF-effect on the ocean systems leads to the results that beside the ocean depth primarily the wind wake defines the intensity and dimension of the OWF induced effect on the ocean system:

- Shallower waters intensify the up- and downwelling cells in the vertical and hence stronger hydrographic changes are detected at the depth of thermocline.
- A more intense wind wake leads to greater magnitudes of the up- and downwelling cells and a stronger changes in the hydrography. Additional the vertical exclusion of thermocline increases with the intensity of the wind wake as well as the depth of the thermocline towards lower ocean layers.
- A wider wind wake (orthogonal to the wind direction) leads to a greater horizontal dimension of the velocity wake, which triggers the horizontal dimension of vertical cells and of the thermocline exclusion. The effect is positive linked, so a greater wake results in a greater horizontal OWF-effect in the ocean.

The wind wake itself and so the wake in the ocean velocity field is defined dominantly by the wind speed, by the number of wind turbines of an OWF, respectively the number of wind turbines within one model grid cell and by the OWF-size, respectively the number of grid cells comprising the OWF-district. Here the wind wake follows the relation the stronger the wind speed within the range of OWF's operation mode is the stronger the wind wake, the higher the amount of wind turbines within one grid cell is the more intense is the wind wake and the larger the OWF-district with operating wind turbines is the lager is the affected area of extreme wind reduction.
Additional the choice of the ocean forcing influences the OWF-effect. The use of a full meteorological forcing for ocean simulations shows that the influence of temperature and humidity forcing is the OWF-effect on the SST field positive overlaid. But the influence of offshore wind farms is dominantly driven by the 10m-wind forcing field.

The OWF impact on the ocean system occurs within minutes after switching into the operational OWF-mode. Simulations show that the duration of the OWF-effect lasted over two days after turning off wind turbines but due to the appearance of inertial oscillation in model runs the OWF-effect on the ocean system can vanish faster.

Evaluation with model results, taken around the test wind farm alpha ventus, shows a good agreement of the OWF-effect on ocean's temperature stratification. The model restrictions only lead to expected discrepancies in the horizontal but the main simulated phenomena of up- and downwelling cells causing changes in the temperature stratification are also established in nature.

Simulations over the German Bight underline that detected influences of OWFs, presented under theoretical assumptions, and show that the impact can be intensified in reality. Addicted to meteorological situation and conditions of boundary layer OWF mostly have a cooling affect under realistic conditions. Instead of the vertical cells belts of vertical motion, with maxima of ±10 m/d, occur in dependence on wind direction, which controls the establishment of the surface elevation dipole-structure. The OWF induced atmospheric cooling, respectively warming, is stamped on SST, which is also changed by an identified switch of the SST-front due to wake in the ocean horizontal velocity field. Theoretically SST can vary due to the operating wind turbines by plus minus one degree Celsius.

Finally such imposed dynamical and hydrographic modification on ocean system by OWFs yields to questions about possible variations on the ocean ecosystem and especially about biological consequences.
The theoretical approach of the dynamical analysis, influenced by OWF results, can be transferred to each offshore wind farm location in the world. Technical it is possible to build OWFs along all coasts around the world. Independent of the habitat physically up- and downwelling will occur. And there are plans all over the world to use offshore wind energy. So assuming that installed offshore wind farms will consistently operate the described influence of OWF on atmosphere and especially on ocean will be of permanent duration in future. The meteorological warming and cooling as well as cloud dissipation and fog production can affect local climates over time.
Regarding the ocean effect the surface elevation can impact shipping and storm surges but the important OWF-effect on ocean is the occurrence of vertical motion and so the influence on ocean's stratification will be dominant. A warming or cooling of the upper layers and mixing over the whole water depth will have consequences on the ecosystem. The response of the ecosystem to the vertical mixing regarding nutrients, plankton and other microorganism depends on the habitat. But the OWF induced upwelling in comparison to the coastal up- and downwelling is special because here water that carries the properties of the ecosystem will have relevant consequences on the mixed layer, as mentioned already by Broström [2008].
Additional an impact on mammals is possible. For example the simulated up- and downwelling belts in the North Sea can trigger distribution of common porpoise (personal correspondence with Michael Dähne).

Hence the OWF induced dynamical changes of ocean on the biology as well as on the chemistry should be a next step to estimate OWF-impacts on the ecosystem.

But beside the question about consequences for the ecosystem the back coupling of ocean with atmosphere should be considered in future as well. A change in SST of one/two degrees again affects the atmospheric boundary layer and the atmosphere-ocean interaction. Analysis of OWF impacts on local climates as well as impacts on ocean will need fully coupled atmospheric-ocean simulation to judge the strength of possible changes due to offshore wind farming.

BIBLIOGRAPHY

Arakawa, A., and V. R. Lamb (1977), Computational design of the basic dynamical processes of the UCLA general circulation model, *Methods in Computational Physics*, *17*, 173.

Backhaus, J. O. (1983), A semi-implicit scheme for the shallow water equations for application to shelf sea modelling, *Continental Shelf Research*, *2*(4), 243–254.

Backhaus, J. O. (1996), Climate-sensitivity of European marginal seas, derived from the interpretation of modelling studies, *Journal of Marine Systems*, *7*(2-4), 361–382, doi:10.1016/0924-7963(95)00034-8.

Backhaus, J. O. (1985), A three-dimensional model for the simulation of shelf sea dynamics, *Ocean Dynamics*, *38*(4), 165–187, doi:10.1007/BF02328975.

Backhaus, J. O., and D. Hainbucher (1987), A Finite Difference General Circulation Model for Shelf Seas and Its Application to Low Frequency Variability on the North European Shelf, in *Elsevier Oceanography Series*, vol. 45, pp. 221–244, Elsevier.

Baidya Roy, S. (2004), Can large wind farms affect local meteorology? *J. Geophys. Res.*, *109*(D19), D19101, doi:10.1029/2004JD004763.

Baidya Roy, S., and J. J. Traiteur (2010), Impacts of wind farms on surface air temperatures, *Proceedings of the National Academy of Sciences*, *107*(42), 17899–17904, doi:10.1073/pnas.1000493107.

Becker, G. A., H. Giese, K. Isert, P. König, H. Langenberg, T. Pohlmann, and C. Schrum (1999), Mesoskalige Strukturen, Flüsse und Wassermassen-VariabilitÄt in der Deutschen Bucht, dargestellt durch die Kustos-Experimente und numerische Modelle, *Deutsche Hydrographische Zeitschrift*, *51*(2-3), 155–179, doi:10.1007/BF02764173.

Betz, A. (1926a), Windenergie und ihre Ausnutzung durch Windmühlen, *Naturwissenschaften und Technik, Heft 2*.

Betz, A. (1926b), Wirbelschichten und ihre Bedeutung für die Strömungsvorgänge, *Naturwissenschaften*, *14*(50-51), 1228–1233, doi:10.1007/BF01451780.

BMU (2013), Offshore-Windparks in Betrieb, *www.offshore-windenergie.net*. [online] Available from: http://www.offshore-windenergie.net/windparks/windparks-in-betrieb (Accessed 2 December 2013)

BMWi, BMU (2012), Erster Monitoring-Bericht "Energie der Zukunft," *BMWi und BMU Report, Öffentlichkeitsarbeit*, 1–132. [online] Available from: http://www.bmwi.de/DE/Mediathek/publikationen,did=543190.html

Boyer, T., S. Levitus, H. Garcia, R. A. Locarnini, C. Stephens, and J. Antonov (2005), Objective analyses of annual, seasonal, and monthly temperature and salinity for the World Ocean on a 0.25° grid, *Int. J.*

Climatol., *25*(7), 931–945, doi:10.1002/joc.1173.

Broström, G. (2008), On the influence of large wind farms on the upper ocean circulation, *Journal of Marine Systems*, *74*(1-2), 585–591.

BSH (2013), Meeresnutzung-Windparks, *www.bsh.de*. [online] Available from: http://www.bsh.de/de/Meeresnutzung/Wirtschaft/Windparks/ (Accessed 20 November 2013)

Burchard, H. et al. (2008), Effects of wind farm foundations on the water exchange between North Sea and Baltic Sea - A first careful assessment derived from the QuantAS-Off project, *Projektbericht QuantAS-Off*, 27.

BWE (Ed.) (2013), *Konstruktiver Aufbau von Windanlagen*, Bundesverband WindEnergie. [online] Available from: http://www.wind-energie.de/infocenter/technik/konstruktiver-aufbau/fundament (Accessed 1 December 2013)

Carbajal, N. (1993), Modelling of the circulation in the Gulf of California, *Reports Centre of Marine Climate Research*, 1–186.

Carbajal, N. (1997), Two applications of Taylor's problem solution for finite rectangular semi-enclosed basins, *Continental Shelf Research*.

Carbajal, N., and Y. Montaño (2001), ScienceDirect.com - Estuarine, Coastal and Shelf Science - Comparison between Predicted and Observed Physical Features of Sandbanks, *Estuarine*.

Castro Mora, J., J. M. Calero Barón, J. M. Riquelme Santos, and M. Burgos Payán (2007), An evolutive algorithm for wind farm optimal design, *Neurocomputing*, *70*(16-18), 2651–2658, doi:10.1016/j.neucom.2006.05.017.

Christiansen, M. B. (2006), Wind Energy Applications of Synthetic Aperture Radar, *PhD Thesis, Risø National Laboratory*, 1–54.

Christiansen, M. B., and C. B. Hasager (2005), Wake studies around a large offshore wind farm using satellite and airborne SAR, *31st Int. Symp. on Remote Sensing of Environment, St. Peteresburg (Russian Federation)*.

Damm, P. E. (1997), *Die saisonale Salzgehalts- und Frischwasserverteilung in der Nordsee und ihre Bilanzierung.*, University Hamburg, Institute for Oceanography.

dena, D. E. A. (2013), Offshore-Windenergie, *www.effiziente-energiesysteme.de*. [online] Available from: http://www.effiziente-energiesysteme.de/themen/erneuerbare-energien/offshore-windenergie/ (Accessed 1 December 2013)

Fiedler, B. H., and M. S. Bukovsky (2011), The effect of a giant wind farm on precipitation in a regional climate model, *Environ. Res. Lett.*, *6*(4), 045101, doi:10.1088/1748-9326/6/4/045101.

Fitch, A. C., J. B. Olson, J. K. Lundquist, J. Dudhia, A. K. Gupta, J. Michalakes, and I. Barstad (2012), Local and Mesoscale Impacts of Wind Farms as Parameterized in a Mesoscale NWP Model, *Mon. Wea. Rev.*, *140*(9), 3017–3038, doi:10.1175/MWR-D-11-00352.1.

GWEC, and G. International (2012), Global Wind Energy Outlook, 2012, *REPORT*, 1–52.

Haffmans, C. (2005), *Flächenerhebung für Hamburg und Schleswig-Holstein 2005*, Statistisches Amt für Hamburg und Schleswig-Holstein, Antsalt des öffentlichen Rechts. [online] Available from:

http://www.hamburg.de/info/3277402/hamburg-in-zahlen.html

Hainbucher, D., and J. O. Backhaus (1999), Circulation of the eastern North Atlantic and north-west European continental shelf - a hydrodynamic modelling study, *Fisheries Oceanography*, *8*, 1–12, doi:10.1046/j.1365-2419.1999.00009.x.

Hasager, C., L. Rasmussen, A. Peña, L. Jensen, and P.-E. Rethore (2013), Wind Farm Wake: The Horns Rev Photo Case, *Energies*, *6*(2), 696–716, doi:10.3390/en6020696.

Hau, E. (2008), *Windkraftanlagen*, 4 ed., Springer. ISBN: 9783540721505, 910p.

Hein, B. (2013), Processes of stratification and destratification in the Mekong ROFI, *Dissertation Universität Hamburg*, 156.

Huang, D., J. Su, and J. O. Backhaus (1999), Modelling the seasonal thermal stratification and baroclinic circulation in the Bohai Sea, *Continental Shelf Research*, 1485–1505.

Jenkins, N. (1993), Engineering wind farms, *Power Engineering Journal*, *7*(2), 53–60.

Jimenez, A., A. Crespo, E. Migoya, and J. Garcia (2007), Advances in large-eddy simulation of a wind turbine wake, *J. Phys.: Conf. Ser.*, *75*, 012041, doi:10.1088/1742-6596/75/1/012041.

Jimenez, A., A. Crespo, E. Migoya, and J. Garcia (2008), Large-eddy simulation of spectral coherence in a wind turbine wake, *Environ. Res. Lett.*, *3*(1), 015004, doi:10.1088/1748-9326/3/1/015004.

Keith, D. W., J. F. DeCarolis, D. C. Denkenberger, D. H. Lenschow, S. L. Malyshev, S. Pacala, and P. J. Rasch (2004), The influence of large-scale wind power on global climate, *Proceedings of the national academy of sciences of the United States of America*, *101*(46), 16115–16120.

Kirk-Davidoff, D. B., and D. W. Keith (2008), On the Climate Impact of Surface Roughness Anomalies, *J. Atmos. Sci.*, *65*(7), 2215–2234, doi:10.1175/2007JAS2509.1.

Lackner, M. A., and C. N. Elkinton (2009), An Analytical Framework for Offshore Wind Farm Layout Optimization, *Wind Engineering*, *31*(1), 17–31, doi:10.1260/030952407780811401.

Lange, M., B. Burkhard, S. Garthe, and K. Gee (2010), Analyzing Coastal and Marine Changes: Offshore Wind Farming as a Case Study, edited by GKSS Research Center, Geesthacht, *LOICZ Research and Studies*, *36*, 212.

Lax, P. D., and B. Wendroff (1964), Difference schemes for hyperbolic equations with high order of accuracy, *Comm. Pure Appl. Math.*, *17*(3), 381–398, doi:10.1002/cpa.3160170311.

Lax, P., and B. Wendroff (1960), Systems of conservation laws, *Comm. Pure Appl. Math.*, *13*(2), 217–237, doi:10.1002/cpa.3160130205.

Li, X., and S. Lehner (2012), Sea surface wind field retrieval from TerraSAR-X and its applications to coastal areas, pp. 2059–2062, IEEE.

Linde, M., P. Hoffmann, H. J. Lenhart, and K. H. Schlünzen (n.d.), *Influence of large offshore wind farms on urban climate*, Meteorologische Zeitschrift (in progress).

Loewe, P. (2009), Bundesamt für Seeschifffahrt und Hydrographie - Berichte des BSH - System Nordsee, *REPORTs by German Federal Maritime and Hydrographic Agency*, 1–270.

Lu, H., and F. Porté-Agel (2011), Large-eddy simulation of a very large wind farm in a stable atmospheric boundary layer, *Phys. Fluids*, *23*(6), 065101, doi:10.1063/1.3589857.

Mathis, M. (2013), Projected Forecast of Hydrodynamic conditions in the Norths Sea for the 21st Century, *Dissertation Universität Hamburg*, 182.

Meyers, J., and C. Meneveau (2012), Optimal turbine spacing in fully developed wind farm boundary layers, *Wind Energ.*, *15*, 305–317, doi:10.1002/we.469.

Mikkelsen, R. (2003), Actuator disc methods applied to wind turbines, *PhD Thesis, Technical University of Denmark*.

Morris, N. (2006), *Wind Power*, Black Rabbit Books. ISBN: 9781583409107, 32p.

Mosetti, G., C. Poloni, and B. Diviacco (1994), Optimization of wind turbine positioning in large windfarms by means of a genetic algorithm, *Journal of Wind Engineering and Industrial Aerodynamics*, *51*(1), 105–116, doi:10.1016/0167-6105(94)90080-9.

Moum, J. N., and W. D. Smyth (2001), Upper ocean mixing processes, *Encyclopedia of Ocean Sciences*, 3093–3100, doi:10.1006/rwos.2001.0156.

Nunneri, C., H. J. Lenhart, B. Burkhard, and W. Windhorst (2008), Ecological risk as a tool for evaluating the effects of offshore wind farm construction in the North Sea, *Reg Environ Change*, *8*(1), 31–43, doi:10.1007/s10113-008-0045-9.

O'Driscoll, K., B. Mayer, T. Ilyina, and T. Pohlmann (2012), Modelling the cycling of persistent organic pollutants (POPs) in the North Sea system: Fluxes, loading, seasonality, trends, *Journal of Marine Systems*, *111-112*(2013), 69–82.

Orlanski, I. (1976.), A simple boundary condition for unbounded hyperbolic flows, *J. Phys. Oceanogr.*, *12*, 251–269.

OSPAR (2000), Quality Status Report 2000: Region II: Greater North Sea, *Marine, OSPAR Commission for the Protection of the Marine, London*, *136*, 25.

Otto, L., J. T. F. Zimmermann, G. K. Furnes, M. Mork, R. Saetre, and G. Becker (1990), Review of the physical oceanography of the North Sea, *Netherlands J Sea Res*, *26*(2-4), 161–238.

Paskyabi, M. B., and I. Fer (2012), Upper Ocean Response to Large Wind Farm Effect in the Presence of Surface Gravity Waves, *Energy Procedia*, *24*, 245–254, doi:10.1016/j.egypro.2012.06.106.

Pohlmann, T. (1996a), Calculating the annual cycle of the vertical eddy viscosity in the North Sea with a three-dimensional baroclinic shelf sea circulation model, *Continental Shelf Research*, *16*(2), 147–161.

Pohlmann, T. (1996b), Calculating the development of the thermal vertical stratification in the North Sea with a three-dimensional baroclinic circulation model, *Continental Shelf Research*, *16*(2), 163–194.

Pohlmann, T. (1996c), Simulating the heat storage in the North Sea with a three-dimensional circulation model, *Continental Shelf Research*.

Pohlmann, T. (2006), A meso-scale model of the central and southern North Sea: Consequences of an improved resolution, *Continental Shelf Research*, *26*.

Polinder, H., S. de Haan, and M. R. Dubois (2005), Basic operation principles and electrical conversion systems of wind turbines, *EPE JOURNAL*, *15*(4), 43.

Porté-Agel, F., Y.-T. Wu, H. Lu, and R. J. Conzemius (2011), Large-eddy simulation of atmospheric boundary layer flow through wind turbines and wind farms, *Jnl. of Wind Engineering and Industrial Aerodynamics*, *99*(4), 154–168, doi:10.1016/j.jweia.2011.01.011.

Rhode, J. (1998), The Baltic and North Seas: A process-oriented review of physical oceanography, *Robinson, A. R., Brink, K. H. (Eds.), The Sea. Vol.11, John Wiley & Sons*, 699–732.

Roe, P. L. (1986a), Characteristic-based schemes for the Euler equations, *Annual review of fluid mechanics*, doi:10.1146/annurev.fl.18.010186.002005.

Roe, P. L. (1986b), Discrete models for the numerical analysis of time-dependent multidimensional gas dynamics, *Journal of Computational Physics*, *63*(2), 458–476, doi:10.1016/0021-9991(86)90204-4.

Rubin, H., and J. Atkinson (2001), *Environmental Fluid Mechanics*, 10 ed., edited by M. Dekker, Eastern Hemisphere Distribution. Marcel Dekker AG. [online] Available from: http://www.dekker.com

Schlünzen, H. (1988), *Das mesoskaligen Transport- und Strömungsmodell "METRAS" -Grundlagen, Validierung, Anwendung-*, Hamburger Geophysikalische Einzelschriften: G.M.L. Wittenborn Söhne. 139p.

Schrum, C. (1997), Thermohaline stratification and instabilities at tidal mixing fronts: results of an eddy resolving model for the German Bight, *Continental Shelf Research*, *17*(6), 689–716.

Schrum, C., and J. O. Backhaus (1999), Sensitivity of atmosphere-ocean heat exchange and heat content in the North Sea and the Baltic Sea, *Tellus A*, *51*(4), 526–549, doi:10.1034/j.1600-0870.1992.00006.x.

Steele, J. H., S. A. Thorpe, and K. K. Turekian (2009), North Sea Circulation, *Encyclopedia of Ocean Sciences.Vol. 4. Academic Press, London, 2nd Edition, 73–81.*

Sutherland, H. J., and J. F. Mandell (1996), Application of the US high cycle fatigue data base to wind turbine blade lifetime predictions, *Proceeding of Energy Week, AMSE*.

Sündermann, J., and T. Pohlmann (2011), A brief analysis of North Sea physics, *Oceanologia*, *53*(3), 663–689, doi:10.5697/oc.53-3.663.

Vestas Wind Systems, V. G. (2013), Vestas product brochures, *www.vestas.com*. [online] Available from: http://www.vestas.com/en/media/brochures.aspx (Accessed 9 December 2013)

Wang, C., and R. G. Prinn (2010), Potential climatic impacts and reliability of very large-scale wind farms, *Atmos. Chem. Phys.*, *10*(4), 2053–2061, doi:10.5194/acp-10-2053-2010.

Wolsink, M. (2000), Wind power and the NIMBY-myth: institutional capacity and the limited significance of public support, *Renewable Energy*, *21*(1), 49–64, doi:10.1016/S0960-1481(99)00130-5.

Wu, Y.-T., and F. Porté-Agel (2010), Large-Eddy Simulation of Wind-Turbine Wakes: Evaluation of Turbine Parametrisations, *Boundary-Layer Meteorol*, *138*(3), 345–366, doi:10.1007/s10546-010-9569-x.

Zettler, M. L., and F. Pollehne (2006), The impact of wind engine constructions on benthic growth

patterns in the western Baltic, *Offshore Wind Energy. Research on Environmental Impacts. J. Köller, J. Köppel, W. Peters (eds.): Springer, Berlin*, 201–222.

Zhou, L., Y. Tian, S. B. Roy, C. Thorncroft, L. F. Bosart, and Y. Hu (2012), Impacts of wind farms on land surface temperature, *Nature Climate Change*, *2*(6), 1–5, doi:10.1038/nclimate1505.

PERSONAL CORRESPONDENCES

Marita Linde

Meteorologisches Institut der Universität Hamburg

Bundesstrasse 55

20146 Hamburg

Germany

Michael Dähne

Institute for Terrestrial and Aquatic Wildlife Research (ITAW)

University of Veterinary Medicine Hannover (Foundation)

Werftstraße 6

25761 Büsum

Germany

DATA OVERVIEW

ECMWF ERA-Interim data used in this thesis have been obtained from the ECMWF data server http://www.ecmwf.int/products/data and additional ECMWF forcing data are a courtesy of the Meteorological Institute of the University of Hamburg.

METRAS data used in this thesis were simulated by M. Linde and are a courtesy of the Meteorological Institute of the University of Hamburg.

HAMSOM data used in this thesis were simulated by myself.

WOA-01 data used in this thesis are a courtesy of the Institute of Oceanography of the University of Hamburg.

ADCP and CTD data used in this thesis were supported by the BSH and measured by myself.

ABBREVIATIONS

variables

ζ	surface elevation [m]
p	pressure [Pa]
uv10	horizontal wind field in 10 m [m/s]
ug	geostrophic wind [m/s]
velh	ocean's horizontal velocity field
velc.u	ocean's velocity component u [m/s]
velc.v	ocean's velocity component v [m/s]
velc.w	ocean's velocity component w [m/s]
SST	sea surface temperature [ºC]

abbreviations in analysis

OWF	offshore wind farm
TOS	type of simulation (TOS-01, TOS-2)
UG*	Prescribed geostrophic wind speed (UG5, UG8, UG16) [m/s]
T*	wind turbine number (T012, T048, T080, T160, T8590) [#]
F*	forcing fields (F01, F02, F03, F04)
wd*	wind direction (N, NE, E, SE, S, SW, W, NW, N) [º]
HD*	depth of ocean (HD60, HD30) [m]
TS*	temperature and salinity (TS01, TS02, TS03)
BTM	HAMSOM simulations in barotropic mode
src•	Source code manipulation
REFr	reference without wind turbines
OWFr	simulations considering wind turbines

model & data

HAMSOM	Hamburg Shelf Ocean Model
METRAS	mesoscale transport and stream model
ECMWF	European Centre for Medium-Range Weather Forecasts
WOA	World Ocean Atlas
NOAA	National Oceanic and Atmospheric Administration
ADCP	Acoustic Doppler Current Profiler
CTD	Conductivity-Temperature-Depth

institutions & additionals

BMU	Bundesministerium für Umwelt, Naturschutz und Reaktorsicherheit
BMWi	Bundesministerium für Wirtschaft und Technologie
BWE	Bundesverband Wind Energie
BSH	Federal Maritime and Hydrographic Agency
dena	Deutsche Energie-Agentur GmbH
EEZ	Exclusice Economy Zone
IMPRS	International Max Planck Research School

APPENDIX

A.A The Numerical Model HAMSOM

The **HAM**burg **S**helf **O**cean **M**odel (HAMSOM) is a numerical three-dimensional baroclinic hydrostatic dynamical model developed by Backhaus in 1985 [*Backhaus,* 1985]. Papers related to HAMSOM model description are for example Pohlmann (2006), Pohlmann (1996a-c), Orlanksi (1976), Schrum (1997), Lax and Wendroff (1960 &1964), Roe (1986a-b) and several more. Some details of model structure is given here:

Essential Equations:

The main equations are the momentum equations in x- and y-coordinate, the vertical motion in z-coordinate, which is approximated by the vertical hydrostatic equation, the continuity equation, temperature and salinity conservation equation and the state equation of sea water.

$$\frac{\partial \mathbf{u}}{\partial t} + \mathbf{u}\frac{\partial u}{\partial x} + v\frac{\partial u}{\partial y} + w\frac{\partial u}{\partial z} - fv = -\frac{1}{\rho}\frac{\partial p}{\partial x} + A_H\nabla^2 u + \frac{\partial}{\partial z}\left(A_v\frac{\partial u}{\partial z}\right) + F_x \qquad \textbf{(EQ.a 1)}$$

$$\frac{\partial \mathbf{v}}{\partial t} + \mathbf{u}\frac{\partial v}{\partial x} + v\frac{\partial v}{\partial y} + w\frac{\partial v}{\partial z} + fu = -\frac{1}{\rho}\frac{\partial p}{\partial y} + A_H\nabla^2 v + \frac{\partial}{\partial z}\left(A_v\frac{\partial v}{\partial z}\right) + F_y \qquad \textbf{(EQ.a 2)}$$

$$\frac{\partial p}{\partial z} = -\rho g \qquad \textbf{(EQ.a 3)}$$

$$\frac{\partial u}{\partial x} + \frac{\partial v}{\partial y} + \frac{\partial w}{\partial z} = 0 \qquad \textbf{(EQ.a 4)}$$

$$\frac{\partial T}{\partial t} + u\frac{\partial T}{\partial x} + v\frac{\partial T}{\partial y} + w\frac{\partial T}{\partial z} = K_H\nabla^2 T + \frac{\partial}{\partial z}\left(K_v\frac{\partial T}{\partial z}\right) + S_T \qquad \textbf{(EQ.a 5)}$$

$$\frac{\partial S}{\partial t} + u\frac{\partial S}{\partial x} + v\frac{\partial S}{\partial y} + w\frac{\partial S}{\partial z} = K_H\nabla^2 S + \frac{\partial}{\partial z}\left(K_v\frac{\partial S}{\partial z}\right) + S_S \qquad \textbf{(EQ.a 6)}$$

$$\rho = \rho(S,T,p) = \rho_0 + \rho' \qquad \textbf{(EQ.a 7)}$$

The equations are solved with finite differences.

Approximations and Parameterizations:

HAMSOM is treated as hydrostatic model, which means vertical momentum equation is replaced by the hydrostatic equilibrium of perturbation pressure and density fields.

Boussinesq-approximation is adapted as well. The vertical sub-grid scale turbulence is parameterized by means of a second order turbulent closure approach. The vertical eddy viscosity and the vertical eddy diffusivity are explained in section 4.2.2. The horizontal sub-scale processes (diffusion of horizontal momentum) are parameterized through the implementation of the Smagorinsky scheme (section 4.2.2) The scheme is used to obtain variable values of the horizontal turbulent exchange coefficient which depend on the horizontal velocity shear of the flow.

Boundary Conditions

HAMSOM uses a free surface and can be run with open and closed boundary conditions. At the surface it is assumed that z=ζ (ζ:= surface elevation) and at the bottom z=-H (H:= water depth below the mean sea level). Then the following boundary is used:

Kinematic boundary conditions:

$$\boldsymbol{w_\zeta = \frac{\partial \zeta}{\partial t} + u_\zeta \frac{\partial \zeta}{\partial x} + v_\zeta \frac{\partial \zeta}{dy}} \qquad \textbf{(EQ.a 8)}$$

$$\boldsymbol{w_{-H} = u_{-H} \frac{\partial H}{\partial x} + v_{-H} \frac{\partial H}{dy}} \qquad \textbf{(EQ.a 9)}$$

dynamic boundary conditions at surface (s) and bottom (b):

$$\boldsymbol{\tau_s^{(x)} = A_{vc} \frac{\partial u_\zeta}{\partial z} - A_{dc} \cdot \left(\frac{\partial u_\zeta}{\partial x} \frac{\partial \zeta}{\partial x} + \frac{\partial u_\zeta}{\partial y} \frac{\partial \zeta}{\partial y} \right)} \qquad \textbf{(EQ.a 10)}$$

$$\boldsymbol{\tau_s^{(y)} = A_{vc} \frac{\partial v_\zeta}{\partial z} - A_{dc} \cdot \left(\frac{\partial v_\zeta}{\partial x} \frac{\partial \zeta}{\partial x} + \frac{\partial v_\zeta}{\partial y} \frac{\partial \zeta}{\partial y} \right)} \qquad \textbf{(EQ.a 11)}$$

$$\boldsymbol{\tau_b^{(x)} = A_{vc} \frac{\partial u_{-H}}{\partial z} - A_{dc} \cdot \left(\frac{\partial u_{-H}}{\partial x} \frac{\partial H}{\partial x} + \frac{\partial u_{-H}}{\partial y} \frac{\partial H}{\partial y} \right)} \qquad \textbf{(EQ.a 12)}$$

$$\boldsymbol{\tau_b^{(y)} = A_{vc} \frac{\partial v_{-H}}{\partial z} - A_{dc} \cdot \left(\frac{\partial v_{-H}}{\partial x} \frac{\partial H}{\partial x} + \frac{\partial v_{-H}}{\partial y} \frac{\partial H}{\partial y} \right)} \qquad \textbf{(EQ.a 13)}$$

with A_{vc}/A_{dc} as vertical/horizontal eddy viscosity/diffusion coefficients.

In case of closed boundaries the normal velocity component and the elevation are zero at the boundaries. While for the lateral velocity a semi-slip condition is applied, i.e., the gradients of the tangential velocity components at the closed boundaries are set to zero.

In case of open boundaries, as used here, the sea surface elevation ζ are obtained from data which are calculated from the tidal components.

Sea surface temperature and salinity are changed due to heat fluxes. It is assumed that no heat and salt fluxes occur across the seabed floor, thus at bottom is obtained:

$$\boldsymbol{\left(\frac{\partial T}{\partial z}\right)_{-H} = \left(\frac{\partial S}{\partial z}\right)_{-H} = 0} \qquad \textbf{(EQ.a 14)}$$

At the open lateral boundaries Temperature and salinity are adapted from observed values by Newtonian damping. The variable can also be damped to a reference value:

$$\frac{\partial T}{\partial t} = \frac{T_{clim} - T}{T_d} \quad \textbf{(EQ.a 15)}$$

$$\frac{\partial S}{\partial t} = \frac{S_{clim} - S}{T_d} \quad \textbf{(EQ.a 16)}$$

With T_{clim} and S_{clim} as climatological temperature and salinity, which are taken from WOA-01 as references; T_d is the damping scale, i.e., the smaller the value T_d, the stronger the property is kept to the reference value.

Additional for temperature and salinity "active boundary conditions" are adopted which means that in case of an inflow to the internal model area, the temperature and the salinity references are dominant, in contrary, if the transport causes an outflow, temperature and salinity from interior influence the boundary data. As outflow condition a Sommerfeld radiation condition is adopted (Orlanski, 1976).

The source and sink term of salinity is represented by the river inflow at the lateral boundary and by evaporation and rainfall at the sea surface. The source and sink term of temperature is represented by heat fluxes at the sea surface.

Numerical Method:

HAMSOM is using transports instead of velocities in the horizontal momentum equations and the continuity equation. Hence, the water column is split into N layers with a layer thickness of $h_k=d_k-d_{(k-1)}$ where d_k is the depth of the lower boundary.

HAMSOM makes use of Arakawa C grid, which was extended in the vertical by Backhaus [1980] for the spatial discretization.

For time discretization HAMSOM uses a semi-implicit scheme including the Crank-Nicholson method and a second staggered two time level scheme for temperature and salinity (half time step apart from the time steps of velocity and surface elevation).

Horizontal discretization is considered by semi-implicit and explicit scheme and vertical discretization by the semi-implicit scheme. The advective terms of the momentum equation and of the transport equation of salinity and temperature are solved explicitly. The implicit numerical scheme is applied for the free surface and vertical shear stress terms in the equation of motion to avoid stability constraints for surface gravity waves as well as for vertical diffusion. Numerical stability of Coriolis and pressure gradient terms is guaranteed by a stable second order approximation.

A.B The Numerical Model METRAS

The following provisions are based on Schlünzen's dissertation [*Schlünzen*, 1988] and briefly introduce the model METRAS.

Essential Equations:

The basic prognostic equations are the equations of motion and continuity, and the balance equations for heat and humidity or harmful substances. The diagnostic equations are the zeroth law of thermodynamics and the equation for the potential temperature. In an arbitrary with earth rotating coordinate system these equations can be written as follows:

$$\frac{\partial \vec{v}}{\partial t} + (\vec{v} \cdot \nabla)\vec{v} = -\frac{1}{\rho} \nabla p - 2[\Omega \times \vec{v}] - \nabla\vec{\Phi} + \vec{F} \qquad \textbf{(EQ.b 1)}$$

$$\frac{\partial \rho}{\partial t} + \nabla \cdot (\rho\vec{v}) = 0 \qquad \textbf{(EQ.b 2)}$$

$$\frac{\partial \chi}{\partial t} + \vec{v} \cdot \nabla\chi = Q_\chi + F_\chi \qquad \textbf{(EQ.b 3)}$$

$$v_l^k = \frac{R_l^k T}{p} \qquad \textbf{(EQ.b 4)}$$

$$\theta = T\left(\frac{1000[hPa]}{p}\right)^{R/c_p} \qquad \textbf{(EQ.b 5)}$$

Coordinates and Averaging:

The equations in METRAS are solved on a topographic grid, which means a substitution of the vertical coordinate z to η with

$$\eta = z_t \frac{z - z_s(x,y)}{z_t - z_s(x,y)} \qquad \textbf{(EQ.b 6)}$$

The vertical coordinate η is zero at the height of orography $z_s(x,y)$ and at top of model at $z=z_t$ the η-coordinate is constant in time and space, defined as $\eta=z_t$. Additional METRAS uses a non-equidistance but horizontal orthogonal grid, adaptive for 1km up to 50km size of grid cell. In this thesis METRAS was run with a mesh size of 3km, which is comparable to HAMSOM. METRAS' coordinate system is so chosen that there is the same number of grid cells in x- (east-west) direction and y- (north-south) direction. This asks for a transformation of model equations changing coordinates from X (x, y, z) to $\dot{X}$ $(\dot{x}^1, \dot{x}^3, \dot{x}^3)$ then equations can be solved as long as space derivations are constant for an area and time interval. In the atmosphere a lattice separation in order of one centimeter and a time interval of 1 second

should not be exceeded (Pielke, 1984,2002). Hence the model equation would have been solved in a lot of grid cells. Due to computer capacity and efficient issued simulations of mesoscale phenomena. Therefore the model equations are averaged in space and time. This is done by separating variables ψ into a part, which is averaged in space and time (integrated over Δt, Δx, Δy and Δz), and into a part showing deviating fluctuations ψ':

$$\bar{\psi} := \int_t^{t+\Delta t} \int_x^{x+\Delta x} \int_y^{y+\Delta y} \int_z^{z+\Delta z} \psi \, dx\, dy\, dz\, dt / (\Delta t\, \Delta x\, \Delta y\, \Delta z) \qquad \textbf{(EQ.b 7)}$$

In the model equations the variable $\boldsymbol{\psi}$ is separated by $\bar{\psi} + \psi'$. Thereby micro scale changes of pressure and density are neglected.

Beside that temperature, humidity, pollutant concentration, pressure and density are separated into a mesoscale part $\tilde{\psi}$ and a large-scale part ψ_0:

$$\psi_0 := \int_x^{x+\Delta x} \int_y^{y+\Delta y} \bar{\psi}\, dx\, dy \,/ (\,\Delta x \cdot \Delta y\,) \qquad \textbf{(EQ.b 8)}$$

Due to numerical reasons the mesoscale pressure $\tilde{p}$ is split into p_1 and $p_2 = \tilde{p} - p_1$. Summarized the meteorological variables are:

$$u = \bar{u} + u' \qquad \textbf{(EQ.b 9)}$$

$$v = \bar{v} + v' \qquad \textbf{(EQ.b 10)}$$

$$w = \bar{w} + w' \qquad \textbf{(EQ.b 11)}$$

$$\rho = \rho_0 + \tilde{\rho} \quad (\textbf{Assumption}: \rho' \ll \tilde{\rho}) \qquad \textbf{(EQ.b 12)}$$

$$p = p_0 + p_1 + p_2 \quad (\textbf{Assumption}: p' \ll \tilde{p}) \qquad \textbf{(EQ.b 13)}$$

$$\chi = \chi_0 + \tilde{\chi} + \chi' \qquad \textbf{(EQ.b 14)}$$

Approximation:

Several approximations are adopted in METRAS considering the scale meso-γ an meso-β. This scale allows the simulation of mesoscale phenomena with a size of 2.5 km to 250km. These approximations are the hydrostatic approximation, geostrophic approximation, inelastic approximation, and Boussinesq approximation.

Hydrostatic Approximation:

$$\frac{\partial p}{\partial z} = -\rho g \qquad \textbf{(EQ.b 15)}$$

The hydrostatic balance describes the balance between pressure gradient force and gravity force. Thereby the vertical acceleration within in the equation of vertical motion is negligible small compared to the gravity acceleration g. This approximation can be adopted for phenomena with a characterized horizontal extension of 10 km and more.

Inelastic Approximation:

$$\nabla \cdot (\rho \vec{v}) = 0 \qquad \textbf{(EQ.b 16)}$$

Here the assumption is that the density ρ does not change partial. A nice side effect of this assumption is the elimination of sound waves and that it is valid for the whole mesoscale.

Geostrophic Approximation:

The geostrophic balance is the balance between the horizontal gradient pressure force and the Coriolis force considering that this is valid in a frictionless, non-curving stream in a non-rotating fluid, which can be adopted in the macro-scale starting from 25.000km. So the geostrophic approximation ($\vec{v} = \overrightarrow{v_g}$) is not allowed in the mesoscale. But it is assumed that the large-scale pressure p_0 achieves the geostrophic approach. Which means that in METRAS' horizontal equations of motion the large-scale pressure is substitute by the geostrophic wind. In the new coordinate system, $\dot{X}$, the following applies:

$$\mathbf{U}_g = -\frac{1}{\rho_0 f}\left\{\frac{\partial \dot{x}^2}{\partial y}\frac{\partial p_0}{\partial \dot{x}^2} + \frac{\partial \dot{x}^3}{\partial y}\frac{\partial p_0}{\partial \dot{x}^3}\right\} \qquad \textbf{(EQ.b 17)}$$

$$\mathbf{V}_g = +\frac{1}{\rho_0 f}\left\{\frac{\partial \dot{x}^1}{\partial x}\frac{\partial p_0}{\partial \dot{x}^1} + \frac{\partial \dot{x}^3}{\partial x}\frac{\partial p_0}{\partial \dot{x}^3}\right\} \qquad \textbf{(EQ.b 18)}$$

In METRAS it is also assumed that the Coriolis force and so the Coriolis parameter $f = 2\Omega \sin\varphi$ (Ω:= rotation rate of earth, φ:=latitude) is fixed. This is allowed up to a characteristically horizontal phenomena's extension of 1.500 km. Thus **f** is constant in area of METRAS.

Boussinesq Approximation:

In METRAS the Boussineq Approximation is supposed which is caused by the fact that horizontal fluctuations of density are mostly small compared to the large-scale density part and can neglected everywhere with the exception of the lift-term in the equation of vertical motion. So it is imposed that

$$\overline{\rho} = \rho_0\left(1 + \frac{\tilde{\rho}}{\rho_0}\right) \cong \rho_0 \qquad \textbf{(EQ.b 19)}$$

The mesoscale density anomaly $\tilde{\rho}$ is derived by the linearized gas equation as a function of the mesoscale part of potential temperature $\tilde{\theta} = \bar{\theta} - \theta_0$, of pressure $\tilde{p} = p_1 + p_2$, and of specific humidity (considering wet atmosphere) $\tilde{q}_1^1 = \bar{q}_1^1 - q_0{}_1^1$. With the specific heat at constant pressure c_p and accordingly at constant volume c_v for dry air the mesoscale density anomaly is given by

$$\frac{\tilde{\rho}}{\rho_0} = -\frac{\tilde{\theta}}{\theta_0} + \frac{c_v}{c_p}\frac{p_1+p_2}{p_0} - \left(\frac{R_1^1}{R_0} - 1\right)\cdot \tilde{q}_1^1 + \tilde{q}_1^2 + \tilde{q}_1^3 \qquad \textbf{(EQ.b 20)}$$

In case of a neutral atmosphere $\tilde{\rho}$ is zero.

Parameterization

Due to a relative big grid some physical processes cannot be resolved. Therefore it is necessary to parameterize such processes to describe their influences on the whole system. In METRAS subscale turbulences are parameterized as well as cloud formation and precipitation formation, and radiation. Further details see Schlünzen (1988). Regarding turbulences METRAS uses the 1st order closure instead of a 2nd order (using prognostic equations) to reduce integration costs.

Numeric Methods:

As well as HAMSOM, METRAS equations are spatially discretized on an ARAKAWA-C-Grid. As mentioned before here the grid for the vectorial value is shifted form the grid of scalar values by a half grid cell. This placement improves numerical precision in case of calculating divergences and is an essential tool to calculate gravity waves.

Due to the non-linear instabilities of the model equations 2Δx-waves can occur and fudges the solution. To avoid and to damp 2Δx-waves and METRAS works with different filters.

Initialization:

The initialization of METRAS works in three steps. First step is the definition of model area and the calculation of the model grid considering ground levels and land use classes. Second step is the definition of balanced starting profile calculated with the help of a one-dimensional model. To determine this profile large-scale profiles temperature, humidity and geostrophic wind have to be purported. The dynamical field and the thermodynamically field are not adopted at the beginning that is why the dynamical equations are calculated as long till the wind profile is stationary. After that the third step is the horizontal homogeny extension of the 1D stationary initialized profiles to the model area of the three dimensional model. After three hours of simulation time the model is independent of the initialization method (Hoffmann, 2009).

B. Worldwide Offshore Wind Farming Worldwide

The United Nations Convention of the Law of the Sea (UNCLOS) only allows nations to economical use their adjoining oceans within the zone called Exclusive Economic Zone (EEZ). Only within the EEZ constructions of offshore wind farms all over the world are possible. A definition of ocean zones before nations coasts are given by graphic B01. The EEZ can reach till 220 miles from coast into ocean. Hence a huge area along coasts around the world is possible for wind farming especially if offshore wind turbines become independent of ocean depth due to swimming fundaments.

But currently offshore wind farming is more concentrated to Europe and China like Graphic B02 shows based on LORC Knowledge. **LORC Knowledge** is a Danish database collecting all offshore wind farm information worldwide. The Database is supervised by **L**indoe **O**ffshore **R**enewable **C**enter. Beside statistics they also provides maps illustrating places of OWFs in commission and under installation. The website is www.lorc.dk.

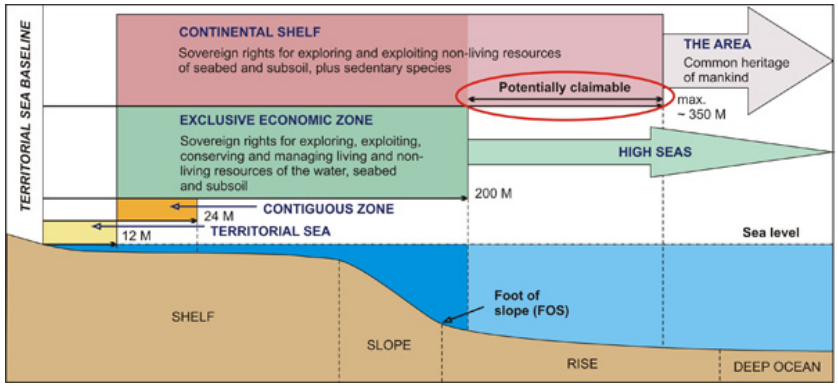

Graphic B01: Definition of Exclusive Economy zone in coastal areas after UNCLOS. Source: BGR after Symonds et al. 1998. [www.bgr.bund.de/EN/Themen/Zusammenarbeit/TechnZusammenarb/UNCLOS/ UNCLOS_Article76/UNCLOS_Article76_node_en.html]

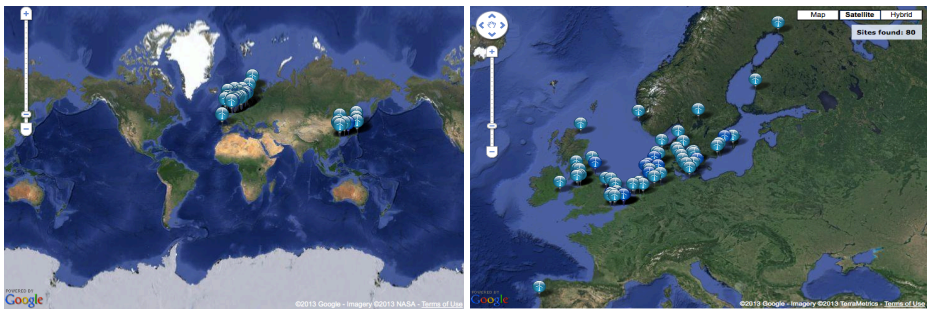

Graphic B02: OWFs in commission and under installation around the world (left)and in Europe (right). Core areas are Europe with North Sea and China in 2013. Dark blue signs means OWF is installation progress; light blue signs are commissioned OWFs. Taken from www.lorc.dk/offshore-wind-farms-map.

C. WEGA Cruise 141

C.1 Impressions of WEGA Cruise 141

Due to security instructions offshore wind turbines cannot be easily observed from close. In exception of people being involved in this wind business nobody else has really the opportunity to visit such an offshore wind farm, indeed there exist some tours for example from Helgoland going close to German's test wind park *alpha ventus*. To get a feeling of the dimension of wind turbines here some pictures photographed during the "WEGA Cruise in May 2013" helps to see what happened outside on the North Sea. It is impressive how big even the smaller offshore wind turbines compared to onshore wind turbines, which let expect a rotor diameter of 200 meters, and may more in future, are. On the other hand it shows a proud technique, designed for more than 15 years challenges against salty water and air, gears and high swell.
At this point I would like to take again the opportunity of thanking the BSH for its special support.
Image D01 shows VWFS WEGA, image D02 – D05 illustrates *alpha ventus* with wind turbines, research platform Fino1 and relay station.

ship type: research/survey vessel
year of construction: 1990
length x width: 52m x 10m
register ton: 969 t
load rating: 160 t
registered speed (max/mean): 13/11.6 kn
flag: Germany [DE]
Rufzeichen: DBBC
IMO: 8901054, **MMSI:** 211205970

Image C01: VWFS WEGA , sounding, wreck searching and research vessel of the BSH

Image C02: Impression of German test wind park alpha ventus on 12th May 2013 in the morning (left) and in the evening (right).

Image C03: Research platform Fino1 (left and middle) close to alpha ventus and relay/transformer station close to alpha ventus wind turbine AV12 (right), taken at 12th/13th May 2013.

Image C04: Impressions of dimension of offshore wind turbine and nacelle. Helicopters bring people to offshore wind farm and let them down on a rope for maintenance work at wind turbine.

Image C05: Left) Dinghy for diving within *alpha ventus*. Divers checking, lying-up and obtain measuring instruments in test district *alpha ventus*. Right) Construction boat for offshore wind farm mounting close to *alpha ventus*.

C.2 CTD probe

Image C06 shows CTD (conductivity, temperature, depth) measuring station at research vessel WEGA with winch and CTD probe and sensing elements. A CTD probe determines conductivity, temperature and pressure of water and based on that measures salinity and density can be calculated.

Image C06: Winch and CTD probe (left) and sensing elements (middle and right). Number through images: 1) data transfer and power supply cable and connection an rope of winch; 2) Oxygen sensor; 3) temperature probe; 4) pressure sensor; 5) conductivity cell.

Temperature measurement:

A platinum-thermometer Pt100 is common used for temperature measurement via CTD. That is a resistance wire, which has at 0 ºC an electrical resistance of 100 Ohm. Platinum is used due to its long-term stability and reproductivity of electrical conditions. The coefficient of specific resistance

is positive, which means the resistance grows with temperature. The relationship is linear but the temperature coefficient of platinum is small, $3.85x10^{-3}$/ºC. The level of measured accuracy requires a value of 0.01 ºC, the aimed resolution is 0.001 ºC. That means, connected with small temperature coefficient, that $2.5x10^{-6}$ parts of the resistance value must be resolved. Therefor Pt100 is used as resistance within as Wheatstone-bridge-circuit.

Conductivity measurement:

The used technique for conductivity is a galvanic method with two electrodes via a bridge circuit. The electrodes are sensitive against exterior electrical and magnetic fields. They have to be protected towards outside then surrounding cannot take influence on measuring signal.

Pressure measurements:

Pressure measurements with electrical technique are done by diaphragm capsule. The bending of a membrane determined the measurement. The bending is gathered piezo-resistive.

In sum 42 CTD profiles at different positions were taken by cranking the CTD probe from sea surface to bottom and back during WEGA cruise 141 on 12th May 2013.

C.3 ADCP

Image C07 shows the instrument ADCP (Acoustic Doppler Current profiler) with it is four sensors and construction for placement at sea ground. The ADCP is fixed within a ground track, which again is connected to some weight via a cable to make sure that the rack will be placed at ground. The connected buoys swimming at surface and mark position of dropped ADCP.

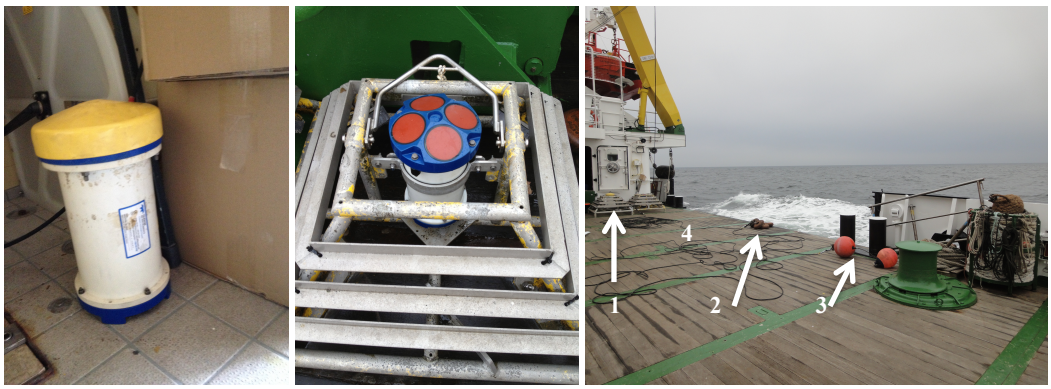

Image C07: Measuring instrument ADCP with yellow protecting above sensors (left), ADCP with four red transducer faces within ground rack (middle) and right image shows construction of ADCP ground rack (1), weights (2) and buoy (3) connected with cable rope(4) before dropping.

ADCPs are used to measure how fast water is moving across an entire water column, so water velocity over a profile. The water currents are measured via sound considering the Doppler effect. The ADCP transmits pings of sound at a constant frequency into the water from bottom to surface. As the wave sounds travel, they ricochet off particles suspended in the moving water and reflect back to the instrument. Due to the Doppler Effect, sound waves bounced back from a particle moving away from the profiler have a slightly lowered frequency when they return. Particles moving toward the instrument send back higher frequency waves. Then the difference in frequency between the waves the profiler sends out and the waves it receives is called the Doppler shift. The shift is used to calculate how fast the particle and the water around it are moving. But ADCP does not send a single wave but several pulses – broadband technology. So finally it is not the difference of frequency between the emitted wave and the reflected wave that is measured but the variation of phase between several reflected pulses. The depth of velocity through the measured profiles is calculated by considering the time of return of the wave and the speed of sound. The column of water is partitioned into vertical elements (bins) and the ADCP "listens" to the reflected echoes at different time interval, which correspond to given depths.

During WEGA cruise 141 three ADCPs were sank into the North Sea at three different positions around wind farm *alpha ventus*. They were dropped in the morning of 11th May 2013 and collected at 13th May 2013 as well in the morning. At 08:30 UTC all three instruments started measures on 11th May 2013.
The ADCP worked with a broadband of 614.4 kHz with 50 pings per ensemble, a time per ping of 12.0", so an ensemble interval of 600.0 seconds and a bin size in the vertical of 0.5 m, so sixty vertical elements.

The postprocessing of ADCP data included a filtering of the tidal signal. That was necessary to actually have a change to detect upwelling and downwelling structures in the data set because here tides impose the dominant signal on each dynamical measurement. The done tide filtering followed the principle of the harmonic analysis.
The ADCP measurements are illustrated in figure C08. On the one hand data are shown including the tidal signal, on the other hand the tidal signal is filtered by the harmonic analysis. The order of vertical velocities, after tidal extraction, is higher than in the case of model simulation, shown in figure C09. For most of the time the measurements show a positive vertical component (greenish, reddish color gives positive values in figure C08). In connection with the analysis of the CTD-temperature profiles, in chapter 4.2.4, the used ADCP positions seems to be as well outside of the downwelling region, which is expected within and close around the wind farm alpha ventus, but they even do not strike the upwelling region, shown in figure C09 by means of modeled velocity components w.

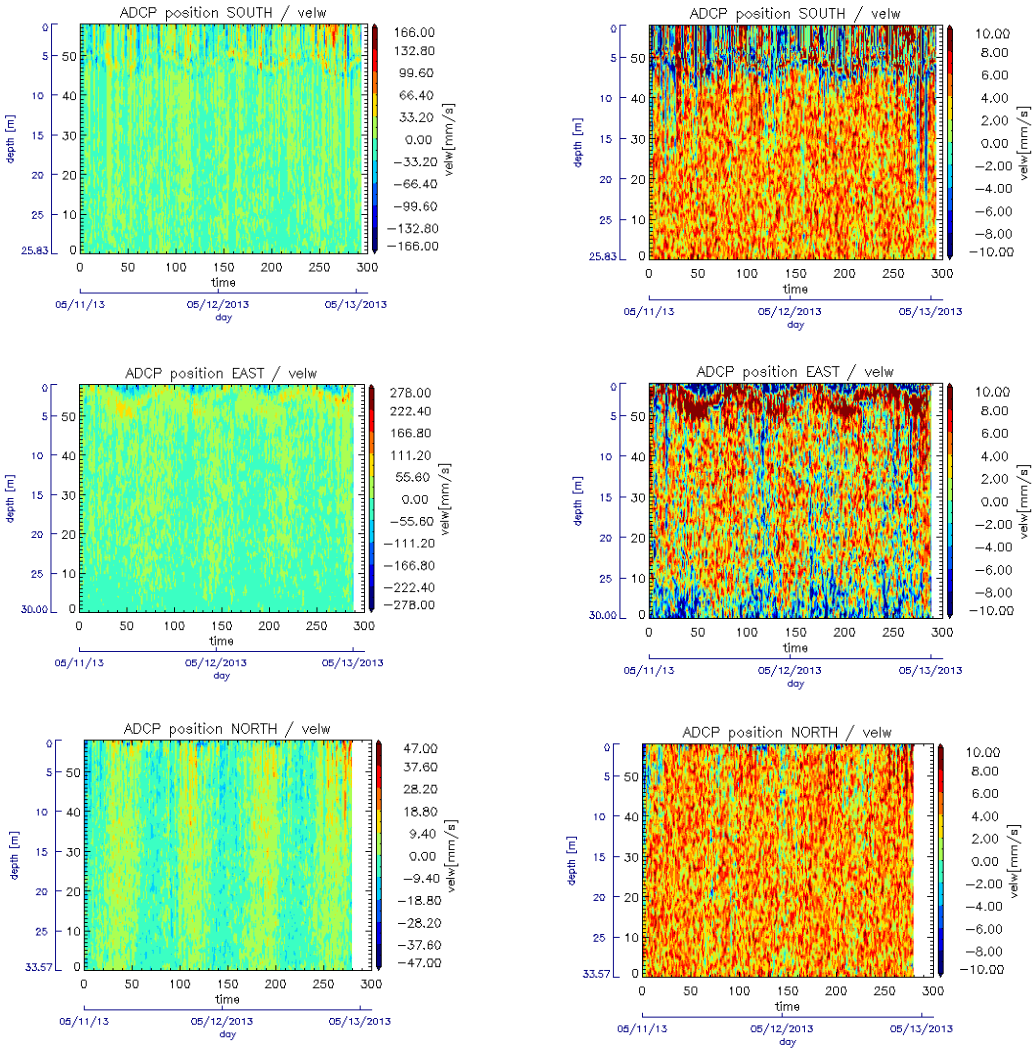

Graphic C08: Vertical velocity component w in mm/s for the three ADCPs around wind farm alpha ventus including tidal signal (left) and without tidal signal (right). Black colored x- and y-axis gives time and depth at measure-index. Blue colored x- and y-axis gives the corresponding real depths and times for the measure-index.

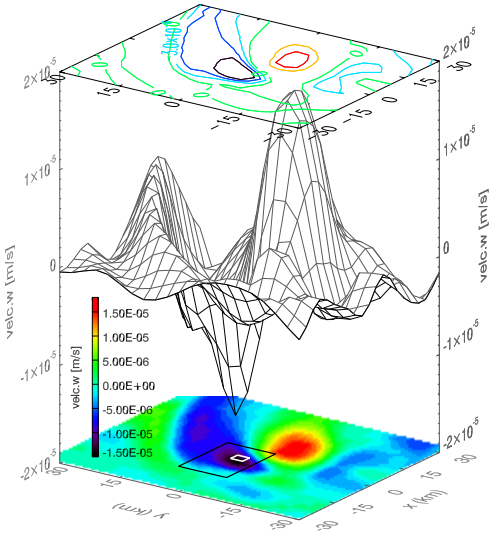

Graphic C09: Simulated vertical velocity component w with the ocean model HAMSOM at 2m depth. White square shows position of the OWF, black square illustrates the big square around the wind farm after modification of horizontal dimension in chapter 4.2.4.

D. Additions and Notes to OWF Analysis

D.1 Handling METRAS data

Comment on indirect coupling of HAMSOM with METRAS:

One main work was the preparation of METRAS data to make them useable in HAMSOM. Simplifying only a semi-directional coupling was adapted. Although METRAS was simulated with a similar grid size of 3x3 km data asked for a horizontal interpolation of METRAS forcing to longitude-latitude grid of HAMSOM. METRAS is isometric, while HAMSOM is orthomorphic. Therefore METRAS data were projected and interpolated to HAMSOM grid.

Another issue in using METRAS data as forcing for HAMSOM occurs regarding surface data. In case of METRAS it is not possible to exactly calculate 2 m temperature and humidity fields. Instead of 2 m values the 10 m values were used as forcing for HAMSOM. Based on evaluation of model data and data of Weather Mast Hamburg that approach is acceptable because differences between surface an 10 m lie between 1ºC (personal correspondence with M.Linde). In case of theoretical simulation an error of 1 ºC does not change declaration. Hazarding the consequences of a temperature error of 1ºC in forcing, the error is considered in ocean surface for realistic simulations of the North Sea (TOS-02). Using 10m-temperature and humidity values are more consequent than extrapolation by ignoring stabilities and other conditions, which can result in absolutely wrong near surface data.

Array transformation:

Data of the atmosphere model METRAS are used in this thesis as meteorological forcing for ocean simulations with HAMSOM. Due to differences between METRAS and HAMSOM a post processing regarding adjustment of METRAS data to HAMSOM needs is necessary.

In this connection one important point is the transformation of METRAS data array to HAMSOM array. Graphic 2 illustrates the projection of Cartesian based model array with a dimension of x=164 and y=149 and horizontal resolution of 3x3 km on a spherical map. Northerly and southerly length of boundaries disagrees and area is not rectangular, like HAMSOM. METRAS is isometric, while HAMSOM is orthomorphic. So METRAS coordinates from Cartesian (x,y) coordinates were transformed to the spherical longitude and latitude grid considering the center-longitude and center-latitude of model mid-point MP(6.3º, 55º). Exemplified each value of grid box was taken with corresponding longitude/latitude position and placed on HAMSOM array into the grid box having the closest (maximal 0.1’ discrepancies) longitude/latitude position to the one of METRAS.

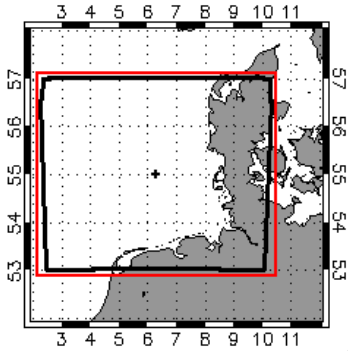

Graphic D01: Projection of METRAS horizontal array (NX1=164,NX2=149) with resolution of 3x3 km on spherical map without array transformation based on provided corresponding longitude, latitude data. Mid point of model area at MP(6.3º,55º) is marked with '+'. Northerly and southerly length of METRAS model area (black square) disagree. Finally METRAS data were transformed to red HAMSOM area.

Gaps of filled HAMSOM array with METRAS data were corrected using linear interpolation which slightly expanse METRAS district to red square in graphic 2.

Cloud Determination:

In case of unrestrained meteorological forcing for ocean simulation, HAMSOM need as cloud parameter the presence of cloud defined as 0 for cloud-free and as 1 for cloudiness. Types of clouds or fraction are ignored. ECMWF provide total cloud cover information but METRAS not. To determine cloudiness in METRAS cloud water content and precipitation was considered.

Total cloud water content $\bar{q}_{lc}$ [kg/kg] is given by sum of

$$\bar{q}_{lc} = q_{lc0} + \tilde{q}_{lc}$$

with q_{lc0}:= basic state cloud water [kg/kg] content and $\tilde{q}_{lc}$:= mesoscale specific cloud water content perturbation [kg/kg].

Precipitation is given by total rain water content $\bar{q}_{lr}$[kg/kg],

$$\bar{q}_{lr} = q_{lr0} + \tilde{q}_{lr}$$

with q_{rc0}:= basic state rain water content [kg/kg] and $\tilde{q}_{lr}$:= mesoscale specific rain water content perturbation [kg/kg].

In case of total cloud water content and total rain water content averaged over the vertical being greater 10^{-3} kg/kg the presence of cloud was set to 1.

For the use of precipitation in HAMSOM the rain water content was converted into kg/m^3 multiplying with the density.

Calculation of real temperature:

METRAS provides potential temperature as output. The potential temperature θ is defined as the temperature that a air parcel would have if it were brought adiabatically to some reference pressure and easier allows comparison of temperature in different height.

HAMSOM needs real temperature for forcing in degrees Celsius. The real temperature was calculated from potential temperature and pressure via

$$T = \frac{\theta}{\left(p0/p\right)^{0.286}}, \qquad with\ p0 = 1000.hPa, p[hPa], \theta[K]\ and\ T[K].$$

Finally T[K] was converted into T[ºC].

D.2 Comment on Result Presentation

Analysis of model results and measurements focuses on the one hand of the whole model area but on the other hand also along sections through model area and at special points. With following graphics positions of OWFs and investigation locations, which are used in analysis, are clarified. Graphic D02 shows how small the different OWF-districts are. Graphic D03 underlines cross-sections through OWF which were mostly used to illustrate OWF's effect on ocean in the vertical. Lastly, graphic D03 documents positions of location within the model are. Position P0, respectively P3, is placed within OWF at southeasterly grid box of the 12-turbine OWF-district. Distance to S-N cross section of positive positions (P+…) is 6 km, for negative positions (P-…) is 12 km. P2 is 6 km North to OWF center along S-N section, P3 12 km South to it.

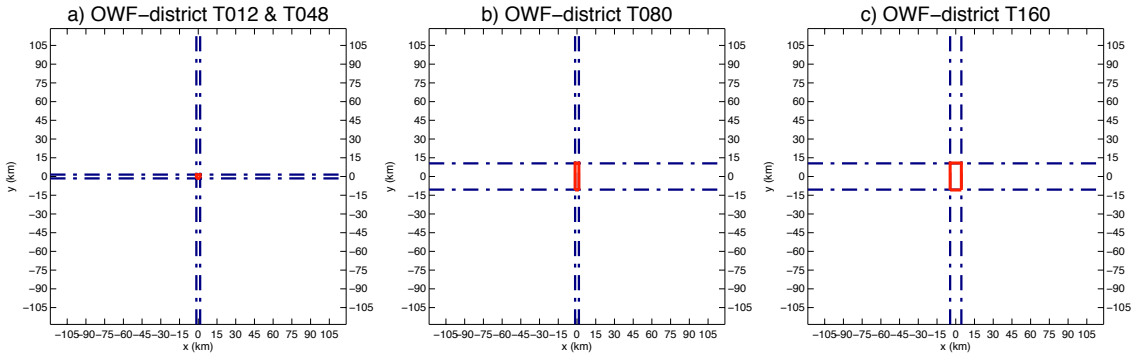

Graphic D02: OWF-districts within model area under TOS-01 (Ocean-Box model), which is marked with a red square. a) clarifies the OWF-district for 12 and 48 turbines, b) for 80 turbines and c) for 160 wind turbines. The blue dashed-dotted lines are used in result presentation; their enclosed area defines the OWF-district.

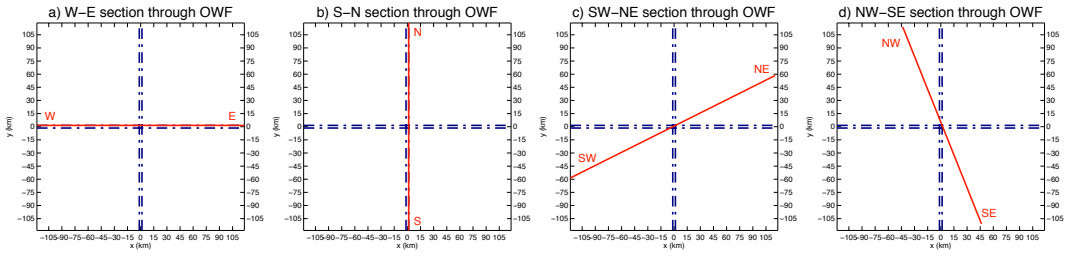

Graphic D03: Cross-sections of analysis through OWFs. a) Cross section through OWF from West to East, b) from South to North, c) from Southwest to Northeast and d) from Northwest to Southeast.

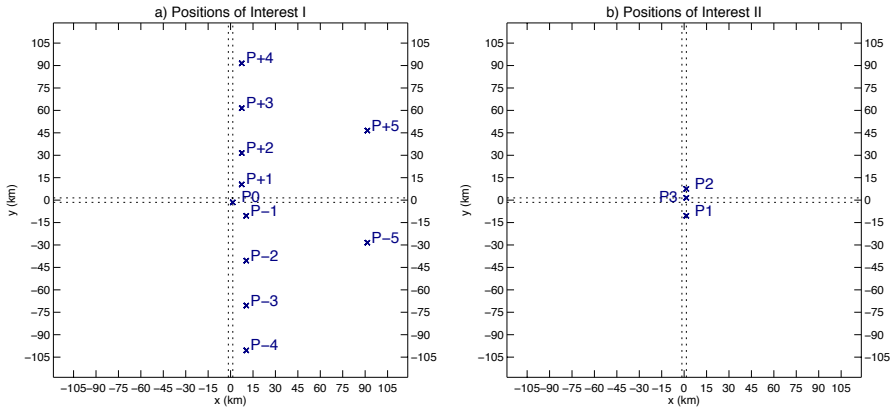

Graphic D03: Positions of interest for OWF analysis. a) Sample of positions based on OWF induced dipole structure of surface elevation. b) Sample of positions along S-N cross-section through OWF based on location of extrema of ocean variables.

E. Table of Statistics

Table of statistics comprises extrema and averages of OWF-effect (OWFr-REFr) of various simulations using the ocean box (TOS-01). These tables are used in analysis of the OWF-effect on ocean related to different wind speed conditions, size of OWF-district and number of wind turbines, ocean depth and forcing assumptions. Those analyses are documented in chapter 4.3.Pmin and Pmax are the positions of extrema of whole model area (overall), at surface and in 12 m depths. 'min' and 'max' give the extreme changes of ocean variables due to OWF. 'mean+' provides the positive averaged OWF-effect, 'mean-' the negative one.

Table of Statistics 1: Master simulation T012ug08 TS01HD60F01 → UG8 / T012 / F01 / HD60

mode (OWFr-REFr)	variable	unit	depth	Pmin (km/km/m)	Pmax (km/km/m)	min	max	mean-	mean+
T012ug08	ζ	[m]	overall	(+09/-09/00)	(+06/+12/00)	-9.16E-03	5.86E-03	-7.71E-04	5.71E-04
	velh	[m/s]	overall	(+12/-09/10)	(+03/ 00/12)	-0.0621	0.0910	-0.0014	0.0036
	velh		surface	(-06/+03/00)	(+03/-15/00)	-0.0581	0.0670	-0.0038	0.0024
	velh		12m	(00/+39/12)	(+03/ 00/12)	-0.0051	0.0910	-0.0012	0.0064
	velc.u	[m/s]	overall	(+03/ 00/00)	(+09/-15/00)	-0.1360	0.0807	-0.0061	0.0019
	velc.u		surface	(+03/ 00/00)	(+09/-15/00)	-0.1360	0.0807	-0.0072	0.0033
	velc.u		12m	(+06/+03/12)	(+09/-18/12)	-0.0719	0.0498	-0.0068	0.0021
	velc.v	[m/s]	overall	(+03/ 00/12)	(+18/-09/10)	-0.0578	0.0700	-0.0018	0.0014
	velc.v		surface	(-03/-12/00)	(-06/+06/00)	-0.0477	0.0544	-0.0013	0.0021
	velc.v		12m	(+03/ 00/12)	(-09/+06/12)	-0.0578	0.0342	-0.0027	0.0016
	velc.w	[m/s]	overall	(+09/+09/12)	(+03/-12/10)	-4.37E-05	5.04E-05	-1.09E-06	1.21E-06
TS01HD60F01	velc.w		2m	(00/+03/02)	(+06/-06/02)	-1.10E-05	1.54E-05	-4.70E-07	5.63E-07
	velc.w		12m	(+09/+09/12)	(+03/-12/12)	-4.37E-05	4.61E-05	-2.32E-06	2.22E-06
	temperature	[°C]	overall	(+06/-09/10)	(+03/+09/14)	-2.7012	1.9250	-0.0087	0.0094
	temperature		surface	(+09/-15/00)	(+03/-03/00)	-0.2317	0.1939	-0.0047	0.0110
	temperature		12m	(+06/-12/12)	(+03/+09/12)	-1.8067	1.6771	-0.0540	0.0663
	salinity	[psu]	overall	(+03/+09/18)	(+09/-09/16)	-5.84E-02	6.16E-02	-9.59E-04	7.68E-04
Master Simulation	salinity		surface	(+03/-03/00)	(+09/-15/00)	-1.13E-03	2.17E-03	-1.05E-04	4.33E-05
	salinity		12m	(+03/+09/12)	(+09/-09/12)	-1.87E-02	5.40E-02	-1.05E-03	1.19E-03
	density	[kg/m^2]	overall	(+03/+09/14)	(+06/-09/10)	-0.3958	0.5605	-0.0025	0.0023
	density		surface	(+03/-03/00)	(+09/-15/00)	-0.0415	0.0498	-0.0024	0.0010
	density		12m	(+03/+09/12)	(+06/-12/12)	-0.3502	0.3727	-0.0138	0.0111

Table of Statistics 2: Simulation T012ug05 TS01HD60F01 → UG5

mode (OWFr-REFr)	variable	unit	depth	Pmin (km/km/m)	Pmax (km/km/m)	min	max	mean-	mean+
T012ug08	ζ	[m]	overall	(+09/-09/00)	(+06/+12/00)	-3.84E-03	2.54E-03	-2.47E-04	2.12E-04
	velh	[m/s]	overall	(-03/+03/00)	(+03/ 00/10)	-0.0360	0.0421	-0.0005	0.0014
	velh		surface	(-03/+03/00)	(+06/-15/00)	-0.0360	0.0335	-0.0027	0.0013
	velh		12m	(+09/+42/12)	(+03/ 00/12)	-0.0014	0.0401	-0.0004	0.0024
	velc.u	[m/s]	overall	(+03/ 00/00)	(+09/-15/00)	-0.0656	0.0372	-0.0022	0.0007
	velc.u		surface	(+03/ 00/00)	(+09/-15/00)	-0.0656	0.0372	-0.0026	0.0014
	velc.u		12m	(+09/+03/12)	(+06/-15/12)	-0.0307	0.0185	-0.0026	0.0008
	velc.v	[m/s]	overall	(00/-03/10)	(-06/+06/00)	-0.0296	0.0286	-0.0006	0.0006
	velc.v		surface	(-03/-12/00)	(-06/+06/00)	-0.0203	0.0286	-0.0005	0.0019
	velc.v		12m	(00/-03/12)	(-03/+12/12)	-0.0262	0.0139	-0.0009	0.0007
	velc.w	[m/s]	overall	(+03/+09/10)	(+06/-09/08)	-2.36E-05	2.56E-05	-5.06E-07	4.99E-07
TS01HD60F01	velc.w		2m	(00/+06/02)	(+06/-06/02)	-7.78E-06	1.04E-05	-3.39E-07	3.63E-07
	velc.w		12m	(+03/+09/12)	(+03/-09/12)	-1.89E-05	1.56E-05	-9.67E-07	8.87E-07
	temperature	[°C]	overall	(+06/-09/12)	(+03/+09/12)	-0.8742	0.8157	-0.0037	0.0036
	temperature		surface	(+12/-12/00)	(+06/ 00/00)	-0.0706	0.0323	-0.0023	0.0018
	temperature		12m	(+06/-09/12)	(+03/+09/12)	-0.8742	0.8157	-0.0200	0.0221
	salinity	[psu]	overall	(+03/+09/16)	(+06/-09/16)	-2.48E-02	2.78E-02	-3.63E-04	3.25E-04
UG5	salinity		surface	(+06/ 00/00)	(+12/-12/00)	-1.60E-04	1.34E-04	-1.56E-05	8.23E-06
	salinity		12m	(+03/+09/12)	(+06/-09/12)	-1.25E-02	2.18E-02	-4.34E-04	4.46E-04
	density	[kg/m^2]	overall	(+03/+09/12)	(+06/-09/10)	-0.1689	0.1804	-0.0010	0.0009
	density		surface	(+06/ 00/00)	(+12/-12/00)	-0.0069	0.0150	-0.0004	0.0005
	density		12m	(+03/+09/12)	(+06/-09/12)	-0.1689	0.1803	-0.0046	0.0041

Table of Statistics 3: Simulation T012ug16 TS01HD60F01 → UG16

mode (OWFr-REFr)	variable	unit	depth	Pmin (km/km/m)	Pmax (km/km/m)	min	max	mean-	mean+
T012ug08	ζ	[m]	overall	(+09/-12/00)	(+03/+09/00)	-2.14E-02	1.42E-02	-2.30E-03	1.88E-03
	velh	[m/s]	overall	(+15/-12/16)	(+06/ 00/22)	-0.1271	0.1761	-0.0049	0.0094
	velh		surface	(-06/+03/00)	(00/-15/00)	-0.1238	0.1214	-0.0078	0.0054
	velh		12m	(+15/-12/12)	(+06/ 00/12)	-0.0936	0.1312	-0.0056	0.0099
	velc.u	[m/s]	overall	(+03/-03/00)	(+09/-18/00)	-0.3299	0.1331	-0.0174	0.0057
	velc.u		surface	(+03/-03/00)	(+09/-18/00)	-0.3299	0.1331	-0.0213	0.0077
	velc.u		12m	(+09/ 00/12)	(+12/-18/12)	-0.1803	0.0896	-0.0183	0.0067
	velc.v	[m/s]	overall	(-03/-09/00)	(+18/-09/16)	-0.1165	0.1190	-0.0057	0.0044
	velc.v		surface	(-03/-09/00)	(-06/+06/00)	-0.1165	0.1031	-0.0048	0.0053
	velc.v		12m	(-06/-12/12)	(+12/-09/12)	-0.0664	0.0962	-0.0043	0.0055
	velc.w	[m/s]	overall	(+09/+03/24)	(+06/-12/16)	-9.36E-05	1.12E-04	-3.41E-06	3.63E-06
TS01HD60F01	velc.w		2m	(-03/-03/02)	(+09/-03/02)	-1.88E-05	2.36E-05	-1.59E-06	1.63E-06
	velc.w		12m	(-03/ 00/12)	(+06/-12/12)	-6.32E-05	7.62E-05	-3.73E-06	3.98E-06
	temperature	[ºC]	overall	(+06/-09/16)	(00/+06/20)	-3.0687	2.6948	-0.0247	0.0233
	temperature		surface	(+12/-15/00)	(00/-06/00)	-0.4346	0.8787	-0.0122	0.0360
	temperature		12m	(+09/-06/12)	(-03/ 00/12)	-2.3055	0.7564	-0.0257	0.0258
	salinity	[psu]	overall	(+03/+09/22)	(+09/-12/18)	-1.70E-01	2.16E-01	-2.32E-03	2.43E-03
UG16	salinity		surface	(00/-03/00)	(+12/-15/00)	-2.18E-02	2.06E-02	-1.19E-03	5.11E-04
	salinity		12m	(-03/ 00/12)	(+06/-09/12)	-2.20E-02	9.16E-02	-1.01E-03	1.05E-03
	density	[kg/m^2]	overall	(00/+06/20)	(+06/-12/16)	-0.5962	0.7119	-0.0061	0.0063
	density		surface	(00/-06/00)	(+12/-15/00)	-0.1942	0.1010	-0.0081	0.0028
	density		12m	(-03/ 00/12)	(+06/-09/12)	-0.1688	0.4963	-0.0059	0.0058

Table of Statistics 4: Simulation T048ug08 TS01HD60F01 → T048

mode (OWFr-REFr)	variable	unit	depth	Pmin (km/km/m)	Pmax (km/km/m)	min	max	mean-	mean+
T012ug08	ζ	[m]	overall	(+09/-09/00)	(+03/+09/00)	-8.86E-03	5.83E-03	-7.45E-04	5.40E-04
	velh	[m/s]	overall	(+18/-12/10)	(+03/ 00/12)	-0.0639	0.0923	-0.0013	0.0034
	velh		surface	(-06/+03/00)	(+03/-15/00)	-0.0575	0.0677	-0.0036	0.0023
	velh		12m	(-03/+36/12)	(+03/ 00/12)	-0.0050	0.0923	-0.0012	0.0063
	velc.u	[m/s]	overall	(+03/ 00/00)	(+06/-15/00)	-0.1389	0.0813	-0.0059	0.0019
	velc.u		surface	(+03/ 00/00)	(+06/-15/00)	-0.1389	0.0813	-0.0071	0.0032
	velc.u		12m	(+06/+03/12)	(+09/-18/12)	-0.0719	0.0478	-0.0067	0.0020
	velc.v	[m/s]	overall	(+03/ 00/12)	(+18/-09/10)	-0.0581	0.0689	-0.0017	0.0014
	velc.v		surface	(-03/-12/00)	(-06/+06/00)	-0.0476	0.0550	-0.0012	0.0020
	velc.v		12m	(+03/ 00/12)	(-09/+06/12)	-0.0581	0.0355	-0.0026	0.0016
	velc.w	[m/s]	overall	(+03/+06/12)	(+03/-12/10)	-4.40E-05	4.94E-05	-1.06E-06	1.15E-06
TS01HD60F01	velc.w		2m	(-03/ 00/02)	(+06/-06/02)	-1.18E-05	1.55E-05	-4.55E-07	5.37E-07
	velc.w		12m	(+03/+06/12)	(+03/-12/12)	-4.40E-05	4.66E-05	-2.26E-06	2.11E-06
	temperature	[ºC]	overall	(+06/-09/10)	(+03/+09/14)	-2.6823	1.9207	-0.0084	0.0091
	temperature		surface	(+09/-15/00)	(+03/-03/00)	-0.2210	0.1895	-0.0046	0.0104
	temperature		12m	(+06/-12/12)	(+03/+09/12)	-1.7905	1.6759	-0.0518	0.0646
	salinity	[psu]	overall	(+03/+09/18)	(+09/-09/16)	-5.78E-02	6.08E-02	-9.25E-04	7.39E-04
T048	salinity		surface	(+03/-03/00)	(+09/-15/00)	-1.11E-03	2.06E-03	-1.02E-04	4.17E-05
	salinity		12m	(+03/+09/12)	(+06/-09/12)	-1.87E-02	5.35E-02	-1.01E-03	1.14E-03
	density	[kg/m^2]	overall	(+03/+09/14)	(+06/-09/10)	-0.3949	0.5569	-0.0024	0.0022
	density		surface	(+03/-03/00)	(+09/-15/00)	-0.0406	0.0475	-0.0023	0.0010
	density		12m	(+03/+09/12)	(+06/-12/12)	-0.3500	0.3690	-0.0134	0.0106

Table of Statistics 5: Simulation T080ug08 TS01HD60F01 → T080

mode (OWFr-REFr)	variable	unit	depth	Pmin (km/km/m)	Pmax (km/km/m)	min	max	mean-	mean+
T012ug08	ζ	[m]	overall	(+09/-15/00)	(+06/+18/00)	-9.69E-03	6.85E-03	-9.39E-04	8.30E-04
	velh	[m/s]	overall	(+09/-03/00)	(+06/+09/12)	-0.0695	0.0702	-0.0065	0.0047
	velh		surface	(+09/-03/00)	(+06/-21/00)	-0.0695	0.0550	-0.0095	0.0035
	velh		12m	(-03/+51/12)	(+06/+09/12)	-0.0059	0.0702	-0.0019	0.0080
	velc.u	[m/s]	overall	(+06/+09/00)	(+09/-21/00)	-0.0965	0.0758	-0.0063	0.0032
	velc.u		surface	(+06/+09/00)	(+09/-21/00)	-0.0965	0.0758	-0.0093	0.0071
	velc.u		12m	(+12/+12/12)	(+09/-24/12)	-0.0526	0.0436	-0.0077	0.0031
	velc.v	[m/s]	overall	(00/-06/12)	(+18/-15/10)	-0.0525	0.0723	-0.0025	0.0043
	velc.v		surface	(-03/-15/00)	(-06/+12/00)	-0.0358	0.0648	-0.0029	0.0070
	velc.v		12m	(00/-06/12)	(-06/+15/12)	-0.0525	0.0371	-0.0038	0.0024
	velc.w	[m/s]	overall	(+06/+15/12)	(+06/-18/10)	-4.19E-05	4.37E-05	-1.31E-06	1.45E-06
TS01HD60F01	velc.w		2m	(-03/+06/02)	(+09/-15/02)	-1.45E-05	1.48E-05	-1.05E-06	1.10E-06
	velc.w		12m	(+06/+15/12)	(+09/-18/12)	-4.19E-05	3.77E-05	-2.47E-06	2.42E-06
	temperature	[ºC]	overall	(+06/-15/10)	(+03/+15/14)	-2.5275	1.6863	-0.0382	0.0282
	temperature		surface	(+09/-21/00)	(+06/+03/00)	-0.1581	0.2038	-0.0131	0.0909
	temperature		12m	(+06/-15/12)	(+03/+15/12)	-1.6415	1.5175	-0.0726	0.1960
	salinity	[psu]	overall	(+03/+15/18)	(+06/-15/16)	-5.06E-02	5.36E-02	-7.96E-04	1.05E-03
T080	salinity		surface	(+06/-06/00)	(+09/-21/00)	-1.16E-03	1.22E-03	-5.47E-04	3.61E-04
	salinity		12m	(+03/+15/12)	(+06/-15/12)	-1.80E-02	4.68E-02	-2.18E-03	9.16E-04
	density	[kg/m^2]	overall	(+03/+15/14)	(+06/-15/10)	-0.3461	0.5243	-0.0064	0.0086
	density		surface	(+06/+03/00)	(+09/-21/00)	-0.0437	0.0339	-0.0195	0.0028
	density		12m	(+03/+15/12)	(+06/-15/12)	-0.3166	0.3384	-0.0396	0.0145

Table of Statistics 6: Simulation T160ug08 TS01HD60F01 → T160

mode (OWFr-REFr)	variable	unit	depth	Pmin (km/km/m)	Pmax (km/km/m)	min	max	mean-	mean+
T012ug08	ζ	[m]	overall	(+09/-15/00)	(+06/+18/00)	-1.27E-02	8.83E-03	-1.38E-03	1.09E-03
	velh	[m/s]	overall	(+12/ 00/00)	(+06/+09/12)	-0.0794	0.0828	-0.0041	0.0067
	velh		surface	(+12/ 00/00)	(+03/-21/00)	-0.0794	0.0681	-0.0060	0.0058
	velh		12m	(-06/+51/12)	(+06/+09/12)	-0.0059	0.0828	-0.0021	0.0092
	velc.u	[m/s]	overall	(+06/+09/00)	(+09/-21/00)	-0.1192	0.0872	-0.0092	0.0034
	velc.u		surface	(+06/+09/00)	(+09/-21/00)	-0.1192	0.0872	-0.0069	0.0062
	velc.u		12m	(+09/+12/12)	(+09/-24/12)	-0.0664	0.0585	-0.0102	0.0036
	velc.v	[m/s]	overall	(00/ 00/12)	(+18/-15/10)	-0.0562	0.0759	-0.0034	0.0033
	velc.v		surface	(-06/-18/00)	(-09/+12/00)	-0.0433	0.0709	-0.0023	0.0052
	velc.v		12m	(00/ 00/12)	(-09/+15/12)	-0.0562	0.0409	-0.0046	0.0028
	velc.w	[m/s]	overall	(+06/+15/12)	(+06/-15/08)	-5.51E-05	5.32E-05	-1.68E-06	1.83E-06
TS01HD60F01	velc.w		2m	(-06/+06/02)	(+06/-12/02)	-1.55E-05	1.95E-05	-8.61E-07	9.53E-07
	velc.w		12m	(+06/+15/12)	(+06/-21/12)	-5.51E-05	4.75E-05	-3.12E-06	3.40E-06
	temperature	[ºC]	overall	(+09/-15/10)	(+03/+15/14)	-2.8230	2.0383	-0.0153	0.0137
	temperature		surface	(+09/-21/00)	(00/-06/00)	-0.2678	0.2182	-0.0155	0.0212
	temperature		12m	(+06/-18/12)	(+03/+15/12)	-1.8902	1.7051	-0.0544	0.1807
	salinity	[psu]	overall	(+03/+15/18)	(+09/-15/16)	-6.26E-02	6.51E-02	-1.02E-03	1.06E-03
T160	salinity		surface	(+03/-06/00)	(+09/-21/00)	-1.19E-03	2.56E-03	-1.36E-04	1.33E-04
	salinity		12m	(00/+15/12)	(+06/-18/12)	-1.89E-02	5.80E-02	-1.74E-03	1.18E-03
	density	[kg/m^2]	overall	(+03/+15/14)	(+09/-15/10)	-0.4190	0.5851	-0.0034	0.0038
	density		surface	(00/-06/00)	(+09/-21/00)	-0.0467	0.0576	-0.0045	0.0033
	density		12m	(+03/+15/12)	(+06/-18/12)	-0.3562	0.3906	-0.0367	0.0111

Table of Statistics 7: Simulation T012ug08 TS01HD60F04 → BROSTRÖM F04

mode (OWFr-REFr)	variable	unit	depth	Pmin (km/km/m)	Pmax (km/km/m)	min	max	mean-	mean+
T012ug08	ζ	[m]	overall	(+003/-012/00)	(+006/+009/00)	-1.55E-02	7.91E-03	-1.48E-03	6.79E-04
	velh	[m/s]	overall	(+003/-015/10)	(000/-003/12)	-0.0655	0.1435	-0.0054	0.0091
	velh		surface	(-066/-120/00)	(+003/-003/00)	-0.0286	0.0994	-0.0100	0.0249
	velh		12m	(-069/-114/12)	(000/-003/12)	-0.0058	0.1435	-0.0031	0.0224
	velc.u	[m/s]	overall	(+003/-003/00)	(+114/-102/14)	-0.2282	0.0630	-0.0175	0.0059
	velc.u		surface	(+003/-003/00)	(000/-021/00)	-0.2282	0.0052	-0.0390	0.0027
	velc.u		12m	(+003/-003/12)	(+102/+114/12)	-0.1343	0.0574	-0.0064	0.0118
	velc.v	[m/s]	overall	(-006/-012/00)	(+117/-114/10)	-0.1067	0.0828	-0.0093	0.0066
	velc.v		surface	(-006/-012/00)	(+117/-114/00)	-0.1067	0.0300	-0.0420	0.0081
	velc.v		12m	(+021/+009/12)	(-114/+114/12)	-0.0643	0.0578	-0.0205	0.0154
	velc.w	[m/s]	overall	(-003/ 000/10)	(+006/-012/10)	-3.81E-05	2.93E-05	-2.21E-06	2.04E-06
TS01HD60F01	velc.w		2m	(-003/-003/02)	(+003/-009/02)	-1.73E-05	9.97E-06	-1.00E-06	9.29E-07
	velc.w		12m	(000/+003/12)	(+003/-015/12)	-3.72E-05	2.22E-05	-2.72E-06	2.74E-06
	temperature	[ºC]	overall	(+003/-009/10)	(+003/+006/14)	-2.6790	2.7477	-0.0473	0.0594
	temperature		surface	(+003/-015/00)	(+084/+108/00)	-0.9161	0.2599	-0.1299	0.1187
	temperature		12m	(+003/-012/12)	(-006/+003/12)	-2.1669	1.6512	-0.3741	0.3655
	salinity	[psu]	overall	(+003/+006/20)	(+003/-012/14)	-9.18E-02	1.11E-01	-1.75E-03	1.24E-03
Broström F04	salinity		surface	(+114/+102/00)	(+003/-015/00)	-3.20E-04	1.75E-02	-1.08E-04	5.78E-04
	salinity		12m	(000/+006/12)	(+003/-012/12)	-1.85E-02	1.02E-01	-1.45E-03	4.78E-03
	density	[kg/m^2]	overall	(+003/+006/14)	(+003/-009/10)	-0.5660	0.5760	-0.0125	0.0106
	density		surface	(+084/+108/00)	(+003/-015/00)	-0.0548	0.2009	-0.0251	0.0275
	density		12m	(-006/+003/12)	(+003/-012/12)	-0.3444	0.4725	-0.0721	0.0762

Table of Statistics 8: Simulation T012ug08 TS01HD60F03 → full meteorlogical forcing F03

mode (OWFr-REFr)	variable	unit	depth	Pmin (km/km/m)	Pmax (km/km/m)	min	max	mean-	mean+
T012ug08	ζ	[m]	overall	(+12/-09/00)	(+03/+09/00)	-8.29E-03	5.48E-03	-7.58E-04	5.59E-04
	velh	[m/s]	overall	(+18/-12/12)	(+06/+03/14)	-0.0609	0.0831	-0.0013	0.0037
	velh		surface	(-06/+03/00)	(+03/-15/00)	-0.0481	0.0668	-0.0024	0.0026
	velh		12m	(+18/-12/12)	(+06/+03/12)	-0.0609	0.0365	-0.0033	0.0021
	velc.u	[m/s]	overall	(+03/ 00/00)	(+06/-15/00)	-0.1069	0.0773	-0.0060	0.0019
	velc.u		surface	(+03/ 00/00)	(+06/-15/00)	-0.1069	0.0773	-0.0065	0.0033
	velc.u		12m	(+06/+03/12)	(+06/-15/12)	-0.0596	0.0327	-0.0047	0.0019
	velc.v	[m/s]	overall	(+03/ 00/14)	(+18/-09/12)	-0.0500	0.0717	-0.0018	0.0015
	velc.v		surface	(-03/-12/00)	(-06/+06/00)	-0.0464	0.0477	-0.0014	0.0016
	velc.v		12m	(+87/+48/12)	(+18/-09/12)	-0.0179	0.0717	-0.0010	0.0038
	velc.w	[m/s]	overall	(+06/+09/14)	(+03/-12/12)	-4.37E-05	4.81E-05	-1.15E-06	1.27E-06
TS01HD60F01	velc.w		2m	(+06/+09/02)	(+06/-09/02)	-8.03E-06	1.34E-05	-4.79E-07	6.44E-07
	velc.w		12m	(+06/+09/12)	(+03/-12/12)	-4.03E-05	4.81E-05	-1.90E-06	1.96E-06
	temperature	[ºC]	overall	(+06/-09/12)	(+03/+09/14)	-2.4067	1.7482	-0.0073	0.0082
	temperature		surface	(+09/-15/00)	(+03/-03/00)	-0.2114	0.3421	-0.0054	0.0111
	temperature		12m	(+06/-09/12)	(00/+03/12)	-2.4067	0.2305	-0.0602	0.0050
	salinity	[psu]	overall	(+03/+09/18)	(+09/-09/16)	-6.42E-02	6.41E-02	-9.05E-04	7.48E-04
full meteorological forcing F03	salinity		surface	(+03/ 00/00)	(+09/-15/00)	-1.22E-02	3.75E-03	-2.27E-04	2.44E-04
	salinity		12m	(+63/+15/12)	(+06/-09/12)	-1.67E-02	2.69E-02	-7.78E-04	2.33E-04
	density	[kg/m^2]	overall	(+03/+09/14)	(+06/-09/12)	-0.3367	0.4680	-0.0022	0.0019
	density		surface	(00/-03/00)	(+09/-15/00)	-0.0771	0.0443	-0.0023	0.0012
	density		12m	(-03/ 00/12)	(+06/-09/12)	-0.0530	0.4680	-0.0011	0.0114

Table of Statistics 9: Simulation T012ug08 TS01HD30F01 → OCEAN DEPTH HD30

mode (OWFr-REFr)	variable	unit	depth	Pmin (km/km/m)	Pmax (km/km/m)	min	max	mean-	mean+
T012ug08	ζ	[m]	overall	(+09/-12/00)	(+06/+12/00)	-1.27E-02	7.56E-03	-1.37E-03	9.82E-04
	velh	[m/s]	overall	(+15/-12/10)	(+06/ 00/12)	-0.0668	0.1200	-0.0024	0.0066
	velh		surface	(-06/+03/00)	(+03/-15/00)	-0.0594	0.0660	-0.0045	0.0034
	velh		12m	(-18/+30/12)	(+06/ 00/12)	-0.0067	0.1200	-0.0017	0.0090
	velc.u	[m/s]	overall	(+03/ 00/00)	(+09/-18/00)	-0.1632	0.0770	-0.0109	0.0035
	velc.u		surface	(+03/ 00/00)	(+09/-18/00)	-0.1632	0.0770	-0.0123	0.0043
	velc.u		12m	(+09/+03/12)	(+09/-18/12)	-0.1050	0.0569	-0.0118	0.0035
	velc.v	[m/s]	overall	(00/-03/12)	(+18/-09/10)	-0.0685	0.0634	-0.0032	0.0026
	velc.v		surface	(-03/-12/00)	(-09/+06/00)	-0.0600	0.0532	-0.0024	0.0028
	velc.v		12m	(00/-03/12)	(-09/+09/12)	-0.0685	0.0357	-0.0041	0.0026
	velc.w	[m/s]	overall	(+03/+06/12)	(+03/-12/10)	-5.46E-05	4.53E-05	-1.27E-06	1.32E-06
TS01HD60F01	velc.w		2m	(00/+03/02)	(+09/-06/02)	-1.24E-05	1.49E-05	-4.51E-07	5.87E-07
	velc.w		12m	(+03/+06/12)	(+03/-12/12)	-5.46E-05	3.97E-05	-2.47E-06	2.27E-06
	temperature	[ºC]	overall	(+06/-09/10)	(+03/+09/14)	-2.3694	1.6882	-0.0134	0.0129
	temperature		surface	(+09/-15/00)	(+03/-03/00)	-0.1811	0.1955	-0.0041	0.0098
	temperature		12m	(+06/-12/12)	(+03/+09/12)	-1.5863	1.5547	-0.0468	0.0571
	salinity	[psu]	overall	(00/+06/16)	(+06/-12/14)	-4.76E-02	4.60E-02	-7.14E-04	6.33E-04
HD30	salinity		surface	(+03/-03/00)	(+09/-15/00)	-1.12E-03	1.72E-03	-9.21E-05	4.30E-05
	salinity		12m	(+03/+09/12)	(+06/-12/12)	-1.81E-02	4.24E-02	-8.85E-04	1.01E-03
	density	[kg/m^2]	overall	(+03/+09/14)	(+06/-09/10)	-0.3462	0.4933	-0.0030	0.0031
	density		surface	(+03/-03/00)	(+09/-15/00)	-0.0419	0.0390	-0.0021	0.0009
	density		12m	(+03/+09/12)	(+06/-12/12)	-0.3244	0.3253	-0.0118	0.0096

ACKNOWLEDGMENT

At this point I want to use the chance to register some attendants supporting me and my work in the last 32 months.

Primarily I have to thank my first adviser and tutor PD Dr. Thomas Pohlmann for his collaboration, for his offer of the scholarship at the *International Max Planck Research School for Maritime Affairs* and especially for his professional support.

I have to thank my second adviser, Prof. Dr. Schlünzen, and the members of my examination committee, Prof. Dr. Gajewski, Prof. Dr. Backhaus and Prof. Dr. Burchard for their expenditure of time for my promotion proceeding.

Particularly I have to mention M. Linde. Thank you for a well collaboration and expenditure of time by simulations, data and questions regarding METRAS.

To the BSH, the WEGA cruise and A. Schneehorst a big thank-you for an interesting cruise to *alpha ventus* and the measurement campaign which ends in a really wonderful revealing data set and a friendly collaboration.

A thank-you is to be addressed to the TO-work group, which provides a nice working atmosphere and thank you to the IMPRS-MA for providing an insight into the law-side of the maritime affairs.

A thank goes also to the department of Informatics Scientific Computing of Hamburg University, especially H. Lenhart, for their interest at my work. I am really curious and looking forward to the simulations considering the OWF-effect on the North Sea's ecosystem.

Last but not least I want to mention my family and want to thank them for supporting my academic studies, my conference and summer school trip and you are always open to me.